

**DOCTORAL THESIS**

Lignin Valorization via  
Chloromethylation as a  
Versatile Approach Towards  
Sustainable Materials

Mahendra Kothottil Mohan

TALLINN UNIVERSITY OF TECHNOLOGY  
DOCTORAL THESIS  
74/2025

**Lignin Valorization  
via Chloromethylation as a Versatile  
Approach Towards Sustainable Materials**

MAHENDRA KOTHOTTIL MOHAN



TALLINN UNIVERSITY OF TECHNOLOGY  
School of Science  
Department of Chemistry and Biotechnology

This dissertation was accepted for the defence of the degree of Doctor of Philosophy  
in Chemistry, on 25/09/2025

<b>Supervisor:</b>	Dr. Yevgen Karpichev School of Science Tallinn University of Technology Tallinn, Estonia
<b>Opponents:</b>	Associate Professor Mika Sipponen Department of Chemistry Stockholm University Stockholm, Sweden
	Professor Timo Kikas Institute of Forestry and Engineering Estonian University of Life Sciences Tartu, Estonia

**Defence of the thesis:** 27/10/2025, Tallinn

**Declaration:**

Hereby I declare that this doctoral thesis, my original investigation and achievement, submitted for the doctoral degree at Tallinn University of Technology has not been submitted for doctoral or equivalent academic degree.

Mahendra Kothottil Mohan

-----  
signature



European Union  
European Regional  
Development Fund



Investing  
in your future

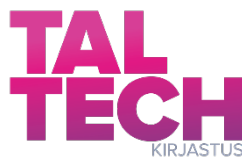
Copyright: Mahendra Kothottil Mohan, 2025  
ISSN 2585-6898 (publication)  
ISBN 978-9916-80-385-1 (publication)  
ISSN 2585-6901 (PDF)  
ISBN 978-9916-80-386-8 (PDF)  
DOI <https://doi.org/10.23658/taltech.74/2025>

Kothottil Mohan, M. (2025). Lignin Valorization via Chloromethylation as a Versatile Approach Towards Sustainable Materials [TalTech Press]. <https://doi.org/10.23658/taltech.74/2025>

TALLINNA TEHNICAÜLIKOO  
DOKTORITÖÖ  
74/2025

# **Ligniini väärindamine klorometüleerimise teel kui mitmekülgne lähenemisviis jätkusuutlike materjalide loomisele**

MAHENDRA KOTHOTTIL MOHAN



# Contents

List of Publications .....	6
Author's Contribution to the Publications .....	7
Introduction .....	8
Abbreviations .....	9
1 Literature Overview .....	11
1.1 Green and sustainable chemistry .....	11
1.2 Renewable vs. fossil resources.....	11
1.3 Lignin .....	12
1.3.1 Lignin Monomers .....	12
1.3.2 Technical Lignin.....	14
1.3.3 Organosolv Lignin.....	14
1.4 Chemical modification of lignin .....	14
1.5 Scope of the Study .....	15
1.5.1 Lignin as Catalyst.....	16
1.5.2 Lignin as an Antibacterial Agent.....	17
1.5.3 Lignin as Thermoplastic Fillers .....	18
2 Objectives of the Study.....	20
3 Results and Discussions .....	22
3.1 Chloromethylation of lignin (Publications I to IV) .....	22
3.1.1 Green chemistry metrics for chloromethylation .....	25
3.2 Lignin catalyst for cross-coupling reactions and click reactions (Publication I) ..	26
3.2.1 Preparation of Lignin@Pd/CuO–NPs .....	26
3.2.2 Evaluation of the catalytic activity of Lignin@Pd/CuO–NPs in batch reaction and packed-bed flow reactor .....	28
3.2.3 Green chemistry metrics for catalytic reactions .....	28
3.3 Antibacterial quaternary ammonium lignin (Publication II) .....	29
3.3.1 Preparation of QALs .....	29
3.3.2 Antibacterial activity of lignin .....	31
3.4 Antibacterial properties of quaternary phosphonium vs ammonium lignin (Publication V) .....	34
3.4.1 Preparation of QHLs .....	34
3.4.2 Antibacterial activity of QHLs.....	36
3.4.3 Morphology of CA–Lignin electrospun nanofibres .....	38
3.4.4 Wettability test .....	39
3.4.5 Biofilm formation .....	40
3.5 Lignin Esters as Advanced Filler to PLA for 3D Printing (Publication III) .....	41
3.5.1 Characterization and thermal properties of esterified lignin and PLA composite.	41
3.5.2 Mechanical testing of esterified lignin PLA composite and 3D printing capabilities .....	43
3.5.3 Morphological characterization of 3D-printed specimens. ....	46
3.6 Organosolv vs technical lignin: Influence of aliphatic and aromatic groups (Publication IV).....	47
3.6.1 Thermal properties of esterified lignin and PLA composite.....	47

3.6.2	Mechanical properties of esterified lignin and PLA composite .....	48
4	Conclusions .....	50
5	Experimental section .....	51
	References .....	55
	Acknowledgements.....	61
	Abstract .....	63
	Lühikokkuvõte.....	65
	Appendix 1 .....	67
	Appendix 2 .....	81
	Appendix 3 .....	95
	Appendix 4 .....	107
	Appendix 5 .....	123
	Curriculum vitae.....	141
	Elulookirjeldus.....	143

## List of Publications

The list of author's publications, on the basis of which the thesis has been prepared:

- I Mohan, M. K.; Silenko, O.; Krasnou, I.; Volobujeva, O.; Kulp, M.; Ošek, M.; Lukk, T.; Karpichev, Y. Chloromethylation of Lignin as a Route to Functional Material with Catalytic Properties in Cross-Coupling and Click Reactions. *ChemSusChem* **2024**. <https://doi.org/10.1002/cssc.202301588>.
- II Mohan, M. K.; Kaur, H.; Rosenberg, M.; Duvanov, E.; Lukk, T.; Ivask, A.; Karpichev, Y. Synthesis and Antibacterial Properties of Novel Quaternary Ammonium Lignins. *ACS Omega* **2024**. <https://doi.org/10.1021/acsomega.4c06000>.
- III Mohan, M. K.; Krasnou, I.; Lukk, T.; Karpichev, Y. Novel Softwood Lignin Esters as Advanced Filler to PLA for 3D Printing. *ACS Omega* **2024**, 9 (44), 44559–44567. <https://doi.org/10.1021/acsomega.4c06680>.
- IV Mohan, M. K.; Ho, T. T.; Köster, C.; Järvi, O.; Kulp, M.; Karpichev, Y. Tuning Ester Derivatives of Organosolv vs Technical Lignin for Improved Thermoplastic Materials. *Faraday Discuss* **2025**. <https://doi.org/10.1039/D5FD00068H>.
- V Mohan, M.K.; Bragina, O.; Mosjakina, S.; Raimundo, J.-M.; Karpichev, Y. Antibacterial Properties of Heteronium Lignin Containing Materials Against ESKAPE Pathogens. *ChemRxiv*. **2025**; <https://doi.org/10.26434/chemrxiv-2025-zmlgw-v2>. This content is a preprint and has not been peer-reviewed.

## **Author's Contribution to the Publications**

Contribution to the papers in this thesis are:

- I The author had a major role in the development of the conceptualization, methodologies, investigation, validation, data curation, and visualization. The author wrote the manuscript, with the contributions from the co-authors, and compiled the supporting information.
- II The author had a major role in the development of the conceptualization, methodologies, investigation (synthesis and characterization of studied compounds), validation, data curation, and visualization. The author co-wrote the manuscript with the contributions from the co-authors and compiled the supporting information.
- III The author had a major role in the development of the conceptualization, methodologies, investigation, validation, data curation, and visualization. The author wrote the manuscript, with the contributions from the co-authors, and compiled the supporting information.
- IV The author had a major role in the development of the conceptualization, methodologies, investigation (esterification through chloromethylation and characterization of studied composites), validation, data curation, and visualization. The author co-wrote the manuscript with the contributions from the co-authors and compiled the supporting information.
- V The author had a major role in the development of the conceptualization, methodologies, investigation (synthesis and characterization of studied compounds and materials), validation, data curation, and visualization. The author wrote the manuscript, with the contributions from the co-authors, and compiled the supporting information.

## Introduction

The exploration of environmental materials continues to progress, emphasizing the harnessing of natural resources and repurposing of waste. The advancement of eco-friendly technologies and methods stands as a cornerstone for building a sustainable society.<sup>1</sup> This highlights the importance of bio-based industries in replacing non-renewable resources for fuel, energy, and manufacturing.<sup>2</sup> Efforts to convert biomass into valuable products must adhere to rigorous standards to guarantee sustainability.

Lignin, Earth's second most prevalent biopolymer and a primary by-product of the cellulose industry, represents a vast reservoir of renewable aromatics, capable of supplanting fossil-derived aromatic compounds.<sup>3</sup> Despite its ubiquity, lignin is relegated mainly to a by-product status in pulp production, with approximately 70 million tons generated annually worldwide. Regrettably, due to the lack of efficient processing techniques, approximately 95% of industrial lignin is currently incinerated for energy.<sup>4</sup> However, given its natural abundance, lignin holds promise for addressing the escalating scarcity of fossil resources if it can be effectively transformed into a renewable commodity or upgraded into higher-value materials. Recent advancements in lignin modification chemistry have yielded a range of functional lignin-based polymers, amalgamating the inherent attributes of lignin with the added functionalities of grafted polymers.<sup>5</sup> Lignin emerges as an underappreciated asset in green chemistry, poised to serve as a foundation for the development of fabrication processes for materials endowed with advanced properties.<sup>6-8</sup>

In this study, I present a novel method for the chloromethylation of lignin, which has paved the way for the creation of a diverse range of lignin-based products utilizing chloromethylated lignin as the starting material. The resulting lignin-based materials encompass catalytic agents (**Publication I**), antibacterial formulations (**Publication II** and **Publication V**), and thermoplastic additives (**Publication III** and **IV**). This research, along with the greener chloromethylation approach for lignin, holds promise for shedding new light on lignin valorization, rendering it both economically attractive and environmentally safe.

Furthermore, I have presented the results of my research at various stages in international conferences held in Estonia, Portugal, the Netherlands, Italy, France, India, and United States.

## Abbreviations

AcOH	Acetic acid
AL	Amino lignin
BAEP	Benzoic acid esterified pine
CA	Cellulose acetate
CFU	Colony-forming units
CHO	Formaldehyde
CM/CML	Chloromethylated lignin
DMF	Dimethylformamide
DMSO- <i>d</i> <sub>6</sub>	Deuterated dimethyl sulfoxide
DSC	Differential scanning calorimetry
EA	Elemental analysis
EtOH	Ethanol
FT-IR	Fourier transform infrared spectroscopy
H	Hydrogen
HCl	Hydrochloric acid
HLE	Hydrolysis lignin ester
Im	Imidazole
L	Lignin
MBC	Minimal bactericidal concentration
Me	Methyl
M <sub>w</sub>	Molecular weight
N6	Trihexylamine
N8	Trioctylamine
NaOH	Sodium hydroxide
NMR	Nuclear magnetic resonance
NPs	Nanoparticles
OH	Hydroxy/hydroxyl
OHLE	Hydroxyl (OH) esterified lignin
OL	Organosolv lignin
P6	Trihexylphosphine
P8	Trioctylphosphine
PC	Positive control
Pd	Palladium
PFA	Paraformaldehyde
PLA	Polylactic acid
QAL	Quaternary ammonium lignin
QAS	Quaternary ammonium salt
QHL	Quaternary heteronium lignin
QHS	Quaternary heteronium salt
QPL	Quaternary phosphonium lignin

QPS	Quaternary phosphonium salt
SEM	Scanning electron microscope
$T_g$	Glass transition temperature
TGA	Thermogravimetric analysis
THF	Tetrahydrofuran
XRF	X-ray fluorescence
ZOI	Zone of inhibition



### 1.3 Lignin

In 1838, French chemist Anselme Payen conducted pioneering experiments by treating wood with nitric acid and sodium hydroxide, which yielded two distinct substances. One of these substances, termed cellulose, emerged as a key discovery, while the other, characterized by a high carbon content and enveloping the cellulose, was termed "encrusting material." This event marked a significant milestone in the understanding of lignin. Subsequently, in 1865, Schulze formally designated this "encrusting material" as lignin, derived from the Latin word "lignum," meaning "wood." Building upon this, in 1868, E. Erdmann identified aromatic compounds as constituents of lignin.<sup>25</sup> Further advancements came in 1890 when Benedikt and Bamberger demonstrated the presence of other functional groups within lignified wood material, such as methoxyl groups. Lignin, a complex biomacromolecule, predominates in the cell wall of lignocellulosic materials like wood, exhibiting a highly branched and amorphous structure whose composition varies based on the plant source.<sup>26</sup>

#### 1.3.1 Lignin Monomers

The chemical structure of lignin from three hydroxycinnamyl alcohols, known as monolignols: p-coumaryl alcohol, coniferyl alcohol, and sinapyl alcohol (see Figure 2). These alcohols differ primarily in the degree of methoxylation at the C3 and C5 positions of the aromatic ring. The p-hydroxyphenyl (H unit) lacks methoxyl groups at these positions, the guaiacyl (G unit) possesses a methoxyl group at the C3 carbon, and the syringyl (S unit) features methoxyl groups at both the C3 and C5 carbons.<sup>27</sup>

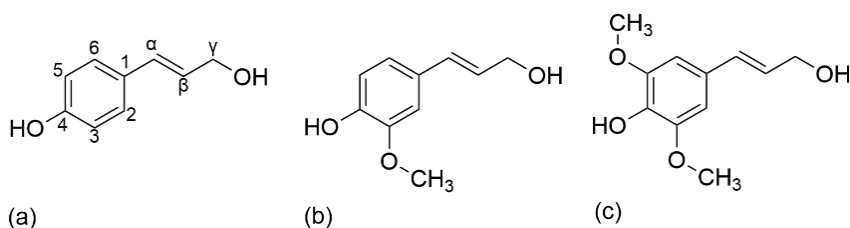


**Figure 2.** Monolignol species: (a) p-coumaryl alcohol (H unit), (b) coniferyl alcohol (G unit), (c) sinapyl alcohol (S unit).

Lignin is a three-dimensional, amorphous heteropolymer lacking a well-defined chemical structure (see Figure 3). Polymerization occurs through the interaction of monomers with polymer stages, as well as through the reaction of pre-existing aggregates (such as di, tri, etc., lignans). Molecular weight stands as another crucial feature of lignin. Typically, the molecular weight of lignin ranges from 1 to 50 kDa.<sup>28</sup> The molecular weight of lignin can undergo substantial changes due to the isolation procedures, the origin of the plant species, and post-refinery processes. The reported molar masses of isolated lignins, such as the approximately 10,000 molecular weight of spruce milled wood lignin (MWL) produced in the laboratory, are variable and method-dependent, thus not uniform or representative.<sup>29</sup> The lignification process in plants involves the formation of a complex, three-dimensional structure through the linking of precursor alcohols, primarily through  $\beta$ -O-4 ether bonds (see Figure 3). Hardwood lignin is mainly composed of guaiacyl and syringyl units with low levels of p-hydroxyphenyl. In contrast, softwood lignin has higher

levels of guaiacyl units and lower levels of p-hydroxyphenyl. Grasses contain guaiacyl, syringyl, and p-hydroxyphenyl units (see Table 1). In all cases, these monomers are linked together without defined repeating units. The lignification process results in the formation of a complex, three-dimensional structure composed of various bonds. The primary linkages in native lignin are  $\beta$ -O-4 and  $\alpha$ -O-4 bonds. Lignin features both hydrophilic and hydrophobic groups; however, due to its three-dimensional chemical structure, it is predominantly hydrophobic in its natural form. This hydrophobic nature plays a crucial role in making the plant cell wall water-repellent, thus facilitating water transport within the plant. The composition and content of lignin can vary depending on the plant species and environmental factors.<sup>30</sup>

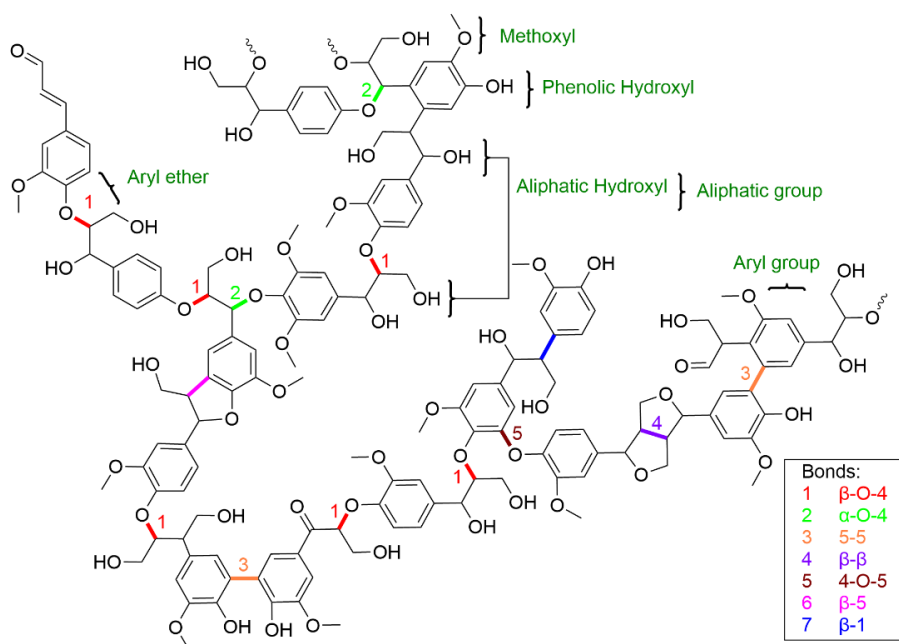


**Figure 3.** Prominent linkages and functional groups in softwood lignin.<sup>31</sup>

**Table 1.** Lignocellulose and lignin composition for softwoods, hardwoods, and grasses.<sup>32</sup>

	Lignocellulose composition (wt.%)			Monolignol distribution in lignin (%)		
	Cellulose	Hemicellulose	Lignin	H	G	S
Softwoods	46-50	19-22	21-29	<10	>95	2-3
Hardwood	40-46	17-23	18-25	<8	20-60	40-75
Grasses	28-37	23-29	17-20	5-33	33-80	20-54

Lignin presents a major opportunity for improving the efficiency of a lignocellulosic biorefinery. As a highly abundant raw material, it constitutes up to 30% of the weight

and 40% of the energy content of lignocellulosic biomass.<sup>33</sup> The inherent structure of lignin indicates its potential as a key chemical feedstock, especially in the production of supramolecular materials and aromatic chemicals.<sup>34</sup>

### **1.3.2 Technical Lignin**

Technical lignin is a byproduct derived from various pretreatments or separation processes involving lignocellulosic biomass. These biomasses are commonly used as raw materials for pulp or second-generation ethanol production. The chemical properties of technical lignin, including its composition, molecular weight, and molecular structure, can be affected by the isolation process, resulting in different types of lignin with diverse applications in biorefinery platforms. Additionally, these types of lignin exhibit variations in physical properties such as solubility, hydrophobicity, and hydrophilicity. Therefore, it is important to consider each technical lignin individually due to these inherent differences.<sup>35,36</sup> Lignin is commonly viewed as a secondary product of pulp manufacturing, with approximately 70 million tons of technical lignin generated globally each year. Due to the lack of efficient processing techniques, about 95% of industrial lignin is currently utilized as a fuel source.<sup>37</sup>

The structure of natural lignin can undergo significant degradation and alteration depending on the process used, resulting in a decrease in aliphatic OH groups,  $\beta$ -O-4 bonds, and  $\beta$ - $\beta$  bonds. This process may also result in the formation of degraded products such as phenolic hydroxyl groups, carboxylic acids, and carbonyl groups.<sup>38</sup> As a result, the composition of technical lignin is generally influenced by the extraction method and the original raw material source (softwood, hardwood, or grasses).<sup>39</sup>

### **1.3.3 Organosolv Lignin**

The organosolv lignin extraction process aims to isolate lignin from the lignocellulosic biomass using organic solvents to dissolve the lignin. This process is exciting for various bioproduct applications, as it can be sulfur-free, depending on the solvents used.<sup>40</sup> The quality of the extracted lignin depends on the pretreatment conditions. Lignin extracted through the organosolv process can have high purity, chemical reactivity, be non-toxic, and exhibit good thermal stability, which benefits its use in high-performance polymer composites, carbon-fiber precursors, and biomedical materials where low impurity levels are crucial. Organosolv lignin typically has a homogeneous structure similar to that of native lignin, characterized by a low molecular weight and polydispersity.<sup>36</sup> Studies have shown that increasing the severity of organosolv processes can reduce the molar mass of extracted lignin by 36 to 56% compared to untreated lignin. Additionally, this process can result in a reduction of aliphatic hydroxyl group content and an increase in syringyl phenolic units and condensed phenolic structures.<sup>41</sup> Organosolv lignin is highly soluble in organic solvents but almost insoluble in water due to its hydrophobic nature. To recover organosolv lignin from the solvent, it must be precipitated, typically by adjusting the concentration, pH, and temperature.<sup>42</sup>

## **1.4 Chemical modification of lignin**

Despite lignin containing various functional groups (hydroxyl, methoxyl, carbonyl, and carboxyl groups), its application is constrained by the presence of one or two methoxyl groups in its structure, which reduces its reactivity and limits its use in certain products. To overcome this challenge, numerous studies have been conducted to enhance lignin's chemical reactivity by altering its structure. These alterations focus on increasing the

reactivity of hydroxyl groups or modifying the nature of the active chemical sites. Various chemical modification pathways have been explored to improve reactivity of lignin.<sup>43</sup> Traditionally, the hydroxyl groups and aromatic units in lignin are extensively used for chemical functionalization. The presence of both aromatic and aliphatic hydroxyl groups enables chemical reactions such as esterification, alkylation, etherification, hydroxypropylation with epoxides, and urethanization through either isocyanate or non-isocyanate routes. Lignin phenolation is particularly interesting because it increases the number of reactive sites for aromatic substitution reactions. Chemical modifications on the aromatic units can include sulfomethylation, hydroalkylation, amination, and nitration. Additionally, azo coupling reactions have been reported to alter lignin properties.<sup>44</sup> Understanding this chemistry is crucial for designing modified lignins with desirable properties and developing new grafting chemistries for polymeric modifications.<sup>43,45</sup>

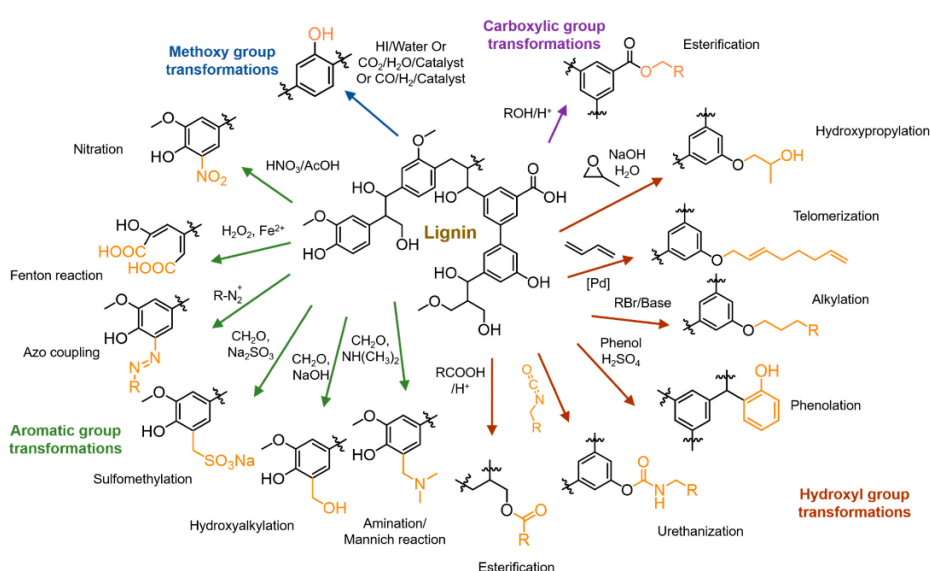


**Figure 4.** Summary of chemical transformations to diversify chemical functionality on lignin.<sup>46</sup> © 2019, MDPI. Licensed under CC BY 4.0.

## 1.5 Scope of the Study

In recent years, there has been a growing interest in exploring the various applications of lignin across different fields such as biomedicine,<sup>47,48</sup> food packaging,<sup>49–51</sup> cosmetics, health products,<sup>52,53</sup> precursor materials for advanced 3D printing,<sup>54</sup> lignin-based aerogels, lignin-derived carbon nanoparticles,<sup>55–57</sup> and antimicrobial applications.<sup>58–60</sup>

Different types of lignin, which depend on their botanical source and extraction method, have unique structural and chemical features that influence how they can be used. Kraft lignin, made through alkaline pulping with sodium hydroxide and sodium sulfide, has a high phenolic hydroxyl content and strong antioxidant capacity, making it suitable to use in antioxidant additives, UV-protective coatings, and polymer stabilization.<sup>61,62</sup> Soda lignin, extracted under alkaline conditions from non-wood sources such as annual plants, is also sulfur-free and eco-friendly, making it appealing for dispersants, emulsifiers, and biodegradable packaging.<sup>63,64</sup> Lignosulfonates, obtained

from sulfite pulping, are naturally water-soluble and surface-active, enabling their use as dispersing agents, binders, and chelants in aqueous systems.<sup>65</sup> Organosolv lignin, produced with organic solvents, is sulfur-free, has high purity, and exhibits excellent thermal stability, which is beneficial for high-performance polymer composites and biomedical materials where low impurity levels are essential.<sup>66</sup> Therefore, choosing materials for specific applications should consider the inherent lignin structure, how compatible the modification method is with the intended end-use, the processing technique (such as extrusion, electrospinning, or 3D printing), and sustainability factors like toxicity, recyclability, and environmental impact over the product's life cycle.

Compared to alternative methods of lignin modification, chloromethylation provides a highly adaptable chemical handle, facilitating rapid and efficient post-functionalization through nucleophilic substitution. This method enables the introduction of ionic, hydrophobic, or polymerizable groups. Its versatility frequently surpasses that of conventional techniques such as esterification or sulfonation, which primarily alter solubility or hydrophobicity but offer limited options for subsequent modification. Nonetheless, these traditional approaches may require longer reaction durations, specialized catalysts, or result in lignin derivatives with reduced chemical reactivity. Therefore, although chloromethylation offers unparalleled functional versatility compared to many other methods, its implementation should be carefully evaluated based on the synthetic benefits, hazard mitigation, and environmental impact throughout the lifecycle.

### **1.5.1 Lignin as Catalyst**

In recent decades, the protocols for cross-coupling reactions have seen significant advancements. Among these, the Suzuki-Miyaura coupling stands out as one of the most effective, powerful, and versatile methods for forming carbon-carbon bonds.<sup>67</sup> These reactions typically rely on homogeneous palladium (Pd) catalysts, paired with ligands such as phosphines or other organic compounds, in organic solvents. The metal catalysts and ligands used are often expensive and non-reusable, making the process economically challenging and coming with significant safety concerns. Additionally, the purification of contaminated products are typically slow and costly. They are also criticized in the context of effective circular economy strategies.<sup>68</sup> Given the increasing demand for resource efficiency and the need to minimize the use of Endangered & critical elements (which face supply limitations in the coming years),<sup>69</sup> there is a shift towards more sustainable alternatives. These alternatives include using metals with higher Chemical Element Sustainability Indexes,<sup>70</sup> such as copper, iron, or manganese, which are more affordable and sustainable. Copper is notable for its versatile catalytic properties, making it a highly appealing alternative.

Therefore, there is an urgent need to develop more efficient and user-friendly approaches that minimize or eliminate the reliance on non-sustainable metals in heterogeneous coupling reactions. Unlike previous examples that have used lignin or plant-based stabilizing agents for Pd catalysts,<sup>71–75</sup> our approach involves the preparation of a Pd/CuO heterogeneous catalyst with a lower content of the non-sustainable noble metal (Pd).<sup>69</sup> This catalyst has the potential to catalyze a broader spectrum of chemical reactions, offering a more sustainable solution. Although heterogeneous catalysts are rarely used for carbon-carbon coupling reactions, they could potentially offer more sustainable and economical alternatives.

In the last 15 years, N-heterocyclic carbenes (NHCs) have gained recognition as ligands for Pd-mediated cross-couplings. NHCs offer robust electron-donating capabilities, enabling oxidative insertion even with challenging substrates. Their steric bulk and distinctive structure also facilitate rapid reductive elimination.<sup>76</sup> Compared to established phosphine ligands, NHCs with bulky ligands have significantly improved catalyst efficiency.<sup>77</sup> However, effective heterogenization is necessary to meet the demands of various applications.<sup>78,79</sup> Despite existing methods for synthesizing Pd nanoparticles from plant extracts, the use of stabilizing agents has not been thoroughly explored.

### 1.5.2 Lignin as an Antibacterial Agent

The World Health Organization (WHO) reports that approximately 700,000 people die globally from antibiotic-resistant bacterial infections each year. In the United States, reported only in 2019, more than 35,000 deaths occurred from 2.8 million cases of antibiotic-resistant bacterial infections.<sup>80</sup> Similarly, Europe reported roughly 33,000 deaths annually attributed to antibiotic-resistant infections.<sup>81</sup> Globally, methicillin-resistant *Staphylococcus aureus* (MRSA) is recognized as a leading cause of human bacterial infection, and in 2017, MRSA alone caused 10,600 deaths from 323,700 cases in the United States.<sup>82</sup> Therefore, new antibacterial agents are needed to battle multidrug-resistant bacteria.

The antimicrobial properties of lignin are not surprising, considering that plants have evolved to use these properties as a defense mechanism against invading pathogenic microbes.<sup>83</sup> Lignin has shown its inhibitory effect against plant pathogens such as *Pseudomonas putida* and *Xanthomonas sp.*,<sup>84–86</sup> as well as against other bacteria that colonize plant surfaces.<sup>87</sup> The mechanism of antibacterial activity of lignin is proposed to rely on its strong affinity for the bacterial cell surface and its interaction with surface proteins and lipids, leading to membrane disruption and inhibition of the respiratory chain.<sup>88</sup> These events are expected to result in the formation of reactive oxygen species (ROS), which cause oxidative damage to cellular components and hinder bacterial growth.<sup>86</sup> In several studies, lignin have been combined with other antimicrobial materials to enhance their antimicrobial effect. For instance, silver nanoparticles have been added to lignin to enhance their activity against a range of bacteria.<sup>89,90</sup> It has been suggested that incorporating silver into lignin and further coating it with a cationic polyelectrolyte layer facilitates the interaction between lignin and the bacterial membrane, resulting in a synergistic antimicrobial effect.<sup>91</sup>

The development of lignin-based surfactants that concurrently demonstrate antibacterial activity signifies a significant advancement in the formulation of multifunctional, bio-derived materials. Lignin's aromatic backbone and inherent phenolic groups provide structural integrity and antimicrobial properties, while chemical modifications—such as quaternization to introduce cationic groups—donate amphiphilic characteristics and enhance interaction with microbial cell membranes, thereby resulting in practical antibacterial effects.<sup>92</sup> This dual functionality extends the applicability of lignin-derived products into sectors such as biomedical coatings, packaging, and water treatment. Additionally, it aligns with principles of green chemistry by employing a renewable biopolymer and reducing reliance on synthetic, petrochemical-derived surfactants.<sup>6,93</sup> The integration of surface activity and antimicrobial properties within a single lignin-based material creates opportunities for cost-effective production, simpler formulations, and environmentally friendly performance, thereby fostering the

development of high-value, sustainable alternatives within the surfactant and antimicrobial industries.

Quaternary heteronium salts (QHSs), including quaternary ammonium and phosphonium compounds, represent a promising path for discovering new antibacterial materials.<sup>94,95</sup> The hydrophobic side chain plays a significant role in influencing the antimicrobial properties of QHSs.<sup>96</sup> Since the 1930s, quaternary ammonium compounds (QASs) have been cationic surfactants widely used for their antimicrobial properties,<sup>97</sup> which result from their ability to disrupt bacterial cell membranes and cause leakage of cellular components.<sup>98–101</sup> This disruption occurs due to the presence of a positively charged nitrogen atom connected to four alkyl or aryl groups,<sup>102</sup> one of which is typically a long hydrocarbon chain (eight or more carbon atoms) that acts as a hydrophobic component.<sup>103</sup> In general, longer alkyl chains have improved penetration capability into bacterial membranes,<sup>100,104</sup> indicating that longer the hydrophobic carbon chain length, higher the antimicrobial activity.<sup>105</sup> However, some studies have shown an optimal side chain length of 10-12 carbons against Gram-negative<sup>106</sup> bacteria and 13-14 carbons against Gram-positive bacteria<sup>107</sup> for the best antimicrobial performance of QASs. This tendency persists in the case of surface-active ionic liquids,<sup>108,109</sup> where the extension of the alkyl chain length often leads to levelling off or fading of antimicrobial activity, known as the cut-off effect.<sup>110</sup> Gram-positive bacteria are expected to be more sensitive to QASs than Gram-negative bacteria, as the former lack the outer membrane that restricts QASs' access to their target site in the cytoplasmic membrane.<sup>111</sup> Dimeric QASs bearing two cationic groups and two hydrophobic carbon chains have been shown to exhibit greater antibacterial and biocidal activity compared to their monomeric counterparts.<sup>112,113</sup> Lignins modified with quaternary ammonium groups have been shown to exhibit substantially higher antibacterial activity than unmodified lignin against *E. coli*, *Listeria monocytogenes*, *Salmonella enterica*, and *S. aureus*.<sup>114,115</sup> Additionally, while QASs have been shown to exhibit notable toxicity to environmental organisms<sup>116</sup> and eukaryotic cells in vitro,<sup>117</sup> QAS-modified lignins are less cytotoxic.<sup>118</sup>

In the mid-20<sup>th</sup> century, quaternary phosphonium salts (QPSs) were widely researched for their antibacterial properties and safety in human applications.<sup>119</sup> These salts share structural similarities with QASs, notably showing antibacterial properties against both Gram-positive and Gram-negative bacteria.<sup>120</sup> Therefore, these compounds, along with lignin (QHLs), can be considered safer analogues to low-molecular-weight QHSs for human use and potentially also from an environmental perspective.

### 1.5.3 Lignin as Thermoplastic Fillers

Plastics are essential in numerous commercial sectors, with a global production volume of approximately 450 million tons in 2019.<sup>121</sup> However, fossil-based plastics are linked to significant environmental issues, including CO<sub>2</sub> emissions and littering, contributing to widespread microplastic pollution. As the global population grows, the demand for plastic products is expected to increase, making the development of renewable alternatives even more critical.<sup>122</sup> Currently, bioplastics account for less than 1% of total plastic production,<sup>123</sup> highlighting the urgent need for innovative solutions to meet the demand for renewable materials and replace fossil-based plastics.<sup>124</sup>

Increasing environmental awareness is driving the adoption of greener, high-thermal-performance sustainable materials in the construction industry. Bio-based materials are becoming increasingly crucial for enhancing the energy efficiency of buildings, offering both environmental and economic benefits.<sup>125</sup> Using plant-based biomass materials in

construction can reduce fossil fuel demand, lower carbon dioxide emissions, and minimize the production of non-degradable waste.

PLA (polylactic acid), a versatile biopolymer derived from the renewable agricultural monomer 2-hydroxy propionic acid (lactic acid), is synthesized through the fermentation of starch-rich materials like sugar beets, sugarcane, and corn.<sup>126</sup> In addition to its natural biocompatibility, PLA is widely used in various fields, including 3D printing.<sup>127,128</sup> The global 3D printing market was valued at approximately USD 15.35 billion in 2024. It is projected to grow from USD 16.16 billion in 2025 to about USD 35.79 billion by 2030, with a compound annual growth rate (CAGR) of 17.2% between 2025 and 2030. This expansion is fueled by advances in additive manufacturing and increasing demand for customized products. Additionally, higher government investments worldwide and a broader selection of industrial-grade materials have further driven adoption. Sectors like healthcare, automotive, and consumer goods are adopting 3D printing for rapid prototyping and personalized manufacturing. These applications improve design flexibility, reduce waste, and shorten product development cycles.<sup>129</sup>

However, PLA has some limitations, such as brittleness, low heat resistance, high cost, and slow crystallization, which have restricted its broader adoption in commercial applications.<sup>130</sup> Furthermore, it is relatively expensive and produced from starch, which competes with the food supply chain. Lignin-based thermoplastic materials have garnered growing attention as sustainable, cost-effective, and biodegradable alternatives to petroleum-derived thermoplastics. Lignin is used without further modification as an antioxidant, UV stabilizer, or flame retardant.<sup>131–133</sup> However, due to its poor miscibility with polymer matrices, it can only be incorporated in small amounts.<sup>134,135</sup> Therefore, developing sustainable bio-additives for plastics possessing lower environmental impact and sustainability concerns is an approach worth further exploration.

## 2 Objectives of the Study

This study aims to develop a more sustainable protocol for the chloromethylation of organosolv lignin to produce chloromethylated lignin (CML), which acts as a versatile intermediate for various functional materials. The CML will undergo further modifications for different applications and will be tested for its performance.

The applications of functionalized lignin include:

- Functionalizing organosolv CML with 1-methylimidazole to stabilize Pd/CuO as a reusable organic catalyst. The resulting Lignin@Pd/CuO–NPs catalyst will be used to explore a range of C–C bond formation reactions, including Suzuki-Miyaura, Sonogashira, Heck, and azide-alkyne cycloaddition (click) reactions. The study will also investigate the reuse of the catalyst in batch reactions and its application in a packed-bed flow reactor.
- Designing a series of quaternary ammonium lignin (QALs) based on three different lignin sources: hardwood (aspen), softwood (pine), and grass (barley straw). The quaternary ammonium groups added to these CMLs will vary in single alkyl chain length, ranging from 6 to 18 carbons. The resulting QALs will be tested for their antibacterial activity against clinical isolates of *Methicillin-Resistant S. aureus* and *K. pneumoniae*.
- Synthesis of quaternary heteronium lignin (QHLs: QALs and QPLs) and its comparative study against ESKAPE. To produce electrospun nanofibers from active QHLs using cellulose acetate (CA) to evaluate their practical applications.
- Functionalizing CML by esterification and incorporating it into PLA as a high-performance filler for 3D printing. This addition aims to reduce the amount of PLA in the filament, thereby lowering the cost of the final material, while enhancing its thermal and mechanical properties.
- Systematic comparison of two distinct strategies for lignin modification: (i) direct esterification of hydroxyl groups with fatty acid chlorides, and (ii) a two-step process involving chloromethylation followed by reactions with aliphatic and aromatic carboxylic acids.

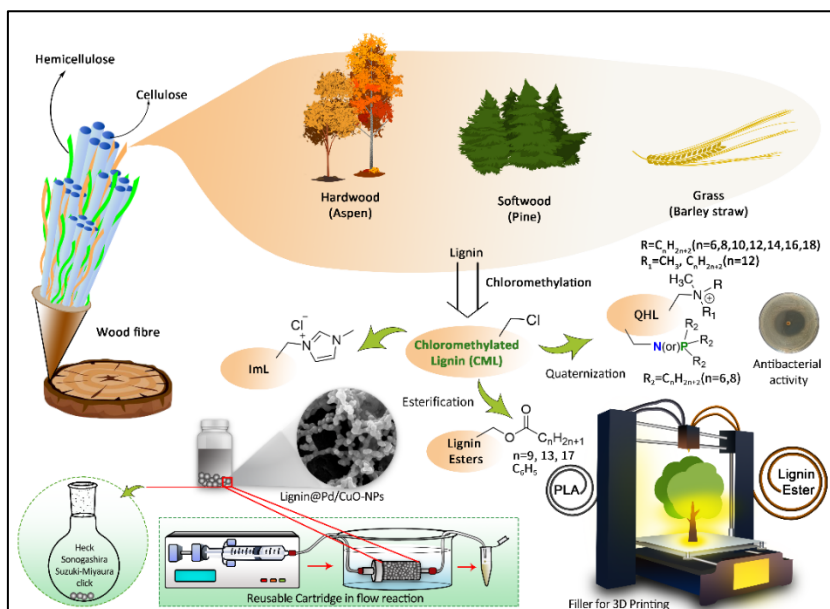


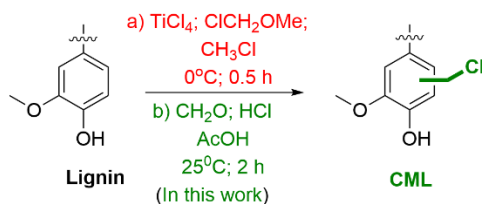
**Figure 5.** The overall visual representation of the study's objectives. Designed with Adobe Photoshop.

## 3 Results and Discussions

### 3.1 Chloromethylation of lignin (Publications I to IV)

In recent years, various chemical modifications have been introduced to incorporate active sites into lignin's complex structure,<sup>7</sup> though they have been explored less extensively than hydroxyl group modifications. These modifications include nitration,<sup>136</sup> amination,<sup>137</sup> alkylation/dealkylation,<sup>138</sup> hydroxylation,<sup>139</sup> carboxylation, and halogenation.<sup>140</sup> This study aims to incorporate the chloromethyl functional group into the aromatic structure of lignin through a chloromethylation step. To develop a more efficient chloromethylation protocol for lignin, two conditions (see Scheme 1) were studied, applied to organosolv aspen lignin. These reactions have been previously shown to be applicable to small aromatic molecules<sup>141,142</sup> and aromatic macrocycles like calix[4]arenes.<sup>143–145</sup>

Our study reveals that the route using methyl-chloromethyl-ether and  $\text{TiCl}_4$  as a Lewis acid catalyst in chloroform is not suitable for lignin (Blanc reaction), resulting in only 1.5% (m/m) of organic chlorine in the final product (see Scheme 1a). Moreover, this reaction needs to be performed with care, as it, like most chloromethylation reactions, produces highly carcinogenic bis(chloromethyl) ether as a by-product. In contrast, the reaction involving paraformaldehyde (PFA) and excess hydrogen chloride in acetic acid as solvent achieved a 7.7%-20% (m/m) yield of organic chlorine in the final product (see Scheme 1b). This newly developed greener route, as evaluated by green chemistry metrics, produces a significantly higher amount of chloromethylated lignin (CML).



**Scheme 1.** Two different strategies were used to explore the chloromethylation of lignin, as illustrated in the guaiacyl (G) unit of lignin.

In the  $^1\text{H}$  NMR spectra of the chloromethylated lignin (CML) product (see Figure 6a), a new peak appears at 4.5-4.75 ppm compared to organosolv lignin, indicating the presence of the  $-\text{CH}_2\text{-Cl}$  group on the benzene ring. Further confirmation was provided by 2D-HSQC measurement of hardwood, which provides a deeper understanding of lignin structure (e.g., inter-unit linkages, and subunits).<sup>146,147</sup> Two informative areas of oxygenated aliphatic side chain (C/H 100-35/6-2.5 ppm) and aromatic or unsaturated carbon (C/H 150-100/8.0-6.0 ppm) were focused for the 2D-HSQC interpretation. DMSO- $d_6$  solvent signal (C/H 39.51/2.5 ppm) was used to calibrate all spectra. Two distinct cross-peaks at C/H 37.97/4.8 and 40.61/4.63 ppm in Figure 7c, marked and an asterisk, confirm the introduction of reactive groups into aromatic rings in lignin compared to the starting material (see Figure 7a). Introduction of new functional groups could occur either orthogonally or metagonally, explaining the emergence of two distinct signals in the HSQC spectra, consistent with previous  $^1\text{H}$  NMR results. Lignin containing abundant methoxy groups, which contribute to the strong and stable cross-peaks at C/H 55.62/3.77 ppm before and after chemical modification. However, chloromethylated

lignin exhibits a significant decrease in ether linkage ( $\beta$ -O-4') peaks ( $A_{\beta(s)}$ : C/H 86.06/4.11). This can be due to the acidic-induced cleavage of lignin's labile bonds during the chloromethylation reaction, likely to depolymerize lignin into smaller fragments. Focusing on the aromatic region of HSQC spectra, prominent cross-peaks at C/H 104.30/6.60 and 118.5-110.11/6.90-6.76 ppm correspond to S and G units of hardwood lignin,<sup>148</sup> drastically decreases for chloromethylated lignin (see Figure 7d) compared to SM (see Figure 7b), confirming the chloromethylation on the aromatic ring. It is worth noting that chloromethylation can occur at any position of phenolic rings. Literature suggests that it may arise in the ortho-position adjacent to the hydroxy group,<sup>149</sup> and even at the meta-position of the syringyl unit of lignin, particularly in compounds like 3,5-dimethyl-4-hydroxyphenyl ethane.<sup>150</sup>

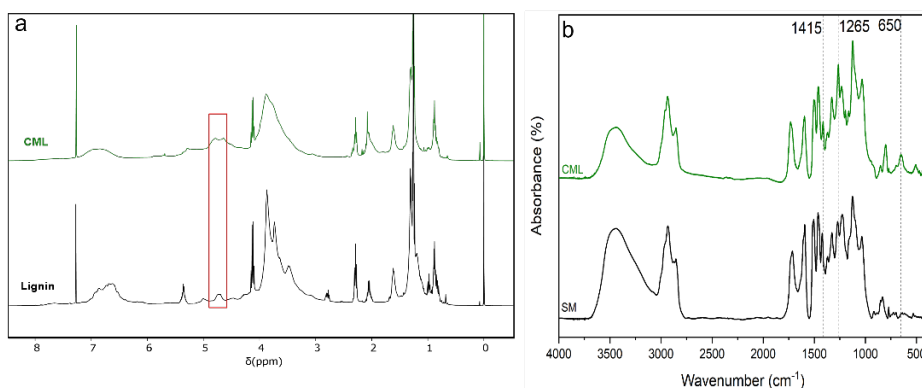


**Figure 6.** An example of  $^1\text{H}$  NMR (a) and FTIR (b) spectra of lignin and CML product.

Similarly, FTIR (see Figure 6b) confirmed characteristic peaks of  $-\text{CH}_2-\text{Cl}$  are observed at  $1264\text{--}1267\text{ cm}^{-1}$  and  $633\text{--}670\text{ cm}^{-1}$ . The peak around  $1413\text{--}1424\text{ cm}^{-1}$  can be attributed to aromatic ring vibrations or C-H deformation vibrations in the methylene ( $-\text{CH}_2-$ ) groups, which are already part of the lignin structure. However, the introduction of  $-\text{CH}_2-\text{Cl}$  groups may not result in a completely new peak but could instead lead to a subtle shift or increase in intensity, making them difficult to distinguish. In certain cases, minor shifts are observed, suggesting potential overlap of peaks. Considering the complexity of lignin structure, non-uniform chloromethylation or low concentration of  $-\text{CH}_2-\text{Cl}$  groups may result in only subtle changes in the FTIR spectrum. X-ray fluorescence (XRF) analysis shows that chloromethylated lignin contained 7.7 to 20 w/w% of chlorine.

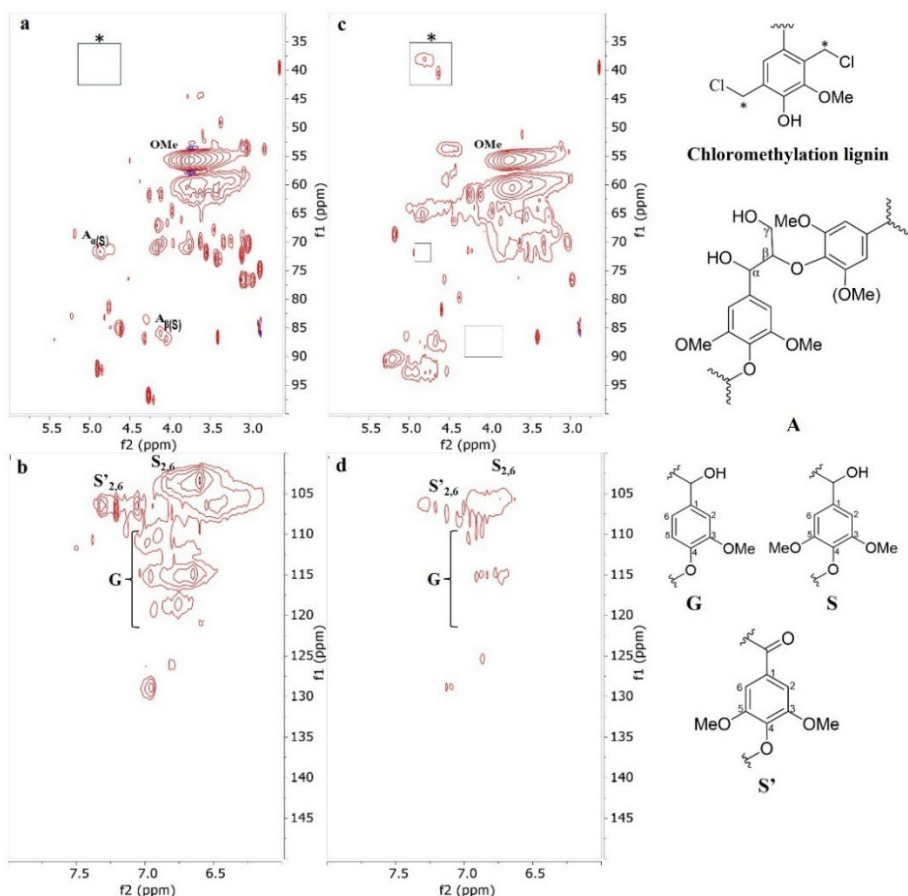


**Figure 7.** 2D-HSQC of lignin (a, b), chloromethylated lignin (c, d). Two regions of investigation: oxygenated aliphatic side chain (C/H 100–35/6.0–2.5 ppm) (top), aromatic/unsaturated region (C/H 150–100/8.0–6.0 ppm) (bottom). The lignin's subunits are presented on the right.

The size exclusion chromatography (SEC) results indicate that molecular changes occurred during the reaction process, resulting in the formation of heterogeneous lignin (see Figure 8). The elevated polydispersity index (PI) of chloromethylated lignin (CML) sample indicates a broader molecular weight distribution compared to the starting material.

A sharp peak at around 10 minutes corresponds to the exclusion limit of the SEC column, indicating the presence of a broad range of molecular weights condensed into a sharp peak. This suggests that some lignin crosslinking occurred during chloromethylation, possibly due to side reactions with formaldehyde. Additionally, potential side products or low-molecular-mass lignin fragments may have formed post-chloromethylation, as indicated by a significant peak at 16.5 minutes. Despite the similarity in molecular weights among different lignin types, our focus remains on utilizing the entire lignin material.

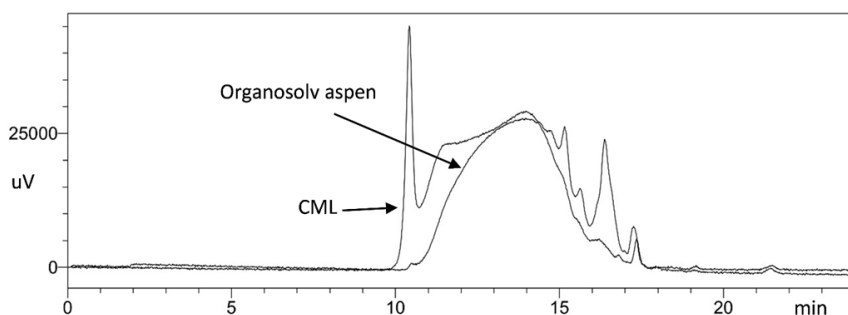


**Figure 8.** An example of size exclusion chromatography (SEC) curve of organosolv aspen lignin vs CML.

### 3.1.1 Green chemistry metrics for chloromethylation

Clark et al.'s CHEM21 toolkit<sup>151</sup> was used to evaluate the parameters listed in Table 2. For assessing the atom economy (AE) of reactions involving lignin, a polymer with an average molecular weight, the guaiacyl lignin monomer unit (G-unit) is considered as part of the green chemistry metrics to enhance our understanding. Method 1 (the CML protocol developed in this study) outperformed Method 2 (CML-TiCl<sub>4</sub>, a Blanc reaction procedure using a Lewis acid catalyst) in terms of yield, selectivity, atom economy, and overall efficiency. However, both methods can still improve in terms of conversion rates and reaction mass efficiency. Method 2, in particular, needs attention to reduce its environmental impact, especially concerning the use of solvents and reagents (red flag). In the proposed synthetic Method 1, more environmentally favorable solvents were used, resulting in better yields and a positive impact on overall green metrics, making it the greener choice. The reactions avoided using critical elements (with 5-50 years of supply remaining).<sup>69</sup>

**Table 2.** Green Chemistry metrics calculated for the processes studied.

Method No.	Method	Yield	Conversion	Selectivity	AE	RME	OE	PMI (total)	PMI Reaction solvents
1	CML	20	20	99.9	92.5	12.7	13.7	286.6	41.5
2	CML-TiCl <sub>4</sub>	1.2	1.5	78.9	61.7	0.8	1.2	7899.6	3973.3

The process mass intensity (PMI) parameters revealed that the major contribution to total PMI came from the PMI of reaction solvents, with Method 2 being significantly more unfavorable compared to Method 1. This analysis underscores the importance of addressing the choice of solvents as a critical issue in the synthetic process. Among the solvents used for reactions and workup, "recommended" solvents (green flag) such as water, ethanol (EtOH), and acetic acid (AcOH) were employed. It is worth noting that in this study, AcOH was considered "recommended or problematic," as stated in the CHEM21 toolkit. However, AcOH, along with some "intermediate" solvents, has been

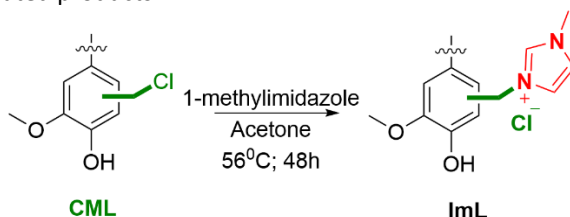
criticized for its unfavorable health score and is classified as "problematic" by default.<sup>152,153</sup> The energy parameters were marked with a green flag, as the reactions were conducted between 0 and 70°C.

The optimized protocol for CML preparation, which resulted in higher content of the chloromethylated product, was selected for scaling up and further transformation into functional materials. These transformations include the development of lignin-based N-heterocyclic carbene (NHC) complexes for cross-coupling reactions, quaternary heteronium lignin (QAL, QPL) for antibacterial applications, and fillers to PLA for 3D printing.

## 3.2 Lignin catalyst for cross-coupling reactions and click reactions (Publication I)

### 3.2.1 Preparation of Lignin@Pd/CuO-NPs

The chloromethylated lignin was further transformed into methyl imidazolium lignin (ImL) as illustrated in Scheme 2. The formation of ImL was confirmed through <sup>1</sup>HNMR and FTIR spectroscopy (Appendix I). Elemental analysis showed that the nitrogen content in the imidazolium lignin is 4.65%, compared to the starting chloromethylated lignin (CML), which contains only 0.01% nitrogen. It is important to note that some of the ImL-lignin may dissolve in the reaction solvent or be lost during the filtration process, which could contribute to discrepancies in nitrogen content. The reported nitrogen content only applies to isolated products.



**Scheme 2.** Schematic representation of ImL from CML.

The isolated products were further utilized as stabilizing agents for Pd and CuO to prepare heterogeneous Lignin@Pd/CuO nanoparticles (NPs) (see Experimental section). The SEM image of Lignin@Pd/CuO confirms that the Lignin@Pd/CuO nanoparticles (NPs) have an average size of 40 nm, as shown in Figure 9a. According to the SEM-EDX (Energy Dispersive X-ray analysis) results, the elemental composition of the catalyst includes 2.384% Pd (w/w) and 3.047% Cu (w/w) loaded onto the modified lignin, along with oxygen (O), nitrogen (N), and carbon (C).

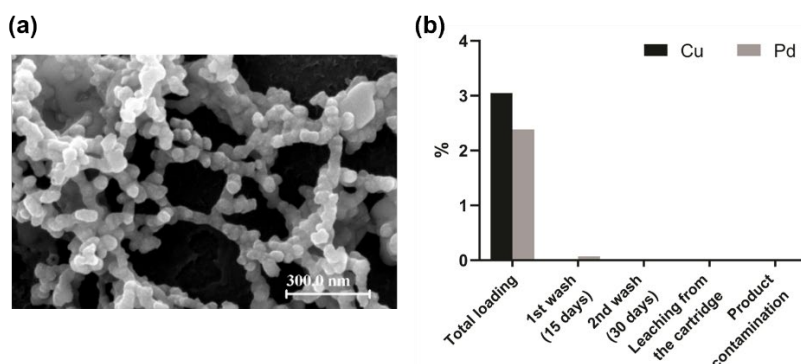


**Figure 9.** Characterization of Lignin@Pd/CuO-NP material. (a) SEM image; (b) Pd/Cu leaching determined by AAS.

An investigation was carried out to evaluate how much Pd and Cu leach into the solution and to determine their reusability. The concentration of Pd and Cu in the treated ethanol (w/w) serves as an indirect measure of the structural stability of the Lignin@Pd/CuO nanoparticles (NPs) under conventional batch reaction conditions. The test was carried out over 30 days with conventional mechanical stirring at 50°C. As shown in Figure 9b, after 15 days, only 0.015% of Cu and 0.0728% of Pd were detected in the solution. Upon completion of the 30 days, the leaching was found to be minimal of 0.011% for Cu and 0.012% for Pd, compared to the initial 3.047% Cu and 2.384% Pd present in the starting Lignin@Pd/CuO-NP material.

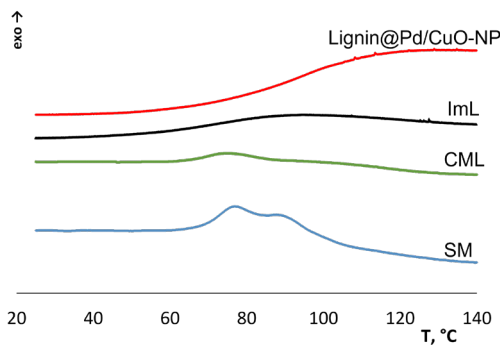


**Figure 10.** DSC curve for lignin derivatives.

The thermal properties (see Figure 10) of chloromethylated lignin (CML) are similar to those of the starting organosolv lignin, with both materials exhibiting a glass transition temperature ( $T_g$ ) around 70°C, which is typical for chemically modified lignin. The glass transition step in the DSC curves appears distorted, likely due to the material's heterogeneity (see Figure 10). Two enthalpy recovery peaks observed in the heating curve of organosolv lignin may be attributed to material aging upon heating. The slightly lower glass transition and onset temperatures for CML may be attributed to partial depolymerization of the lignin. The incorporation of 1-methylimidazole into CML appears to enhance hydrogen bonding in ImL, which is subsequently further stabilized by the embedding of metal, as evidenced by the pronounced glass transition peak for Lignin@Pd/CuONP, with the  $T_g$  increasing to 89.9°C.

### 3.2.2 Evaluation of the catalytic activity of Lignin@Pd/CuO-NPs in batch reaction and packed-bed flow reactor

The Suzuki-Miyaura coupling reaction is renowned for its effectiveness, versatility, and power in forming C-C bonds. Assessed the catalytic activity of Lignin@Pd/CuO-NPs for various reactions, including Suzuki-Miyaura, Sonogashira, Heck, and azide-alkyne cycloaddition (click) reactions. The catalyst demonstrated the highest activity for the click and Suzuki-Miyaura reactions, as shown in Figure 11a. Furthermore, its reusability was assessed by recovering the heterogeneous catalyst through simple filtration after each reaction, followed by washing, drying, and repeating the process up to 10 times. Notably, the catalytic efficiency remained consistent across all reactions for up to 10 cycles, with the catalyst being successfully recovered and reused after each run.

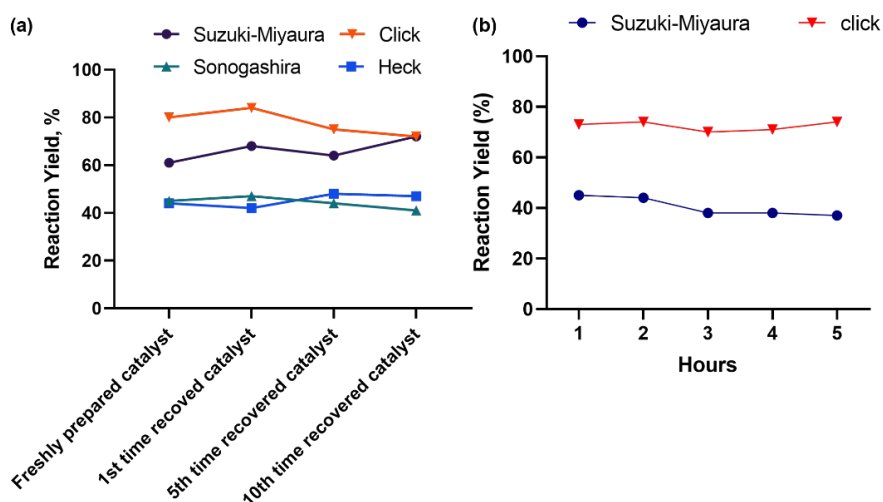


**Figure 11.** Yields for the studied reaction in batch (a) and continuous flow reaction (b).

Flow chemistry techniques have garnered significant attention for meeting the growing demand for chemical sustainability by reducing the use of reagents and materials, optimizing energy consumption, and enhancing process safety. Based on the batch reaction, the best-performing reactions, click and Suzuki-Miyaura reactions, were performed in continuous flow reaction (see Figure 11b). The experiment was conducted at 40°C, using 50 mg of supported catalyst, resulting in yields of up to 74% and 45%, respectively. The click reaction was then scaled up by preparing a larger volume of the reaction mixture and pumping it for 16 hours and 40 minutes under the same conditions, corresponding to a 5.0 mmol scale, yielding the product in 63% (0.74 g) isolated yield. While the click reaction proved to be very efficient under these conditions, the Suzuki-Miyaura reaction was slower and required longer reaction times, achieved using a lower flow rate and higher dilution.

### 3.2.3 Green chemistry metrics for catalytic reactions

The green chemistry metrics for the preparation of ImL, the azide-alkyne cycloaddition (click) reaction, and Suzuki-Miyaura cross-coupling reaction in both batch and continuous flow were studied (see Table 3). The preparation of ImL, click reaction, both in batch and continuous flow modes, and the Suzuki-Miyaura batch reaction are the most efficient

and environmentally friendly among the five methods studied. The flow-based Suzuki-Miyaura reaction shows moderate efficiency but could benefit from improvements in atom economy, waste reduction, and overall performance. Transitioning from batch to continuous flow reactions represents a significant step toward greener and more sustainable processes. These findings can guide the optimization of these chemical methods to improve sustainability and efficiency. Ultimately, choosing solvents and reagents should be carefully balanced to maximize yield while minimizing potential risks to safety, health, and the environment.

**Table 3.** Green Chemistry metrics calculated for the processes studied (1-5).

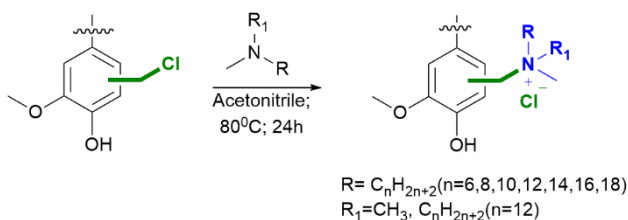
Method No.	1	2	3	4	5
Method	1mL (Acetone/ Me-THF)	Suzuki- Miyaura reaction (batch)	Suzuki- Miyaura reaction (flow)	Click reaction (batch)	Click reaction (flow)
Yield	99.8	65	43.8	76.8	73.8
Conversion	100	66	45	70	73.8
Selectivity	99.8	98.5	97.3	109.7	100
AE	100	57.7	57.7	100	100
RME	68	31.9	45	69	57
OE	67.9	55.3	78	69	57
PMI (total)	19.3	279.1	710.1	90.6	94.7
PMI Reaction solvents	11.5	239.1	704.0	89.2	92.7

### 3.3 Antibacterial quaternary ammonium lignin (Publication II)

In this study, the quaternization approach was used to create a series of quaternary ammonium lignin (QALs) derived from three distinct lignin sources: hardwood (aspen), softwood (pine), and grass (barley straw). Each source has unique monolignol compositions and different constituent units, which are expected to influence their antibacterial properties. The quaternary ammonium groups attached to these lignins had alkyl chains ranging from 6 to 18 carbons in length. The resulting QALs were evaluated for their physicochemical characteristics and antibacterial effectiveness against clinical isolates of *S. aureus* and *K. pneumoniae*.

#### 3.3.1 Preparation of QALs

Here, chloromethylation was employed, followed by quaternization of the chloromethylated sites (see Scheme 3). Previously, the successful integration of chloromethylation into aspen lignin (see Scheme 1) was demonstrated; the same methodology was applied in this study to aspen, barley, and pine lignin. Further quaternization was performed according to scheme 3, the resulting quaternary ammonium lignins (QALs) were named C6, C8, C10, C12, C14, C16, and C18 corresponding to the amines  $[C_6H_{13}N(CH_3)_2, C_8H_{17}N(CH_3)_2, C_{10}H_{21}N(CH_3)_2, C_{12}H_{25}N(CH_3)_2, C_{14}H_{29}N(CH_3)_2, C_{16}H_{33}N(CH_3)_2, \text{ and } C_{18}H_{37}N(CH_3)_2]$  respectively. Additionally, a modified CM lignin was synthesized using a ternary double n-alkyl chain amine,  $(C_{12}H_{25})_2N(CH_3)$ . This variant was designated as (C12)<sub>2</sub>.



**Scheme 3.** Schematic synthesis pathway of quaternary ammonium lignin, QALs from CML as shown for G unit of lignin.

The preparation of quaternary ammonium lignin from CML was confirmed using  $^1H$  NMR and FT-IR spectroscopy (see Figure 1, Appendix II). The FT-IR spectra of the QALs also retained most of the characteristic features of their starting material counterparts, indicating that the structural integrity of lignin remained largely unchanged during the modification process. Further evidence of successful tertiary amine incorporation is the presence of nitrogen in the lignin after quaternization (see Figure 12a). The nitrogen content in the quaternary ammonium lignins (QALs) ranged from 0.77% to 2.74%, varying based on the lignin source. Our findings suggest that the quaternization process is influenced by the solubility of lignin, which affects the accessibility of reactive chloromethyl sites to tertiary dimethyl amines, especially those with longer carbon chains. When comparing the nitrogen content of QALs with single (C12) and double (C12)<sub>2</sub> alkyl chains, the nitrogen content was consistently lower in the double-chain variants across all lignins, likely due to steric hindrance. Additionally, the nitrogen content reported is specifically for isolated products; some variation may also arise from the loss of dissolved lignin during the isolation process. As anticipated, the QALs displayed a positive surface charge, whereas the lignins without quaternary ammonium modification exhibited slightly negative, positive, or nearly neutral surface charges (see Figure 12b).

Since some of the lignin samples appeared aggregated, the hydrodynamic particle size of all lignin samples was analyzed to assess the stability of their suspensions (see Figure 12c). The measurements revealed that both chloromethylated (CML) and starting material (SM) lignin without quaternary ammonium groups aggregated significantly in 1.5% DMSO (the final environment for antibacterial testing). In contrast, the particle sizes of the QALs were significantly smaller. This indicates that the high positive surface charge of the QALs enabled better dispersion compared to the SM and CM lignin. There was no significant correlation found between the hydrodynamic diameter and the alkyl chain length of the QALs.

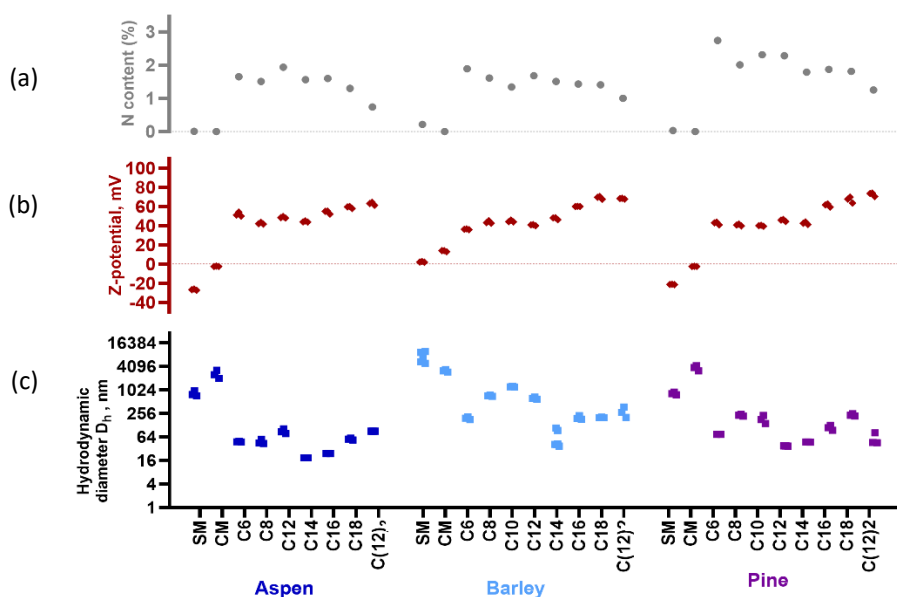


**Figure 12.** Properties of the lignin (SM) and QALs (a) N-content (%); (b)  $\zeta$ -potential (mV); (c) Hydrodynamic diameter (nm) of the lignin samples.

### 3.3.2 Antibacterial activity of lignin

The antibacterial properties of lignin and its derivatives were assessed by determining their bactericidal effect (measured as the minimal bactericidal concentration, MBC) in water, and their bacteriostatic effect (growth inhibition, indicated by the zone of inhibition, ZOI) in a semi-solid agar medium (see Figure 13). The maximum concentration of DMSO used was 1.5%. The study found that the maximum bactericidal effect of quaternary ammonium lignin (QALs), with an MBC of approximately 0.012 mg/L after 24 hours of exposure, was consistent across samples from different lignin sources (aspen, barley, pine) and against both tested bacterial strains (*K. pneumoniae* and *Methicillin-resistant S. aureus*). However, the bactericidal action speed of the QALs varied against these bacteria.

Based on the MBC values, non-quaternized lignin (SM, CML) from all sources was more effective against *S. aureus* than *K. pneumoniae* after 24 hours. Our findings support the general understanding that lignin exhibits greater antibacterial activity against Gram-positive bacteria compared to Gram-negative bacteria. Specifically, much lower concentrations of SM (8–15 times) and CM (2–4 times) were needed to kill *S. aureus* compared to *K. pneumoniae*. CML was typically 2 to 8 times more effective at killing bacteria than SM for both bacterial species. However, its ability to kill *S. aureus* did not significantly increase with quaternization. Furthermore, SM from all lignin sources exhibited either a more negative charge or a less positive charge compared to CML (see Figure 12). A reduction in negative charge or an increase in positive charge can decrease electrostatic repulsion or strengthen attraction to the bacterial cell surface, respectively. Additionally, the chloromethylation process itself might play a role in antibacterial activity. Previous literature indicates that chlorine-containing compounds tend to exhibit higher activity against Gram-positive bacteria than Gram-negative bacteria.<sup>154</sup>

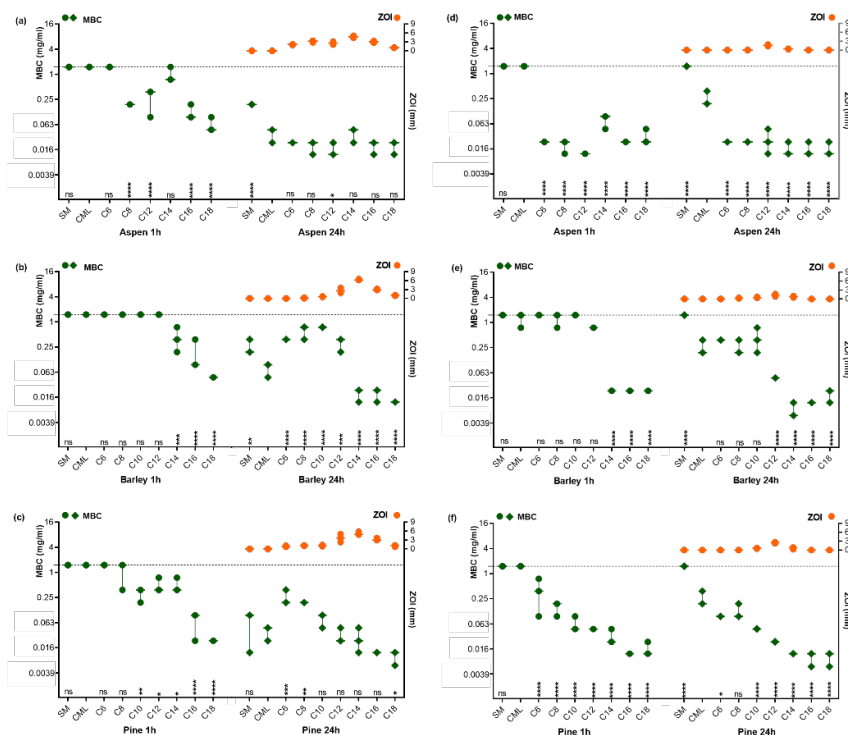


**Figure 13.** Minimal bactericidal concentration (MBC) of lignin samples against *S. aureus* (a-c). *K. pneumoniae* (d-f). MBC values for (a, d) aspen, (b, e) barley, and (c, f) pine after 1 h, and 24 h of exposure are plotted on the left Y-axis, and zone of inhibition (ZOI) values for 24 h incubation period on right Y-axis. The highest concentration (1.5 mg/ml) used in MBC assay is shown as a grey dotted line on the left Y-axis. The median and range of three biological replicates are shown. Statistically significant differences from control (CML) are presented above X-axis for each respective alkyl chain length (C), denoted by ns (not significant), \*\*\*\* ( $p \leq 0.0001$ ), \*\*\* ( $p \leq 0.001$ ), \*\* ( $p \leq 0.01$ ), and \* ( $p \leq 0.05$ )

The antimicrobial activity of QALs against *K. pneumoniae* was quicker than against *S. aureus* within the first hour of exposure, but the differences in MBC values became negligible after 24 hours (see Figure 13). QALs with longer alkyl chains (C14-C18) demonstrated more consistent antimicrobial effects across various bacterial species and plant sources, compared to those with shorter chains. The longest-chain QALs also showed the highest positive charge during exposure, likely enhancing electrostatic attraction to the negatively charged bacterial surfaces and improving their bactericidal efficiency. In contrast, QALs with shorter alkyl chains (C6-C12) were generally less effective, except for the rapid antimicrobial action of aspen-derived C6-C12 against *K. pneumoniae*.

Previous research generally indicates that quaternary ammonium compounds (QACs) with alkyl chain lengths from C8 to C18 provide optimal antibacterial activity, usually when chains contain more than 10 carbons. The effectiveness of this approach depends on the specific compound, exposure duration, and the type of bacterial cell wall. In contrast, QACs with alkyl chains shorter than C4 or longer than C18 are generally seen as nearly inactive. Our research showed that in MBC assays, QALs with the longest alkyl chains had the most potent bactericidal effects, and no clear shorter optimal chain length

was identified. Earlier research determining the best alkyl chain length for antibacterial effects mainly used growth inhibition tests on semi-solid (agar) media by measuring zones of inhibition (ZOI). In this assay utilizing QALs, the most pronounced bacteriostatic effect was observed at chain lengths of C12 to C14. Conversely, QALs with the longest alkyl chains did not exhibit growth inhibition. (see Figure 13). This suggests that the alkyl chain lengths that achieve maximum growth inhibition on agar (ZOI) are quite different from those effective in liquid environments (MBC). Specifically, the ZOI peaks sharply at C12 or C14, depending on the bacterial species, and then declines towards C18. Conversely, the MBC assay shows that bactericidal activity increases with longer alkyl chains, reaching a maximum at C16-C18. It is worth considering that the optimal lengths of the ZOI may be attributable to variations in hydrophobic aggregation and/or the restricted diffusion of longer-chain QALs within agar, rather than their intrinsic biological activity.

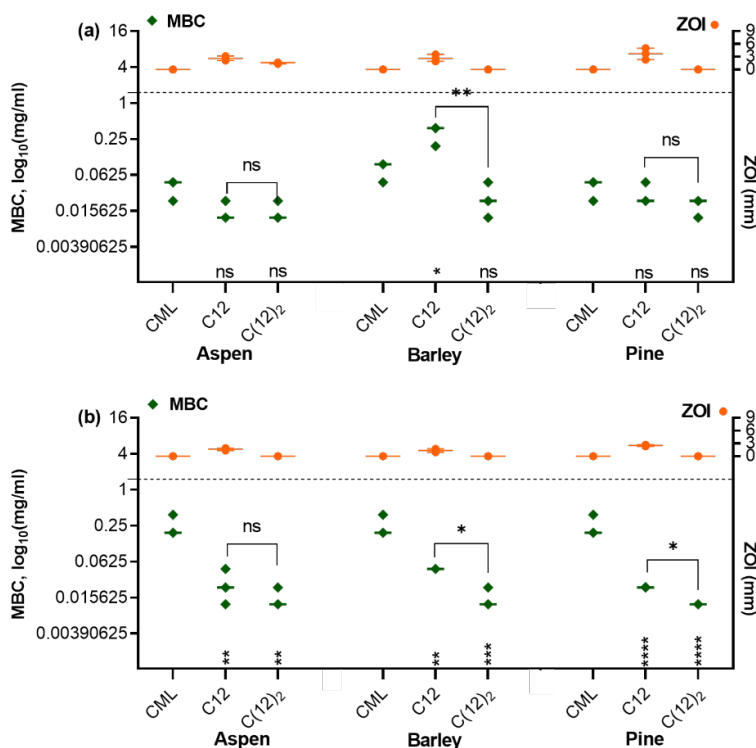


**Figure 14.** Minimal bactericidal concentration (MBC) of lignin samples modified with single and double alkyl chains, tested against (a) *S. aureus* and (b) *K. pneumoniae*. MBC values for aspen, barley and pine after 24 h of exposure are plotted on the left Y-axis, and zone of inhibition (ZOI) values for 24 h of incubation period on right Y-axis. CML - chloromethylated lignin, C12, C(12)<sub>2</sub> - quaternary ammonium lignins, QAL. The highest concentration (1.5 mg/ml) used in MBC assay is shown as a grey dotted line on the left Y-axis. Statistical significance of differences ( $p < 0.05$ ) of MBC values from the CM is presented under each respective alkyl chain length, and between the single and double chains are marked above (ns(non-significant), \*\*\*\* ( $p \leq 0.0001$ ), \*\*\* ( $p \leq 0.001$ ), \*\* ( $p \leq 0.01$ ) and \* ( $p < 0.05$ )).

Modifying QALs by replacing a single C12 alkyl chain with a double C(12)<sub>2</sub> chain resulted in inconsistent changes in antibacterial activity (see Figure 14). Compared to the single C12 chain, the MBC value of the double chain decreased for *K. pneumoniae* in barley and pine lignin, but for *S. aureus*, this decrease was only seen with barley lignin. In the case of aspen lignin, the MBC values for both bacteria were similar, whether the QAL had a single C12 or a double C(12)<sub>2</sub> chain. These variations in MBC values between single and double-alkyl chain QALs may partly result from the significant reduction in nitrogen content in the double-chain QALs compared to their single-chain versions. This suggests that the double alkyl chain modification was less effective, resulting in fewer antibacterial components at the same QAL concentration.

Although the ZOI consistently decreased for double chains compared to single chains, the MBC for double chains either remained unchanged or decreased. These differences highlight that inhibition zones should only be compared when the tested substances diffuse equally in the water-based environment of the semisolid agar medium. Our results indicate that evaluating bacteriostatic properties based on ZOI for QALs with longer or double alkyl chains—a hydrophobic group—can be misleadingly underestimated in diffusion-limited testing formats.

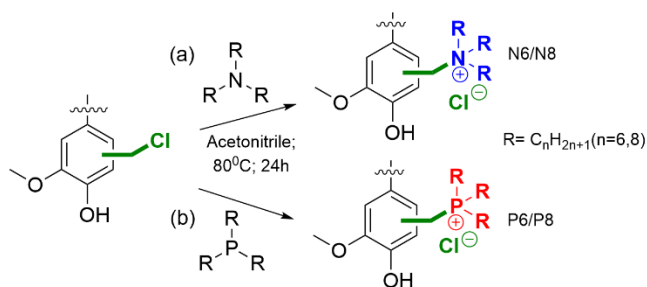
Furthermore, prepared and compared lignin-based trialkyl quaternary ammonium (QAL) and quaternary phosphonium (QPL) compounds against the ESKAPE pathogens (*Enterococcus faecium*, *Staphylococcus aureus*, *Klebsiella pneumoniae*, *Acinetobacter baumannii*, *Pseudomonas aeruginosa*, and *Enterobacter species*), which are the leading cause of nosocomial infections worldwide.

### **3.4 Antibacterial properties of quaternary phosphonium vs ammonium lignin (Publication V)**

In this study, a novel lignin-based phosphonium compound was developed to assess the molecular diversity of quaternary heteronium lignin compounds (QHLs) utilizing our prior data. The efficacy of both quaternary ammonium lignins (QALs) and quaternary phosphonium lignins (QPLs) was evaluated through growth inhibition assays and determination of minimum bactericidal concentrations (MBCs) and zone of inhibition (ZOI) against laboratory and multi-resistant strains of ESKAPE pathogens. Further development of electrospun nanostructures of the highest performing QHL with cellulose acetate has been conducted, alongside an assessment of their antibacterial properties in a real-world scenario.

#### **3.4.1 Preparation of QHLs**

In this investigation, chloromethylated pine lignin was additionally quaternized utilizing tertiary amines and phosphines in accordance with Scheme 4. The resulting quaternary heteronium lignins (QHLs) were named N6, N8, P6, and P8, corresponding to the amines [trihexylamine and trioctylamine], and phosphines [trihexylphosphine and trioctylphosphine], respectively.



**Scheme 4.** Schematic synthesis pathway of quaternary ammonium (QALs) and phosphonium (QPLs) lignin, from CM, as shown for the G unit of lignin.

FT-IR spectroscopy confirmed the preparation of quaternary ammonium lignin from CML (see Figure 15). Characteristic peaks at 643 cm<sup>-1</sup> and 1262 cm<sup>-1</sup> indicate -CH<sub>2</sub>-Cl groups in CM lignin. The absorption band of -(CH<sub>2</sub>)- groups appears at 723 cm<sup>-1</sup>, while bands for CH<sub>3</sub> and CH<sub>2</sub> are observed at 2953 cm<sup>-1</sup> and 1464 cm<sup>-1</sup> in QHLs. The <sup>1</sup>H NMR spectrum shows strong peaks at δ 0.88 and δ 1.25 ppm, confirming the presence of CH<sub>3</sub> and CH<sub>2</sub> groups that make up the hydrophobic tails of the alkyl chains in both QALs and QPLs. Additionally, <sup>31</sup>P NMR analysis reveals a peak at δ 33.38 for P6 and P8, confirming the presence of a quaternary phosphonium group in the lignin structure. Additionally, CHN analysis revealed that all modified QHLs have increased C and H% compared to the CM lignin, and N% was observed only in the QAL samples (see Table 4).

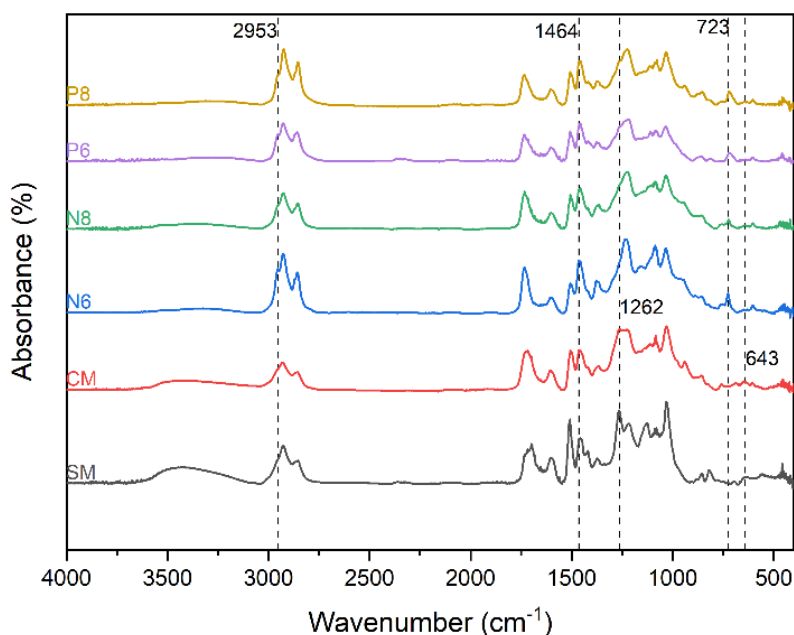


**Figure 15.** FTIR spectra of starting materials (SM), chloromethylated lignin (CM), and quaternary ammonium (N6, N8) and phosphonium lignin (P6, P8).

**Table 4.** CHN content (%) of the QHL samples.

	N%, average	C%, average	H%, average
CM	0	62.08	6.595
P6	0.055	65.08	8.435
P8	0	66.89	8.855
N6	1.2	67.235	8.245
N8	0.675	65.065	7.4

### 3.4.2 Antibacterial activity of QHLs

Here, lignin SM was considered a negative control, and C18 from our previous set of experiments (see Figure 13) was a positive control (PC). The antibacterial activity of QHLs was tested against both Gram-positive (*E. faecium*, *S. aureus*) and Gram-negative (*K. pneumoniae*, *A. baumannii*, *P. aeruginosa*, *E. cloacae*) pathogens (ESKAPE) at 1h and 24h post-treatment (see Figure 16). The minimal bactericidal concentration (MBC) values indicate a time-specific response to the tested samples.

MBC against *E. faecium* (see Figure 16a): both sample groups showed moderate inhibition after 1h and 24h. Compounds P6 and P8 demonstrated a strong effect comparable to the starting material (SM), while N6 and N8 showed moderate activity. By 24 hours, P6 exhibited the most significant increase, suggesting a strong time-dependent killing effect. P8 showed slight improvements. The lignin SM did not inhibit growth. Similar results appeared with *S. aureus* (see Figure 16b): initial inhibition at 1h was limited, but most samples became more effective after 24h, especially P6 and P8 compared to PC. N6 and N8 did not significantly reduce the MBC. The SM remained inactive, consistent with earlier observations. These findings demonstrate that P6 has significant time-dependent killing activity against gram-positive bacteria and is the most effective among the tested compounds against *S. aureus* and *E. faecium*. Meanwhile, P8 also shows promise as a moderately active agent.

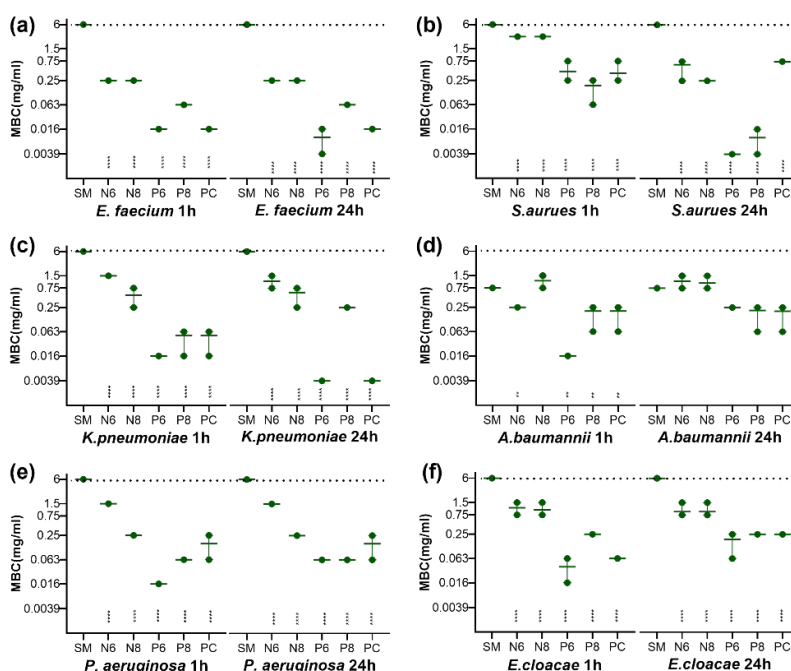


**Figure 16.** Minimal bactericidal concentration (MBC) of lignin samples (QHLs) against ESKAPE after 1 h, and 24 h of exposure are plotted. The highest concentration (6 mg/ml) used in MBC assay. Statistically significant differences from control (SM) are presented above X-axis for each respective modification denoted by ns (non significant), \*\*\*\* ( $p \leq 0.0001$ ), \*\*\* ( $p \leq 0.001$ ), \*\* ( $p \leq 0.01$ ), and \* ( $p \leq 0.05$ ).

The gram-negative strains responded differently. For *K. pneumoniae* (see Figure 16c), the bactericidal effectiveness of the tested compounds varied notably over time. At 1 hour, compounds P6, P8, and PC showed significant activity, while N6 and N8 had moderate effects, and SM remained inactive. By 24 hours, P6's potency increased, with its MBC dropping to 0.0039 mg/mL, demonstrating strong time-dependent activity. Similarly, PC's efficacy improved considerably, also reaching an MBC of 0.0039 mg/mL, indicating highly potent bactericidal action. N6 and N8 showed moderate improvements in efficacy.

*A. baumannii* (see Figure 16d), *P. aeruginosa* (see Figure 16e), and *E. cloacae* (see Figure 16f) showed a complex antibacterial response profile, highlighting notable differences in compound efficacy over time. At the 1h time point, compounds P6, P8, and PC exhibited the most prominent bactericidal effects. These results indicate that all three compounds possess rapid antimicrobial activity against these bacteria. However, after 24 hours, the MBC of P6 increases, suggesting a reduction in potency over prolonged exposure, potentially due to the activation of bacterial resistance mechanisms such as efflux systems or biofilm formation. In contrast, P8 and PC maintained a very similar MBC at their 1h time point, indicating bacteriostatic activity. These findings highlight P8 have near-identical activity compared to the PC, whereas P6 retains the highest activity for 1h incubation, even though some reduction in efficacy over time was observed. Compounds N6 and N8 demonstrated more modest or delayed activity, with some improvements at

24 hours, indicating potential for further optimization or use in combination therapy. SM, by contrast, remained largely inactive against all tested organisms at both time points, suggesting limited bactericidal potential.

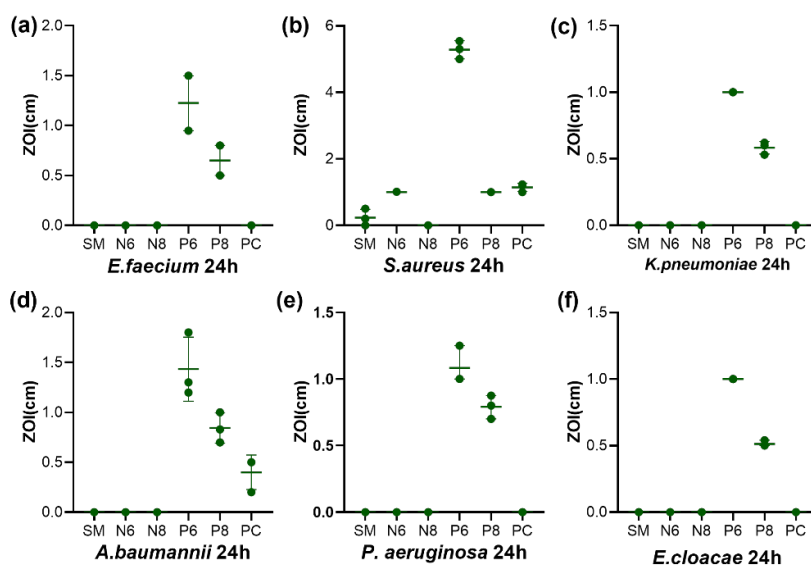


**Figure 17.** Zone of inhibition (ZOI) of lignin samples (QHLs) against ESKAPE after 24 h of incubation is plotted. The median and range of three biological replicates are shown.

ZOI test (see Figure 17) reveals that across all six tested bacterial strains—*Staphylococcus aureus*, *Enterococcus faecium*, *Klebsiella pneumoniae*, *Acinetobacter baumannii*, *Enterobacter cloacae*, and *Pseudomonas aeruginosa*—compound P6 consistently demonstrated the strongest and broadest antibacterial activity. It produced clear and measurable zones of inhibition against every strain tested, indicating potent efficacy against both Gram-positive and Gram-negative bacteria, and highlighting its potential as a lead compound for further antimicrobial development. Compound P8 showed moderate activity against five of the six strains, with particularly consistent inhibition of Gram-negative species, though its overall potency was lower than that of P6. PC exhibited only limited antibacterial effects, with weak inhibition observed against *S. aureus* and *A. baumannii*, and no activity against the other tested bacteria. In contrast, compounds N6 and N8, as well as SM, showed no detectable antibacterial activity against any of the tested strains, suggesting a lack of intrinsic antimicrobial properties under the conditions used. Overall, P6 emerges as the most promising candidate because of its consistent and high activity against a broad range of clinically relevant pathogens. Additionally, this lignin-based material can be further utilized in the development of effective bactericidal products. Here, the development of electrospun nanostructures of the top-performing QHL (P6) using cellulose acetate has been carried out.

### 3.4.3 Morphology of CA–Lignin electrospun nanofibres

Electrospinning has been widely employed as a versatile and efficient technique in the fabrication of micro- and nanofibers. Compared to traditional spun fibers, electrospun

fibers can possess significantly smaller diameters at the nanometric scale, thereby offering a high surface area with a porous structure.<sup>155</sup> These nanofibers, characterized by their extensive surface area, have demonstrated potential for use in various applications, including healthcare, biotechnology, environmental engineering, and energy storage.<sup>156,157</sup> Cellulose, the most abundant natural polymer on Earth, is renewable, cost-effective, and readily accessible, making it highly appealing for use in biomedical, food packaging, and pharmaceutical sectors.<sup>158–160</sup> Cellulose acetate, a derivative of cellulose, has garnered significant interest owing to its biocompatibility, biodegradability, non-toxicity, and cost-effectiveness.<sup>161</sup> It exhibits substantial potential for electrospinning, as it can be readily fashioned into fibers or thin film materials.

Figure 18 shows SEM images of pure cellulose acetate (CA) electrospun nanofibers and CA-lignin derivative nanofibers. The pure CA fibers are free of beads, thicker, and more uniform than the others (see Figure 18b). Conversely, CA-lignin fibers exhibit minor structural changes, including the presence of beads and thinner fibers (see Figure 18c). This may result from lignin's complex, irregular structure, its lower molecular weight, and reduced chain entanglement compared to cellulose acetate at this concentration. Such disruption can promote bead formation, especially at higher lignin levels, like 10%.

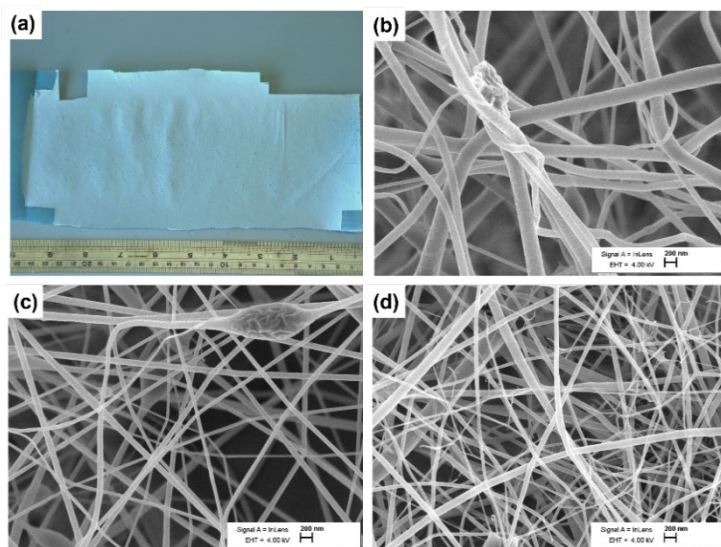


**Figure 18.** Electrospun nanofibers deposited on non-woven fabric (a), along with SEM images of pure CA nanofibers (b), CA containing 10% unmodified lignin (c), and P6 (d).

When cellulose acetate is mixed with lignin modified by quaternary phosphonium salt—particularly at 10% concentration—fiber thinning and breakage are observed, as shown in Figure 18d. This is believed to result from the ionic properties of quaternary phosphonium salts. Their addition increases electrical conductivity, promoting greater stretching of the electrospinning jet. However, this can cause the fibers to thin excessively, destabilizing the jet and often leading to fiber breakage or a spray of discontinuous fibers.

### 3.4.4 Wettability test

The graph shows how contact angle changes with aging time during a wettability test (see Figure 19). In all three samples, the contact angle decreases consistently as aging

time increases. This pattern indicates that the surface becomes more hydrophilic over time, demonstrating improved wettability as it ages. The steady decrease also suggests that the measurements are consistent and reliable across multiple tests. Both cellulose acetate (CA, without lignin) and P6 display similar trends, starting from about 18° and dropping to around 6.8° at 3.5 seconds. In contrast, SM (cellulose acetate with 10% unmodified lignin) reaches a maximum contact angle of approximately 31.5°, then decreases to about 20.5°. This may be due to the hydrophobic properties of organosolv lignin. Conversely, the combination of quaternary phosphonium lignin and CA behaves similarly to cellulose acetate, likely because the increased polarity from the quaternary groups makes the surface more hydrophilic. Overall, the data support the trend of increasing surface hydrophilicity over time, with most contact angles below 30°, indicating very hydrophilic surfaces.

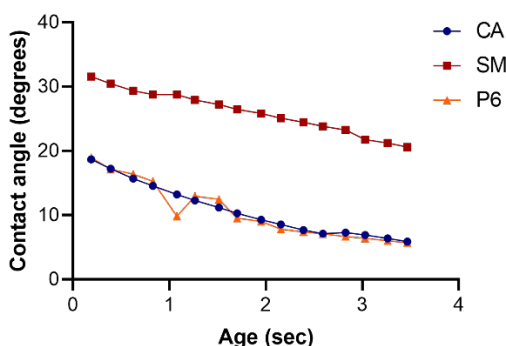


**Figure 19.** Changes in contact angle over time for cellulose acetate (CA-10%), cellulose acetate with 10% unmodified lignin (SM), and cellulose acetate with 10% P6 lignin (P6).

### 3.4.5 Biofilm formation

Microorganisms often adhere to various surfaces, including medical equipment and food packaging, resulting in the formation of biofilms that facilitate multiplication, growth, maturation, and dispersion.<sup>161,162</sup> Consequently, issues such as bio-corrosion and bio-fouling occur, presenting significant risks to human health and the ecological environment. To address these challenges, the integration of antibacterial agents into materials has become a standard strategy to inhibit microorganisms and reduce the aforementioned problems.

Anti-biofilm assessments of CA-Lignin electrospun nanofibers were conducted on two microbial species: the Gram-positive *S. aureus* and the Gram-negative *K. pneumoniae*. These microorganisms are among the most extensively studied model organisms for examining pathogenicity, resistance, the development of infectious processes, and biofilm formation. It was observed that P6 demonstrated a significant anti-biofilm effect against both bacteria compared to SM, as shown in Figure 20. A reduction factor of 1.7 colony-forming units per milliliter (CFU/ml) was noted for *S. aureus*, and a reduction factor of 2 colony-forming units per milliliter (CFU/ml) was observed for *K. pneumoniae*.

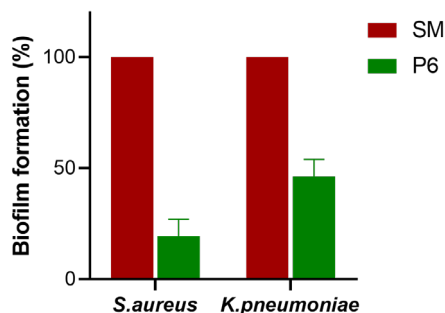


**Figure 20.** CFU/ml values were obtained following the assessment of viable counts of *S. aureus* and *K. pneumoniae* microbial cells derived from biofilms cultivated for 24 hours.

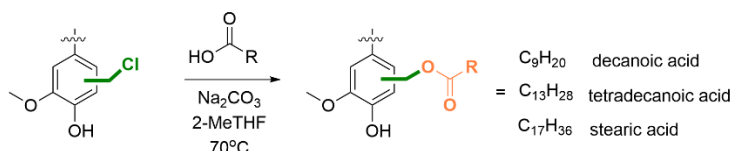
This indicates that cellulose acetate nanofibers with P6 exhibit superior antimicrobial properties, making them a promising candidate for applications that require effective bacterial suppression. Further research is recommended to augment antibacterial efficacy and expand the range of activity.

### 3.5 Lignin Esters as Advanced Filler to PLA for 3D Printing (Publication III)

This study explores incorporating organosolv pine lignin, chemically modified through a greener chloromethylation method followed by esterification, into PLA as a high-performance filler. This approach aims to reduce the amount of PLA needed in filament production, lowering costs while also improving thermal and mechanical properties. Since unmodified lignin alone does not enhance thermal performance, a straightforward two-step esterification was performed using decanoic, tetradecanoic, and stearic acids. This process was designed to chemically modify lignin from chloromethylated lignin while keeping its hydroxyl groups intact. Further preparations involved creating various lignin/PLA composites through solvent casting. The long-chain fatty acid esters on lignin's surface are anticipated to enhance adhesion to the PLA matrix during processing. Additionally, the unmodified hydroxyl groups on lignin are presumed to augment intermolecular forces, interchain attraction, and cohesion, thereby increasing the glass transition temperature ( $T_g$ ) by reducing molecular mobility.

#### 3.5.1 Characterization and thermal properties of esterified lignin and PLA composite

The success of the esterification reaction (see Scheme 5) was confirmed through  $^1\text{H}$  NMR and FTIR analyses (see Appendix III). The PLA/lignin composite spectra displayed similar bands to those of pure PLA, as shown in Figure 21. In addition, biocomposites containing lignin exhibited a small peak at  $1510\text{ cm}^{-1}$ , attributed to C=C groups in aromatic rings, and at  $2885\text{ cm}^{-1}$  from  $\text{CH}_2$  stretching modes in the methyl and methylene groups of the ester side chain. Differential Scanning Calorimetry (DSC) is widely recognized as a reliable method for determining the glass transition temperature ( $T_g$ ) of lignin polymer. This thermal parameter is crucial for understanding the potential of lignin in polymer applications and for processing it, using current industrial techniques such as hot pressing.



**Scheme 5.** Schematic synthesis pathway of lignin esterification from CML as shown for G unit of lignin.

Initial studies on lignin modification with fatty acids revealed that esterified lignin exhibited novel properties, including changes in solubility and thermal behavior.<sup>163</sup> Subsequent research observed a consistent decrease in  $T_g$  with larger ester substituents,<sup>164</sup> with longer chains causing a more significant reduction in  $T_g$ . However, determining the  $T_g$  of lignin is challenging due to its complex chemistry and broad molecular weight distributions, which result in a wide temperature range for this transition.<sup>165</sup> Previous research has discussed the thermoplasticity of lignin,<sup>166</sup> indicating that lignin molecules have a thermal softening point,<sup>167</sup> typically occurring at high temperatures between 90°C and 180°C for non-derivatized lignins.<sup>168</sup> In this study, the  $T_g$  values for isolated pine lignins were determined to be 111°C, while PLA had a  $T_g$  of 68°C.

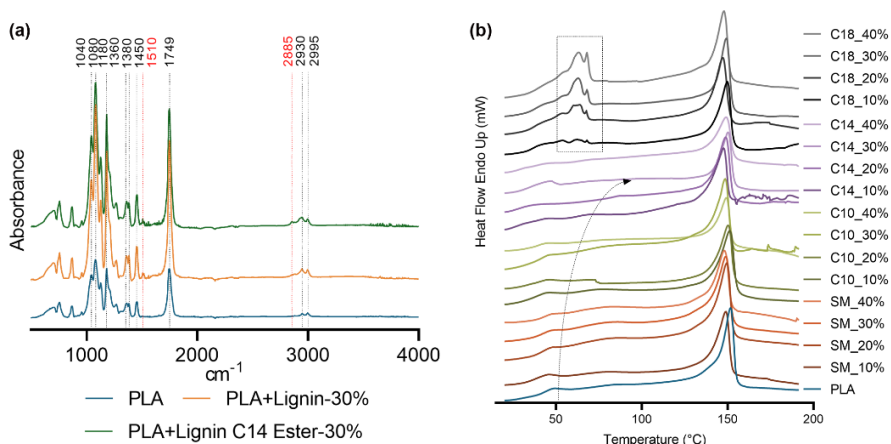


**Figure 21.** FT-IR spectra of PLA/Lignin blends(a), and DSC graph for all prepared blends(b)

Interestingly, PLA combined with lignin-ester derivatives showed significant changes in thermal properties. The lignin esters examined showed good compatibility with PLA. The most common esterification on phenol hydroxy groups on lignin reduces hydrogen bonding and increases molecular free volume. Consequently, this enhances chain mobility and lowers the  $T_g$  of esterified lignin. However, according to our scheme 4, the unmodified OH groups are expected to enhance the intermolecular forces and interchain attraction, consequently raising  $T_g$  by reducing mobility. Figures 21b and 22 present the thermograms for all PLA-lignin-ester derivatives. Unmodified lignin samples and lignin esters with decanoic acid (C10) did not improve  $T_g$ . However, lignin esters with tetradecanoic acid (C14) at a 30% concentration achieved the highest  $T_g$  of 72.12°C, which decreased with further incorporation. The glass transition step in the DSC curves was distorted in the case of stearic acid (C18), likely due to material heterogeneity (see Figure 21b). These results reveal that the optimal chain length and concentration are crucial for the maximum compatibility. Based on the results, PLA + Lignin C14 ester at 30% was selected as the best candidate for further application.

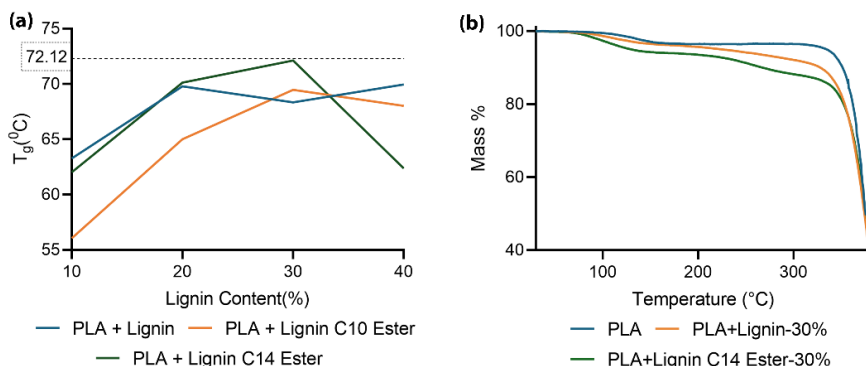


**Figure 22.** Glass transition temperature for PLA/Lignin blends(a) and TGA plot of PLA and PLA/Lignin composites obtained under nitrogen atmosphere at 20°C/min heating rate(b).

The thermogravimetry (TG) curves, which depict the percentage of weight loss in PLA/lignin blends, are presented in Figure 22b. These curves were recorded at a heating rate of 20 °C/min under a nitrogen atmosphere. The thermal degradation data reveal the rate of weight loss, allowing for a comparison of the thermal stability of different lignin materials. As shown in Figure 22b, thermal decomposition occurs in two distinct temperature ranges, starting at approximately 80°C and 245°C. The weight loss observed at 80°C is attributed to the evaporation of moisture and chemically bound water.<sup>169</sup> The major decomposition, which begins at 245°C, marks the onset of thermal degradation, with further breakdown occurring at higher temperatures. This suggests that the PLA/lignin blends maintain thermal stability between 210°C and 230°C, making them well-suited for 3D printing applications.

### 3.5.2 Mechanical testing of esterified lignin PLA composite and 3D printing capabilities

The tensile test results of PLA/lignin solvent-cast films (see Figures 23 and 24(a-c)) indicate that adding lignin to PLA impacts its mechanical properties. The Young's modulus of the PLA/lignin films (see Figure 24a) varies depending on the type of lignin used, with lignin generally reducing the stiffness of the PLA matrix, resulting in lower values compared to pure PLA. The PLA + Lignin C14-30% blend exhibited the lowest modulus, signifying a significant decrease in stiffness. Interestingly, this blend also showed the highest tensile stress at maximum load compared to both neat PLA and PLA + Lignin-30% (see Figure 24b), suggesting that lignin ester can act as a reinforcing filler in the polymer matrix under stress. However, the tensile extension at maximum load for this blend was moderate to slightly lower than neat PLA but higher than PLA + Lignin-30% (see Figure 24c), indicating that the modified lignin contributes to increased flexibility. These findings suggest that while incorporating lignin into PLA through solvent casting reduces stiffness, this effect is most pronounced with the Lignin C14 ester.

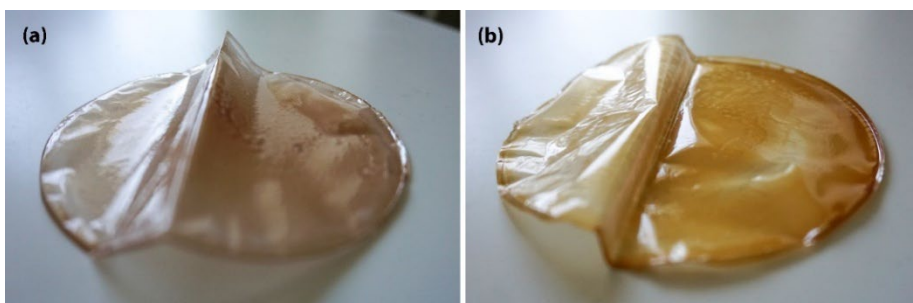


**Figure 23.** PLA + Lignin-30% film (a) and PLA + Lignin C14 Ester-30% film (b)

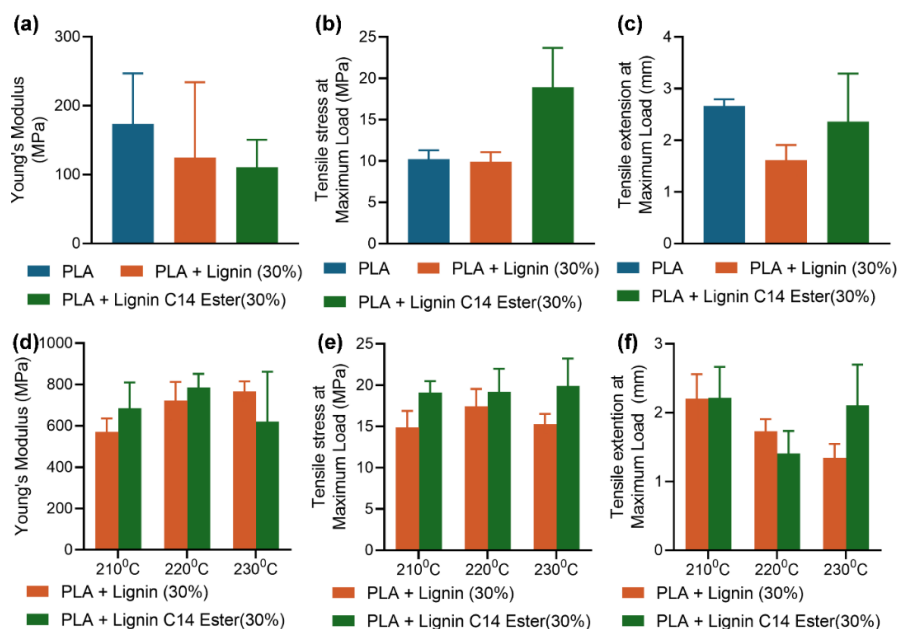


**Figure 24.** (a)(d) Young's modulus, (b)(e) stress at maximum load, (c)(f) tensile extension at maximum load of PLA/lignin film (a, b, c), and PLA/lignin extruded filament (d, e, f).

Extruded filaments produced at various temperatures and compositions exhibit distinct mechanical properties (see Figure 24(d-f), Figure 25). At different temperatures, filaments containing unmodified lignin and lignin C14 ester exhibited variations in tensile stress, tensile extension, and Young's modulus. Compared to unmodified lignin filaments, specimens with lignin C14 ester exhibit significantly higher tensile stress at maximum load. The improvement is consistent across all temperatures (see Figure 24e). Despite the fact that tensile extension decreases with increasing temperature, filaments containing lignin C14 ester tend to exhibit greater extension at higher temperatures (see Figure 24f). The blending process and lignin content significantly affect stiffness, as indicated by Young's modulus data. Figure 24d shows that modulus increases with processing temperature, peaking at 230°C for native lignin and 220°C for lignin C14 ester samples.

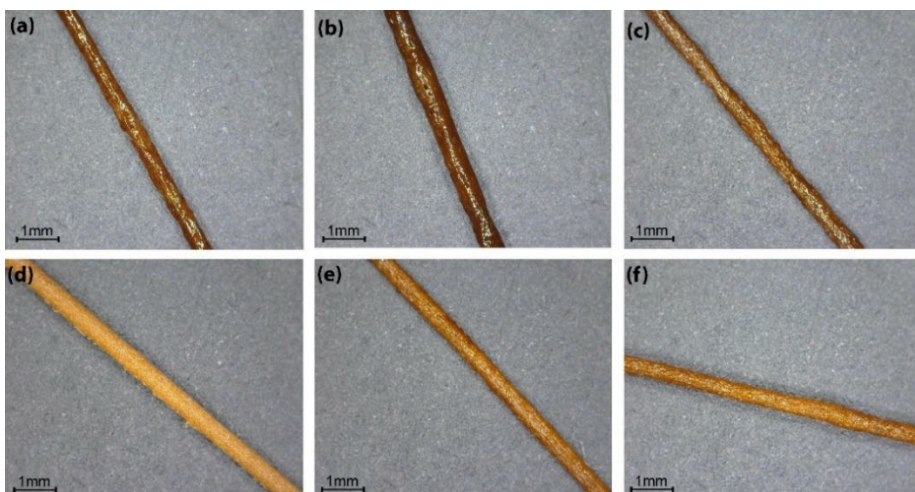


**Figure 25.** Individual filaments extruded from 0.4 mm nozzle at 210°C (a, d), 220°C (b, e), 230°C (c, f) for PLA+ Lignin-30% (a-c), and PLA + Lignin C14 Ester-30% (d-f)

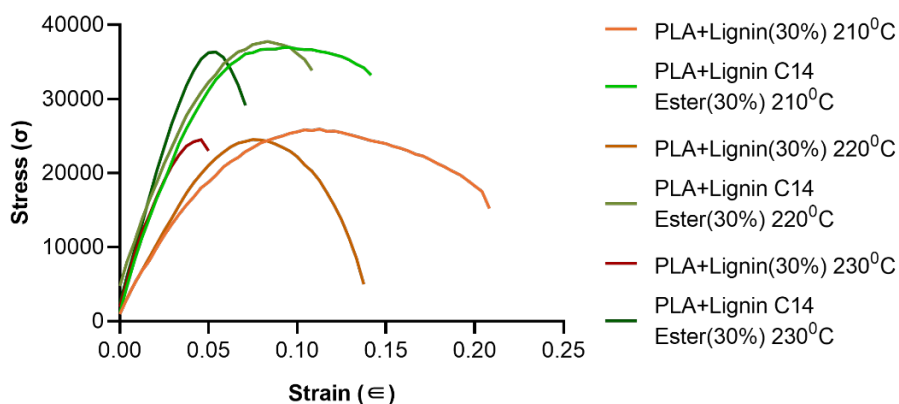


**Figure 26.** Stress-Strain curve for PLA/lignin filaments.

Furthermore, the stress-strain curve indicates that PLA + lignin (30%) at 210°C exhibits moderate tensile strength and a reasonable level of strain before fracture (see Figure 26). This indicates reasonable flexibility but relatively lower strength compared to others. Among the tested samples, PLA blended with 30% lignin C14 ester demonstrates the highest strength and strain capacity, exhibiting a superior ability to endure stress and deformation before breaking, and thus becomes the strongest and most flexible material in the dataset. In contrast, filament processed at 230°C exhibits reduced tensile strength and a shorter strain range, indicating that the material has become more brittle and has a greater tendency to break more readily under stress, which is true for both modified and unmodified lignin.

In conclusion, incorporating lignin into PLA significantly impacts the mechanical properties of both films and extruded filaments, with our study demonstrating enhanced mechanical performance in composites with higher lignin content than previously

reported in the literature. While the addition of neat lignin slightly reduced tensile stress and extension, the incorporation of lignin C14 ester significantly improved these properties at the break, indicating better compatibility and interaction within the PLA matrix. Lignin generally decreases the Young's modulus of the PLA matrix film, potentially making the polymer composite more elastic. Additionally, lignin imparts unique characteristics that could be beneficial for specific applications, such as biodegradable packaging and low-load structural components. These findings underscore the importance of optimizing both the lignin content and type to achieve desirable mechanical properties in PLA/lignin composites, particularly for 3D printing and other additive manufacturing technologies, where material performance under mechanical stress is crucial.

### 3.5.3 Morphological characterization of 3D-printed specimens.

The morphology of filaments (see Figure 25) reveals that adding Lignin C14 Ester to PLA results in filaments with improved surface smoothness, particularly at higher extrusion temperatures. The smoother surface morphology observed at 220°C suggests better compatibility and processing stability for the PLA + Lignin C14 Ester-30% composite, which could lead to enhanced mechanical properties and overall material performance.

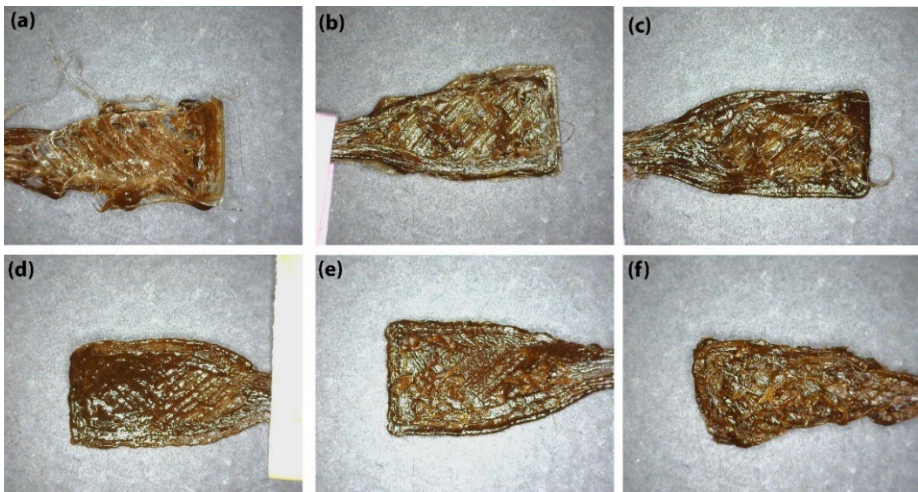


**Figure 27.** 3D-printed bone-shaped samples at 210°C (a, d), 220°C (b, e), 230°C (c, f) for PLA+ Lignin-30% (a-c), and PLA + Lignin C14 Ester-30% (d-f).

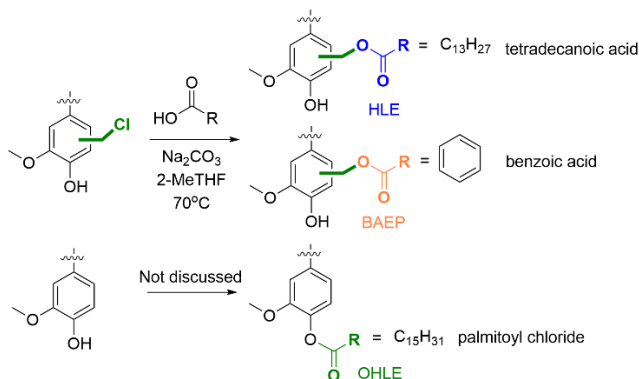
Figure 27 shows 3D-printed bone-shaped samples produced at various temperatures for PLA + Lignin-30% and PLA + Lignin C14 Ester-30% composites. The samples with PLA + Lignin-30% (see Figure 27a-c) exhibit significant structural irregularities and poor layer adhesion, indicating suboptimal printing conditions across all three temperatures. In contrast, the PLA + Lignin C14 Ester-30% samples (see Figure 27d-f) show better structural integrity compared to the PLA + Lignin-30% samples, although some defects are still visible. The sample printed at 220°C (see Figure 27e) displays the highest quality, with a uniform surface texture and strong layer cohesion, indicating optimal printing conditions. This comparison suggests that incorporating Lignin C14 Ester into PLA enhances 3D printability, particularly at higher extrusion temperatures. The improved layer adhesion and structural integrity of the PLA + Lignin C14 Ester-30% composites at 220°C underscore the enhanced

compatibility and stability of this material combination, making it more suitable for 3D printing applications than PLA + Lignin-30%.

Furthermore, to demonstrate the compatibility and tunability of PLA with lignin esters, three different types of lignin functionalization were investigated, and their properties were examined, as outlined in the following chapter.

### 3.6 Organosolv vs technical lignin: Influence of aliphatic and aromatic groups (Publication IV)

In this study, the previously transferred esterification strategy (see Scheme 5) was employed, and the optimal functional group (C14-30%) for technical lignin (birch-derived) was selected. Furthermore, to understand the influence of hydrocarbon chain (C14), a new group that is esterified with aromatic acid (e.g., benzoic acid) (see Scheme 6). Similarly, to understand the importance of phenolic hydroxyl group, direct esterification of lignin hydroxyl groups is added for the thermal and mechanical testing. Utilized 10% as the minimum and 30% as the maximum lignin concentrations for the PLA composites.



**Scheme 6.** Schematic synthesis pathway of lignin esterification from CML and hydroxyl group, as shown for G unit of lignin. OHLE is used to compare the thermal and mechanical properties of Cl esterified lignin.

#### 3.6.1 Thermal properties of esterified lignin and PLA composite

Our previous study of PLA with C14 organosolv lignin ester showed an increasing  $T_g$  with increasing lignin concentration, reaching a maximum  $T_g$  of 72.12°C (see Figure 22a) at 30%. A similar result was found in the case of hydrolysis lignin esters (HLE) with PLA (see Figure 28a); the maximum observed  $T_g$  (70°C) was at 30%. However, hydroxy group esterified lignin (OHLE) with PLA exhibited a reduction in  $T_g$  (up to 55 °C) and  $\Delta C_p$ , as shown in Figure 28b, indicating strong crystallinity while increasing the lignin content. Benzoic acid ester (BAEP) showed an increase in  $T_g$  similar to HLE, reaching up to 70°C, while moderately increasing  $\Delta C_p$ , indicating less crystalline or plasticization effect.

The thermogravimetric analysis (TGA) (see Figure 28c) illustrated the thermal stability profile of PLA/lignin composites. A gradual mass loss is observed in all the samples with increasing temperature. The initial mass loss, occurring around 80°C, is attributed to the evaporation of moisture. At 245°C, significant thermal decomposition begins, accelerating at higher temperatures. PLA, BAP, and HLE exhibit a similar degradation

pattern, whereas the OHLE sample displays the lowest thermal stability. Notably, BAP shows slightly higher mass loss in the initial mass loss range. Differential thermogravimetric analysis (DTG) (see Figure 28d) highlights differences in thermal degradation behavior among the samples. BAP and HLE follow a similar DTG profile as PLA, whereas OHLE sample begins to degrade at lower temperatures, indicating early thermal breakdown. These findings suggest that OHLE is the least thermally stable, likely due to the absence of phenolic hydroxyl groups that can form hydrogen bonds. In contrast, esterification through chloromethylation retains free hydroxyl groups, which can engage in stronger intermolecular interactions, contributing to enhanced thermal stability in corresponding composites.

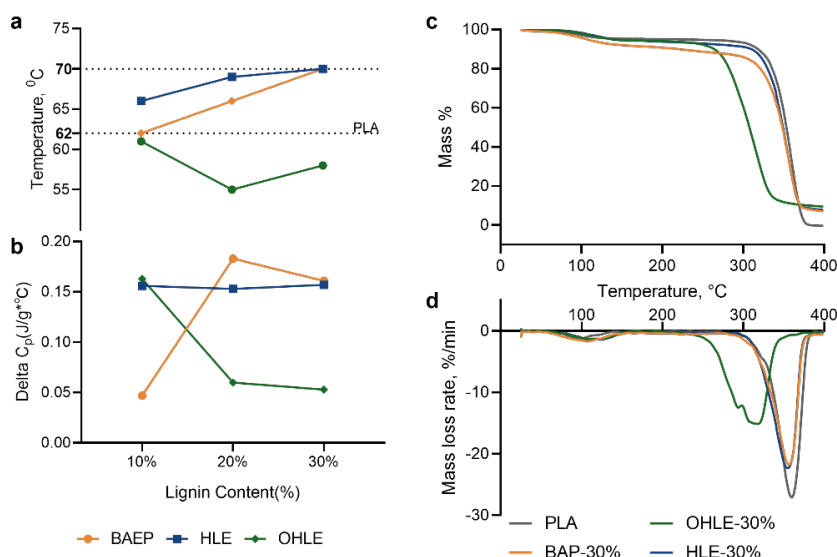


**Figure 28.** Glass transition temperature (a), delta  $C_p$  (b), thermogravimetric (c), and differential thermogravimetric (d) studies for PLA/lignin film.

### 3.6.2 Mechanical properties of esterified lignin and PLA composite

The tensile properties of PLA/lignin composite are plotted in Figure 29. The neat PLA film exhibited superior load-bearing capacity (see Figure 29a) compared to other modified lignin/PLA films. Notably, the PLA+HLE showed a reduced maximum load but exhibited the highest tensile stress among all modified composites (see Figure 29b). This might be due to inhomogeneous sample preparation, leading to higher true tensile strength despite lower load. However, PLA composites with OHLE and BAP demonstrated lower maximum load and tensile stress values, with BAP showing the lowest tensile stress, indicating loss of strength.

Tensile extension at maximum load increased for all lignin ester samples (see Figure 29c) compared to neat PLA, reflecting enhanced ductility in the composites. These results show that lignin ester incorporation reduces PLA's brittleness and improves its flexibility.

The modulus of elasticity (see Figure 29d), which reflects material stiffness, showed PLA+HLE showed the highest modulus, followed by neat PLA, OHLE, and

BAEP, respectively, indicating that HLE addition enhances the composite stiffness. These results contradict our previous study on organosolv pine lignin (see Figure 24a). The more phenolic hydroxyl groups and crosslinked structure of hydrolysis lignin could be the reason for this observation.

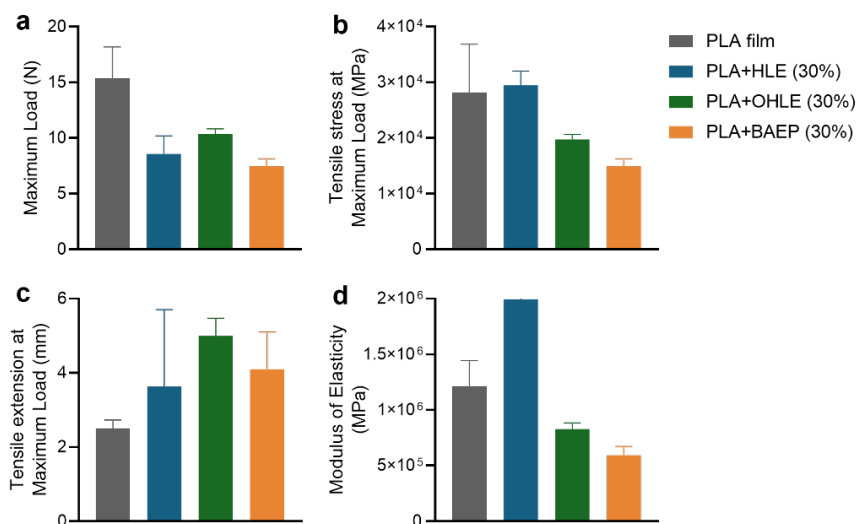


**Figure 29.** (a) Maximum load, (b) tensile stress at maximum load, (c) tensile extension at maximum load, (d) Young's modulus of PLA/lignin film.

Among the different modifications, HLE and BAEP improve the thermal properties of PLA, while OHLE enhances flexibility through plasticizing effect. These findings highlight that the overall performance of PLA composite is influenced by the specific type of lignin ester incorporated. The results demonstrate how selectively esterifying lignin can tailor the thermal and mechanical properties of PLA, offering a promising approach to developing high-performance, eco-friendly bioplastics.

## 4 Conclusions

This study has explored the potential of lignin as a versatile and sustainable material through various innovative approaches.

- The investigation of chloromethylation reactions has expanded the chemical modification possibilities for lignin. The development of novel lignin-derived materials under environmentally friendly conditions, including mild temperatures and greener solvents, highlights the commitment to sustainable practices.
- The use of sustainable copper nanoparticles supported on imidazolium lignin for catalytic applications, in comparison to traditional noble metals such as palladium, highlights the potential of lignin in green chemistry.
- The preparation of lignin-based quaternary ammonium and phosphonium surfactants from different biomass sources further demonstrates lignin's adaptability and functional diversity. The evaluation of antibacterial activity against both Gram-positive and Gram-negative clinical isolates underscores lignin's potential in biomedical applications. The development of electrospun nanostructures of the highest performing QPL with cellulose acetate has been undertaken, and their antibacterial properties have been evaluated in a real-world scenario.
- The preparation of lignin-based esters for the development of 3D printing materials presents a greener and more sustainable alternative, showcasing lignin's promise in advanced manufacturing technologies.

Overall, these findings contribute to the growing body of knowledge on lignin's potential as a renewable and eco-friendly resource for various industrial applications.

## 5 Experimental section

A brief description of the synthetic methods is provided below. Further details on the synthesis, characterisation, and studies of the properties can be found in Publications I–IV.

### Reagents and materials

All reagents used were of analytical reagent grade and were purchased from Sigma-Aldrich, Merck, Alfa Aesar, or TCI Europe and were used without further purification. Deionized water from a Milli-Q water purification system (Millipore S.A., Molsheim, France) was used throughout the study. Aspen wood chips were supplied by Estonian Cell AS in Kunda, Estonia. Longitudinally sawn pine timber sawdust was provided by Prof. Jaan Kers from Tallinn University of Technology. Barley straw came from Prof. Timo Kikas at the Estonian University of Life Sciences in Tartu. All feedstocks were dried in a convection oven at 50 °C until they reached 8% moisture, then ground into a fine powder, and stored in plastic bags at room temperature.

### Organosolv lignin extraction

A 50 g sample of ground and dried aspen chips, pine sawdust, or barley straw was refluxed in a 2 L round-bottom flask equipped with a mechanical stirrer and a condenser. The reflux used 1.5 L of solvent for 6 hours. The solvent mixture comprised 0.28 M HCl (37% purity) dissolved in absolute ethanol. After refluxing, the mixture was filtered through Whatman filter paper to remove the solid residue. The collected filtrate was concentrated to approximately 100 mL using a rotary evaporator. The concentrated liquor was diluted in 100 mL of acetone and then introduced into a vigorously stirred 2 L volume of cold Milli-Q water, which reduced the solubility of lignin. The precipitated lignin was separated by centrifugation at 4200 rpm. The recovered lignin was washed three times with 1 L of ultrapure water, centrifuged, and then dried in a convection oven at 40 °C for 24 hours. The dried organosolv lignin was weighed, yielding a 6% yield, and was then used for further analysis or subsequent procedures.

### Characterization of lignin and lignin materials

NMR spectra of lignin samples were obtained using a Bruker Avance III 400MHz spectrometer (USA) and a Bruker Avance III 800 MHz spectrometer. Each sample, approximately 60 mg, was dissolved in DMSO- $d_6$  or  $CDCl_3$  in a 5mm NMR tube. The spectra were plotted using MestReNova software.

The FTIR spectra of lignin were obtained using a Shimadzu IR Tracer-100 spectrometer (Kyoto, Japan). Samples were prepared as KBr pellets with a 1:100 weight ratio. The spectra were recorded at a resolution of 2  $cm^{-1}$  over 80 scans. Data analysis was performed with Shimadzu LabSolutions software.

Elemental analysis was carried out using an Elementar Vario MICRO cube (Langensfeld, Germany) in CHNS mode. Organic chlorine in lignin was analyzed with a Bruker S4 Pioneer XRF spectrometer (USA) employing a pre-calibrated MultiRes measurement method. For this analysis, lignin samples were mixed with  $NaHCO_3$  at a 1:10 ratio.

The hydrodynamic diameter (Dh) and  $\zeta$ -potential of the QALs were assessed using a Zeta sizer Nano ZSP (Malvern Panalytical, UK) from a lignin suspension at 1.5 mg/mL

in 1.5% DMSO in water. For each sample, three to five measurements were conducted, each consisting of 12–15 runs, depending on the sample's homogeneity.

Differential scanning calorimetry (DSC) analysis was carried out with a PerkinElmer DSC 6000 calorimeter, equipped with an IntraCooler II cooling system, at a steady heating rate of 10°C/min in a pure nitrogen environment (purity 99.999%, purge flow of 20 mL/min). A consistent sample weight of 5 mg  $\pm$  2 mg was used across all materials. The samples were pressed into aluminium crucibles and covered with aluminium lids to ensure good thermal contact.

Thermogravimetric analysis (TGA) was conducted using a NETZSCH STA 449 F3 Jupiter® instrument. Samples, weighing 4.8  $\pm$  0.9 mg, were heated in a pure nitrogen atmosphere (99.999% purity, flow rate of 40 mL/min) from 25°C to 400°C at a steady rate of 10°C/min. Aluminium crucibles were employed for the measurements.

Mechanical testing involved evaluating specimens produced via solvent casting (film) and 3D printing extrusion (filament). An Instron 5866 machine (US) was used following ASTM D638 standards, equipped with a 2.5 kN load cell for tensile tests. Five specimens from each series were tested. The testing parameters included a speed of 20 mm/min and a grip distance of 30 mm for the 10 mm wide films, and 50 mm/min with a 30 mm grip distance for the extruded filaments.

**3D-Printing Capability**—The bone-shaped test specimen, measuring 30  $\times$  4.96  $\times$  0.94 mm, was printed using the respective extruded materials on a Wanhao Duplicator 4s dual-extruder 3D printer (China) equipped with a 0.4 mm nozzle. The print bed was heated to 70 °C, and the extruder temperature was varied from 210 to 230 °C for all compositions.

## **Synthesis of Chloromethylated Lignin**

One gram of organosolv lignin and one gram of paraformaldehyde (PFA) were dissolved in 10 mL of glacial acetic acid (AcOH). The solution was then bubbled with hydrochloric acid (HCl) gas for 2 hours. The reaction was halted by adding 30 mL of water. The crude CML product was subsequently filtered, washed with water, and dried under vacuum, yielding 1.2 grams.

## **Synthesis of Iml-lignin**

1 g of 1-methylimidazole was added dropwise to a solution containing 1 g of CML in 20 mL of acetone. The reaction mixture was heated while stirring at 56 °C. After 48 hours, the precipitate was filtered, washed with 10 mL of a 70% ethanol/water mixture, and then dried under vacuum. The precipitated and washed product, yielding 350 mg, was selected for characterization and further functionalization.

## **Preparation of Lignin@Pd/CuO-NPs**

A solution of 20 mg of Imidazolium lignin (ImL) was dissolved in 2 mL of ethanol at 70 °C for 10 to 20 minutes. Once the solution became transparent, 2 mL of a mixture containing 0.9 mM CuCl<sub>2</sub> and 0.1 mM PdCl<sub>2</sub> was added, and the entire reaction mixture was stirred for 30 minutes at 70 °C. Next, 2 mM NaBH<sub>4</sub> was added, and the reaction mixture was kept stirring at ambient temperature for 12 hours. As the nanoparticles formed, the color of the reaction mixture changed from brown to black. The mixture was then centrifuged at 7000 rpm for 30 minutes, washed three times with water and ethanol, and dried.

## **Synthesis of QHLs**

To prepare QHLs, a solution of a CML lignin (1g in 20 mL of acetonitrile), 1 g of one of the following ternary amines or phosphines (ternarydimethyl amines, trihexylamine,

trioctylamine, trihexylphosphine, and trioctylphosphine) was added. The mixtures were heated at 80°C for 24h, after which the resulting QHLs were filtered, washed with hexane, and dried under vacuum.

### **Synthesis of lignin esters**

For the esterification of chloromethylated lignin, 1 g (1 equivalent) of acids—such as decanoic, tetradecanoic, stearic, or benzoic acid—and 1.2 equivalents of Na<sub>2</sub>CO<sub>3</sub> were added to 10 mL of 2-MeTHF. The mixture was heated to 70 °C and kept at this temperature for 30 minutes. Next, 1 g of chloromethylated lignin, dissolved in 10 mL of 2-MeTHF, was added to the reaction mixture, which was stirred overnight at 70 °C. After the reaction was complete, the mixture was poured into cold brine, yielding a brown precipitate. The precipitate was then filtered and washed with water to remove any remaining salts. Finally, the brown precipitate was dried under vacuum for further processing.

### **Preparation of PLA Lignin Composites**

PLA was separately dissolved in DCM within a 15 mL glass vial at 45 °C. Lignin was dissolved in THF at room temperature and then mixed to obtain a content of 10–40% w/w. The dissolved solutions were combined in a Petri dish and left to dry overnight. After this initial drying, the composite material was further dried in a vacuum oven at 40 °C for 12 hours.

### **Electrospinning of CA-Lignin nanofibers**

A solution comprising 15 wt.% cellulose acetate (CA) was formulated through the combination of acetone and dimethylacetamide in a volume ratio of 2:1 (v/v), with continuous stirring at ambient temperature until a homogeneous and transparent solution was obtained. Subsequently, P6 was incorporated into the CA solution to achieve a final concentration of 10% (v/v) of P6, and the mixture was stirred once more at ambient temperature to ensure homogeneity.

Cellulose acetate (CA) solutions, both with and without Lignin\_P6 (10%), were electrospun at room temperature using a horizontal electrospinning setup. Each polymer solution was placed in a 5 mL syringe fitted with a 0.6 mm diameter needle. The electrospinning process was carried out at a voltage of 20–25 kV using a power supply (Gamma High Voltage Research, ES 40R-20W/DM/M1127, Ormond Beach, FL), with the distance between the needle and the collector set between 8 and 10 cm. The feed rate was maintained at 0.8 mL/h, controlled by a syringe pump (NE-1010 Programmable Single Syringe Pump, New Era Pump Systems, Inc.). The electrospun nanofibers were collected on a cylindrical rotary drum covered with non-woven fabric. The CA and CA-Lignin\_P6 membranes were then removed from the fabric and dried at room temperature for 24 hours. Scanning electron microscopy (SEM, Zeiss FEG-SEM Ultra-55) was used to evaluate the morphology and average diameter of the nanofibers.

### **Antibacterial Activity Assessment**

Growth Inhibition Assay: A single colony was picked from overnight plates and inoculated into 5 mL of LB broth. The culture was then grown for 16 hours at 37°C with shaking at 150 rpm. Next, the bacterial culture was diluted 1:50 with fresh medium and incubated for 2 hours to reach the exponential growth phase. The OD at 600 nm was measured, and the culture was diluted to a target OD of 0.1. Then, 100 µL of this bacterial suspension was evenly spread on TSA agar plates using sterile glass beads. After allowing the plates to dry for 5 minutes, 3 µL drops of test compounds at 100 mg/mL in DMSO were pipetted

onto the inoculated plates, with 3  $\mu$ L of DMSO serving as a control. The plates were incubated at 37°C for 24 hours to ensure optimal growth. Following incubation, the zone of growth inhibition around the compound droplets was measured in millimeters using a caliper. The experiment was performed in three biological replicates.

**Minimal Bactericidal Concentration (MBC).** A single colony from the LB agar plate was inoculated into LB broth and grown for 16 hours at 150 rpm and 37 °C. The bacterial culture was then diluted 1:50 with fresh media and incubated at 37 °C and 150 rpm until reaching exponential growth phase (OD 0.6 at 600 nm). Cells were pelleted by centrifugation at 5000 g for 10 minutes at 4 °C, resuspended in an equal volume of sterile water, and washed twice more. The final pellet was suspended in water to achieve a target optical density (OD<sub>600</sub>) of 0.2. Compounds were diluted to the specified concentrations in 3% DMSO, based on pre-experiments showing that a 1:1 dilution of 3% DMSO (final concentration, 1.5%) had no significant effect on the viability of *S. aureus* and *K. pneumoniae* after 24 hours. Consequently, the highest lignin concentration tested was 1.5 mg/mL or 6mg/mL, always in a 1.5% DMSO-water solution. Then, 100  $\mu$ L of bacterial suspension was mixed with 100  $\mu$ L of lignin solution and incubated at 37 °C for 24 hours. After 1 and 24 hours of exposure, 3  $\mu$ L of the cell suspension was drop-plated onto LB agar and incubated at 37 °C for 24 hours. The MBC was defined as the lowest concentration of the compound that resulted in no visible colonies on the agar spot. All MBC tests were performed with three biological replicates.

### **Biofilm formation**

To assess the antimicrobial and biofilm-inhibitory effects of the tested materials, monospecies biofilms of *Staphylococcus aureus* HUMB 19594 and *Klebsiella pneumoniae* HUMB 01336 were developed. Experiments utilized sterile 6-well plates (Nunc) with coated samples that were UV-sterilized for 15 minutes beforehand. Each well received 2 mL of nutrient broth inoculated with approximately 10<sup>6</sup> CFU/mL bacterial suspension prepared in sterile saline. The coated samples were placed into the wells and incubated at 37 °C for 24 hours to promote bacterial adhesion, colonization, and biofilm formation on the surfaces. After incubation, the samples were gently rinsed with 1 mL of sterile saline to remove planktonic (non-adherent) cells. To extract biofilm-associated bacteria, samples were transferred into 1 mL of sterile saline and mechanically homogenized by vigorous vortexing and pipetting. The suspensions containing detached biofilm cells were serially diluted, and 100  $\mu$ L of each dilution was spread on nutrient agar plates. After incubation at 37 °C for 24 hours, CFU/mL counts were performed to determine the number of viable bacteria on each sample.

### **Statistical Analysis**

Statistical analysis of the data was conducted using GraphPad Prism 8 (GraphPad Software, San Diego, USA). The methods included correlation analysis, multiple linear regression, and analysis of variance (ANOVA), with post hoc tests for multiple comparisons when appropriate, all at a significance level of  $\alpha = 0.05$ .

## References

- 1 T. Kobayashi and L. Nakajima, *Curr Opin Green Sustain Chem*, 2021, **28**, 100439.
- 2 P. Anastas, M. Nolasco, F. Kerton, M. Kirchhoff, P. Licence, T. Pradeep, B. Subramaniam and A. Moores, *ACS Sustain Chem Eng*, 2021, **9**, 8015–8017.
- 3 C. Wang, S. S. Kelley and R. A. Venditti, *ChemSusChem*, 2016, **9**, 770–783.
- 4 R. Sun, *ChemSusChem*, 2020, **13**, 4385–4393.
- 5 D. Kai, M. J. Tan, P. L. Chee, Y. K. Chua, Y. L. Yap and X. J. Loh, *Green Chemistry*, 2016, **18**, 1175–1200.
- 6 V. K. Thakur, M. K. Thakur, P. Raghavan and M. R. Kessler, *ACS Sustain Chem Eng*, 2014, **2**, 1072–1092.
- 7 B. Jacobs, Y. Yao, I. Van Nieuwenhove, D. Sharma, G.-J. Graulus, K. Bernaerts and A. Verberckmoes, *Green Chemistry*, 2023, **25**, 2042–2086.
- 8 P. Jędrzejczak, M. N. Collins, T. Jesionowski and Ł. Klapiszewski, *Int J Biol Macromol*, 2021, **187**, 624–650.
- 9 P. T. Anastas and J. C. Warner, *Green Chemistry*, Oxford University PressOxford, 2000.
- 10 M. Lancaster, *Handbook of Green Chemistry and Technology*, 2008.
- 11 T. E. Graedel, *Handbook of GREEN CHEMISTRY AND TECHNOLOGY*, 2008.
- 12 P. J. Dunn, A. S. Wells and M. T. Williams, Eds., *Green Chemistry in the Pharmaceutical Industry*, Wiley, 2010.
- 13 J. Butlin, *J Int Dev*, 1989, **1**, 284–287.
- 14 S. K. Sikdar, *AIChE Journal*, 2003, **49**, 1928–1932.
- 15 S. Shafiee and E. Topal, *Energy Policy*, 2009, **37**, 181–189.
- 16 F. Gironi and V. Piemonte, *Energy Sources, Part A: Recovery, Utilization, and Environmental Effects*, 2011, **33**, 1949–1959.
- 17 W. Wang, J. Ge, X. Yu and H. Li, *Science of The Total Environment*, 2020, **708**, 134841.
- 18 C. U. Pittman and C. E. Carraher, in *Applications of Polymers*, Springer US, Boston, MA, 1988, pp. 113–124.
- 19 S. A. Miller, *Polym Chem*, 2014, **5**, 3117.
- 20 Y. Zhu, C. Romain and C. K. Williams, *Nature*, 2016, **540**, 354–362.
- 21 S. Mecking, *Angewandte Chemie International Edition*, 2004, **43**, 1078–1085.
- 22 S. J. Rowan, *ACS Macro Lett*, 2021, **10**, 466–468.
- 23 F. G. Calvo-Flores and J. A. Dobado, *ChemSusChem*, 2010, **3**, 1227–1235.
- 24 G. H. G. Gellerstedt, *Monomers, Polymers and Composites from Renewable Resources*, 2008.
- 25 Z. Mahmood, M. Yameen, M. Jahangeer, M. Riaz, A. Ghaffar and I. Javid, in *Lignin - Trends and Applications*, InTech, 2018.
- 26 EERO SJÖSTRÖM, *Wood Chemistry*, Elsevier, 1993.
- 27 H. Erdtman, *J Polym Sci B*, 1972, **10**, 228–230.
- 28 A. Tolbert, H. Akinosho, R. Khunsupat, A. K. Naskar and A. J. Ragauskas, *Biofuels, Bioproducts and Biorefining*, 2014, **8**, 836–856.
- 29 E. Windeisen and G. Wegener, in *Reference Module in Materials Science and Materials Engineering*, Elsevier, 2016.
- 30 B. M. Upton and A. M. Kasko, *Chem Rev*, 2016, **116**, 2275–2306.
- 31 E. Windeisen and G. Wegener, in *Reference Module in Materials Science and Materials Engineering*, Elsevier, 2016.

- 32 W. Schutyser, T. Renders, G. Van den Bossche, S. Van den Bosch, S. Koelewijn, T. Ennaert and B. F. Sels, in *Nanotechnology in Catalysis*, Wiley, 2017, pp. 537–584.
- 33 J. J. Bozell, J. E. Holladay, D. Johnson and J. F. White, *Top Value Added Chemicals from Biomass - Volume II, Results of Screening for Potential Candidates from Biorefinery Lignin*, 2007.
- 34 H. Hatakeyama and T. Hatakeyama, 2009, pp. 1–63.
- 35 A. Vishtal and A. Kraslawski, *Bioresources*, 2011, **6**, 3547–3568.
- 36 A. Kumar, Anushree, J. Kumar and T. Bhaskar, *Journal of the Energy Institute*, 2020, **93**, 235–271.
- 37 R. Sun, *ChemSusChem*, 2020, **13**, 4385–4393.
- 38 Ewellyn A. Capanema and Mikhail Balakshin, In *Proceedings of 18th ISWFPC–International Symposium on Wood, Fiber and Pulp Chemistry.*, 2015, 120–123.
- 39 F. José Borges Gomes, R. E. de Souza, E. O. Brito and R. C. Costa Lelis, *Journal of Applied Biotechnology & Bioengineering*, 2020, 100–105.
- 40 M. Yáñez-S, B. Matsuhira, C. Nuñez, S. Pan, C. A. Hubbell, P. Sannigrahi and A. J. Ragauskas, *Polym Degrad Stab*, 2014, **110**, 184–194.
- 41 M. Yáñez-S, B. Matsuhira, C. Nuñez, S. Pan, C. A. Hubbell, P. Sannigrahi and A. J. Ragauskas, *Polym Degrad Stab*, 2014, **110**, 184–194.
- 42 G. Vázquez, G. Antorrena, J. González and S. Freire, *Journal of Wood Chemistry and Technology*, 1997, **17**, 147–162.
- 43 S. Laurichesse and L. Avérous, *Prog Polym Sci*, 2014, **39**, 1266–1290.
- 44 J. Wang, B. Wu, S. Li, G. Sinawang, X. Wang and Y. He, *ACS Sustain Chem Eng*, 2016, **4**, 4036–4042.
- 45 P. Figueiredo, K. Lintinen, J. T. Hirvonen, M. A. Kostainen and H. A. Santos, *Prog Mater Sci*, 2018, **93**, 233–269.
- 46 M. S. Ganewatta, H. N. Lokupitiya and C. Tang, *Polymers (Basel)*, 2019, **11**, 1176.
- 47 E. Larrañeta, M. Imízcoz, J. X. Toh, N. J. Irwin, A. Ripolin, A. Perminova, J. Domínguez-Robles, A. Rodríguez and R. F. Donnelly, *ACS Sustain Chem Eng*, 2018, **6**, 9037–9046.
- 48 D. Gan, W. Xing, L. Jiang, J. Fang, C. Zhao, F. Ren, L. Fang, K. Wang and X. Lu, *Nat Commun*, 2019, **10**, 1487.
- 49 S. Shankar and J.-W. Rhim, *Food Hydrocoll*, 2017, **71**, 76–84.
- 50 W. Yang, J. S. Owczarek, E. Fortunati, M. Kozanecki, A. Mazzaglia, G. M. Balestra, J. M. Kenny, L. Torre and D. Puglia, *Ind Crops Prod*, 2016, **94**, 800–811.
- 51 W. Yang, Y. Weng, D. Puglia, G. Qi, W. Dong, J. M. Kenny and P. Ma, *Int J Biol Macromol*, 2020, **144**, 102–110.
- 52 Y. Qian, X. Qiu and S. Zhu, *Green Chemistry*, 2015, **17**, 320–324.
- 53 C. E. de Araújo Padilha, C. da Costa Nogueira, M. A. Oliveira Filho, D. F. de Santana Souza, J. A. de Oliveira and E. S. dos Santos, *Process Biochemistry*, 2020, **91**, 23–33.
- 54 O. Cusola, O. J. Rojas and M. B. Roncero, *ACS Appl Mater Interfaces*, 2019, **11**, 45226–45236.
- 55 C.-W. Wu, P.-H. Li, Y.-M. Wei, C. Yang and W.-J. Wu, *RSC Adv*, 2022, **12**, 10755–10765.
- 56 P. Jõul, O. Järvik, H. Lees, U. Kallavus, M. Koel and T. Lukk, *Front Chem*, DOI:10.3389/fchem.2023.1326454.
- 57 C. Li, W. Li, H. Liu, Y. Li, L. Dai, C. Li and C. Si, *Ind Crops Prod*, 2024, **222**, 120123.
- 58 A. G. Morena and T. Tzanov, *Nanoscale Adv*, 2022, **4**, 4447–4469.

- 59 A. G. Morena, A. Bassegoda, M. Natan, G. Jacobi, E. Banin and T. Tzanov, *ACS Appl Mater Interfaces*, 2022, **14**, 37270–37279.
- 60 K. Li, W. Zhong, P. Li, J. Ren, K. Jiang and W. Wu, *Int J Biol Macromol*, 2023, **252**, 126281.
- 61 J. Domínguez-Robles, N. K. Martin, M. L. Fong, S. A. Stewart, N. J. Irwin, M. I. Rial-Hermida, R. F. Donnelly and E. Larrañeta, *Pharmaceutics*, 2019, **11**, 165.
- 62 D. D. S. Argyropoulos, C. Crestini, C. Dahlstrand, E. Furusjö, C. Gioia, K. Jedvert, G. Henriksson, C. Hultberg, M. Lawoko, C. Pierrou, J. S. M. Samec, E. Subbotina, H. Wallmo and M. Wimby, *ChemSusChem*, DOI:10.1002/cssc.202300492.
- 63 J. Sameni, S. A. Jaffer and M. Sain, *Compos Part A Appl Sci Manuf*, 2018, **115**, 104–111.
- 64 S. Kirar, D. Mohne, M. Singh, V. Sagar, A. Bhise, S. Goswami and J. Bhaumik, *Sustainable Materials and Technologies*, 2024, **40**, e00864.
- 65 T. Aro and P. Fatehi, *ChemSusChem*, 2017, **10**, 1861–1877.
- 66 O. Yu and K. H. Kim, *Applied Sciences*, 2020, **10**, 4626.
- 67 A. Fihri, M. Bouhrara, B. Nekoueishahraki, J.-M. Basset and V. Polshettiwar, *Chem Soc Rev*, 2011, **40**, 5181.
- 68 A. Charpentier Poncelet, C. Helbig, P. Loubet, A. Beylot, S. Muller, J. Villeneuve, B. Laratte, A. Thorenz, A. Tuma and G. Sonnemann, *Nat Sustain*, 2022, **5**, 717–726.
- 69 A. J. Hunt, T. J. Farmer and J. H. Clark, in *Element Recovery and Sustainability*, The Royal Society of Chemistry, 2013, pp. 1–28.
- 70 A. Charpentier Poncelet, C. Helbig, P. Loubet, A. Beylot, S. Muller, J. Villeneuve, B. Laratte, A. Thorenz, A. Tuma and G. Sonnemann, *Nat Sustain*, 2022, **5**, 717–726.
- 71 A. Khazaei, S. Rahmati, Z. Hekmatian and S. Saeednia, *J Mol Catal A Chem*, 2013, **372**, 160–166.
- 72 M. Nasrollahzadeh, S. M. Sajadi, A. Rostami-Vartooni and M. Bagherzadeh, *J Colloid Interface Sci*, 2015, **448**, 106–113.
- 73 D. Baruah, R. N. Das, S. Hazarika and D. Konwar, *Catal Commun*, 2015, **72**, 73–80.
- 74 M. B. Marulasiddeshwara and P. R. Kumar, *Int J Biol Macromol*, 2016, **83**, 326–334.
- 75 F. Coccia, L. Tonucci, N. d’Alessandro, P. D’Ambrosio and M. Bressan, *Inorganica Chim Acta*, 2013, **399**, 12–18.
- 76 S. P. Nolan, Ed., *N-Heterocyclic Carbenes*, Wiley, Weinheim, 2014.
- 77 E. A. B. Kantchev, C. J. O’Brien and M. G. Organ, *Angewandte Chemie International Edition*, 2007, **46**, 2768–2813.
- 78 R. Narayanan and M. A. El-Sayed, *J Am Chem Soc*, 2003, **125**, 8340–8347.
- 79 Y. Huang, Z. Zheng, T. Liu, J. Lü, Z. Lin, H. Li and R. Cao, *Catal Commun*, 2011, **14**, 27–31.
- 80 *Antibiotic resistance threats in the United States*, 2019, Atlanta, Georgia, 2019.
- 81 World Health Organization report. *2021 Antibacterial agents in clinical and preclinical development: an overview and analysis*. Geneva: World Health Organization; 2022.
- 82 D. Tălăpan, A.-M. Sandu and A. Rafila, *Antibiotics*, 2023, **12**, 974.
- 83 N. H. Bhuiyan, G. Selvaraj, Y. Wei and J. King, *Plant Signal Behav*, 2009, **4**, 158–159.
- 84 J. L. Espinoza-Acosta, P. I. Torres-Chávez, B. Ramírez-Wong, C. M. López-Saiz and B. Montaño-Leyva, *Bioresources*, 2016, **11**, 5452–5481.
- 85 M. J. Alves, I. C. F. R. Ferreira, H. J. C. Froufe, R. M. V. Abreu, A. Martins and M. Pintado, *J Appl Microbiol*, 2013, **115**, 346–357.

- 86 W. Yang, E. Fortunati, D. Gao, G. M. Balestra, G. Giovanale, X. He, L. Torre, J. M. Kenny and D. Puglia, *ACS Sustain Chem Eng*, 2018, **6**, 3502–3514.
- 87 T. He, Y. Jiang, S. Chang, X. Zhou, Y. Ji, X. Fang and Y. Zhang, *Ind Crops Prod*, 2023, **191**, 115930.
- 88 A. Alzagameem, S. E. Klein, M. Bergs, X. T. Do, I. Korte, S. Dohlen, C. Hüwe, J. Kreyenschmidt, B. Kamm, M. Larkins and M. Schulze, *Polymers (Basel)*, 2019, **11**, 670.
- 89 D. M. Rocca, J. P. Vanegas, K. Fournier, M. C. Becerra, J. C. Scaiano and A. E. Lanterna, *RSC Adv*, 2018, **8**, 40454–40463.
- 90 Ł. Klapiszewski, T. Rzemieniecki, M. Krawczyk, D. Malina, M. Norman, J. Zdarta, I. Majchrzak, A. Dobrowolska, K. Czaczek and T. Jesionowski, *Colloids Surf B Biointerfaces*, 2015, **134**, 220–228.
- 91 A. P. Richter, J. S. Brown, B. Bharti, A. Wang, S. Gangwal, K. Houck, E. A. Cohen Hubal, V. N. Paunov, S. D. Stoyanov and O. D. Velev, *Nat Nanotechnol*, 2015, **10**, 817–823.
- 92 D. Kai, M. J. Tan, P. L. Chee, Y. K. Chua, Y. L. Yap and X. J. Loh, *Green Chemistry*, 2016, **18**, 1175–1200.
- 93 M. Vinardell and M. Mitjans, *Int J Mol Sci*, 2017, **18**, 1219.
- 94 X. Xie, W. Cong, F. Zhao, H. Li, W. Xin, G. Hou and C. Wang, *J Enzyme Inhib Med Chem*, 2018, **33**, 98–105.
- 95 V. V. Ermolaev, D. M. Arkhipova, V. A. Miluykov, A. P. Lyubina, S. K. Amerhanova, N. V. Kulik, A. D. Voloshina and V. P. Ananikov, *Int J Mol Sci*, 2021, **23**, 86.
- 96 Y. Ma, J. Dai, L. Wu, G. Fang and Z. Guo, *Polymer (Guildf)*, 2017, **114**, 113–121.
- 97 Y. Jiao, L. Niu, S. Ma, J. Li, F. R. Tay and J. Chen, *Prog Polym Sci*, 2017, **71**, 53–90.
- 98 S. P. Denyer and G. S. A. B. Stewart, *Int Biodeterior Biodegradation*, 1998, **41**, 261–268.
- 99 T. Thorsteinsson, M. Másson, K. G. Kristinsson, M. A. Hjálmarsdóttir, H. Hilmarsson and T. Loftsson, *J Med Chem*, 2003, **46**, 4173–4181.
- 100 D. Kwaśniewska, Y.-L. Chen and D. Wieczorek, *Pathogens*, 2020, **9**, 459.
- 101 F. Kopecky, *Pharmazie*, 1996, **51**, 135–44.
- 102 G. Sun, Ed., *Functional Textiles for Improved Performance, Protection and Health*, Elsevier, Gang , 2011.
- 103 J. C. Tiller, C.-J. Liao, K. Lewis and A. M. Klibanov, *Proceedings of the National Academy of Sciences*, 2001, **98**, 5981–5985.
- 104 K. Li, S. Bian, W. Zhen, H. Li and L. Zhao, *React Funct Polym*, 2021, **158**, 104791.
- 105 M. N. Nadagouda, P. Vijayasathya, A. Sin, H. Nam, S. Khan, J. B. M. Parambath, A. A. Mohamed and C. Han, *Medicinal Chemistry Research*, 2022, **31**, 1663–1678.
- 106 S. Buffet-Bataillon, P. Tattevin, M. Bonnaure-Mallet and A. Jolivet-Gougeon, *Int J Antimicrob Agents*, 2012, **39**, 381–389.
- 107 M. D. Culler, J. Bitman, M. J. Thompson, W. E. Robbins and S. R. Dutky, *J Dairy Sci*, 1979, **62**, 584–595.
- 108 I. V. Kapitanov, A. Jordan, Y. Karpichev, M. Spulak, L. Perez, A. Kellett, K. Kümmerer and N. Gathergood, *Green Chemistry*, 2019, **21**, 1777–1794.
- 109 D. K. A. Kusumahastuti, M. Sihtmäe, I. V. Kapitanov, Y. Karpichev, N. Gathergood and A. Kahru, *Ecotoxicol Environ Saf*, 2019, **172**, 556–565.
- 110 P. Balgavý and F. Devínsky, *Adv Colloid Interface Sci*, 1996, **66**, 23–63.
- 111 J. M. Boyce, *Antimicrob Resist Infect Control*, 2023, **12**, 32.
- 112 J. Haldar, P. Kondaiah and S. Bhattacharya, *J Med Chem*, 2005, **48**, 3823–3831.
- 113 S. Zhang, S. Ding, J. Yu, X. Chen, Q. Lei and W. Fang, *Langmuir*, 2015, **31**, 12161–12169.

- 114 L. An, J. W. Heo, J. Chen and Y. S. Kim, *J Clean Prod*, 2022, **368**, 133219.
- 115 L. Chang, W. Duan, S. Huang, A. Chen, J. Li, H. Tang, G. Pan, Y. Deng, L. Zhao and D. Li, *R Soc Open Sci*, 2021, **8**, rsos.201904.
- 116 W. A. Arnold, A. Blum, J. Branyan, T. A. Bruton, C. C. Carignan, G. Cortopassi, S. Datta, J. DeWitt, A.-C. Doherty, R. U. Halden, H. Harari, E. M. Hartmann, T. C. Hrubec, S. Iyer, C. F. Kwiatkowski, J. LaPier, D. Li, L. Li, J. G. Muñiz Ortiz, A. Salamova, T. Schettler, R. P. Seguin, A. Soehl, R. Sutton, L. Xu and G. Zheng, *Environ Sci Technol*, 2023, **57**, 7645–7665.
- 117 Y. Liang, H. Li, J. Ji, J. Wang and Y. Ji, *Molecules*, 2023, **28**, 5469.
- 118 K. Acurio Cerda, M. Kathol, G. Purohit, E. Zamani, M. D. Morton, O. Khalimonchuk, R. Saha and S. K. Dishari, *ACS Sustain Chem Eng*, 2023, **11**, 10364–10379.
- 119 V. V. Ermolaev, D. M. Arkhipova, V. A. Miluykov, A. P. Lyubina, S. K. Amerhanova, N. V. Kulik, A. D. Voloshina and V. P. Ananikov, *Int J Mol Sci*, 2021, **23**, 86.
- 120 M. V. Pugachev, N. V. Shtyrlin, S. V. Sapozhnikov, L. P. Sysoeva, A. G. Iksanova, E. V. Nikitina, R. Z. Musin, O. A. Lodochnikova, E. A. Berdnikov and Y. G. Shtyrlin, *Bioorg Med Chem*, 2013, **21**, 7330–7342.
- 121 Global Plastics Outlook: Economic drivers, environmental impacts and policy options. P. Chalmin, *Field Actions Sci Rep*, 2019, 6–11.
- 122 M. Weiss, J. Haufe, M. Carus, M. Brandão, S. Bringezu, B. Hermann and M. K. Patel, *J Ind Ecol*, DOI:10.1111/j.1530-9290.2012.00468.x.
- 124 I. Ribca, M. E. Jawerth, C. J. Brett, M. Lawoko, M. Schwartzkopf, A. Chumakov, S. V. Roth and M. Johansson, *ACS Sustain Chem Eng*, 2021, **9**, 1692–1702.
- 125 J. Adamczyk and R. Dylewski, *Renewable and Sustainable Energy Reviews*, 2017, **80**, 421–429.
- 126 M. A. Elsayy, K.-H. Kim, J.-W. Park and A. Deep, *Renewable and Sustainable Energy Reviews*, 2017, **79**, 1346–1352.
- 127 A. Haryńska, H. Janik, M. Sienkiewicz, B. Mikolaszek and J. Kucińska-Lipka, *ACS Sustain Chem Eng*, 2021, **9**, 6923–6938.
- 128 S. Bhagia, K. Bornani, R. Agrawal, A. Satlewal, J. Đurkovič, R. Lagaña, M. Bhagia, C. G. Yoo, X. Zhao, V. Kunc, Y. Pu, S. Ozcan and A. J. Ragauskas, *Appl Mater Today*, 2021, **24**, 101078.
- 129 3D Printing market size, share & trends, 2025 to 2030.
- 130 H. Balakrishnan, A. Hassan, M. Imran and M. U. Wahit, *Polym Plast Technol Eng*, 2012, **51**, 175–192.
- 131 S. Domeneek, A. Louaifi, A. Guinault and S. Baumberger, *J Polym Environ*, 2013, **21**, 692–701.
- 132 C. Pouteau, P. Dole, B. Cathala, L. Averous and N. Boquillon, *Polym Degrad Stab*, 2003, **81**, 9–18.
- 133 A. De Chirico, M. Armanini, P. Chini, G. Cioccolo, F. Provasoli and G. Audisio, *Polym Degrad Stab*, 2003, **79**, 139–145.
- 134 G. UZUN and D. AYDEMİR, *Bulletin of Materials Science*, 2017, **40**, 383–393.
- 135 L. Hu, T. Stevanovic and D. Rodrigue, *J Appl Polym Sci*, DOI:10.1002/app.41040.
- 136 L. Zhang and J. Huang, *J Appl Polym Sci*, 2001, **80**, 1213–1219.
- 137 M. Arend, B. Westermann and N. Risch, *Angewandte Chemie International Edition*, 1998, **37**, 1044–1070.
- 138 Y. Liu and K. Li, *J Adhes*, 2006, **82**, 593–605.
- 139 P. Truter, A. Pizzi and H. Vermaas, *J Appl Polym Sci*, 1994, **51**, 1319–1322.
- 140 S. Laurichesse and L. Avérous, *Prog Polym Sci*, 2014, **39**, 1266–1290.

- 141 *Organic Syntheses*, 1956, **36**, 50.
- 142 Nenad Maraš, *ChemSpider SyntheticPages*, 2011, 518.
- 143 R. V. Rodik, A.-S. Anthony, V. I. Kalchenko, Y. Mély and A. S. Klymchenko, *New Journal of Chemistry*, 2015, **39**, 1654–1664.
- 144 V. Burilov, R. Garipova, E. Sultanova, D. Mironova, I. Grigoryev, S. Solovieva and I. Antipin, *Nanomaterials*, 2020, **10**, 1143.
- 145 European Patent Organization, EP1110964 A1, 2001.
- 146 J.-L. Wen, S.-L. Sun, B.-L. Xue and R.-C. Sun, *Materials*, 2013, **6**, 359–391.
- 147 T.-Q. Yuan, S.-N. Sun, F. Xu and R.-C. Sun, *J Agric Food Chem*, 2011, **59**, 10604–10614.
- 148 Z. Wang and P. J. Deuss, *ChemSusChem*, 2021, **14**, 5186–5198.
- 149 A. R. Gonçalves and P. Benar, *Bioresour Technol*, 2001, **79**, 103–111.
- 150 P. Truter, A. Pizzi and H. Vermaas, *J Appl Polym Sci*, 1994, **51**, 1319–1322.
- 151 C. R. McElroy, A. Constantinou, L. C. Jones, L. Summerton and J. H. Clark, *Green Chemistry*, 2015, **17**, 3111–3121.
- 152 D. Prat, A. Wells, J. Hayler, H. Sneddon, C. R. McElroy, S. Abou-Shehada and P. J. Dunn, *Green Chemistry*, 2016, **18**, 288–296.
- 153 B. Jacobs, Y. Yao, I. Van Nieuwenhove, D. Sharma, G.-J. Graulus, K. Bernaerts and A. Verberckmoes, *Green Chemistry*, 2023, **25**, 2042–2086.
- 154 M. Rbaa, S. Jabli, Y. Lakhrissi, M. Ouhssine, F. Almalki, T. Ben Hadda, S. Messgo-Moumene, A. Zarrouk and B. Lakhrissi, *Heliyon*, 2019, **5**, e02689.
- 155 E. Zussman, A. Theron and A. L. Yarin, *Appl Phys Lett*, 2003, **82**, 973–975.
- 156 S. Agarwal, J. H. Wendorff and A. Greiner, *Polymer (Guildf)*, 2008, **49**, 5603–5621.
- 157 S. Ramakrishna, K. Fujihara, W.-E. Teo, T. Yong, Z. Ma and R. Ramaseshan, *Materials Today*, 2006, **9**, 40–50.
- 158 S. Majumder, M. A. Matin, A. Sharif and M. T. Arafat, *Journal of Polymer Research*, 2020, **27**, 381.
- 159 M. Masłowski, J. Miedzianowska and K. Strzelec, *Polymers (Basel)*, 2019, **11**, 972.
- 160 A. M. Borrero-López, C. Valencia, A. Blázquez, M. Hernández, M. E. Eugenio and J. M. Franco, *Polymers (Basel)*, 2020, **12**, 2822.
- 161 M. Seifert, S. Hesse, V. Kabrelian and D. Klemm, *J Polym Sci A Polym Chem*, 2004, **42**, 463–470.
- 162 F. C. M. Lobo, A. R. Franco, E. M. Fernandes and R. L. Reis, *Molecules*, 2021, **26**, 1749.
- 163 H. F. Lewis, F. E. Brauns, M. A. Buchanan and E. B. Brookbank, *Ind Eng Chem*, 1943, **35**, 1113–1117.
- 164 W. G. Glasser and R. K. Jain, *hfs*, 1993, **47**, 225–233.
- 165 Z. Guo, A. Gandini and F. Pla, *Polym Int*, 1992, **27**, 17–22.
- 166 H. Funakoshi, N. Shiraishi, M. Norimoto, T. Aoki, H. Hayashi and T. Yokota, *Holzforschung*, 1979, **33**, 159–166.
- 167 In *Lignin in Polymer Composites*, Elsevier, 2016, p. iii.
- 168 H. Li and A. G. McDonald, *Ind Crops Prod*, 2014, **62**, 67–76.
- 169 E. Gkartzou, E. P. Koumoulos and C. A. Charitidis, *Manuf Rev (Les Ulis)*, 2017, **4**, 1.

## Acknowledgements

This doctoral journey was carried out at the Department of Chemistry and Biotechnology, School of Science, Tallinn University of Technology (TalTech). I am sincerely grateful to the Estonian Research Council for their generous support through the grants temTa49, RESTA11, and COVSG5, which enabled and sustained this research.

Life is often described as a corridor of countless doors—some remain closed, many we pass by, and a rare few we knock on, not knowing what lies beyond. I am thankful I knocked on the right one. Maksim Ošeka—you were the first door I approached. Through you, I heard about TalTech, and with that, the path ahead quietly unfolded. You pointed me toward a possibility that would become my reality. Thank you for that nudge, for being the beginning.

On the other side of that door stood two guiding lights—Yevgen Karpichev and Tiit Lukk, my supervisors. You were not just mentors but steady anchors through this long and often uncertain journey.

Yevgen, your impact on me has been immeasurable. You shaped my scientific thinking, gave me freedom to grow, and created a work environment where I felt both valued and supported. Your patience, clarity, and calm strength have left a mark on the person I have become.

Thank you, Tiit, for your wise insights and for believing in the process and in me.

No journey is walked alone, and in the vast corridors of research, I found a companion, a friend, and a fellow explorer in Denys Bonder. You were more than a labmate—you guided me through both the technical corners of our laboratory and the everyday rhythm of life in Estonia. Thank you for your constant support and advice, both scientific and personal.

To my colleagues in Lab 445, thank you for the shared workspaces, shared ideas, and shared laughter. Your presence made the lab a space of learning and comfort. I'm equally grateful to all other collaborators and colleagues who were part of my scientific projects. Each of you contributed a unique thread to the tapestry of this thesis. I would like to sincerely thank Mikk Kaasik, Epp Väli, Eve-Ly Ojangu, Kairit Zovo, and Piia Jõul for kindly reviewing my Estonian abstract. Your feedback and support made a real difference, and I'm very grateful for the time and effort you shared with me. To Jagadeesh, Kannan, and Tran—thank you for standing beside me not only as departmental colleagues but as friends who enriched my life far beyond the academic walls, with conversations, laughter, and unwavering support.

I want to express my heartfelt gratitude to my former supervisor, Dr. Praveen, for his invaluable guidance, constant support, and encouragement throughout my time in the PKV lab. His mentorship played a significant role in shaping my academic and professional growth. I am also deeply thankful to all my colleagues in the PKV lab for creating such a collaborative and inspiring environment. I learned a great deal from each of you—your insights, enthusiasm, and camaraderie made my time in the lab both enriching and memorable. Thank you all for being such an important part of my journey.

I want to express my deepest gratitude to Hasim and Sadik, who have been by my side throughout my academic journey, from the early days of my bachelor's studies to the completion of my master's degree. Thank you for your constant support, friendship, and encouragement.

Outside the lab, I found places that gave me joy, meaning, and a sense of belonging. To my dear friends in the 'Wait for it' art community—thank you for helping me keep my creativity alive when the science became too heavy. To the beautiful circle of 'Mallus in Estonia', thank you for bringing the warmth of home to foreign winters, for the food, the conversations, and the companionship that helped balance work with life.

To my family, who have been my first teachers, first friends, and forever supporters—Amma, Acha, Midhu, and Anju—your love has been the invisible thread that kept me grounded across borders and time zones. A special note of love to the little one, Peelu—the newest light in our family, whose arrival brought joy, hope, and a reminder of all that truly matters.

And finally, to my wife, Nivu—you came into my life as a partner, a pillar, and a calm voice in the chaos. Your love, understanding, and unwavering belief in me have truly made this journey special. Thank you for being my sharp-eyed reviewer when I can't see any difference anymore. I feel so grateful to have your support every step of the way, making it bearable. Thank you for being my home through it all.

If I have missed any names, know that your presence—whether in a conversation, a moment, or a gesture—still echoes in the pages of this work.

This thesis is not just a culmination of academic effort—

It is a journey of people, places, and moments.

To all who walked even a few steps with me, thank you.

This is as much yours as it is mine.

## Abstract

### Lignin Valorization via Chloromethylation as a Versatile Approach Towards Sustainable Materials

Lignin, a highly abundant biopolymer with a high carbon content and significant aromaticity, holds considerable potential as a resource for fuel production and the synthesis of platform chemicals. Despite its promising attributes, lignin remains underutilized compared to other lignocellulosic biopolymers. However, its inherent versatility can be unlocked through various chemical modifications applied at both "upstream" and "downstream" stages after extraction.

Efforts to enhance lignin's utility have primarily focused on "upstream" chemical modifications, targeting the hydroxyl groups for alteration or introducing new reactive sites to broaden its applications. However, the search for versatile and environmentally friendly methods for these modifications is ongoing. In this context, the concept of a greener chloromethylation process, which is gaining renewed interest for its potential in sustainable applications, remains largely unexplored in lignin chemistry.

This study presents a novel chloromethylation technique for lignin, enabling the production of diverse lignin-based materials from chloromethylated lignin. These materials include (i) catalysts, (ii) antibacterial surface agents, and (iii) thermoplastic additives. Lignin-based catalyst (Lignin@Pd/CuO-NPs) offers benefits such as simple synthesis, heterogeneity, recoverability, and recyclability. Demonstrated its effectiveness in multiple carbon-carbon bond-forming reactions, including Suzuki-Miyaura, Sonogashira, Heck, and azide-alkyne cycloaddition (click) reactions. The heterogeneous catalyst demonstrated excellent recyclability, allowing for reuse in at least 10 consecutive cycles while maintaining yields between 42% and 84%. Furthermore, a continuous flow reactor cartridge prototype using Lignin@Pd/CuO-NPs was developed, producing results comparable to batch reactions. This highlights its potential to facilitate diverse carbon-carbon bond formations and emphasizes its recyclability, supporting green chemistry and sustainability efforts.

The introduction of various quaternary amines with differing chain lengths (C6-C18) to chloromethylated lignin derived from hardwood (aspen), softwood (pine), and grass (barley straw) led to the development of innovative surface-active materials (QALs) with enhanced antibacterial activity against both Gram-negative (*Klebsiella pneumoniae*) and Gram-positive (*methicillin-resistant Staphylococcus aureus*) clinical bacterial isolates. The antibacterial performance of QALs was superior to that of unmodified lignin, with QALs featuring longer alkyl chains demonstrating an MBC of 0.012 mg/L against *K. pneumoniae* after just 1 hour of exposure. A similar effect was observed after 24 hours for *S. aureus*. For all lignin samples, an increase in alkyl chain length resulted in enhanced bactericidal activity. The MBC values of C14-C18 QALs were consistently lower than those of QALs with shorter alkyl chains. The agar-based zone of inhibition (ZOI) test indicated an antibacterial optimum for QALs at C12-C14, likely due to the limited diffusion of longer alkyl chain QALs in the semi-solid medium. This understanding was further explored by comparing quaternary ammonium (QALs) and phosphonium (QPLs) lignin for their activity against ESKAPE pathogens (*E. faecium*, *S. aureus*, *K. pneumoniae*, *A. baumannii*, *P. aeruginosa*, *E. cloacae*). MBC and ZOI results of all tested samples, N6, N8, P6, and P8, corresponding to the amines [Trihexylamine and Trioctylamine], and phosphines [Trihexylphosphine and Trioctylphosphine], respectively, P6 stands out as the most

promising candidate due to its consistent and high-level activity across a broad spectrum of clinically relevant pathogens. The development of an electrospun nanostructured film made from the top-performing QPL with cellulose acetate has been carried out, characterized morphologically using scanning electron microscopy, and tested for its biofilm inhibitory properties against both Gram-positive and Gram-negative bacteria for practical applications.

Chloromethylated lignin (CML) was esterified with decanoic acid (C10), tetradecanoic acid (C14), and stearic acid (C18). Esterified lignin was incorporated into polylactic acid (PLA) at varying proportions (10%, 20%, 30%, and 40%) using the solvent casting technique. The thermal and mechanical properties of the solvent-casted films were analyzed, with lignin-loaded PLA composites showing the highest enhancement in glass transition temperature ( $T_g$ ), reaching  $72.12^\circ\text{C}$  for 30% loading of tetradecanoic acid (C14). This composition exhibited a tensile strength of  $18.9 \pm 4.7$  MPa and a maximum load of  $5.5 \pm 1$  N, compared to the stiffer and more rigid native PLA, which had values of  $10.2 \pm 1$  MPa and  $4.6 \pm 0.3$  N, respectively. The unmodified lignin-PLA composite showed intermediate properties. The optimal composition was selected for producing 3D printing filament, with three extrusion temperatures evaluated. The advanced mechanical properties and surface morphology of the 3D-printed filament were then analyzed. Further studies were conducted on organosolv pine and hydrolysis birch lignin, which were chemically modified through esterification at hydroxyl groups using palmitoyl (C16) chlorides, and through chloromethylation and subsequent esterification using tetradecanoic acid (C14) and benzoic acid. Esterified lignin was incorporated into PLA at varying proportions (10%, 20%, and 30%) using the solvent casting technique. These results showed that 30% of hydrolysis lignin ester (HLE) and benzoic acid ester (BAEP) enhanced the heat stability of PLA, while esterification by palmitoyl chloride (OHLE) made it more elastic through plasticization.

This research, in conjunction with the greener chloromethylation approach for lignin, provides new insights into lignin valorization, making it both sustainable and economically attractive.

## Lühikokkuvõte

### Ligniini väärindamine klorometüleerimise teel kui mitmekülgne lähenemisviis jätkusuutlike materjalide loomisele

Ligniin on laialdaselt esinev kõrge süsinikusisaldusega aroomaatne biopolümeer, mis omab toorainena märkimisväärsed potentsiaali kütuse tootmisel ja platvormkemikaalide sünteesimisel. Hoolimata sellest on ligniin, võrreldes teiste lignotselluloosset päritolu biopolümeeridega, endiselt alakasutatud. Ligniini mitmekülgsus tuleneb keemilistest modifikatsioonidest, mida teostatakse ekstraheerimise käigus nii eel- kui ka järeltöötamise etappides.

Ligniini kasutusvõimaluste laiendamiseks on seni keskendunud peamiselt eeltöötlusel tehtavatele keemilistele modifikatsioonidele, mille käigus muudetakse hüdroksüülrühmi või lisatakse uusi reaktiivseid rühmasid. Siiski otsitakse jätkuvalt uusi töötlusmeetodeid, mis oleksid ühtlasi nii universaalsed kui ka keskkonnasõbralikud. Selles kontekstis on taas hakatud huvi tundma rohelisema klorometüleerimise protsessi vastu, mida on ligniinikeemias seni vähe uuritud, kuid millel võiks olla potentsiaali jätkusuutlike rakenduste jaoks.

Käesolev uurimus tutvustab uut ligniini modifitseerimise tehnikat, mis võimaldab klorometüleeritud ligniinist toota mitmesuguseid ligniinipõhiseid materjale. Nendeks materjalideks on (i) katalüsaatorid, (ii) antibakteriaalsed pinnakaitsevahendid, (iii) termoplastsed lisaained.

Ligniiniipõhisel katalüsaatoril (Lignin@Pd/CuO-NPs) on mitmeid eeliseid, see on lihtsasti sünteesitav, heterogeenne, reaktsioonikeskkonnast kergesti eraldatav ja taaskasutatav. Nimetatud katalüsaator on näidanud head efektiivsust mitmesugustes süsinik-süsinik sidemaid moodustavates reaktsioonides, sealhulgas Suzuki–Miyaura, Sonogashira, Heck ja asiidi-alküüni tsükliiseerimisreaktsioonides (nn *click*-reaktsioonid). Lisaks osutus see heterogeenne katalüsaator väga hästi taaskasutatavaks, nimelt jäid vähemalt kümnes järjestikuses reaktsioonis saavutatud reaktsiooni saagised vahemikku 42–84%. Lisaks töötati Lignin@Pd/CuO-NPs katalüsaatorit kasutades välja läbivoolureaktori kolonni prototüüp, millega saadud tulemused olid võrreldavad nendega, mis saadi partiireaktsioonidega. Saadud tulemused näitavad Lignin@Pd/CuO-NPs katalüsaatori potentsiaali erinevate C–C sidemete moodustamisel, rõhutavad taaskasutatavust ning toetavad rohelise keemia ja jätkusuutlikkuse kontseptsiooni.

Uudsete pindaktiivsete materjalide (QAL-ide) väljatöötamiseks lisati klorometüleeritud lehtpuu (harilik haab), okaspuu (mänd) ja rohhtaime (odrapõhk) ligniinidele erineva ahelapikkusega (C6–C18) kvaternaarseid amiine. Saadud materjalid näitasid tugevat antibakteriaalset toimet nii Gram-negatiivsete (*Klebsiella pneumoniae*) kui ka Gram-positiivsete (metitsilliiniresistentne *Staphylococcus aureus*) kliiniliste tüvede vastu. QAL-ide antibakteriaalne toime oli oluliselt tõhusam kui töötlemata ligniinil. Pikema alküülahelaga QAL-ide korral oli minimaalseks bakteritsiidseks kontsentratsiooniks (MBC) 0,012 mg/L, mis toimis *K. pneumonia* puhul juba pärast ühetunnist kokkupuudet. Sarnane mõju oli 24 tunni järel nähtav ka *S. aureus* puhul. Kõigi modifitseeritud ligniinide korral täheldati, et mida pikem on alküülahel, seda suurem on ka selle bakteritsiidne aktiivsus. C14–C18 ahelapikkusega QAL-ide puhul olid MBC

väärtused järjepidevalt madalamad, kui lühema ahelaga QAL-ide korral. Agarplaatidel läbi viidud inhibeerimistsooni (ZOI) test näitas optimaalset antibakteriaalset toimet C12–C14 ahelapikkusega QAL-ide puhul, mida saab selgitada pikema ahelaga QAL-ide piiratud difusiooniga pooltahkes keskkonnas. Selle nähtuse paremaks mõistmiseks võrreldi omavahel QAL-de ja fosfoonium-liigendatud ligniinide (QPL-ide) toimet ESKAPE (*E. faecium*, *S. aureus*, *K. pneumoniae*, *A. baumannii*, *P. aeruginosa*, *E. cloacae*) patogeenidele. Kõigi testitud proovide N6, N8, P6 ja P8 (vastavad amiinidele triheksüülamiin ja trioktüülamiin ning fosfiinidele triheksüülfosfiin ja trioktüülfosfiin) puhul eristus MBC- ja ZOI-tulemuste põhjal silmatorkavalt P6, näidates kõrget antibakteriaalset aktiivsust nimetatud patogeenide vastu.

Järgnevalt töötati välja QPL-il ja atsetüülselluloosil põhinev elektrokedratud nanostruktureeritud kile, mille mikrostruktuuri iseloomustati skaneeriva elektronmikroskoopia abil ning mille biofilmi inhibeerivaid omadusi testiti praktiliste rakenduste tarbeks nii Gram-positiivsete kui ka Gram-negatiivsete bakterite peal. Klorometüülitud ligniin (CML) esterdati dekaan- (C10), tetradekaan- (C14) ja steariinhappega (C18). Kasutades lahustipõhist valamistehnikat segati saadud esterifitseeritud ligniin polüpiimhappega (PLA) erinevates kontsetratsioonides (10%, 20%, 30%, 40%). Saadud kilede termiliste ja mehaaniliste omaduste analüüs näitas, et kõige suurem klaasistumistemperatuur ( $T_g$ ) (kuni 72,12 °C-ni) oli täheldatav PLA-komposiidi puhul, mis sisaldasid 30% C14–esterifitseeritud ligniini. Selle esterifitseeritud ligniin-PLA komposiidi venitustugevuseks oli  $18,9 \pm 4,7$  MPa ja maksimaalseks koormustaluvuseks  $5,5 \pm 1$  N. Võrreldes tavalise PLA-ga ( $10,2 \pm 1$  MPa ja  $4,6 \pm 0,3$  N) oli saadud filament elastsem ja tugevam. Muundamata ligniin-PLA komposiit jäi omaduste poolest vahepealseks. 3D-prinditud filamendi valmistamiseks sobiv optimaalne koostis valiti testides kolme erinevat ekstrusioonitemperatuuri. Seejärel analüüsiti 3D-prinditud filamendi mehaanilisi omadusi ja pinna mikrostruktuuri. Täiendavad uuringud viidi läbi organosolv männiligniini ja hüdrolüüsi kaseligniiniga, mida oli keemiliselt hüdroksüülrühmade esterifitseerimisega muudetud, kasutades palmitoüülkloriide (C16); ning modifitseeritud klorometüülamise ja järgneva esterifitseerimisega, kasutades tetradekaanhapet (C14) ja bensoehapet. Esterifitseeritud ligniin segati PLA-ga (10%, 20%, 30%) lahustipõhise valamistehnika teel. Saadud tulemused näitasid, et 30%-ne hüdrolüüsiligniiniestri (HLE) ja bensoehappeestri (BAEP) sisaldus tõstis PLA kuumakindlust, samas kui palmitoüülkloriidiga esterifitseerimine (OHLE) muutis PLA elastsemaks.

Antud töös kasutatud rohelisema klorometüülamise meetodika pakub ligniini väärindamiseks uusi teadmisi ning on ühtlasi ka majanduslikult atraktiivne ning jätkusuutlik lähenemisviis.

## Appendix 1

### Publication I

Mohan, M. K.; Silenko, O.; Krasnou, I.; Volobujeva, O.; Kulp, M.; Ošek, M.; Lukk, T.; Karpichev, Y. Chloromethylation of Lignin as a Route to Functional Material with Catalytic Properties in Cross-Coupling and Click Reactions. *ChemSusChem* **2024**. <https://doi.org/10.1002/cssc.202301588>.

Reprinted with permission from John Wiley and Sons.





# Chloromethylation of Lignin as a Route to Functional Material with Catalytic Properties in Cross-Coupling and Click Reactions

Mahendra K. Mohan,<sup>[a]</sup> Oleg Silenko,<sup>[a, b]</sup> Illia Krasnou,<sup>[c]</sup> Olga Volobujeva,<sup>[c]</sup> Maria Kulp,<sup>[a]</sup> Maksim Ošeka,<sup>[a]</sup> Tiit Lukk,<sup>[a]</sup> and Yevgen Karpichev<sup>\*[a]</sup>

We present a novel, greener chloromethylation procedure for organosoluble lignin under mild reaction conditions without Lewis acid as a catalyst and in acetic acid as a solvent. This synthetic protocol provides a reliable approach to chloromethylated lignin (CML) and means to obtain valuable lignin derivatives. The resulted CML was subsequently transformed into 1-methylimidazolium lignin (ImL), which effectively serves as a stabilizing agent for Pd/CuO nanoparticles (Pd/CuO–NPs). To evaluate the versatility of developed lignin-based catalyst, we investigate its performance in a series of carbon-carbon bond formation reactions, including Suzuki-Miyaura, Sonogashira, Heck reactions, and azide-alkyne cycloaddition (click) reaction. Remarkably, this catalyst exhibited a high degree of

catalytic efficiency, resulting in reactions with yields ranging from average to excellent. The heterogeneous catalyst demonstrated outstanding recyclability, enabling its reuse for at least 10 consecutive reaction cycles, with yields consistently falling within the range of 42% to 84%. A continuous flow reactor cartridge prototype employing Lignin@Pd/CuO–NPs was developed, yielding results comparable to those achieved in batch reactions. The utilization of Lignin@Pd/CuO–NPs as a catalyst showcases its potential to facilitate diverse carbon-carbon bond formation reactions and underscores its promising recyclability, aligning with the green chemistry metrics and principles of sustainability in chemical processes.

## Introduction

Advances in environmental materials are described with a focus on the utilization of natural resources and their waste. The development of green technologies and processes is a key to a sustainable society,<sup>[1]</sup> highlighting importance of the bio-based industries to replace the existing, non-renewable raw materials for fuel, energy, and manufacturing.<sup>[2]</sup> Strategies to transform biomass into useful products must be accomplished with appropriate standards to ensure their sustainability, in alignment with the Sustainable Development Goals of the United Nations.<sup>[3,4]</sup>

Lignin, the second most abundant biopolymer on Earth and the main byproduct of the cellulose industry is a global source of renewable aromatics that offers the possibility of replacing fossil-based aromatic compounds.<sup>[5]</sup> Currently, lignin is generally

considered just a by-product of pulp production, and up to 100 Mt of it is produced worldwide each year. Since effective methods for its processing have not been developed, around 95% of industrial lignin is burned as fuel.<sup>[6]</sup> However, its abundance in nature could potentially solve the problem of the rapidly depleting fossil-based resources if it was successfully translated into a renewable resource or valorized to higher value materials. In recent years, advanced lignin modification chemistry has generated a number of functional lignin-based polymers that integrate both the intrinsic features of lignin and additional properties of the grafted polymers.<sup>[7]</sup> Lignin is an underestimated green chemistry material that could be a promising base for developing a fabrication process for materials with advanced properties.<sup>[8–10]</sup>

Two generalized approaches to using lignin as a starting material can be considered: downstream fragmentation or depolymerization to obtain platform chemicals, and chemical transformation chains to functionalize lignin and expand its potential in real-life applications.<sup>[11]</sup> Chloromethylation is a basic organic chemistry reaction that opens wide opportunities for further functionalization of natural raw materials. Interest in this reaction was boosted in 2022 when the US Environmental Protection Agency Green Chemistry Award was given for the development of the greener chloromethyl furfural synthesis, a chemocatalytic approach to biorefining in pulp production and building multifunctional chemical platforms.<sup>[12]</sup>

Lignin's complex structure limits its use in high-end applications, but modification can overcome this limitation and expand its range of applications. Typically, modification involves modifying chemically active sites or increasing the reactivity of

[a] M. K. Mohan, O. Silenko, M. Kulp, M. Ošeka, T. Lukk, Dr. Y. Karpichev  
Department of Chemistry and Biotechnology, Tallinn University of Technology (TalTech), Akadeemia tee 15, 12618 Tallinn, Estonia  
phone: +372 620 4381  
fax: +372 620 2994  
E-mail: yevgen.karpichev@taltech.ee

[b] O. Silenko  
Institute of Organic Chemistry, National Academy of Science of Ukraine,  
5 Akademika Kukharis Str., 02094, Kyiv, Ukraine

[c] I. Krasnou, O. Volobujeva  
Department of Materials and Environmental Technology, Tallinn University  
of Technology (TalTech), Ehitaajate tee 5, 19086, Tallinn, Estonia

Supporting information for this article is available on the WWW under  
<https://doi.org/10.1002/cssc.202301588>

both aromatic and aliphatic hydroxyl groups. However, this strategy only aims to produce more efficient, more reactive macromonomers. Although the Blanc reaction, a chemical method to form chloromethyl arenes with formaldehyde and hydrogen chloride catalyzed by Lewis's acids has been widely used for about 100 years,<sup>[13]</sup> to the best of our knowledge, no evidence of its successful application in lignin modification can be found in the literature. However, chloromethylation without a Lewis acid was reported for a model compound for syringyl unit of lignin, 3,5-dimethyl-4-hydroxyphenyl ethane<sup>[14]</sup> and for aromatic macrocycles, calix[4]arenes.<sup>[15]</sup>

Chloromethylation of lignin may lead towards simple, convenient, and sustainable protocols for preparation of functional materials from biomass, including catalysts. In the past decades, protocols for cross-coupling reactions have improved significantly. The Suzuki-Miyaura coupling is one of the most effective, powerful, and versatile reactions for forming carbon-carbon bonds.<sup>[16]</sup> Cross-coupling reactions typically use homogeneous Pd/ligand catalysts with phosphines or other organic compounds as ligands in organic solvents, which can make them economically challenging and environmentally harmful. Homogeneous catalysis is limited by expensive, non-reusable metal catalysts and ligands, slow and expensive purification of contaminated products, and the rare use of heterogeneous catalysts for C–C coupling reactions. In the past 15 years, N-heterocyclic carbenes (NHCs) have gained recognition as ligands for Pd-mediated cross-couplings. With NHCs' robust electron-donating capabilities, oxidative insertion is possible even on challenging substrates and their steric size and distinctive structure facilitate rapid reductive elimination.<sup>[17]</sup> Compared with established phosphine ligands, carbenes with bulky ligands have produced substantial improvements in catalyst efficiency<sup>[18]</sup> but demand effective heterogenization to meet the needs of many applications.<sup>[19,20]</sup> Despite existing

methods for synthesizing Pd nanoparticles from plant extracts, stabilizing agents have not been explicitly explored.

The chemical structure of lignin originates from three hydroxycinnamyl alcohols, known as monolignols: *p*-coumaryl alcohol, coniferyl alcohol, and sinapyl alcohol. These alcohols differ solely in the degree of methoxylation at the C3 and C5 positions of the aromatic ring. In essence, the *p*-hydroxyphenyl (H-unit) lacks methoxy groups at carbon C3 and C5 of the aromatic ring, the guaiacyl (G-unit) features a methoxy group at carbon C3, and the syringyl (S-unit) presents methoxy groups at carbon C3 and C5, see Figure 1.<sup>[21]</sup> In softwoods, lignin is predominantly composed of coniferyl alcohol (95 %), with minimal presence of *p*-coumaryl and sinapyl alcohols. Hardwoods exhibit a more balanced distribution coniferyl and sinapyl alcohols, and a minor proportion of *p*-coumaryl alcohol. Grassy biomasses display a diverse composition, featuring a range of percentages for *p*-coumaryl, coniferyl, and sinapyl alcohols. These variations highlight the unique biochemical profiles of different plant species, contributing to the diversity in lignin composition and structure across plant types.<sup>[22]</sup> Based on <sup>31</sup>P NMR, our recent study delineated the distribution of monolignols across various biomasses revealed a higher S/G ratio in hardwoods (aspen) when compared to softwoods (pine), whereas lignins derived from grass (barley straw) biomass encompass all three components (H-, G-, and S-units).<sup>[23]</sup>

In this study, we report the green protocol for chloromethylation of organosolv aspen lignin to prepare chloromethylated lignin (CML), a versatile product for various functional materials. The CML was further modified by 1-methylimidazole to stabilize Pd/CuO. The Lignin@Pd/CuO–NPs catalyst was employed to explore a range of C–C bond formation reactions, including Suzuki-Miyaura, Sonogashira, Heck reactions and azide-alkyne cycloaddition (click) reaction. The reuse of the catalyst in batch

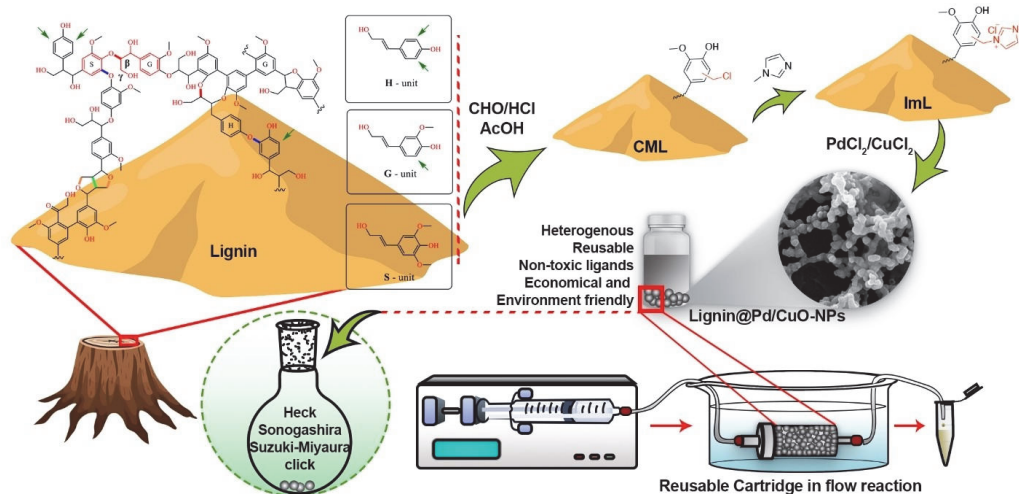


**Figure 1.** Modification of organosolv aspen lignin via chloromethylation and further preparation of Lignin@Pd/CuO–NP catalyst to use in C–C bond formation reactions and azide-alkyne cycloaddition (click) reaction in batch and in the packed-bed flow reactor.

and its application in the packed-bed flow reactor were developed, see Figure 1.

## Experimental Methods

### Materials and methods

All the reagents were used of analytical reagent (AR) grade without any further purification. Organosolv lignin was obtained from the aspen wood chips (provided by Estonian Cell AS) by extraction in EtOH according to the previously described procedure.<sup>[23]</sup> Reagents and solvents were purchased from Sigma-Aldrich (Taufkirchen, Germany). All the chemicals were of analytical grade and used as received. Deionized water from a Milli-Q water purification system (Millipore S.A., Molsheim, France) was used throughout the study.

The NMR spectra were recorded by Bruker Avance III 400 MHz spectrometer; MestReNova x64 software was used to analyse the <sup>1</sup>H spectra and contours in 2D HSQC plots. The FT-IR was recorded by a Shimadzu IRTTracer-100 spectrometer (Kyoto, Japan) as used; KBr pellets were used to prepare the samples at 1% weight by weight with a resolution of 2 cm<sup>-1</sup> and 80 scans. All samples within the 400–4,000 cm<sup>-1</sup> range were analysed using Shimadzu Lab Solutions software. The surface morphology was performed with a high-resolution scanning electron microscope HR-SEM Zeiss Merlin (Germany). Measurements were made at an operating voltage of 7 kV. The chemical composition was determined using an energy dispersive X-ray analysis (EDS) Bruker EDX-XFlash6/30 detector system (USA) (operating voltage 7 kV and the concentrations of elements were calculated by using PB-ZAF standardless mode) and Elementar vario MICRO cube (USA) (operating mode: CHNS mode). Gas chromatography (GC) performed on an Agilent Technologies 7890 A GC system (USA) equipped with an ultra-inert split liner (Agilent Technologies, type 5190–2293) and ZB-5MSi capillary column (30 m\*250 μm\*0.25 μm) using helium as carrier gas at a constant flow rate of 1.3 mL/min.

Size exclusion chromatography (SEC) was employed to determine the weight-averaged molecular weight (MW) and molecular weight distributions (MWD) of lignin samples. The MW data were correlated with calibration standards of known MW. For analysis, lignin samples were dissolved in tetrahydrofuran (THF) at a concentration of 1 mg/mL and subjected to examination using a Prominence LC-20 A Modular HPLC System (Shimadzu, Japan) equipped with a photodiode array detector. The chromatographic columns consisted of a pair of Agilent MesoPore columns with dimensions 300 mm x 7.5 mm, 3 μm, and a guard column of the same material with dimensions 50 mm x 7.5 mm (Agilent Technologies). Elution was carried out at 40 °C with a flow rate of 1 mL/min

using THF stabilized with 250 ppm butylated hydroxytoluene (BHT); detection was performed at 254 nm. The system calibration was executed using polystyrene GPC/SEC calibration standards (EasiVial PS–L, Agilent Technologies). The parameters of Mp, number-averaged molecular weight (Mn), MW, and polydispersity (MW/Mn) were determined using the Lab Solutions software (Shimadzu).

Differential scanning calorimetry (DSC) was performed with a Perkin Elmer Diamond DSC calorimeter (USA) at a scanning rate of 1 °C/min in nitrogen atmosphere (purge at 20 mL/min). A sample weight of 3.00 ± 0.02 mg was used for all materials to avoid variations in thermal properties. Powdered samples were pressed into the aluminium cup to improve contact between the material and the heating furnace. The elemental analysis was performed using Elementar vario MICRO cube (USA) in CHNS mode with 2 mg of sample weighed for one run. Metal content of Pd and Cu was determined by flame atomic absorption spectrometer Varian SpectraAA 220FS instrument (USA). Organic chlorine content in CML samples was analysed by means of Bruker S4 Pioneer XRF spectrometer (USA) using precalibrated MultiRes measurement method. For sample preparation, the dilution method was used with 1:10 sample to NaHCO<sub>3</sub> ratio.

### Procedures of lignin modification

#### Chloromethylation of organosolv lignin

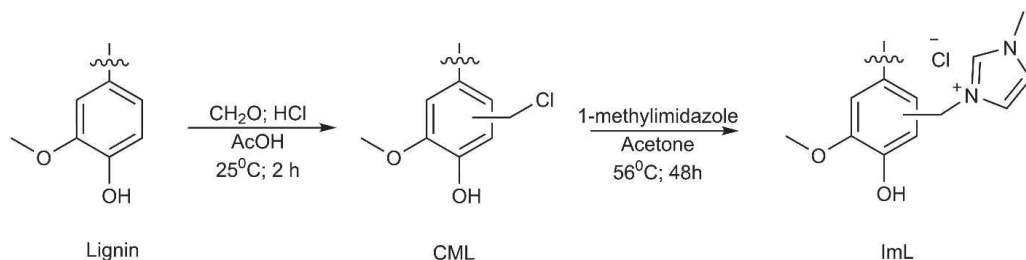
1 g of organosolv lignin and 1 g of paraformaldehyde (PFA) were dissolved in 10 mL of glacial acetic acid (AcOH), then bubbled with HCl gas for 2 h (see Scheme 1); the reaction was stopped by adding 30 mL of water. The crude CML product was filtered off, washed with water, and dried *in vacuo* (yield 1.2 g). The conversion into chloromethylated product was monitored by organic chlorine content analysis.

#### Preparation of 1-methylimidazolium-functionalized (ImL)

1 g of 1-methylimidazole was added dropwise to a solution of 1 g of CML in 20 mL in acetone. The reaction mixture was heated while stirring at 56 °C (see Scheme 1). After 48 h, the precipitate was filtered and washed with 10 mL of 70% ethanol/water mixture and dried *in vacuo*. Only the precipitated and washed product (yield 350 mg) was chosen for characterization and further functionalization.

#### Preparation of Lignin@Pd/CuO–NP

20 mg of ImL were dissolved in 2 mL of ethanol at 70 °C for 10–20 minutes. When the solution became transparent, 2 mL of



**Scheme 1.** Chemical transformation of lignin into 1-methylimidazolium-functionalized product (ImL) via chloromethylation and amination stages, envisaged for G unit.

0.9 mM of  $\text{CuCl}_2$ /0.1 mM  $\text{PdCl}_2$  were added and the whole reaction mass was stirred for 30 min at 70 °C. The  $\text{NaBH}_4$  (2 mM) were added, and the reaction mixture kept stirring for 12 h at ambient temperature. The color of the reaction mixture will change from brown to black as nanoparticles form. The mixture was centrifuged at 7000 rpm for 30 min, washed 3 times with water/ethanol, and dried.

#### Metal leaching from Lignin@Pd/CuO–NP

50 mg of Lignin@Pd/CuO–NP was suspended in 50 mL of EtOH at 50 °C for 30 days. The filtrate was collected at two different time points (15 days and 30 days) and quantified using flame atomic absorption spectrometry.

#### Reactions in Batch and Packed-Bed Flow Procedure for the cross-coupling reactions in batch

Reactions were performed with 1 eq. of 4-bromotoluene, 1.5 eq of phenylboronic acid/styrene/phenylacetylene, 3 eq of  $\text{K}_2\text{CO}_3$ , and 0.5 mg catalyst at 50 °C in EtOH for 14 h; yield was calculated using GC–MS. After filtering, the catalyst was washed several times with water and ethanol, dried, and reused in up to 10 batches of the same reactions.

#### Procedure for the click reaction in batch

The azide-alkyne cycloaddition reaction was performed with 1 eq of phenylacetylene, 1.5 eq of benzyl azide, and 0.5 mg catalyst at 40 °C in EtOH for 5 h; yield was calculated using GC–MS. After filtering, the catalyst was washed several times with water and ethanol, dried, and reused in up to 10 batches of the same reactions.

#### Designing cartridge for continuous flow reaction

A mixture of 50 mg catalyst and 200 mg Celite was used to fill the cartridge of 1 cm inner diameter and 1 cm of loading height, see Figure 2, according to the guidance reported previously for Pd/C packed-bed reactor in flow.<sup>[24]</sup> Tests were performed to determine the possible metal leached from the cartridge after (i) a fraction of the initial solvent passed through it and (ii) the reaction product were collected.

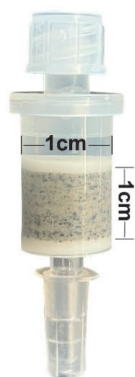


**Figure 2.** Packed-bed flow reactor cartridge loaded with Lignin@Pd/CuO–NP catalyst.

#### Reaction in the packed-bed flow reactor

The reaction mixture for click reaction was prepared from phenylacetylene (1.25 mmol, 125 mg, 1 equiv.) and benzyl azide (1.875 mmol, 244 mg, 1.5 equiv.) in 25 mL volumetric flask filled with EtOH (0.05 M). The KD Scientific syringe pump (USA) was used to pump the reaction mixture at 0.1 mL/min flow rate through the cartridge loaded with Lignin@Pd/CuO–NP placed in a water bath at 40 °C. Similarly, the Suzuki–Miyaura reaction mixture was prepared in MeOH (0.0146 M) with 62.5 mg of 4-bromotoluene (0.365 mmol, 62.5 mg, 1 equiv.), 89.1 mg of phenylboronic acid (0.730 mmol, 89 mg 2 equiv.) and 59.6 mg of sodium acetate (0.730 mmol, 60 mg, 2 equiv.) in a 25 mL volumetric flask. The KD Scientific syringe pump was used to pump the reaction mixture through the catalyst-filled cartridge placed in a water bath at 0.016 mL/min flow and 50 °C. The yields were calculated using GC–MS.

## Results and Discussions

To introduce chemical active sites into lignin's complex structure, different chemical modifications have been published in recent years,<sup>[10]</sup> albeit less thoroughly than hydroxyl group modifications. These modifications include, in essence, nitration,<sup>[25]</sup> amination,<sup>[26]</sup> alkylation/dealkylation,<sup>[27]</sup> hydroxylation,<sup>[14]</sup> carboxylation, and halogenation.<sup>[28]</sup> To identify more efficient and greener chloromethylation protocol for lignin, two conditions of Blanc reaction implied to organosolv aspen lignin were studied, both shown to be applicable for small aromatic molecules<sup>[29,30]</sup> and for aromatic macrocycles, calix[4]arenes.<sup>[15,31,32]</sup> Our study demonstrates that the route with dichloromethyl ether and  $\text{TiCl}_4$  as Lewis acid catalyst in chloroform can hardly be applicable for lignin, yielding only 1.5% (m/m) of organic chlorine in the final product, see Table S1. The reaction route involving PFA and excess of hydrogen chloride in AcOH as a solvent resulted in 20% (m/m) of organic chlorine in the final product. This developed greener route (see green chemistry metrics section below) for obtaining CML yielding about an order on magnitude higher content of chloromethylated product, according to the organic chlorine analysis (see Table S1). The new protocol of CML preparation was optimized and chosen for scaling up and further transformation towards functional materials studied in this work, e.g. towards lignin-based NHCs for Pd-mediated cross-coupling reactions.

#### Characterization of CML

A new peak at 4.5–4.75 ppm appears in the  $^1\text{H}$  NMR spectra of the CML product (Figure S2, b) compared to organosolv lignin (Figure S2, a), which confirms the presence of  $-\text{CH}_2-\text{Cl}$  group on the benzene ring. The HSQC signal at (4.63, 40.87) (Figure S3) shows a new C–H bond formation that confirms chloromethylation. Distinctive signals indicative of distal chloromethylated lignin were identified in the NMR spectra, confirming the chloromethylation on the aromatic ring similarly to reported in the literature.<sup>[33,34]</sup> It was reported that the in-plane stretching vibration of  $\text{CH}_2(\text{CH}_2\text{Cl})$  was responsible for

$\text{CH}_2(\text{CH}_2\text{Cl})$ 's absorption peak at  $1415\text{ cm}^{-1}$ .<sup>[35–37]</sup> Due to the electron withdrawal effect of Cl, the peak vibration is shifted to a lower frequency. A characteristic peak of  $-\text{CH}_2\text{Cl}$  can be seen at  $1269\text{ cm}^{-1}$  and  $644\text{ cm}^{-1}$  (Figure S3). The absorption peak observed at  $1269\text{ cm}^{-1}$  corresponds to the in-plane stretching vibration of C–H in 1,2,4-substituted benzene.<sup>[38]</sup> The XRF method revealed that the chloromethylated product contained 20% organic chlorine. However, chloromethylation can happen in any of the phenolic rings. Chemical modification reported in literature demonstrates that it can occur at *ortho*-position adjacent to the hydroxy group<sup>[39]</sup> but also even at *meta*-position of the syringyl unit of lignin, specifically 3,5-dimethyl-4-hydroxyphenyl ethane.<sup>[40]</sup> Given the polymeric nature of lignin and the available data, our suggestion is that chloromethylation may result in multiple substitutions per monomer unit and consequently contributing to the elevated chlorine content.

The SEC results show that the molecular events that occurred during the reaction process, led to the form of the heterogeneous lignin, see Table S2, Figure S1. The higher polydispersity index (PI) value for CML sample indicates a broader molecular weight distribution compared to the starting material. The ethyl ester of *p*-coumaric acid was shown recently to be a primary low molecular weight species identified occurring along at ethanosolv extraction from aspen.<sup>[41]</sup> As far as the high molecular weight species are concerned, condensation reactions with non-stabilized organosolv lignins that have not been stabilized can appear.<sup>[42]</sup> The sharp peak at ca. 10 minutes aligns with the exclusion limit of the column, thus containing a broad range of molecular weights appeared as a sharp compressed peak. This would indicate that some lignin crosslinking occurred during chloromethylation, following side reaction with formaldehyde as a reagent. The low molar mass fragments appeared only after the chloromethylation (big peak at 16.5 min on the SEC of chloromethylated lignin, Figure S1). This can be due to acid-induced cleavage of lignin inter-unit linkages during chloromethylation reaction. Likewise, we suppose potential presence of side products or lignin fragments post-chloromethylation. Yet, given their origin from lignin sources, our objective remains centered on utilizing the entirety of the lignin, despite the similarity in molecular weight among the various lignin types.

### Characterization of 1-methylimidazolium-functionalized lignin (ImL)

The bands at  $3000\text{--}2800\text{ cm}^{-1}$  in FT-IR spectrum confirm that the presence of N–H stretching from the imidazolium salt and the bands at  $1250\text{--}1020\text{ cm}^{-1}$  are associated with the C–N stretching from the ImL, see Figure S5. The new peaks at 5.49 ppm and 3.89 ppm in the  $^1\text{H}$  NMR spectra confirm  $\text{NCH}_2\text{Ph}$  and  $\text{NCH}_3$ , respectively (Figure S7). Peaks at 9.04 ppm and 7.6 ppm correspond to imidazolium  $-\text{CHs}$ . Nitrogen content in amino lignin is 4.65%, according to elemental analysis, in contrast to starting CML showing only 0.01% of Nitrogen content. It is noteworthy that a portion of dissolved lignin in the reaction solvent is observed or lost during this process. We

suggest that this phenomenon may contribute to the discrepancy in nitrogen content. The reported nitrogen content is specifically applicable to isolated products.

### Characterization of Lignin@Pd/CuO nanoparticle

Palladium catalysts commonly employed to transform C–H bonds into C–C bonds, come with significant cost and safety concerns and are criticized as regards to the effective circular economy strategies.<sup>[43]</sup> Excluding platinum-group metal based catalysts, minimizing use of Endangered & Critical Elements (those will face supply limitations in the coming years)<sup>[44]</sup> and the metals with low Chemical Element Sustainability Index<sup>[45]</sup> combined with maximizing resource efficiency increases demand of copper, iron, or manganese as more affordable catalysts. Among the transition metals, copper stands out for its versatile catalytic properties, making it particularly appealing. Therefore, there is a pressing need to devise a more efficient and user-friendly approach that minimizes or eliminates the reliance on non-sustainable metals in heterogeneous coupling reactions. In contrast to the previously reported examples on using lignin or plant-based stabilizing agent for the Pd catalyst,<sup>[46–50]</sup> our approach included preparation of the Pd/CuO heterogeneous catalyst with lower content of the non-sustainable noble metal (Pd)<sup>[44]</sup> and with potential to catalyse broader spectrum of the chemical reactions.

The SEM image of the Lignin@Pd/CuO confirms that the Lignin@Pd/CuO–NPs have an average size of 40 nm, Figure 3a. According to EDS results, the elemental composition of the catalyst is 2.384% Pd (w/w) and the 3.047% Cu (w/w) loaded on modified lignin along with O, N, and C, Figure S9.

### Lignin@Pd/CuO–NPs leaching study

An investigation has been performed to study the level of Pd/Cu leach in the solution. Pd/Cu concentration (w/w) in the treated ethanol will indirectly indicate the structural stability of Lignin@Pd/CuO–NPs under conventional batch reaction. The test was conducted for continues 30 days under conventional mechanical stirring at  $50^\circ\text{C}$ . Figure 3b shows that after 15 days of the studies only 0.015% of Cu and 0.0728% of Pd were detected in the solution. Further completion of the 30 days, 0.011% of Cu and 0.012% of Pd were detected to leach from 3.047% of Cu and 2.384% of Pd presented in starting Lignin@Pd/CuO–NP material.

As expected, the concentration of Pd/Cu ions in the solutions is minimal. Moreover, the Pd/Cu ions concentration in the collected fraction from the cartridge and the product was below 0.002%, which is, in the case of copper, lower than reported  $\text{L(E)C}_{50}$  values for environmentally relevant organisms<sup>[51]</sup> and less than is has been stated for commercially available Cu-containing catalysts.<sup>[52,53]</sup>

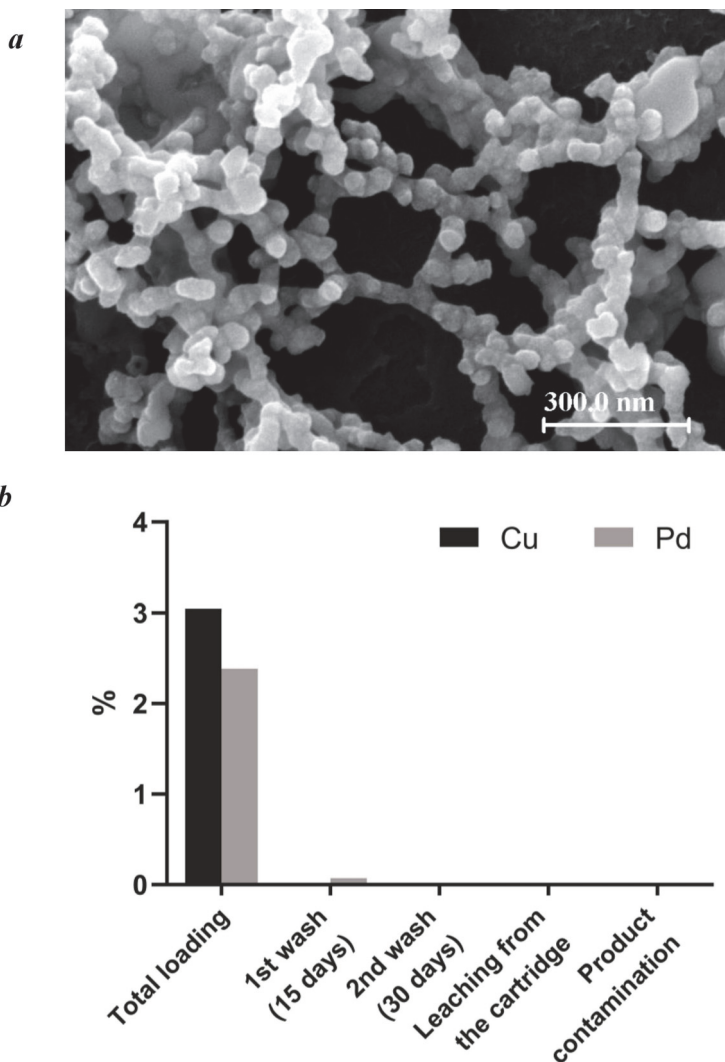


Figure 3. Characterization of Lignin@Pd/CuO-NP material. (a) SEM image; (b) Pd/Cu leaching determined by AAS.

### Thermal Properties

The thermal properties of the CML and starting organosolv lignin are similar; materials have glass transition temperature ( $T_g$ ) near 70 °C, which is typical for chemically modified lignin.<sup>[54]</sup> The glass transition step in DSC curves is distorted, probably due to the heterogeneity of the material, see Figure S8. Two enthalpy recovery peaks are present at the heating curve of organosolv lignin; those may occur due to the aging of the material upon heating. Similar observations were reported in literature for fatty acid-esterified lignin.<sup>[55]</sup> The slightly lower glass transition and onset temperatures for CML may be due to a partial depolymerization of lignin.<sup>[56,57]</sup> The introduction of 1-

metylimidazole fragment seemed to enhance hydrogen bonding in ImL and induces sheet-like structure formation.<sup>[58]</sup> Consequent incorporation of metal nanoparticles improves the structural stability what results in appearance of remarkable glass transition peak for Lignin@Pd/CuO-NP material on the DSC curve (Figure S8) and increasing  $T_g$  up to 89.9 °C. The structural stabilization effect correlates well with the results of SEM imaging, where distinct uniform nanoscale structures were found.

### Evaluation of the catalytic activity of Lignin@Pd/CuO-NPs in batch reaction

In the formation of C–C bonds, Suzuki-Miyaura coupling has proven to be one of the most effective, powerful, and versatile reactions.<sup>[16,46,59]</sup> Using Lignin@Pd/CuO-NPs, we assessed their catalytic activity for the Suzuki-Miyaura, Sonogashira, and Heck reactions, as well as azide-alkyne cycloaddition (click) reaction. The catalytic activity was maximum for the click and the Suzuki-Miyaura reaction, see Table 1. The catalytic efficacy for all the reactions remained comparable or same for up to 10 cycles with the catalyst recovered after each run.

### Evaluation of catalytic efficacy in packed-bed flow reactor

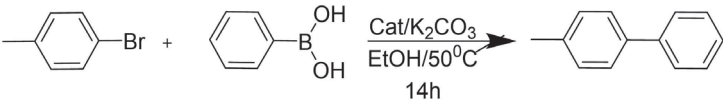
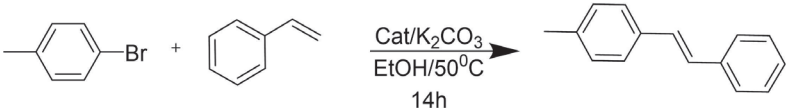
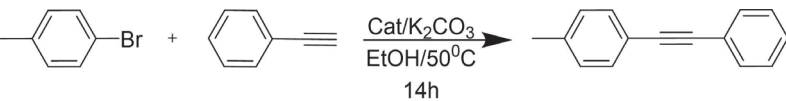
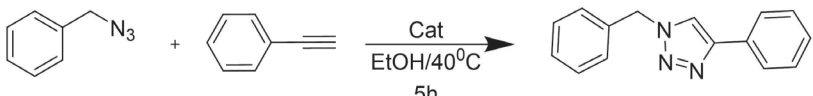
Flow chemistry techniques have attracted significant interest to satisfy the growing demand for chemical sustainability by reducing amount of reagents and materials, optimize use of energy, and enhance process safety.<sup>[60]</sup> The click reaction was studied in flow by pumping the reaction mixture [phenylacetylene (1 equiv.), benzyl azide (1.5 equiv.), EtOH (0.05 M)] continuously through the cartridge using a syringe pump at 0.1 mL/min flow rate, see Scheme 2 (top). The experiment was carried out at 40 °C and 50 mg of supported catalyst allowed us to detect up to 74% yield. The reaction was then scaled up by preparing a larger volume of the reaction mixture and pumping

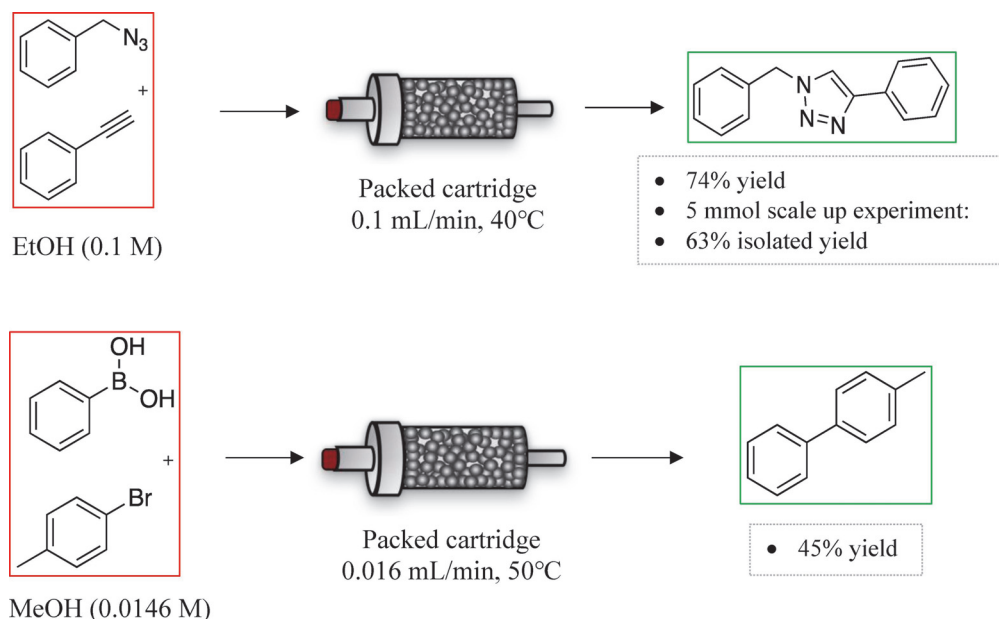
it for 16 h 40 min at the same conditions, which corresponds to 5.0 mmol scale, providing the product in 63% (0.74 g) isolated yield. Although the click reaction was very efficient under the established conditions, the Suzuki-Miyaura reaction was much slower and required longer reaction time achieved by lower flow rate and dilution, see Scheme 2 (bottom). The coupling product was detected in up to 45% yield, when the mixture [4-bromotoluene (1 equiv.), phenylboronic acid (2 equiv.), sodium acetate (2 equiv.), MeOH (0.0146 M)] was pumped at 0.016 mL/min flow rate and 50 °C.

### Green chemistry metrics

CHEM21 toolkit by Clark et al.<sup>[61]</sup> (see Supporting Information) was used for evaluation of the parameters shown in Table 2. To evaluate the atom economy (AE) parameter for reaction involving lignin, a polymer with an average molecular weight, we have considered the guaiacyl lignin monomer unit (G-unit) to use as a part of the green chemistry metric, to enhance our comprehension, see Supporting Information. Method 1 (CML protocol developed in this work) outperforms the method 2 (CML–TiCl<sub>4</sub>, a Blanc reaction procedure with Lewis acid as a catalyst) in terms of yield, selectivity, atom economy, and overall efficiency. However, both processes have room for improvement in conversion rates and reaction mass efficiency, and method 2 specifically needs attention to reduce its environmental impact, especially regarding the use of reaction solvents and reagents (red flag). In the proposed synthetic method 1 we

**Table 1.** Conditions, schemes, and yields for the studied reaction in batch.

Reaction	Yield from freshly prepared catalyst, %	Yield from 1 <sup>st</sup> time recovered catalyst, %	Yield from 5 <sup>th</sup> time recovered catalyst, %	Yield from 10 <sup>th</sup> time recovered catalyst, %
	61	68	64	72
	44	42	48	47
	45	47	44	41
	80	84	75	72



**Scheme 2.** The azide-alkyne cycloaddition (click) reaction (top) and cross-coupling (Suzuki-Miyaura) reaction (bottom) scheme in the packed-bed flow reactor.

**Table 2.** Green Chemistry metrics calculated for the processes studied (1–7).

Method No.	Method	Yield	Conversion	Selectivity	AE	RME	OE	PMI (total)	PMI Reaction	PMI reactants, reagents, catalyst	PMI reaction solvents
1	CML	20	20	99.9	92.5	12.7	13.7	286.6	168.8	126.5	41.5
2	CML-TiCl <sub>4</sub>	1.2	1.5	78.9	61.7	0.8	1.2	7899.6	4840	866.7	3973.3
3	ImL (Dioxan)	100	100	100	100	68	68	24.2	16.6	1.5	15.1
4	ImL (Acetone)	99.8	100	99.8	100	68	67.9	19.3	13	1.5	11.5
5	ImL (Me-THF)	99.8	100	99.8	100	68	67.9	20.3	14	1.4	12.6
6	Suzuki-Miyaura reaction (batch)	65	66	98.5	57.7	31.9	55.3	279.1	279.1	40	239.1
7	Suzuki-Miyaura reaction (flow)	43.8	45.0	97.3	57.7	45	78	710.1	710.1	6.1	704.0
8	Click reaction (batch)	51	70	72.9	100	69	69	90.6	90.6	1.5	89.2
9	Click reaction (flow)	62.9	62.9	100	100	56.6	56.6	457.8	108.5	1.8	106.6

used more favorable from a green chemistry point of view solvents, which have better yields and had a positive impact on the overall green metrics and, thus, is greener (Table S3). The reactions did not use critical elements (with 5–50 years supply remaining).<sup>[44]</sup>

Analysis of the process mass intensity (PMI) parameters has demonstrated that a major contribution to the total PMI is contributed by the PMI (reaction solvents), with about two orders of magnitude more unfavorable for method 2 compared to method 1. The analysis of PMI helps to determine reaction solvents as one of the problematic issues of the synthetic procedure. Among solvents used for reactions and workup, the

“recommended” solvents (green flag) were used – water, EtOH, and AcOH. It should be noted that in this work the AcOH was considered as “recommended or problematic” as mentioned in the CHEM21 toolkit,<sup>[61]</sup> although AcOH, along with several “intermediate” solvents, was criticized to be claimed as a “recommended” because of its unfavorable health score, and ranked as “problematic” by default.<sup>[10,62]</sup> Energy parameters were marked with a green flag (reaction run between 0 to 70 °C).

Optimisation of the preparation for ImL (method 3 in Table 2) included comparison of three solvents, dioxane, acetone, and 2-methyltetrahydrofuran (Me-THF) classified on the different scores in the range from “problematic” to

"recommended".<sup>[62]</sup> Despite its high yield, use of dioxane (method 3 in Table 2) as a reaction solvent is classified as hazardous in terms of safety and health. In order to minimize the hazards associated with the ImL reaction, acetone and Me–THF were proposed as alternative solvents (see Table S4).

Preparation of ImL (methods 3–5), azide-alkyne cycloaddition (click) reaction both in batch (method 8) and in continuous flow (method 9), and the cross-coupling (Suzuki-Miyaura) reaction in batch (method 6) are the most efficient and environmentally friendly processes among the five methods analyzed. The cross-coupling (Suzuki-Miyaura) reaction in flow (method 7) shows moderate efficiency but may benefit from optimization in various aspects, including atom economy, waste reduction, and overall efficiency. The transition from batch reactions (methods 6 and 8) to continuous flow reactions (methods 7 and 9, correspondingly) signifies an upgrade from amber to green status in terms of process sustainability. These findings can guide efforts to optimize these chemical processes for improved sustainability and efficiency. Ultimately, the choice of solvent and reagents in a chemical process should be made with careful consideration of these factors to strike a balance between high yield and minimal impact on safety, health, and the environment.

## Conclusions

In adherence to the principles of green chemistry, we have achieved the successful synthesis of Pd/CuO-coordinated imidazolium lignin via a pioneering chloromethylation process applied to organosolv aspen lignin. This lignin-based catalyst Lignin@Pd/CuO–NPs offers distinct advantages over conventional alternatives, including ease of synthesis, heterogeneity, recoverability, and recyclability. The characterization of the modified lignin was substantiated through a comprehensive array of analytical techniques, encompassing Fourier-transform infrared spectroscopy (FTIR), size exclusion chromatography (SEC), nuclear magnetic resonance (NMR), elemental analysis (EA) for nitrogen content, and X-ray fluorescence (XRF) for organic chlorine content. Scanning electron microscopy (SEM) was employed to validate the morphology of the Lignin@Pd/CuO–NPs catalyst. The efficacy of the Lignin@Pd/CuO–NPs catalyst in facilitating diverse C–C bond formation reactions, including Suzuki-Miyaura, Sonogashira, and Heck reactions as well as azide-alkyne cycloaddition (click) reaction was demonstrated. The heterogeneous catalyst demonstrated robust recoverability and the ability to be reused across multiple consecutive batches. A reusable cartridge for the continuous flow reactor was designed, the catalytic activity under conditions of minimal catalyst loading was evaluated, and reaction times in flow were optimized to carry out studied processes without compromising chemical yield of the reaction. A thorough analysis of green chemistry metrics throughout the entire process of the preparation and use of the novel catalytic material was performed. These findings serve as valuable guidance for optimizing chemical processes, ranging from lignin

modification to the advancement of sustainable applications, in line with the principles of green chemistry.

## Supporting Information

The following files are available free of charge:

Organic chlorine content in CML products

Size exclusion chromatography for studied CML

<sup>1</sup>H and HSQC NMR spectra of CML

FT-IR spectra of CML and ImL products NMR spectrum of ImL

Thermal properties of studied lignin products

Elemental composition of Lignin@Pd/CuO–NP

Catalytic efficacy of Lignin@Pd/CuO–NPs in the packed-bed flow reactor

Schematic illustration of the comparison of methods using Green Chemistry tool

Excel toolkit files:

Green Chemistry metrics for chloromethylation process and amination procedure (zero pass and first pass)

Green Chemistry metrics for Suzuki-Miyaura and click reactions in batch and in continuous flow using Lignin@Pd/CuO–NP as a catalyst (zero pass and first pass)

## Abbreviations

AAS	Atomic Absorption Spectroscopy
AcOH	Acetic acid
CML	Chloromethylated Lignin
CHO	formaldehyde, HC I- Hydrochloric acid
DMSO	Dimethylsulfoxide
EA	Elemental analysis
EtOH	Ethanol
FT-IR	Fourier-Transform Infrared Spectroscopy
HPLC	High-Performance Liquid Chromatography
NaBH <sub>4</sub>	Sodium borohydride
NMR	Nuclear Magnetic Resonance
NPs	Nanoparticles
SEC	Size Exclusion Chromatography
SEM	Scanning Electron Microscopy
GCMS	Gas Chromatography Mass Spectrometry
PFA	paraformaldehyde
XRF	X-Ray Fluorescence.

## Author Contributions

The manuscript was written through contributions of all authors. All authors have given approval to the final version of the manuscript. Mahendra K. Mohan: Conceptualization; Methodology; Investigation (synthesis and characterization of studied compounds); Validation; Data curation; Visualization; Writing – Original draft preparation. Oleg Silenko: Conceptualization; Methodology; Investigation. Illia Krasnou: Investigation (thermal properties). Olga Volobujeva: Investigation (SEM). Maria Kulp: Investigation (GC-MS analysis, SEC, elemental analysis). Maksim Ošeka: Conceptualization (flow reaction); Resources; Writing– Reviewing and Editing. Tiit Lukk: Conceptualization, Methodology; Resources; Funding acquisition; Writing – Reviewing and Editing; Project administration. Yevgen Karpichev: Conceptualization, Methodology; Resources; Funding acquisition; Writing – Original draft preparation; Writing – Reviewing and Editing; Project administration.

## Acknowledgements

This research was funded by Estonian Research Council grants RESTA11 (for M.K.M., M.K., T.L., Y.K.), PSG828 (for M.O.) and COVSG5 (for M.K.M., O.S., Y.K.), and ERDF Dora Plus program (for O.S.). Authors express their appreciation to Siim Pajusaar for XRF experiment, and Marina Kudrjašova for valuable discussions on NMR data.

## Conflict of Interests

The authors declare no conflict of interest.

## Data Availability Statement

The data that support the findings of this study are available in the supplementary material of this article.

**Keywords:** Biomass valorization · Lignin · Chloromethylation · Heterogeneous catalysts · Continuous flow reactions

- [1] T. Kobayashi, L. Nakajima, *Curr. Opin. Green Sustain. Chem.* **2021**, *28*, 100439.
- [2] P. Anastas, M. Nolasco, F. Kerton, M. Kirchhoff, P. Licence, T. Pradeep, B. Subramaniam, A. Moores, *ACS Sustainable Chem. Eng.* **2021**, *9*, 8015–8017.
- [3] <https://www.un.org/sustainabledevelopment/sustainable-development-goals/>, n.d.
- [4] F. I. Gómez-Castro, C. Gutiérrez-Antonio, in *Biofuels and Biorefining*, Elsevier, **2022**, pp. 1–23.
- [5] C. Wang, S. S. Kelley, R. A. Venditti, *ChemSusChem* **2016**, *9*, 770–783.
- [6] R. Sun, *ChemSusChem* **2020**, *13*, 4385–4393.
- [7] D. Kai, M. J. Tan, P. L. Chee, Y. K. Chua, Y. L. Yap, X. J. Loh, *Green Chem.* **2016**, *18*, 1175–1200.
- [8] V. K. Thakur, M. K. Thakur, P. Raghavan, M. R. Kessler, *ACS Sustainable Chem. Eng.* **2014**, *2*, 1072–1092.
- [9] P. Jędrzejczak, M. N. Collins, T. Jesionowski, Ł. Klapiszewski, *Int. J. Biol. Macromol.* **2021**, *187*, 624–650.
- [10] B. Jacobs, Y. Yao, I. Van Nieuwenhove, D. Sharma, G.-J. Graulus, K. Bernaerts, A. Verberckmoes, *Green Chem.* **2023**, *25*, 2042–2086.
- [11] R. J. Khan, C. Y. Lau, J. Guan, C. H. Lam, J. Zhao, Y. Ji, H. Wang, J. Xu, D.-J. Lee, S.-Y. Leu, *Bioresour. Technol.* **2022**, *346*, 126419.
- [12] M. Mascari, *ACS Sustainable Chem. Eng.* **2019**, *7*, 5588–5601.
- [13] G. L. Blanc, *Bull. Soc. Chim. Fr.* **1928**, *33*, 313–319.
- [14] P. Truter, A. Pizzi, H. Vermaas, *J. Appl. Polym. Sci.* **1994**, *51*, 1319–1322.
- [15] V. Burilov, R. Garipova, E. Sultanova, D. Mironova, I. Grigoryev, S. Solovieva, I. Antipin, *Nanomaterials* **2020**, *10*, 1143.
- [16] A. Fihri, M. Bouhrara, B. Nekouishahraki, J.-M. Basset, V. Polshettiwar, *Chem. Soc. Rev.* **2011**, *40*, 5181.
- [17] S. P. Nolan, Ed., *N-Heterocyclic Carbenes*, Wiley, Weinheim, **2014**.
- [18] E. A. B. Kantchev, C. J. O'Brien, M. G. Organ, *Angew. Chem. Int. Ed.* **2007**, *46*, 2768–2813.
- [19] R. Narayanan, M. A. El-Sayed, *J. Am. Chem. Soc.* **2003**, *125*, 8340–8347.
- [20] Y. Huang, Z. Zheng, T. Liu, J. Lü, Z. Lin, H. Li, R. Cao, *Catal. Commun.* **2011**, *14*, 27–31.
- [21] R. Katakira, T. J. Elder, G. T. Beckham, **2018**, pp. 1–20.
- [22] M. N. Belgacem, A. Gandini, Eds., *Monomers, Polymers and Composites from Renewable Resources*, Elsevier, **2008**.
- [23] P. Jöul, T. T. Ho, U. Kallavus, A. Konist, K. Leiman, O.-S. Salm, M. Kulp, M. Koel, T. Lukk, *Materials* **2022**, *15*, 2861.
- [24] M. Ošeka, G. Laudadio, N. P. van Leest, M. Dyga, A. de A Bartolomeu, L. J. Goößen, B. de Bruin, K. T. de Oliveira, T. Noël, *Chem* **2021**, *7*, 255–266.
- [25] L. Zhang, J. Huang, *J. Appl. Polym. Sci.* **2001**, *80*, 1213–1219.
- [26] M. Arend, B. Westermann, N. Risch, *Angew. Chem. Int. Ed.* **1998**, *37*, 1044–1070.
- [27] Y. Liu, K. Li, *J. Adhes.* **2006**, *82*, 593–605.
- [28] S. Laurichesse, L. Avérous, *Prog. Polym. Sci.* **2014**, *39*, 1266–1290.
- [29] *Org. Synth.* **1956**, *36*, 50.
- [30] N. Maraš, *ChemSpider SyntheticPages* **2011**, 518.
- [31] R. V. Rodik, A.-S. Anthony, V. I. Kalchenko, Y. Mély, A. S. Klymchenko, *New J. Chem.* **2015**, *39*, 1654–1664.
- [32] T. Kim, *Synthesis of Calixcrown Derivatives for Immobilizing Proteins*, **2001**, EP1110964A1.
- [33] Y. L. Hu, Q. Ge, Y. He, M. Lu, *ChemCatChem* **2010**, *2*, 392–396.
- [34] V. Burilov, R. Garipova, E. Sultanova, D. Mironova, I. Grigoryev, S. Solovieva, I. Antipin, *Nanomaterials* **2020**, *10*, 1143.
- [35] X. Zhang, Q. Jin, L. Dai, S. Yuan, *Bull. Mater. Sci.* **2011**, *34*, 735–738.
- [36] J. Huang, K. Huang, S. Liu, Q. Luo, S. Shi, *J. Colloid Interface Sci.* **2008**, *317*, 434–441.
- [37] Z. Bin Chen, L. Kang, D. L. Di, F. Dong, H. Yu, *Adv. Mater. Res.* **2011**, *233–235*, 2893–2897.
- [38] V. G. Teixeira, F. M. B. Coutinho, *J. Appl. Polym. Sci.* **2010**, *118*, 2389–2396.
- [39] A. R. Gonçalves, P. Benar, *Bioresour. Technol.* **2001**, *79*, 103–111.
- [40] P. Truter, A. Pizzi, H. Vermaas, *J. Appl. Polym. Sci.* **1994**, *51*, 1319–1322.
- [41] H. Pupart, P. Jöul, M. I. Bramanis, T. Lukk, *Energies* **2023**, *16*, 1557.
- [42] R. Rinken, D. Posthuma, R. Rinaldi, *ChemSusChem* **2023**, *16*, DOI 10.1002/cssc.202201875.
- [43] A. Charpentier Poncelet, C. Helbig, P. Loubet, A. Beylot, S. Muller, J. Villeneuve, B. Laratte, A. Thorenz, A. Tuma, G. Sonnemann, *Nat Sustain* **2022**, *5*, 717–726.
- [44] A. J. Hunt, T. J. Farmer, J. H. Clark, in *Element Recovery and Sustainability*, The Royal Society Of Chemistry, **2013**, pp. 1–28.
- [45] A. Charpentier Poncelet, C. Helbig, P. Loubet, A. Beylot, S. Muller, J. Villeneuve, B. Laratte, A. Thorenz, A. Tuma, G. Sonnemann, *Nat Sustain* **2022**, *5*, 717–726.
- [46] A. Khazaei, S. Rahmati, Z. Hekmatian, S. Saeednia, *J. Mol. Catal. A* **2013**, *372*, 160–166.
- [47] M. Nasrollahzadeh, S. M. Sajadi, A. Rostami-Vartooni, M. Bagherzadeh, *J. Colloid Interface Sci.* **2015**, *448*, 106–113.
- [48] D. Baruah, R. N. Das, S. Hazarika, D. Konwar, *Catal. Commun.* **2015**, *72*, 73–80.
- [49] M. B. Marulasiddeshwara, P. R. Kumar, *Int. J. Biol. Macromol.* **2016**, *83*, 326–334.
- [50] F. Coccia, L. Tonucci, N. d'Alessandro, P. D'Ambrosio, M. Bressan, *Inorg. Chim. Acta* **2013**, *399*, 12–18.
- [51] O. Bondarenko, K. Juganson, A. Ivask, K. Kasemets, M. Mortimer, A. Kahru, *Arch. Toxicol.* **2013**, *87*, 1181–1200.
- [52] A. Santos, P. Yustos, A. Quintanilla, G. Ruiz, F. Garcia-Ochoa, *Appl. Catal. B* **2005**, *61*, 323–333.
- [53] W. Yang, B. Vogler, Y. Lei, T. Wu, *Environ. Sci.: Water Res. Technol.* **2017**, *3*, 1143–1151.

- [54] A. Orebom, D. Di Francesco, P. Shakari, J. S. M. Samec, C. Pierrou, *Molecules* **2021**, *26*, 3219.
- [55] E.-L. Hult, J. Ropponen, K. Poppius-Levlin, T. Ohra-Aho, T. Tamminen, *Ind. Crops Prod.* **2013**, *50*, 694–700.
- [56] A. M. da Costa Lopes, K. G. João, D. F. Rubik, E. Bogel-Lukasik, L. C. Duarte, J. Andreus, R. Bogel-Lukasik, *Bioresour. Technol.* **2013**, *142*, 198–208.
- [57] S. K. Singh, S. Banerjee, K. Vanka, P. L. Dhepe, *Catal. Today* **2018**, *309*, 98–108.
- [58] S. K. Callear, M. B. Hursthouse, T. L. Threlfall, *CrystEngComm* **2010**, *12*, 898–908.
- [59] Y. Ma, J. Dai, L. Wu, G. Fang, Z. Guo, *Polymer (Guildf)* **2017**, *114*, 113–121.
- [60] J. A. Bennett, Z. S. Campbell, M. Abolhasani, *Curr. Opin. Chem. Eng.* **2019**, *26*, 9–19.
- [61] C. R. McElroy, A. Constantinou, L. C. Jones, L. Summerton, J. H. Clark, *Green Chem.* **2015**, *17*, 3111–3121.
- [62] D. Prat, A. Wells, J. Hayler, H. Sneddon, C. R. McElroy, S. Abou-Shehadeh, P. J. Dunn, *Green Chem.* **2016**, *18*, 288–296.

---

Manuscript received: November 3, 2023

Revised manuscript received: January 24, 2024

Accepted manuscript online: January 27, 2024

Version of record online: February 20, 2024



## Appendix 2

### Publication II

Mohan, M. K.; Kaur, H.; Rosenberg, M.; Duvanova, E.; Lukk, T.; Ivask, A.; Karpichev, Y. Synthesis and Antibacterial Properties of Novel Quaternary Ammonium Lignins. *ACS Omega* **2024**. <https://doi.org/10.1021/acsomega.4c06000>.

Reprinted with permission from American Chemical Society.



# Synthesis and Antibacterial Properties of Novel Quaternary Ammonium Lignins

Mahendra K. Mohan,<sup>||</sup> Harleen Kaur,<sup>||</sup> Merilin Rosenberg, Ella Duvanova, Tiit Lukk, Angela Ivask,\* and Yevgen Karpichev\*



Cite This: *ACS Omega* 2024, 9, 39134–39145



Read Online

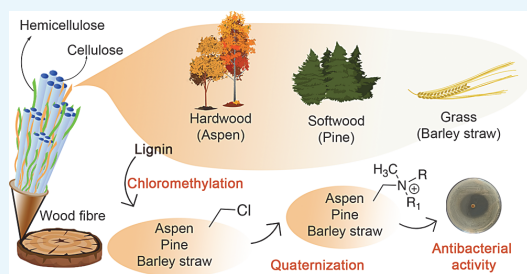
ACCESS |

Metrics & More

Article Recommendations

Supporting Information

**ABSTRACT:** The ongoing demand for effective antimicrobial materials persists, and lignin emerges as a promising natural antibacterial material with renewable properties. The adaptability of lignin to various chemical modifications offers avenues to enhance its antimicrobial activity. Here, we employed chloromethylation and subsequent functionalization with variable tertiary *N*-alkyl dimethyl amines to produce C6–C18 quaternary ammonium lignins (QALs) from hardwood (aspen), softwood (pine), and grass (barley straw). Successful synthesis of QALs was confirmed through NMR and FTIR analysis results along with an increase in the surface  $\zeta$ -potential. Antibacterial activity of QALs against clinical strains of *Klebsiella pneumoniae* and methicillin-resistant *Staphylococcus aureus* was assessed using minimal bactericidal concentration (MBC) assay and agar growth inhibition zone (ZOI) test. The antibacterial activity of QALs was found to be higher than that of the unmodified lignins. QALs with longer alkyl chains demonstrated an MBC of 0.012 mg/L against *K. pneumoniae* already after 1 h of exposure with similar effect size reached after 24 h for *S. aureus*. For all the lignins, an increase in alkyl chain length resulted in an increase in their bactericidal activity. MBC values of C14–C18 QALs were consistently lower than the MBC values of QALs with shorter alkyl chains. Besides the alkyl chain length, MBC values of barley and pine QALs were negatively correlated with the surface  $\zeta$ -potential. While alkyl chain length was one of the key properties affecting the MBC values in a liquid-based test, the agar-based ZOI test demonstrated an antibacterial optimum of QALs at C12–C14, likely due to limited diffusion of QALs with longer alkyl chains in a semisolid medium.



## 1. INTRODUCTION

Biorenewable polymers characterized by high biocompatibility, biodegradability, and cost-effectiveness have emerged as compelling alternatives for a diverse range of applications.<sup>1</sup> Among the various sources of renewable carbon, lignocellulosic biomass has gained prominence, with lignin being the most abundant polyphenolic resource.<sup>2</sup> Lignins have various advantages because of their biocompatibility, antioxidant properties, protection against ultraviolet radiation, and antibacterial activity.<sup>3</sup>

Lignocellulosic biomass is typically composed of 10–40% lignin, with its composition and structure varying depending on the source of lignocellulose.<sup>4</sup> Postextraction, lignin undergoes several chemical transformations that encompass depolymerization, creation of chemically active sites, chemical alteration of hydroxyl groups, and the generation of lignin graft copolymers.<sup>5</sup> The final lignin is a three-dimensional network structure, composed of coniferyl alcohol, *p*-hydroxyphenyl, and syringyl groups interconnected by diverse ester and C–C bonds.<sup>5</sup> Around 70 Mt of lignin is produced by the pulp and paper industry annually, but alarmingly, a mere 5% of it is harnessed into high value added products, such as polymer

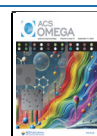
reinforcement,<sup>6–9</sup> stabilizers in emulsions, colloidal suspensions,<sup>10,11</sup> and concrete plasticizers.<sup>12,13</sup> Approximately 95% of lignin residues are either employed as fuel or discarded directly as liquid waste. Considering the wide variety of application areas of lignin, such practices not only deplete valuable raw material resources but also contribute substantially to environmental pollution.<sup>2,14</sup> However, recent years have witnessed a growing interest toward exploring lignin's applications across diverse fields including biomedicine,<sup>15,16</sup> food packaging,<sup>17–19</sup> cosmetics, health products,<sup>20,21</sup> precursor materials for advanced 3D printing,<sup>22</sup> and antimicrobial applications.<sup>23–25</sup> The observation on lignin's antimicrobial properties is not surprising, as plants have evolved to harness these properties as a defense mechanism against invading pathogenic microbes.<sup>26</sup> Lignin has not only demonstrated its inhibitory effect against

Received: June 28, 2024

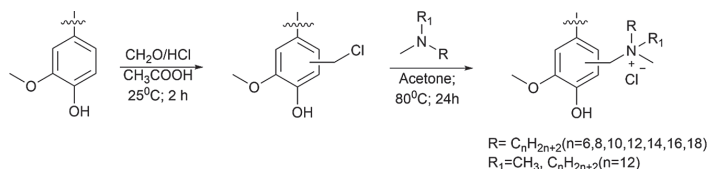
Revised: August 17, 2024

Accepted: August 27, 2024

Published: September 2, 2024



## Scheme 1. Schematic Synthesis Pathway of Quaternary Ammonium Lignins, as Shown for G Unit of Lignin



plant pathogens *Pseudomonas putida* and *Xanthomonas* sp.<sup>27–29</sup> but also against other bacteria, e.g., those colonizing plastic surfaces.<sup>30</sup> In general, the mechanism of lignin's antibacterial activity is proposed to rely on its strong affinity for bacterial cell surface and interaction with surface proteins and lipids, leading to membrane disruption and inhibition of the respiratory chain.<sup>31</sup> The described events are expected to result in the formation of reactive oxygen species (ROS), causing oxidative damage to cellular components and hindering the bacterial growth.<sup>29</sup> In a number of studies, lignins have been further combined with other antimicrobial materials to enhance their antimicrobial effect. Silver nanoparticles have been added to lignins to secure their activity against *Escherichia coli*, *S. aureus*, *Pseudomonas aeruginosa*, *Bacillus subtilis*, and *K. pneumoniae*.<sup>32,33</sup> It has been proposed that incorporation of silver to lignin and further coating with cationic polyelectrolyte layer eases the interaction between lignin and bacterial membrane and leads to a synergistic antimicrobial effect.<sup>34</sup>

In order to increase the cationic charge density of lignins and their bacteriostatic and bactericidal activity, some of the recent studies have incorporated quaternary ammonium groups to the lignin structure.<sup>35</sup> Quaternary ammonium compounds (QAC) are cationic surfactants that belong to a group of the most widely used antimicrobials,<sup>36</sup> which exhibit significant antimicrobial activity due to disruption of bacterial cell membrane and leakage of cellular components.<sup>37–40</sup> This mechanism occurs due to the presence of a positively charged nitrogen atom connected with four alkyl or aryl groups,<sup>41</sup> among which one stands out as a lengthy hydrocarbon chain usually with eight or more carbon atoms, therefore acting as a hydrophobic component. It has been clearly shown that the properties of this hydrophobic side chain play a significant role in influencing the antimicrobial properties of QAC.<sup>42</sup> In general, due to the improved penetration capability of longer alkyl chains to bacterial membranes,<sup>39,43</sup> the tendency shows that the longer hydrophobic carbon chain length, the higher antimicrobial activity.<sup>44</sup> However, some studies have demonstrated an optimal side chain length for the best antimicrobial performance of QACs being 10–12 carbons against Gram-negative<sup>45</sup> and 13–14 carbons against Gram-positive bacteria.<sup>46</sup> Other studies have shown that this tendency persists in case of surface-active ionic liquids, i.e., QAC with a structure altered by an insertion of an amino acid moiety between quaternary ammonium head group and the side chain.<sup>47,48</sup> Extension of the alkyl chain length often leads to leveling off or fading of antimicrobial activity, due to the so-called cutoff effect<sup>49</sup> caused by limited aqueous solubility, kinetic effects, or interactions with biological molecules. In general, Gram-positive bacteria are expected to be more sensitive to QACs than Gram-negative bacteria as the prior lack the outer membrane that restricts QACs access to their target site in cytoplasmic membrane.<sup>50</sup> Dimeric QACs bearing two cationic

groups and two hydrophobic carbon chains have been shown to exhibit greater antibacterial and biocidal activity compared to their monomeric counterparts.<sup>51,52</sup> Lignins modified with quaternary ammonium groups have been shown to exhibit substantially higher antibacterial activity than unmodified lignins against *E. coli*, *Listeria monocytogenes*, *Salmonella enterica*, and *S. aureus*.<sup>53,54</sup> Moreover, while QACs have been shown to exhibit notable toxicity to environmental organisms<sup>55</sup> and eukaryotic cells in vitro,<sup>56</sup> QAC-modified lignins have been shown to be less cytotoxic.<sup>57</sup> Therefore, quaternary ammonium lignins (QALs) can be considered as safer analogs to low molecular weight QACs for human use and potentially also from an environmental perspective.

The main strategy of synthesis of QALs involves Mannich amination combined with attachment of the quaternary alkyltrimethyl or alkyltriethylammonium group to the OH groups.<sup>53,57,58</sup> Recently, our group has presented a greener approach for QAL synthesis that uses chloromethylation step carried out under mild reaction conditions with no Lewis acid catalyst followed by the reaction with a corresponding amine.<sup>59</sup> In this study, we employed the latter synthesis strategy to design a series of QALs based on three different lignin materials originating from hardwood (aspen), softwood (pine), and grass (barley straw). Quaternary ammonium groups added to those lignins varied between 6 and 18 carbons in their alkyl chain length. The resulting QALs were tested for their physicochemical properties and antibacterial activity against clinical isolates of *S. aureus* and *K. pneumoniae*.

## 2. RESULTS AND DISCUSSION

**2.1. Characterization of Lignins.** Considering the constituent units of lignin monomers and their structural composition, lignin is identified as a significantly branched irregular polymer featuring diverse functional groups such as aliphatic and phenolic hydroxyls, carboxylic, carbonyl, and methoxyl groups.<sup>60–62</sup> In this study, biomasses from three different sources known to have different monolignol compositions and different constituent units were used. The softwood (pine) lignin is primarily (>95%) composed of guaiacyl (G) units, with very minimal contribution (<5%) of hydroxyphenyl (H) units.<sup>63</sup> The hardwood (aspen) lignin exhibits a more balanced distribution, with H units ranging between 0 and 8%, G units between 25 and 50%, and syringyl (S) units between 45 and 74%. Grass (barley) lignin, on the other hand, displays a wider variability, with H ranging between 5 and 35%, G between 35 and 80%, and S between 20 and 55%.<sup>63</sup>

The richness of chemical sites within lignin has the potential for chemical modifications. In this study, chloromethylation and further quaternization of the chlorinated sites (Scheme 1) were used. Previous studies have demonstrated the successful integration of chloromethylation into aspen lignin,<sup>59</sup> and the same methodology was used in this study for aspen, barley, and

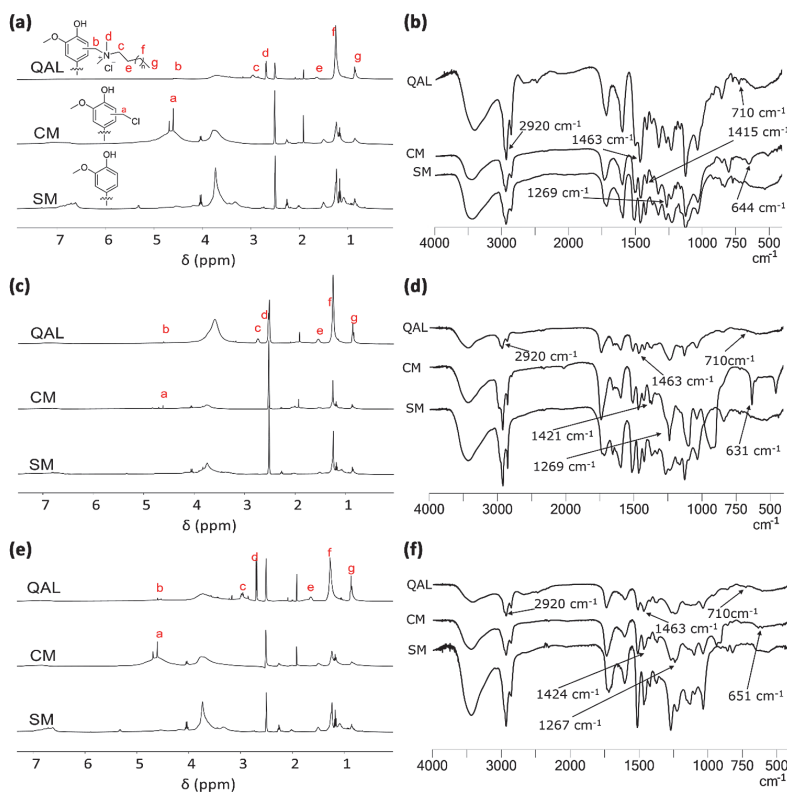


**Figure 1.**  $^1\text{H}$  NMR and FTIR spectra of starting materials (SM), chloromethylated lignins, and quaternary ammonium lignins (as illustrated by the example of C12).  $^1\text{H}$  NMR (a, d, e) and FTIR (b, d, f) spectra of aspen (a, b), barley (c, d), and pine (e, f) lignins. Designation on  $^1\text{H}$  NMR spectra corresponds to the sites highlighted on the molecular formulas drawn in panel (a). In FTIR spectra, characteristic peaks are indicated with arrows.

pine lignins. The analysis of  $^1\text{H}$  NMR spectra of original organosolv (SM) and chloromethylated (CM) lignins, as depicted in Figure 1 unequivocally, verifies the chloromethylation process. A distinct new peak (peak (a) in Figure 1) emerges consistently across all three lignin samples, registering at 4.5–4.75 ppm. This peak corresponds specifically to the presence of  $-\text{CH}_2-\text{Cl}$  within the benzene ring, offering compelling evidence of the successful chloromethylation process in all tested lignin variants. Similarly, distinctive peaks in FTIR at 633–670  $\text{cm}^{-1}$  are indicative of  $-\text{CH}_2-\text{Cl}$  groups (Figure 1). However, the peak around 1413–1424  $\text{cm}^{-1}$  can be attributed to aromatic ring vibrations or C–H deformation vibrations in the methylene ( $-\text{CH}_2-$ ) groups, which are already part of the lignin structure. This means that even without chloromethylation, lignin itself shows an absorption peak in this region, making it less distinctive for identifying the incorporation of  $-\text{CH}_2-\text{Cl}$  groups specifically. Chloromethylation introduces  $-\text{CH}_2-\text{Cl}$  groups into the lignin, which should theoretically give rise to new or enhanced peaks in the FTIR spectrum. However, if the existing lignin structure already has vibrations in the same region (1413–1424  $\text{cm}^{-1}$ ), the addition of  $-\text{CH}_2-\text{Cl}$  groups might not result in a completely new peak but rather a subtle shift or increase in intensity, which could be difficult to distinguish. In some cases (Figure 1b,d,f), a slight shift is observed, suggesting that these

peaks might be overlapping. Similarly, the peak at 1264–1267  $\text{cm}^{-1}$  is typically associated with C–O stretching in ether groups or possibly with C–Cl stretching. Since lignin has abundant ether linkages, the overlap with the new C–Cl bonds formed during chloromethylation might result in only a slight shift or broadening of the peak rather than a distinct new peak. The similarity between lignin and chloromethylated lignin in this region could be due to the fact that the chloromethyl groups do not significantly alter the existing vibrational characteristics of ether linkages. The extent of chloromethylation and the distribution of  $-\text{CH}_2-\text{Cl}$  groups within the lignin matrix may also affect the FTIR spectrum. Considering the lignin structure, if the chloromethylation is not uniform or if the concentration of  $-\text{CH}_2-\text{Cl}$  groups is low, the changes in the FTIR spectrum might be subtle. This could explain why the differences in the range of 1264–1267  $\text{cm}^{-1}$  are not pronounced. These findings provide compelling evidence of the successful incorporation of chloromethane into the lignin structure. However, chloromethyl substitutions in the different lignins were different. XRF analysis shows that CM variants of aspen, barley, and pine lignins were functionalized with 20.0, 10.5, and 7.7% chloromethane, respectively. According to earlier studies, chloromethylation may be significantly affected by the monolignol composition of lignins and the presence of hydroxyphenyl (H) units and guaiacyl (G) units, which

generally indicate a greater potential for chemical reactivity and functionalization. Our findings show that pine exhibits a relatively restricted distribution of these active sites, whereas aspen and barley offer more diverse monolignol structures, making them potentially more versatile for chloromethylation.

Addition of tertiary dimethyl amines to CM lignins resulted in the formation of QALs as proven by  $^1\text{H}$  NMR and FTIR spectra (Figure 1).  $^1\text{H}$  NMR spectrum demonstrated the “g” and “f” peaks at  $\delta$  0.88 and  $\delta$  1.25 ppm, indicating the presence of  $\text{CH}_3$  and  $\text{CH}_2$  moieties constituting hydrophobic tails of the alkyl chains. The singlet peak “d” at  $\delta$  2.69 ppm indicated the presence of  $\text{CH}_3$  groups connected to quaternary nitrogen. “e” and “c” peaks at  $\delta$  1.64 and 2.96 ppm were attributed to the presence of  $\text{CH}_2$  groups next to the quaternary nitrogen. Singlet “b” peaks at  $\delta$  4.66 ppm indicated the presence of  $\text{CH}_2$  groups connecting the quaternary nitrogen [ $\text{ph}-(\text{CH}_2)-\text{N}$ ]. These findings from NMR spectra aligned well with FTIR, which revealed the appearance of the characteristic absorption band of  $-(\text{CH}_2)-$  groups at  $710\text{ cm}^{-1}$  in the case of QALs (Figure 1). Moreover, the characteristic absorption bands of  $\text{CH}_3$  and  $\text{CH}_2$  were observed at  $2920$  and  $1463\text{ cm}^{-1}$  regions in the FTIR spectra of all QALs (Figures 1 and S2). Additionally, FTIR spectra of QALs retained most of the characteristics of their SM predecessors, supporting the assertion that the structural integrity of lignin remained largely undisturbed throughout the modification process.

An additional proof of the successful incorporation of tertiary amines is the appearance of nitrogen in lignins after quaternization (Figure 2, Table S1). Compared with pine and

followed by barley and aspen QALs (Table S1). Considering that one quaternary ammonium group reacted with one chloromethyl group, the amount of chlorine could be used as a predictor for quaternization. However, the finding that pine lignin contained the highest amount of nitrogen and the lowest amount of chlorine (XRF data to determine the content of organic chlorine were discussed above) contradicts the idea of a straightforward relationship. The discrepancy is most likely due to the incomplete reaction of alkyl chains with chloromethyl groups. One likely cause for this could be the solubility of lignin in quaternization reactions affecting the accessibility of reactive chloromethyl sites by the tertiary dimethyl amines, especially those with longer carbon chain lengths. Our earlier observations indicated the superior solubility of pine lignin compared with the other two lignins. This may explain the higher concentration of nitrogen in pine lignin. Furthermore, the structure of aspen lignin has been shown to be relatively inflexible, likely due to the higher number of methyl groups in its monolignols, leading to increased steric hindrance and, consequently, reduced reactivity.<sup>53</sup> When the N content and carbon chain length of QALs of different lignins was correlated, a significant negative correlation ( $r = -0.80$ ; Table S1) was found for pine lignin, suggesting similar incorporation efficacy of alkyl chain lengths with different number of C atoms. The fact that no statistically significant correlation between N content and C chain length was found for barley and aspen lignins (Table S1 and comparison can also be seen in Figure 2) suggests nonlinearity of quaternization reaction in these lignins in case of different tertiary dimethyl amines. When comparing the nitrogen content of C12 and  $(\text{C}_{12})_2$  QALs, the N content was consistently lower in the case of double chains for all lignins. The reason for the lower incorporation of double chains was likely the steric hindrance. Since the nitrogen content reported in this work is provided specifically for the isolated products, we also suppose that among the factors contributing to the variation in nitrogen content for the different QALs could be some dissolved lignin lost during the isolation step.

The incorporation of quaternary ammonium groups into lignins was also evaluated by  $\zeta$  potential (mV). Expectedly, the QALs exhibited a positive surface charge, while lignins without quaternary ammonium chain modification exhibited slightly negative, positive, or close to neutral surface charge (Table S1 and Figure 2). For most QALs, the  $\zeta$ -potential values were higher than  $+40\text{ mV}$ , and in the case of barley and pine, the surface charge was also significantly positively correlated with alkyl chain length (Pearson  $r = 0.89$  and  $0.83$ , respectively) (Table S1). In case of aspen lignin, the charge did not show significant correlation with alkyl chain length.

As some of the lignin samples were visually aggregated, hydrodynamic particle size of all lignins was analyzed in order to evaluate the stability of their suspensions. These particle size measurements showed that CM and SM without a quaternary ammonium group aggregated significantly in 1.5% DMSO (the final antibacterial test environment), while the particle sizes of QALs were significantly smaller. Therefore, clearly, the high positive surface charge of QALs allowed better dispersion of lignins than the mild positive or negative or close to neutral surface charge of SM and CM. There was no significant correlation between hydrodynamic diameter and alkyl chain length of QALs (Table S1).

**2.2. Antibacterial Activity of Lignins.** Antibacterial activity of SM, CM, and QALs was evaluated by measuring

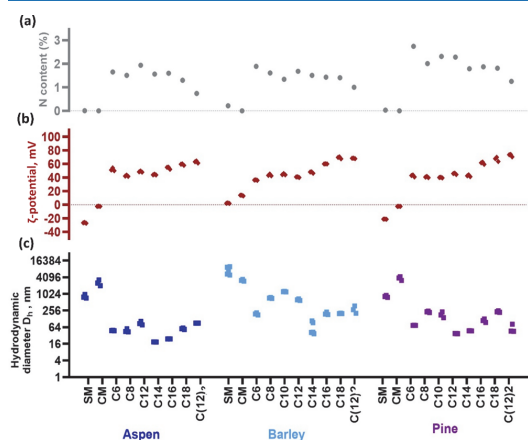


**Figure 2.** Properties of the lignins and quaternary ammonium lignins (QALs) potentially affect antibacterial activity in minimal biocidal concentration test conditions (1.5% DMSO in water). (a) N content (%) of the samples as a proxy of active moiety content in QALs, (b) hydrodynamic diameter (nm), and (c)  $\zeta$ -potential (mV). Dotted red and gray lines for  $\zeta$ -potential and N content represent 0 values.

aspen lignin, barley straws contained some nitrogen before the addition of tertiary dimethyl amines. This nitrogen could be attributed to the natural composition of barley material, e.g., the presence of amino acids, and other nitrogen-containing compounds that were retained during lignin extraction process.<sup>64</sup> The nitrogen content in QALs varied between 0.77 and 2.74% and was dependent on the source of lignin. The highest nitrogen content was detected in pine QALs

their bactericidal (minimal biocidal concentration, MBC) effect in water and bacteriostatic (growth inhibition, ZOI) effect in a semisolid (agar) medium. For both tests, aggregation behavior of the QALs and intrinsic antibacterial activity of their solvent DMSO determined the types of tests and maximum QAL concentrations that could be tested. Pilot experiments showed that while DMSO toxicity was not limiting the ZOI assay, then in the MBC assay, the highest concentration of DMSO that could be tested with Gram-negative *K. pneumoniae* and Gram-positive *S. aureus* was 1.5% (Figures S1 and S3) inherently also limiting the upper concentration limit of QALs (Figures 3 and 4).

Maximum bactericidal effect inflicted by the QALs (MBC of about 0.012 mg/L after 24 h exposure) was similar across samples from all lignin sources (aspen, barley, and pine) and both bacterial models (*K. pneumoniae*, *S. aureus*). However, there were differences in the bactericidal effect of the controls (SM and CM) as well as in the speed of bactericidal action of the QALs (Figures 3 and 4 and Tables S3 and S4) discussed in more detail below.

Our results agree with the general understanding about higher antibacterial effect of lignins to Gram-positive bacterial species as opposed to Gram-negatives.<sup>53,65,66</sup> Based on MBC values, nonquaternized lignins (SM, CM) from all lignin sources were more bactericidal to *S. aureus* than *K. pneumoniae* after 24 h. Specifically, 8–15 times lower concentrations of SM and 2–4 times lower concentrations of CM were needed to kill *S. aureus* compared to *K. pneumoniae* (Tables S3 and S4). CM was generally 2–8 times more bactericidal than SM across both time points and bacterial species, and its bactericidal activity against *S. aureus* was not significantly enhanced by quaternization (Figure 4 and Table S3). Hydrodynamic size of the lignin aggregates could not directly explain the observed differences in bactericidal efficacy of SM and CM. However, SM of all lignin sources was more negatively charged or less positively charged than CM (Table S1 and Figure 2). A decrease of negative or increase in positive charge could respectively decrease electrostatic repulsion or increase attraction to bacterial cell surface, and/or chloromethylation itself might contribute toward an antibacterial effect.

Contrary to the nonquaternized lignins, QALs were generally more bactericidal towards *K. pneumoniae* (Figure 4) than *S. aureus* (Figure 3) after 1 h exposure, but the difference in MBC values mostly disappeared after 24 h exposure. QALs effect toward *K. pneumoniae* was more rapid than toward *S. aureus* with the exposure time variable contributing to overall MBC value variability by 6 and 33%, respectively, based on main effects in multiple linear regression (among exposure time, lignin source, N content, alkyl chain length, hydrodynamic size, and  $\zeta$ -potential). In comparison, the bactericidal effect of CM substantially increased in time also for *K. pneumoniae*, indicating a different underlying mechanism of action of the CMs lignins compared to QALs. Interestingly, literature reported that quaternary ammonium salts of lignin have been shown to be more effective toward *S. aureus* as opposed to Gram-negatives, e.g., with 3-fold difference in MIC values in liquid test format.<sup>72</sup> However, the exact effect sizes are challenging to compare because antibacterial activity of lignins seems to be dependent on both the extraction method and their chemical structure.<sup>23,25</sup>

QALs with longer alkyl chains (C14–C18) demonstrated more consistent antimicrobial properties across bacterial species and plant origins compared to those with shorter

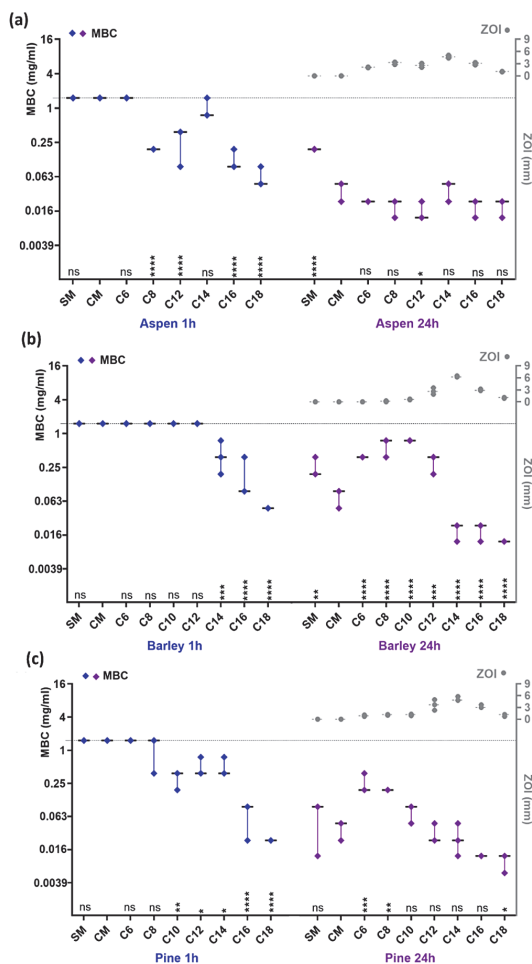


**Figure 3.** Minimal bactericidal concentration (MBC) of lignin sample against *S. aureus*. MBC values for (a) aspen, (b) barley, and (c) pine after 1 and 24 h of exposure are plotted on the left Y-axis, and zone of inhibition values for 24 h of incubation period are on right Y-axis. SM – organosolv lignin, CM – chloromethylated lignin, C6–C18 – quaternary ammonium lignins, QAL. Median and range of three biological replicates are shown. Highest concentration (1.5 mg/mL) used in MBC assay is shown as a gray dotted line on the left Y-axis. Statistically significant differences from control (CM) denoted by ns (not significant), \*\*\*\* ( $p \leq 0.0001$ ), \*\*\* ( $p \leq 0.001$ ), \*\* ( $p \leq 0.01$ ), and \* ( $p < 0.05$ ).

alkyl chains (Figures 3 and 4). QALs with longest alkyl chains also presented the highest positive charge in exposure conditions (Table S1) that could enhance electrostatic attraction toward negatively charged bacterial cell surface and physically enhance the bactericidal effect. QALs with shorter alkyl chains (C6–C12) were generally less effective except for quick-acting antimicrobial potential of C6–C12 of aspen toward *K. pneumoniae* (Figure 4). Interestingly, after 24 h of exposure to *S. aureus*, C6–C12 of barley and pine showed even lower bactericidal effect compared to CM. The latter is largely

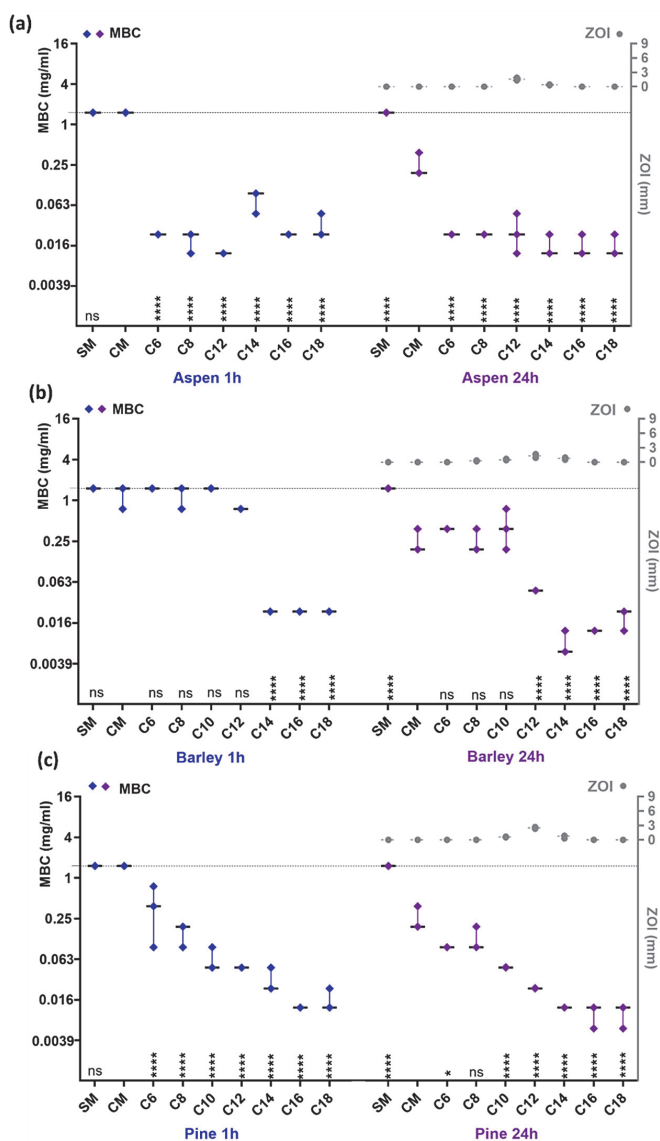


**Figure 4.** Minimal bactericidal concentration (MBC) of lignin samples against *K. pneumoniae*. MBC values for (a) aspen, (b) barley, and (c) pine after 1 and 24 h of exposure are plotted on the left Y-axis, and zone of inhibition values for 24 h of incubation period are on right Y-axis. SM – organosolv lignin, CM – chloromethylated lignin, C6–C18–quaternary ammonium lignins, QAL. Highest concentration (1.5 mg/ml) used in MBC assay is shown as a gray dotted line on the left Y-axis. Median and range of three biological replicates are shown. Statistically significant differences from control (CM) are presented above X-axis for each respective alkyl chain length (C) denoted by ns (not significant), \*\*\* ( $p \leq 0.0001$ ), \*\* ( $p \leq 0.001$ ), \* ( $p \leq 0.01$ ), and \* ( $p < 0.05$ )

explained by comparison to the already quite toxic CM control itself, as explained above.

Modifications with a double C12 alkyl moiety instead of a single C12 alkyl chain resulted in inconsistent changes in antibacterial activity (Figure 5). The MBC value of C(12)<sub>2</sub> of barley and pine decreased for *K. pneumoniae*, in case of *S. aureus*, such a decrease was only observed in case of barley lignin, when compared to C12. In the case of aspen lignin, C12

and C(12)<sub>2</sub> resulted in similar MBC values for both bacteria. Inconsistencies in MBC values of QALs with single and double alkyl chains can at least partly be explained by the substantial decrease of nitrogen content in the double-chain QALs compared to single-chain QALs, indicating that modification with double alkyl chains was less efficient resulting in the presence of smaller amount of the moieties possessing antibacterial activity at the same QAL concentration.

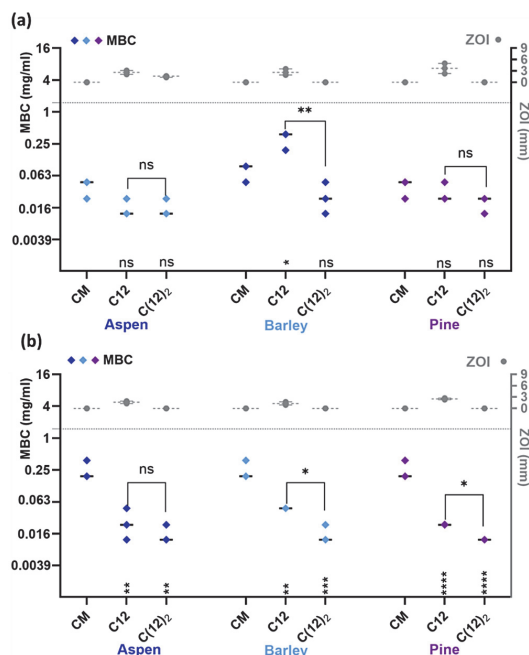


**Figure 5.** Minimal bactericidal concentration (MBC) of lignin samples modified with either single or double alkyl chains, tested against (a) *S. aureus* and (b) *K. pneumoniae*. MBC values for aspen, barley, and pine after 24 h of exposure are plotted on the left Y-axis, and zone of inhibition values for 24 h of incubation period are on right Y-axis. CM – chloromethylated lignin, C12, C(12)<sub>2</sub> – quaternary ammonium lignins, QAL. Median and range of three biological replicates are shown. Highest concentration (1.5 mg/ml) used in MBC assay is shown as a gray dotted line on the left Y-axis. Statistical significance of differences ( $p < 0.05$ ) of MBC values from the CM is presented under each respective alkyl chain length (C) and between the single and double chains are marked above (ns (nonsignificant), \*\*\*\* ( $p \leq 0.0001$ ), \*\*\* ( $p \leq 0.001$ ), \*\* ( $p \leq 0.01$ ), and \* ( $p < 0.05$ )).

Considering the differences in N content, then based on MBC values, QALs with double C12 appear more toxic to bacteria than QALs with single C12.

MBC values of barley and pine QALs consistently negatively correlated with both alkyl chain length and aggregate charge (Table S1) as QALs with longer alkyl chains and higher  $\zeta$ -potential proved to be more bactericidal (Figures 3 and 4). The bactericidal effect of aspen QALs did not correlate with

either alkyl chain length or aggregate charge, possibly due to quick-acting properties and having reached most of their full potential by the 1 h time point. Additionally, although aspen QALs had the same alkyl chain length modifications, they exhibited a substantially narrower range of  $\zeta$  potential values across C6–C18 compared to barley and pine QALs. This suggests that aggregate charge and potential electrostatic attraction to negatively charged cell surfaces could enhance the bactericidal activity. This is further illustrated by a strong positive correlation between alkyl chain length and  $\zeta$ -potential of barley and pine but no significant correlation for aspen QALs (Table S1). Both higher antimicrobial activity at lower alkyl chain lengths and different charge dynamics of aspen QALs could potentially relate to quite different monolignol compositions of aspen lignin compared with pine and barley. It is also not entirely clear what causes the increase of  $\zeta$  potential with the increase of alkyl chain length of pine and barley QALs. Unfortunately, contributions of possibly causal interactions between the variables in Table 1 to changes in MBC values were not evaluated in multiple linear regression due to intervariable dependencies and multicollinearity.

In general, most of the earlier studies have indicated that among quaternary ammonium compounds with the most used alkyl chain lengths of C8–C18, there is an optimal chain length usually above 10 carbons that grants the highest antibacterial efficacy depending on the compound, exposure time, and the type of bacterial cell wall.<sup>44,67–71</sup> At the same time, QACs with alkyl chain lengths  $<4$  or  $>18$  are considered virtually inactive.<sup>72,73</sup> Our study showed that in MBC assays, QALs with the longest alkyl chains were the most bactericidal, and no distinct shorter optimum was revealed. Most of the earlier studies that indicated the existence of alkyl chain length optimum have based their antibacterial effect assessment on growth inhibition tests on semisolid (agar) medium by measuring ZOI. When a similar assay with QALs was carried out in our study, we were also able to demonstrate an optimal bacteriostatic effect at C12–C14, whereas no growth inhibition by the QALs with longest alkyl chains was observed (Figures 4 and 5). The alkyl chain lengths that deliver the maximum effect in growth inhibition on agar medium (ZOI) and bactericidal assay in liquid environment (MBC) differ substantially. ZOI shows a sharp optimum at C12 or C14 (depending on bacterial species), with a decline toward C18. In contrast, the MBC assay shows an increasing bactericidal effect with longer alkyl chains, peaking at C16–C18. Similar discrepancy between the results of growth inhibition and bactericidal assays of benzalkonium chloride with variable alkyl chain lengths has also been noted by Tomlinson et al.<sup>73</sup> We suspect that the ZOI optima are due to differences in

**Table 1.** Correlations between Bactericidal Effects of Quaternary Ammonium Lignins (Minimal Bactericidal Concentration Values after 24 h Exposure) and Their Physicochemical Properties<sup>a</sup>

	origin of lignin	alkyl chain length	N content	hydrodynamic size	$\zeta$ - potential
<i>K. pneumoniae</i>	Aspen	−0.39(ns)	0.41(ns)	0.43(ns)	−0.21(ns)
	Barley	−0.72(****)	0.21(ns)	0.55(**)	−0.52(*)
	Pine	−0.80(****)	0.47(*)	0.29(ns)	−0.54(*)
<i>S. aureus</i>	Aspen	0.043(ns)	−0.15(ns)	−0.52(*)	−0.31(ns)
	Barley	−0.75(****)	0.11(ns)	0.85(****)	−0.61(**)
	Pine	−0.84(****)	0.66(**)	0.08(ns)	−0.52(*)

<sup>a</sup>Pearson correlation coefficients ( $r$ ) and their statistical significance (in brackets) are shown. Statistical significance is ns (not significant), \*\*\*\* ( $p \leq 0.0001$ ), \*\*\* ( $p \leq 0.001$ ), \*\* ( $p \leq 0.01$ ), or \* ( $p < 0.05$ )).

hydrophobic aggregation and/or limited diffusion of the QALs with longer alkyl chains in agar medium, rather than their intrinsic biological activity per se. Notably, C14 QALs also formed the smallest aggregates in the water suspension (Figure 3). Figure 5 further illustrates that modification with double alkyl chains compared to single alkyl chains causes discrepancy between the ZOI and MBC results. While ZOI always decreased for double chains compared to single chains, MBC of double chains either remained similar to single chains or even decreased. These discrepancies highlight that inhibition zones can only be used and compared based on the presumption of equal diffusion of the substances of interest in the water environment of semisolid agar medium. As our results demonstrate, ZOI-based bacteriostatic properties of QALs with longer alkyl chains or double alkyl chains of hydrophobic nature can be falsely underestimated by diffusion-limited test formats.

### 3. CONCLUSIONS

Here, we present the synthesis and antibacterial characterization of quaternary ammonium derivatives of lignin (QAL) sourced from three origins: hardwood represented by aspen, softwood represented by pine, and grass straws represented by barley straw. Lignin was extracted using organosolv methodology, chloromethylated, and subsequently reacted with the corresponding tertiary *n*-alkyl dimethyl amine with alkyl chain lengths ranging from 6 to 18 carbons (C6–C18). Additionally, for C12, double-chain derivatives (C(12)<sub>2</sub>) were prepared by reaction with corresponding dialkyl methylamines. The original organosolv lignin (SM), chloromethylated lignin (CM), and the final QAL products were characterized by <sup>1</sup>H NMR and FTIR analysis to describe the products, elemental analysis to determine nitrogen content, XRF to determine organic chlorine content, and ζ-potential to assess the surface charge and hydrodynamic diameter. Nitrogen content analysis revealed the highest and most consistent incorporation of quaternary ammonium moieties in pine lignin. Compared with SM and CM, the QALs exhibited higher positive charges, with significant positive correlation observed between ζ-potential and alkyl chain length of the quaternary ammonium group in pine and barley lignin.

Antibacterial effect of lignins was evaluated by MBC and agar growth inhibition test (zone of inhibition, ZOI) against clinical isolates of *K. pneumoniae* and *S. aureus* MRSA. The non-quaternized lignins (SM, CM) showed no bactericidal effect after 1 h; however, some level of bactericidal activity was detected after 24 h of exposure, particularly against *S. aureus*. Compared with SM, CM exhibited a higher bactericidal effect, likely due to its less negative surface charge or the presence of chlorine in the molecule. Incorporation of quaternary ammonium groups into the lignin increased the antibacterial activity. QALs with longer alkyl chains demonstrated the MBC of 0.012 mg/L against *K. pneumoniae* after just 1 h of exposure, achieving a similar effect size against *S. aureus* after 24 h. For both tested bacteria, QALs with longer alkyl chains (C14–C18) demonstrated a higher bactericidal effect as compared to those with shorter alkyl chains. MBC values of barley and pine QALs correlated negatively with both the alkyl chain length and surface ζ-potential of the QAL aggregates. However, no such clear correlations were found for aspen QALs, likely due to their more consistent aggregate surface charge across different alkyl chain lengths. QALs with a double C12 alkyl moiety showed inconsistent changes in antibacterial activity

compared to C12 with a single alkyl chain at the same lignin concentration. However, considering large differences in active moiety content (N content) of C12 double and single chains, double C12 appeared more bactericidal than single C12. Contrary to several previous studies demonstrating an optimal alkyl chain length for antibacterial action of QALs, our study showed that in MBC assays, QALs with the longest alkyl chains were the most bactericidal, and no distinct shorter optimum among C6–C18 was revealed. However, a clear optimum at C12–C14 was observed in the growth inhibition test (ZOI), suggesting that in the case of antibacterial tests carried out in agar, the growth inhibiting effect may be restricted by diffusion of QALs with longer alkyl chains along with their bacteriostatic properties. Therefore, semisolid diffusion-limited antibacterial tests should be avoided in the efficacy assessment of compounds with potentially different aggregation and/or diffusion properties in aqueous environments.

Although we demonstrated the incorporation of quaternary ammonium groups with longer alkyl chains into biorenewable lignin material in the development of effective bactericidal materials, concerns have been raised regarding the toxicity of QACs. Therefore, before the actual applications, both the environmental and cytotoxicity of the promising QALs should be investigated.

### 4. METHOD

**4.1. Materials.** Ethanol, acetonitrile, hexane, hydrochloric acid, acetic acid, sulfuric acid, and DMSO-*d*<sub>6</sub> were purchased from Sigma-Aldrich (Taufkirchen, Germany). All of the reagents used were of analytical reagent grade. Deionized water from a Milli-Q water purification system (Millipore S.A., Molsheim, France) was used throughout the study. Aspen wood chips were provided by Estonian Cell AS (Kunda, Estonia); longitudinally sawn pine timber sawdust was provided by Prof. Jaan Kers (Tallinn University of Technology, Tallinn, Estonia); and barley straw was provided by Prof. Timo Kikas (Estonian University of Life Sciences, Tartu, Estonia). All feedstocks were dried in a convection oven at 50 °C up to 8% moisture, followed by grinding to a fine powder and stored in plastic bags at room temperature.

**4.2. Extraction and Modification of Lignins.** Lignin was extracted from aspen, pine, and barley straw according to the previously described organosolv procedure.<sup>74,75</sup> A 50 g sample of ground and dried chips of aspen, sawdust of pine, or barley straws was refluxed in a 2 l round-bottom flask equipped with a mechanical stirrer and a condenser, using 1.5 l of solvent for 6 h. The solvent mixture consisted of 0.28 M HCl (37% purity) in absolute ethanol. Subsequently, the mixture underwent filtration through Whatman filter paper, and the solid residue was removed. The collected filtrate was then concentrated to approximately 100 mL using a rotary evaporator. To recover lignin from the pretreatment solution, a precipitation method was employed. The pretreatment liquor was dissolved in 100 mL of acetone and introduced into a vigorously stirred 2 L volume of cold Milli-Q water, reducing the solubility of lignin. The mixture was stirred for 60 min, followed by the separation of the precipitated lignin via centrifugation at 4200 rpm. The retrieved lignin was washed three times with 1 L of ultrapure water, centrifuged, and subsequently dried in a convection oven at 40 °C for 24 h. The dried organosolv lignin was then weighed (yield 6%) and used for either subsequent analysis or

the following procedures. The extracted lignin was designated as **SM** (starting material).

Chloromethylation of organosolv lignin was performed according to the previously described procedure.<sup>60</sup> 1 g of organosolv lignin and 1 g of paraformaldehyde were dissolved in 10 mL of glacial acetic acid and then bubbled with HCl gas for 2 h after which the reaction was stopped by adding 30 mL of water. The product was then filtered, washed with water, and dried in vacuum. The conversion into chloromethylated products was monitored by organic chlorine content analysis. The resulting chloromethylated lignins were named **CM**.

To prepare QALs, to a solution of a CM lignin (1 g in 20 mL of acetonitrile), 1 g of one of the following ternary dimethyl amines,  $C_6H_{13}N(CH_3)_2$ ,  $C_8H_{17}N(CH_3)_2$ ,  $C_{10}H_{21}N(CH_3)_2$ ,  $C_{12}H_{25}N(CH_3)_2$ ,  $C_{14}H_{29}N(CH_3)_2$ ,  $C_{16}H_{33}N(CH_3)_2$ , and  $C_{18}H_{37}N(CH_3)_2$ , was added. The mixtures were heated at 80 °C for 24 h after which the resulting QALs were filtered, washed with hexane, and dried in vacuum. The resulting QALs were designated as **C6**, **C8**, **C10**, **C12**, **C14**, **C16**, and **C18**, depending on the number of carbons in the alkyl chain. One additional modification of CM lignin was synthesized using ternary double *n*-alkyl chain amine ( $C_{12}H_{25}_2N(CH_3)_2$ ). The resulting double alkyl chain QAL was designated as (**C12**)<sub>2</sub>.

**4.3. Characterization of Lignins.** Proton nuclear magnetic resonance (<sup>1</sup>H NMR) spectra of SM, CM, and QALs were acquired using Bruker Avance III 400 MHz spectrometer (USA). All of the samples (ca. 60 mg) were dissolved in DMSO-*d*<sub>6</sub> in a 5 mm NMR tube; MestReNova x64 software was used to plot the <sup>1</sup>H NMR spectra. Fourier transform infrared spectroscopy (FTIR) spectra of the lignins were collected with the Shimadzu IRTracer-100 spectrometer (Kyoto, Japan). The samples were prepared with KBr pellets at a concentration of 1:100 weight. The resolution was set to 2 cm<sup>−1</sup> with 80 scans recorded. The data analysis was conducted using Shimadzu Lab Solutions software. Elemental analysis for nitrogen was carried out using an Elementar Vario MICRO cube (Langensfeld, Germany) in CHNS mode. XRF analysis of lignins to determine organic chlorine content was carried out using a Bruker S4 Pioneer XRF spectrometer (USA) using a precalibrated MultiRes measurement method. Lignins were mixed 1:10 with NaHCO<sub>3</sub> for the measurement. Hydrodynamic diameter (*D*<sub>h</sub>) and ζ-potential of the QALs were measured from 1.5 mg/mL lignin suspension in 1.5% DMSO in water using a Zetasizer Nano ZSP instrument (Malvern Panalytical, Malvern, UK). Three to five measurements with 12–15 runs of measurements for each repetition were performed for each sample depending on the homogeneity of the sample.

**4.4. Antibacterial Activity Assessment.** Antibacterial activity of lignin compounds was determined by two methods, growth inhibition assay (zone of inhibition, ZOI), and MBC assessment, using two clinical isolates from Estonian Electronic Microbial dataBase (<https://eemb.ut.ee>), *S. aureus* strain HUMB 19594 showing methicillin resistance (MRSA) and *K. pneumoniae* HUMB 01336.<sup>76</sup> Bacteria were routinely cultivated on LB agar medium (5 g/L yeast extract, 10 g/L tryptone, 5 g/L NaCl, 15 g/L agar) and TSA agar medium (17 g/L pancreatic digest of casein, 3 g/L papaic digest of soybean meal, 2.5 g/L dextrose (glucose), and 2.5 g/L dipotassium hydrogen phosphate (5 g/L sodium chloride, 15 g/L agar). Prior to antibacterial tests, lignin samples were dissolved in DMSO at a concentration of 100 mg/mL.

**4.4.1. Growth Inhibition Assay.** A single colony was picked from overnight growth plates and inoculated into 5 mL of LB broth, after which it was grown for 16 h at 37 °C and 150 rpm shaking. Then, the bacterial culture was diluted with fresh medium 1:50 and incubated for 2 h to reach the exponential growth phase. OD at 600 nm of the culture was then diluted to a target value of 0.1, and 100 μL of the resulting bacterial inoculum was spread uniformly on TSA agar plates using sterile glass beads. The plates were allowed to dry for 5 min. To the freshly inoculated plates, 3 μL drops of the test compounds at 100 mg/mL in DMSO were pipetted. A drop of 3 μL of DMSO was used as a control. The plates were incubated at 37 °C for 24 h for optimal growth after which a transparent growth inhibition zone (measured in mm) around the droplets of the compounds was measured using a caliper. The test was performed in three biological replicates.

**4.4.2. Minimal Bactericidal Concentration (MBC).** A single colony from the LB agar plate was inoculated to LB broth and grown for 16 h at 150 rpm at 37 °C. Then, the bacterial culture was diluted with fresh media 1:50 and cultivated at 37 °C and 150 rpm to reach the exponential growth phase (OD 0.6 at 600 nm). The cells were then centrifuged at 5000 g for 10 min at 4 °C, and the pellet was resuspended in an equal volume of sterile water. The previous washing step was repeated twice, and finally, the pellet was suspended in water to target the desired cell density of OD<sub>600</sub> = 0.2. The compounds were diluted to the specified concentrations using 3% DMSO, that was selected according to preexperiments where 1:1 diluted amount of 3% DMSO (final concentration of DMSO 1.5%) had no significant effect on *S. aureus* and *K. pneumoniae* viability after 24 h of exposure (Figure S1). Therefore, the highest tested concentration of lignin in this testing format was 1.5 mg/mL, and the diluent was always 1.5% DMSO in water. 100 μL of the bacterial suspension was mixed with 100 μL of lignin solution and incubated at 37 °C for 24 h. After 1 and 24 h of exposure, 3 μL of the cell suspension was drop-plated onto LB agar medium and incubated at 37 °C for 24 h. The lowest concentration of compounds resulting in no visible viable colony formation on agar medium in the 3 μL spot was defined as MBC. MBC tests were carried out in three biological replicates.

**4.5. Statistical Analysis.** Statistical analysis of the data was performed with GraphPad Prism 10.1.1 (GraphPad Software, San Diego, USA). Correlations, multiple linear regression, and analysis of variance (ANOVA) followed by post hoc testing for multiple comparisons at α = 0.05 were used where appropriate.

## ■ ASSOCIATED CONTENT

### Supporting Information

The Supporting Information is available free of charge at <https://pubs.acs.org/doi/10.1021/acsomega.4c06000>.

Effect of DMSO on bacterial viability FTIR spectra of quaternary ammonium lignins zone of inhibition in growth inhibition test on agar for DMSO and quaternary ammonium lignins for *S. aureus* and *K. pneumoniae*; nitrogen content, hydrodynamic diameter (*D*<sub>h</sub>), and ζ-potential of lignin samples zone of inhibition (ZOI, mm) for *S. aureus* and *K. pneumoniae* MBC of lignin and QAL samples against *S. aureus*; and MBC of lignin and QAL samples against *K. pneumoniae* (PDF)

## AUTHOR INFORMATION

### Corresponding Authors

Angela Ivask – Institute of Molecular and Cell Biology, University of Tartu, 51010 Tartu, Estonia; Phone: +372 737 5020; Email: [angela.ivask@ut.ee](mailto:angela.ivask@ut.ee)

Yevgen Karpichev – Department of Chemistry and Biotechnology, Tallinn University of Technology (TalTech), 12618 Tallinn, Estonia; [orcid.org/0000-0003-2322-6750](https://orcid.org/0000-0003-2322-6750); Email: [yevgen.karpichev@taltech.ee](mailto:yevgen.karpichev@taltech.ee); Fax: +372 620 2994

### Authors

Mahendra K. Mohan – Department of Chemistry and Biotechnology, Tallinn University of Technology (TalTech), 12618 Tallinn, Estonia; [orcid.org/0000-0002-6827-592X](https://orcid.org/0000-0002-6827-592X)

Harleen Kaur – Institute of Molecular and Cell Biology, University of Tartu, 51010 Tartu, Estonia; [orcid.org/0000-0003-3824-7984](https://orcid.org/0000-0003-3824-7984)

Merilin Rosenberg – Institute of Molecular and Cell Biology, University of Tartu, 51010 Tartu, Estonia

Ella Duvanova – Department of Chemistry and Biotechnology, Tallinn University of Technology (TalTech), 12618 Tallinn, Estonia; Vasyil' Stus Donetsk National University, 21027 Vinnytsia, Ukraine

Tiit Lukk – Department of Chemistry and Biotechnology, Tallinn University of Technology (TalTech), 12618 Tallinn, Estonia; [orcid.org/0000-0001-7765-1707](https://orcid.org/0000-0001-7765-1707)

Complete contact information is available at: <https://pubs.acs.org/10.1021/acsomega.4c06000>

### Author Contributions

<sup>||</sup>M.K.M. and H.K. are contributed equally to the publication.

### Author Contributions

The manuscript was written through contributions of all authors. All authors have approved the final version of the manuscript. M.K.M.: conceptualization, methodology, investigation – synthesis and characterization of studied compounds, validation, data curation, visualization, and writing – original draft preparation; H.K.: methodology, investigation (antibacterial properties of studied compounds), data curation, and writing – original draft preparation; M.R.: methodology, investigation, data curation, visualization, writing – original draft preparation, and writing – reviewing and editing; E.D.: investigation (antibacterial properties of studied compounds); T.L.: conceptualization, methodology, resources, funding acquisition, writing – reviewing and editing, and project administration; A.I.: methodology, resources, funding acquisition, writing – original draft preparation, writing – reviewing and editing; and Y.K.: conceptualization, methodology, resources, funding acquisition, writing – original draft preparation, writing – reviewing and editing, and project administration.

### Notes

The authors declare no competing financial interest.

## ACKNOWLEDGMENTS

This study was supported by the Estonian Research Council via projects RESTA11 and TEM-TA49 (for M.K.M., T.L., and Y.K.), COVSGS (for M.K.M., E.D., and Y.K.), and PRG1496 (A.I., H.K., M.R.). Financial support was received from Estonian Ministry of Education and Research (TK210) (A.I.,

M.R.) and ERDF Dora Plus program (for E.D.). Siiri Kõljalg and Tiit Rööp are acknowledged for providing the bacterial strains.

## ABBREVIATIONS

AcOH, Acetic acid; SM, Starting material; CM, Chloromethylated Lignin; QAL, Quaternary ammonium lignin; CHO, Formaldehyde; HCl, Hydrochloric acid; DMSO, Dimethylsulfoxide; EtOH, Ethanol; FTIR, Fourier Transform Infrared Spectroscopy; NMR, Nuclear Magnetic Resonance; PFA, paraformaldehyde; XRF, X-ray Fluorescence

## REFERENCES

- (1) Ramakrishna, S.; Mayer, J.; Wintermantel, E.; Leong, K. W. Biomedical Applications of Polymer-Composite Materials: A Review. *Compos. Sci. Technol.* **2001**, *61* (9), 1189–1224.
- (2) Laurichesse, S.; Avérous, L. Chemical Modification of Lignins: Towards Biobased Polymers. *Prog. Polym. Sci.* **2014**, *39* (7), 1266–1290.
- (3) Figueiredo, P.; Lintinen, K.; Hirvonen, J. T.; Kostianen, M. A.; Santos, H. A. Properties and Chemical Modifications of Lignin: Towards Lignin-Based Nanomaterials for Biomedical Applications. *Prog Mater Sci* **2018**, *93*, 233–269.
- (4) Upton, B. M.; Kasko, A. M. Strategies for the Conversion of Lignin to High-Value Polymeric Materials: Review and Perspective. *Chem Rev* **2016**, *116* (4), 2275–2306.
- (5) He, X.; Luzi, F.; Yang, W.; Xiao, Z.; Torre, L.; Xie, Y.; Puglia, D. Citric Acid as Green Modifier for Tuned Hydrophilicity of Surface Modified Cellulose and Lignin Nanoparticles. *ACS Sustain Chem Eng* **2018**, *6* (8), 9966–9978.
- (6) Fan, Q.; Liu, T.; Zhang, C.; Liu, Z.; Zheng, W.; Ou, R.; Wang, Q. Extraordinary Solution-Processability of Lignin in Phenol–Maleic Anhydride and Dielectric Films with Controllable Properties. *J Mater Chem A Mater* **2019**, *7* (40), 23162–23172.
- (7) Liu, W.; Yao, Y.; Fu, O.; Jiang, S.; Fang, Y.; Wei, Y.; Lu, X. Lignin-Derived Carbon Nanosheets for High-Capacitance Supercapacitors. *RSC Adv.* **2017**, *7* (77), 48537–48543.
- (8) Zhang, X.; Liu, W.; Yang, D.; Qiu, X. Biomimetic Supertough and Strong Biodegradable Polymeric Materials with Improved Thermal Properties and Excellent UV-Blocking Performance. *Adv. Funct. Mater.* **2019**, *29* (4), No. 1806912.
- (9) Liu, W.; Fang, C.; Wang, S.; Huang, J.; Qiu, X. High-Performance Lignin-Containing Polyurethane Elastomers with Dynamic Covalent Polymer Networks. *Macromolecules* **2019**, *52* (17), 6474–6484.
- (10) Gharekhani, S.; Ghavidel, N.; Fatehi, P. Kraft Lignin–Tannic Acid as a Green Stabilizer for Oil/Water Emulsion. *ACS Sustain Chem Eng* **2019**, *7* (2), 2370–2379.
- (11) Bai, L.; Greca, L. G.; Xiang, W.; Lehtonen, J.; Huan, S.; Nugroho, R. W. N.; Tardy, B. L.; Rojas, O. J. Adsorption and Assembly of Cellulosic and Lignin Colloids at Oil/Water Interfaces. *Langmuir* **2019**, *35* (3), 571–588.
- (12) Schmidt, B. V. K. J.; Molinari, V.; Esposito, D.; Tauer, K.; Antonietti, M. Lignin-Based Polymeric Surfactants for Emulsion Polymerization. *Polymer (Guildf)* **2017**, *112*, 418–426.
- (13) Kalliola, A.; Vehmas, T.; Liittä, T.; Tamminen, T. Alkali-O<sub>2</sub> Oxidized Lignin–A Bio-Based Concrete Plasticizer. *Ind Crops Prod* **2015**, *74*, 150–157.
- (14) Lievonen, M.; Valle-Delgado, J. J.; Mattinen, M.-L.; Hult, E.-L.; Lintinen, K.; Kostianen, M. A.; Paananen, A.; Szilvay, G. R.; Setälä, H.; Österberg, M. A Simple Process for Lignin Nanoparticle Preparation. *Green Chemistry* **2016**, *18* (5), 1416–1422.
- (15) Larrañeta, E.; Imizcoz, M.; Toh, J. X.; Irwin, N. J.; Ripolin, A.; Perminova, A.; Domínguez-Robles, J.; Rodríguez, A.; Donnelly, R. F. Synthesis and Characterization of Lignin Hydrogels for Potential Applications as Drug Eluting Antimicrobial Coatings for Medical Materials. *ACS Sustain Chem Eng* **2018**, *6* (7), 9037–9046.



- (50) Boyce, J. M. Quaternary Ammonium Disinfectants and Antiseptics: Tolerance, Resistance and Potential Impact on Antibiotic Resistance. *Antimicrob Resist Infect Control* **2023**, *12* (1), 32.
- (51) Haldar, J.; Kondaliah, P.; Bhattacharya, S. Synthesis and Antibacterial Properties of Novel Hydrolyzable Cationic Amphiphiles. Incorporation of Multiple Head Groups Leads to Impressive Antibacterial Activity. *J. Med. Chem.* **2005**, *48* (11), 3823–3831.
- (52) Zhang, S.; Ding, S.; Yu, J.; Chen, X.; Lei, Q.; Fang, W. Antibacterial Activity, *In Vitro* Cytotoxicity, and Cell Cycle Arrest of Gemini Quaternary Ammonium Surfactants. *Langmuir* **2015**, *31* (44), 12161–12169.
- (53) An, L.; Heo, J. W.; Chen, J.; Kim, Y. S. Water-Soluble Lignin Quaternary Ammonium Salt for Electrospun Morphology-Controlable Antibacterial Polyvinyl Alcohol/ Lignin Quaternary Ammonium Salt Nanofibers. *J Clean Prod* **2022**, *368*, No. 133219.
- (54) Chang, L.; Duan, W.; Huang, S.; Chen, A.; Li, J.; Tang, H.; Pan, G.; Deng, Y.; Zhao, L.; Li, D. Improved Antibacterial Activity of Hemp Fibre by Covalent Grafting of Quaternary Ammonium Groups. *R. Soc. Open Sci.* **2021**, *8* (3), No. 201904.
- (55) Arnold, W. A.; Blum, A.; Branyan, J.; Bruton, T. A.; Carignan, C. C.; Cortopassi, G.; Datta, S.; DeWitt, J.; Doherty, A.-C.; Halden, R. U.; Harari, H.; Hartmann, E. M.; Hrubec, T. C.; Iyer, S.; Kwiatkowski, C. F.; LaPier, J.; Li, D.; Li, L.; Muñoz Ortiz, J. G.; Salamova, A.; Schettler, T.; Seguin, R. P.; Soehl, A.; Sutton, R.; Xu, L.; Zheng, G. Quaternary Ammonium Compounds: A Chemical Class of Emerging Concern. *Environ. Sci. Technol.* **2023**, *57* (20), 7645–7665.
- (56) Liang, Y.; Li, H.; Ji, J.; Wang, J.; Ji, Y. Self-Aggregation, Antimicrobial Activity and Cytotoxicity of Ester-Bonded Gemini Quaternary Ammonium Salts: The Role of the Spacer. *Molecules* **2023**, *28* (14), 5469.
- (57) Acurio Cerda, K.; Kathol, M.; Purohit, G.; Zamani, E.; Morton, M. D.; Khalimonchuk, O.; Saha, R.; Dishari, S. K. Cationic Lignin as an Efficient and Biorenewable Antimicrobial Material. *ACS Sustain Chem Eng* **2023**, *11* (28), 10364–10379.
- (58) Jiao, G.-J.; Peng, P.; Sun, S.-L.; Geng, Z.-C.; She, D. Amination of Biorefinery Technical Lignin by Mannich Reaction for Preparing Highly Efficient Nitrogen Fertilizer. *Int J Biol Macromol* **2019**, *127*, 544–554.
- (59) Mohan, M. K.; Silenko, O.; Krasnou, I.; Volobujeva, O.; Kulp, M.; Ošeka, M.; Lukk, T.; Karpichev, Y. Chloromethylation of Lignin as a Route to Functional Material with Catalytic Properties in Cross-Coupling and Click Reactions. *ChemSusChem* **2024**, *17*, No. e202301588.
- (60) Lignin: Historical, Biological, and Materials Perspectives, Copyright, Advisory Board, Foreword, *Dedication*; **1999**; pp 742i–viii.
- (61) *Methods in Lignin Chemistry*; Lin, S. Y.; Dence, C. W., Eds.; Springer Berlin Heidelberg: Berlin, Heidelberg, 1992.
- (62) *Characterization of Lignocellulosic Materials*; Hu, Q. T., Ed.; Wiley, 2008.
- (63) Gellerstedt, G.; Henriksson, G. Lignins: Major Sources, Structure and Properties. In *Monomers, Polymers and Composites from Renewable Resources*; Elsevier, 2008; pp 201–224.
- (64) Christensen, B. T. Barley Straw Decomposition under Field Conditions: Effect of Placement and Initial Nitrogen Content on Weight Loss and Nitrogen Dynamics. *Soil Biol Biochem* **1986**, *18* (5), 523–529.
- (65) Verrillo, M.; Savy, D.; Cangemi, S.; Savarese, C.; Cozzolino, V.; Piccolo, A. Valorization of Lignins from Energy Crops and Agro-industrial Byproducts as Antioxidant and Antibacterial Materials. *J Sci Food Agric* **2022**, *102* (7), 2885–2892.
- (66) Matos, M.; Claro, F. C.; Lima, T. A. M.; Avelino, F.; Hansel, F. A.; Maciel, G. M.; Lomonaco, D.; Magalhães, W. L. E. Acetone:Water Fractionation of Pyrolytic Lignin Improves Its Antioxidant and Antibacterial Activity. *J Anal Appl Pyrolysis* **2021**, *156*, No. 105175.
- (67) Daoud, N. N.; Dickinson, N. A.; Gilbert, P. Antimicrobial Activity and Physico-Chemical Properties of Some Alkyldimethylbenzylammonium Chlorides. *Microbios* **1983**, *37* (148), 73–85.
- (68) Li, F.; Weir, M. D.; Xu, H. H. K. Effects of Quaternary Ammonium Chain Length on Antibacterial Bonding Agents. *J Dent Res* **2013**, *92* (10), 932–938.
- (69) Zhang, H.; Zhao, S.; Li, A.; Bian, K.; Shen, S.; Tao, M.; Shi, P. Structure-Dependent Antimicrobial Mechanism of Quaternary Ammonium Resins and a Novel Synthesis of Highly Efficient Antimicrobial Resin. *Science of The Total Environment* **2021**, *768*, No. 144450.
- (70) Gilbert, P.; Al-taa, A. Antimicrobial Activity of Some Alkyltrimethylammonium Bromides. *Lett Appl Microbiol* **1985**, *1* (6), 101–104.
- (71) Baudrion, F.; Périchaud, A.; Vacelet, E. Influence of Concentration and Structure of Quaternary Ammonium Salts on Their Antifouling Efficiency Tested against a Community of Marine Bacteria. *Biofouling* **2000**, *14* (4), 317–331.
- (72) Gilbert, P.; Moore, L. E. Cationic Antiseptics: Diversity of Action under a Common Epithet. *J. Appl. Microbiol.* **2005**, *99* (4), 703–715.
- (73) Tomlinson, E.; Brown, M. R. W.; Davis, S. S. Effect of Colloidal Association on the Measured Activity of Alkylbenzyltrimethylammonium Chlorides against *Pseudomonas Aeruginosa*. *J. Med. Chem.* **1977**, *20* (10), 1277–1282.
- (74) Jöul, P.; Ho, T. T.; Kallavus, U.; Konist, A.; Leiman, K.; Salm, O.-S.; Kulp, M.; Koel, M.; Lukk, T. Characterization of Organosolv Lignins and Their Application in the Preparation of Aerogels. *Materials* **2022**, *15* (8), 2861.
- (75) Pupart, H.; Jöul, P.; Bramanis, M. I.; Lukk, T. Characterization of the Ensemble of Lignin-Remodeling DyP-Type Peroxidases from *Streptomyces Coelicolor* A3(2). *Energies (Basel)* **2023**, *16* (3), 1557.
- (76) Parm, Ü.; Metsvaht, T.; Sepp, E.; Ilmoja, M.-L.; Pisarev, H.; Pauskar, M.; Lutsar, I. Impact of Empiric Antibiotic Regimen on Bowel Colonization in Neonates with Suspected Early Onset Sepsis. *European Journal of Clinical Microbiology & Infectious Diseases* **2010**, *29* (7), 807–816.

## Appendix 3

### Publication III

Mohan, M. K.; Krasnou, I.; Lukk, T.; Karpichev, Y. Novel Softwood Lignin Esters as Advanced Filler to PLA for 3D Printing. *ACS Omega* **2024**, 9 (44), 44559–44567. <https://doi.org/10.1021/acsomega.4c06680>.

Reprinted with permission from American Chemical Society.



# Novel Softwood Lignin Esters as Advanced Filler to PLA for 3D Printing

Mahendra K. Mohan, Illia Krasnou, Tiit Lukk, and Yevgen Karpichev\*



Cite This: *ACS Omega* 2024, 9, 44559–44567



Read Online

ACCESS |



Metrics & More

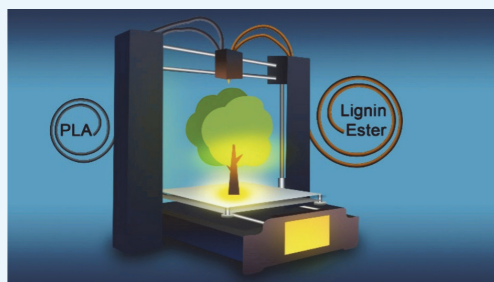


Article Recommendations



Supporting Information

**ABSTRACT:** In this study, we explored the selectivity of softwood lignin toward esterification through chloromethylation. Organosolv pine lignin chloromethylated by a novel greener protocol was subjected to esterification with decanoic acid (C10), tetradecanoic acid (C14), and stearic acid (C18). The success of lignin esterification was confirmed by using FTIR and NMR spectroscopy. For composite preparation, modified lignin was incorporated with PLA in varying proportions (10%, 20%, 30%, and 40%) using the solvent casting technique. The thermal and mechanical properties of the solvent-cast films were analyzed. Notably, lignin esters increased the glass transition temperature ( $T_g$ ) of PLA by a few degrees: tetradecanoic acid (C14) at 30% loading exhibited increases  $T_g$  from approximately 68 to 72 °C. Mechanical testing showed that blending PLA with lignin and its ester derivatives improves its properties. Pure PLA has moderated ductility and stress but lowered stress levels compared to PLA-lignin ester blends. Adding 30% lignin reduced strength and strain, making the material more brittle. In contrast, the PLA + lignin C14 ester (30%) blend achieved the highest stress and strain, enhancing toughness and strength. This makes lignin C14 ester a promising additive for improving the mechanical properties of PLA in applications requiring greater strength and toughness. The composition with optimum properties was selected for production of the 3D-printing filament. Three extrusion temperatures were evaluated, and the advanced mechanical properties of 3D-printed filament along with surface morphology were analyzed.



## INTRODUCTION

The Intergovernmental Panel on Climate Change (IPCC) estimates that global temperatures have risen by about 1.2 °C (2.2 °F) since the preindustrial era. This global warming is mainly driven by human activities, such as burning fossil fuels, deforestation, and industrial processes, which have led to unprecedented levels of greenhouse gas emissions. Approximately one-third of global primary energy demand comes from the building sector, making it a significant source of energy-related greenhouse gas (GHG) emissions.<sup>1</sup> As a result, rapid and extensive climate change has profound impacts on weather patterns, ecosystems, and human societies. Additionally, the manufacturing of construction materials accounts for over 80% of the energy consumption in building construction.<sup>2</sup>

Plastics play a pivotal role in various commercial sectors, contributing to a total production volume of approximately 450 million tons annually in 2019.<sup>3</sup> However, fossil-based plastics are closely associated significant environmental challenges, including CO<sub>2</sub> emissions and littering, which contribute to widespread microplastic pollution. As the global population continues to rise, there is an anticipated surge in the demand for plastic products, even as environmental concerns drive the necessity for the development of renewable alternatives.<sup>4</sup> Presently, the annual production capacity of bioplastics accounts for less than 1% of the total plastic

production volume,<sup>5</sup> underscoring the urgent need for innovative solutions to meet the growing demand for renewable materials and substitute fossil-based plastics.<sup>6</sup>

Increasing environmental awareness is promoting the adoption of greener and high-thermal-performance sustainable materials for construction. Biobased materials are becoming essential for enhancing the energy efficiency of buildings, offering both environmental and economic advantages.<sup>7</sup> Utilizing plant-based biomass materials in construction can decrease fossil energy demand, lower carbon dioxide emissions, and reduce the generation of nondegradable waste.

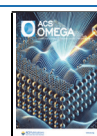
PLA, derived from a renewable agricultural-based monomer, 2-hydroxypropionic acid (lactic acid), is a versatile biopolymer synthesized through the fermentation of starch-rich materials like sugar beets, sugar canes, and corn.<sup>8</sup> Besides its innate biocompatibility, PLA finds extensive application across diverse fields, including 3D printing<sup>9,10</sup> and beyond. However, despite

Received: July 19, 2024

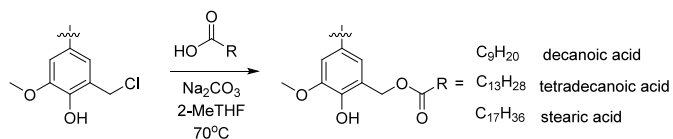
Revised: October 10, 2024

Accepted: October 17, 2024

Published: October 24, 2024



## Scheme 1. Synthesis Pathway of Lignin Esterification



its potential, PLA faces inherent limitations such as brittleness, low heat resistance, high cost and slow crystallization, which have hindered its widespread adoption in commercial applications.<sup>11</sup> Also, it is relatively expensive and produced from starch, which competes with the food supply chain. Thus, the development of sustainable nonfood-based bioadditives for plastics is an approach worthy of further development.

Lignin, an amorphous polyphenol present in plant cell walls, possesses a random, three-dimensional structure formed through an enzyme-mediated dehydrogenative polymerization of phenyl propanoic precursors such as coniferyl, sinapyl, and *p*-coumaryl alcohols. Softwood trees typically contain approximately 28% of lignin, predominantly composed of over 95% guaiacyl units (4-hydroxy-3-methoxy) and traces of *p*-hydroxyphenyl units.<sup>12</sup> It has been clearly observed that the glass transition temperature ( $T_g$ ) of softwood lignin was much higher than that of hardwood lignin.<sup>13</sup> There is increasing interest in leveraging lignin as an affordable and ecofriendly raw material to enhance its utility and broaden its applications. Additionally, there is renewed attention toward producing green and cost-effective polymer composites, where lignin can be incorporated into thermoplastics such as polylactic acid (PLA).<sup>14</sup>

Esterification, which is one of the simplest chemical reactions due to its reaction parameters and reactants, enables the modification of certain properties of lignin.<sup>15</sup> This includes enhancing its hydrophobicity and solubility in organic solvents.<sup>16</sup> Furthermore, esterification functionalizes hydroxyl groups on lignin with ester substituents,<sup>17</sup> reducing hydrogen bonding and increasing molecular free volume.<sup>18</sup> Consequently, this enhances chain mobility and lowers the glass transition point of lignin, thereby increasing its thermoplasticity.<sup>19</sup>

This study aims to incorporate organosolv pine lignin, chemically modified via a greener chloromethylation protocol (reported by our team recently<sup>20,21</sup>) followed by esterification, into PLA as a high-performance filler capable of not only decreasing the amount of PLA in filament targeting a lower price of the final material but also enhancing its thermal and mechanical properties. Given our understanding that unmodified lignin alone does not enhance thermal properties, we chose to conduct a simple two-step esterification process using decanoic, tetradecanoic, and stearic acids. This process aimed to chemically modify lignin obtained from chloromethylated lignin while preserving the hydroxyl groups of lignin. In this research, we synthesized a range of lignin/PLA composites using a solvent casting technique. It is anticipated that the aliphatic groups of long-chain fatty acid esters present on the surface of lignin would enhance adhesion to the PLA matrix during processing. Additionally, the unmodified hydroxyl group on lignin is expected to elevate intermolecular forces, interchain attraction, and cohesion, consequently raising  $T_g$  by reducing mobility. Hence, this study aims to assess the thermal, mechanical, and morphological properties of the resulting

lignin-based PLA biocomposites, demonstrating their suitability as filament materials for 3D printing.

## EXPERIMENTAL SECTION

**Materials and Methods.** *Chemicals.* All reagents utilized, of analytical reagent (AR) grade and procured from Sigma-Aldrich (Taufkirchen, Germany), were employed without further purification. PLA-Ingeo 3D850 was obtained from NatureWorks LLC, US. Deionized water obtained from a Milli-Q water purification system (Millipore S. A., Molsheim, France) was utilized throughout the study. Longitudinally sawn pine timber sawdust was sourced from Prof. Jaan Kers (Tallinn University of Technology, Tallinn, Estonia). The feedstocks underwent drying in a convection oven at 50 °C until reaching 8% moisture content, followed by grinding to a fine powder and subsequent storage in plastic bags at room temperature.

*Methods.* The FT-IR analysis was performed with a Shimadzu IRTracer-100 spectrometer (Kyoto, Japan) in attenuated total reflection (ATR) mode, featuring a resolution of 2  $\text{cm}^{-1}$  and 80 scans. Shimadzu Lab Solutions software was used to analyze all samples within the 400–4000  $\text{cm}^{-1}$  range. For  $^1\text{H}$  NMR analysis, approximately 40 mg of each sample was dissolved in  $\text{DMSO}-d_6$  or  $\text{CDCl}_3$  and placed in a 5 mm NMR tube. The spectra were recorded using a Bruker Avance III 400 MHz spectrometer, and the  $^1\text{H}$  spectra were analyzed with MestReNova x64 software.

*Extraction and Chloromethylation of Lignin.* Lignin was extracted from pine according to the previously described organosolv procedure,<sup>22</sup> and dried organosolv lignin was then weighed (yield 6%) and used for either subsequent analysis or following procedures. Chloromethylation of organosolv lignin was performed according to our previously described procedure<sup>20</sup> (see Scheme 1).

*Esterification of Organosolv Pine.* For esterification of chloromethylated lignin (see Scheme 1), 1 g (1 equiv) of acids (decanoic acid, tetradecanoic acid, and stearic acid) and 1.2 equiv of  $\text{Na}_2\text{CO}_3$  (0.732, 0.552, 0.443 g) were added to 2-MeTHF (10 mL). The mixture was then heated to 70 °C and maintained at this temperature for 30 min. Subsequently, 1 g of dissolved chloromethylated lignin in 10 mL of 2-MeTHF was added to the reaction mixture, which was then stirred overnight at 70 °C. Upon completion of the reaction, the mixture was poured into cold brine, resulting in the formation of a brown precipitate. The precipitate was collected via filtration and washed with water to remove the salts. Finally, the brown precipitate was dried under a vacuum for subsequent steps.

*PLA/Lignin Film Preparation.* PLA was individually dissolved in DCM within a 15 mL glass vial at 45 °C. Lignin was dissolved in THF at room temperature and subsequently mixed to have a content of 10–40% w/w, according to Table S1. The dissolved components were then combined in a Petri dish and left to dry overnight. Following this initial drying

period, the composite material underwent further drying in a vacuum oven at 40 °C for an additional 12 h.

**Differential Scanning Calorimetry.** Differential scanning calorimetry (DSC) was performed by a PerkinElmer Diamond DSC calorimeter (USA) by heating from 0 to 250 °C at a rate of 20 °C/min in a nitrogen atmosphere (purge at 20 mL/min) and then cooling at the same rate. Samples of  $4.00 \pm 0.02$  mg were used for all materials to avoid variations in thermal properties, being pressed into an aluminum cup to improve contact between the material and the heating furnace.

The temperature program started at holding for 1 min, then increased from 0 to 240 °C at a rate of 20 °C/min, followed by a 1 min hold at 240 °C.

**Elemental Analysis.** Elemental analysis was performed using an Elementar Vario MICRO cube apparatus (Langensfeld, Germany) in the CHNS mode. Organic chlorine analysis of lignin was conducted with a Bruker S4 Pioneer XRF spectrometer (USA) using a precalibrated MultiRes measurement method. For the analysis, lignins were mixed with  $\text{NaHCO}_3$  in a 1:10 ratio.

**Thermogravimetry.** TGA experiments on lignin and its derivatives were performed using a Netzsch STA 449F3 thermal analyzer (NETZSCH Instruments North America, Burlington, United States). Samples, weighing  $5 \pm 0.4$  mg, were pyrolyzed in aluminum oxide crucibles under a nitrogen atmosphere at a flow rate of 40 mL/min. The pyrolysis experiments were conducted with a heating rate of 20 K/min, ranging from 20 to 380 °C.

**Mechanical Testing.** Test specimens obtained from the solvent casting (film) and 3D printing extruder process (filament) were mechanically tested with an Instron 5866 instrument (ASTM D638 standard) (Instron, US) and a load cell of 2.5 kN (force sensor capable of measuring up to 2.5 kN of force) used for tensile testing of the biocomposites. Five specimens of each series were tested. The speed and grip distances were 20 and 30 mm for a 10 mm wide film and 50 and 30 mm for extruded filament, respectively.

**3D-Printing Capability.** The test specimen (bone-shaped) with dimensions of  $30 \times 4.96 \times 0.94$  mm was printed with the respective extruded materials using a Wanhao Duplicator 4s dual-extruder 3D printer (China) which was equipped with a 0.4 mm nozzle diameter. The print bed was tempered at 70 °C, and the extruder temperature was varied from 210 to 230 °C for all compositions. See Table S4 for the detailed parameters.

## RESULTS AND DISCUSSION

**Characterization of Organosolv Pine Derivatives.** We previously demonstrated the chloromethylation of aspen lignin<sup>20</sup> and applied the same methodology to pine lignin. A new characteristic peak at 4.5–4.75 ppm in the NMR spectra confirms the presence of  $-\text{CH}_2-\text{Cl}$ . Similarly, absorption peaks in the FT-IR spectra at 1413–142, 1264–1267, and  $633\text{--}670\text{ cm}^{-1}$  indicate the presence of  $-\text{CH}_2\text{Cl}$  groups. XRF analysis further confirms that 11.5% chlorine is present in the chloromethylated sample. These findings provide compelling evidence for the successful incorporation of chloromethyl groups into the lignin structure.

The success of the esterification reaction was confirmed by  $^1\text{H}$  NMR studies. A comparison of the spectra of esterified lignin with the initial substrate, i.e., organosolv pine lignin, revealed the disappearance of the chloromethylated peak ( $\text{ph}-\text{CH}_2-\text{Cl}$ ) and the emergence of a new peak corresponding to

the methylene moieties ( $\text{ph}-\text{CH}_2-\text{O}$ ) indicative of the esters, as illustrated in Figure 1.

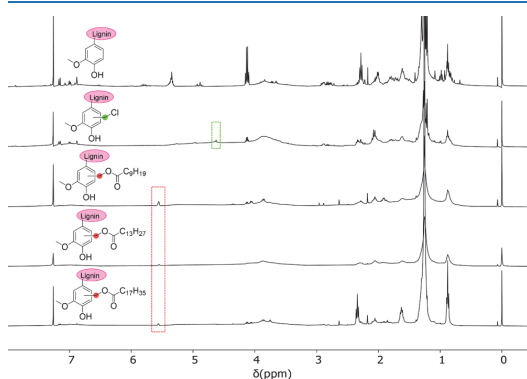


**Figure 1.**  $^1\text{H}$  NMR spectra (from top to bottom) of organosolv pine lignin, chloromethylated lignin, and lignin esters in  $\text{CDCl}_3$ .

The increased intensity of two bands around  $2917$  and  $2850\text{ cm}^{-1}$  is due to  $\text{CH}_2$  stretching modes in the methyl and methylene groups of the ester side chains.<sup>23</sup> Additionally, a major absorption band at  $1735\text{ cm}^{-1}$  and bands at  $1559\text{ cm}^{-1}$  correspond to  $\text{C}=\text{O}$  stretching vibrations and aromatic skeletal vibrations in lignin, respectively,<sup>24</sup> as illustrated in Figure 2a. Lignin's complex and diverse structure can cause considerable variation in the FT-IR spectrum, making it difficult to distinguish between peaks originating from native lignin and those resulting from esterification. In addition, elemental analysis (Table S2) shows that esterified lignin

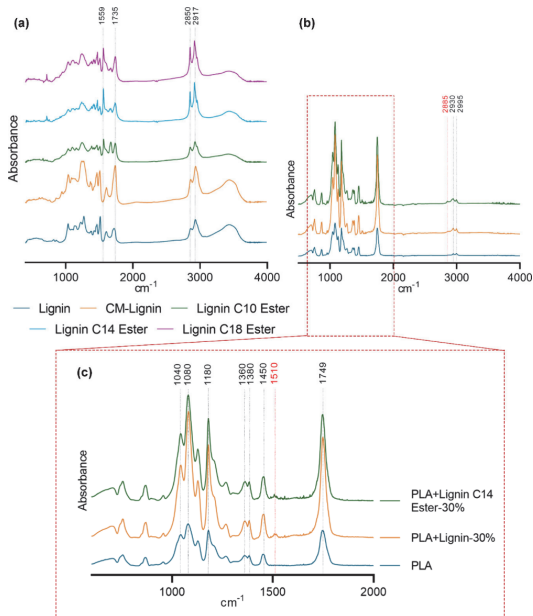


**Figure 2.** FT-IR spectra of organosolv pine lignin and its derivatives (a) and PLA/lignin blends (b,c).

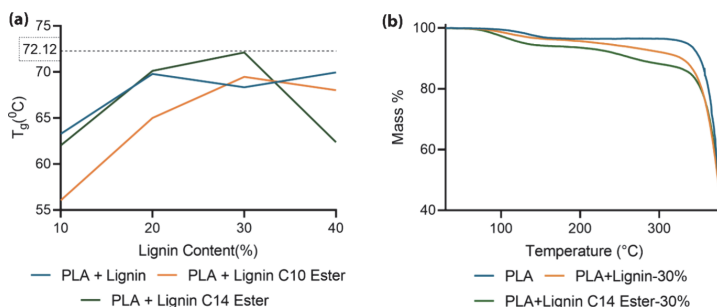


**Figure 3.** Glass transition temperature for PLA/lignin blends (a) and TGA plot of PLA and PLA/lignin composites obtained under a nitrogen atmosphere at 20 °C/min heating rate (b).

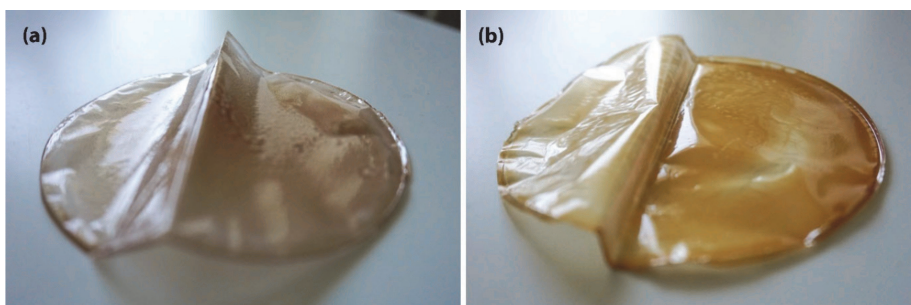


**Figure 4.** PLA + lignin-30% film (a) and PLA + lignin C14 ester-30% film (b).

contains more C and H than native lignin. These changes strongly confirm the lignin esterification;<sup>25</sup> PLA/lignin curves displayed bands similar to those of neat PLA curves (Figure 2b).

The asymmetric and symmetric stretching vibrations of the  $\text{CH}_3$  group were displayed in neat PLA at 2995 and 2930  $\text{cm}^{-1}$ , respectively. A  $\text{C}=\text{O}$  stretching vibration is responsible for the intense peak at 1749  $\text{cm}^{-1}$ . The peak at 1450  $\text{cm}^{-1}$  can be attributed to  $\text{CH}_3$  antisymmetric bending vibrations. Peaks at 1380 and 1360  $\text{cm}^{-1}$  correlate with CH group deformation and bending modes.  $\text{C}-\text{O}-\text{C}$  stretching vibrations are attributed to the peaks at 1180, 1080, and 1040  $\text{cm}^{-1}$ . Interestingly, this peak is notably higher in the PLA/lignin curve, indicating that the addition of lignin increased the hydroxy group content. In addition, biocomposites containing lignin showed a small peak at 1510  $\text{cm}^{-1}$  caused by  $\text{C}=\text{C}$  groups in the aromatic rings and at 2885  $\text{cm}^{-1}$  caused by  $\text{CH}_2$  stretching modes in the methyl and methylene groups of the ester side chain.

**Thermal Behavior: DSC and TGA of Esterified Lignin PLA Composite.** DSC stands as one of the most widely accepted methods for determining the glass transition temperature of lignin molecules. This thermal parameter of polymers yields crucial insights into utilizing lignin in polymer applications and processing it via current industrial techniques such as hot pressing.

Lignin is being explored as fillers, extenders, and reinforcing agents in rubber and thermoset resins,<sup>26</sup> as well as serving as hard segments in the development of toughened thermally simulated shape-memory copolymeric elastomers.<sup>27</sup> The initial study published on lignin modification with fatty acids

demonstrated that esterified lignin acquired novel and intriguing properties, including alterations in solubility and thermal behavior,<sup>28</sup> and a subsequent study noted a steady decline in  $T_g$  with the use of larger ester substituents.<sup>29</sup> It is widely recognized that the reduction of  $T_g$  is more pronounced with longer attached chains. However, determining the  $T_g$  of lignins proves challenging due to the complexity of lignin chemistry and its broad molecular weight distributions, resulting in a typically wide temperature range for this phenomenon.<sup>30</sup> Previous studies have addressed the thermo-plasticity of lignin,<sup>31</sup> suggesting that lignin molecules exhibit a thermal softening point.<sup>32</sup> Typically, this transition occurs at elevated temperatures ranging from 90 to 180 °C for nonderivatized lignins.<sup>33</sup> In this specific case, the  $T_g$  values for isolated pine lignins were determined as 111 and 68 °C for PLA. Nevertheless, PLA with lignin-ester derivatives exhibited a noteworthy alteration in their thermal characteristics. Lignin esters presented in this study show a good compatibility with PLA. Figure 3a and Table S3 illustrate the obtained thermograms for all PLA-lignin-ester derivatives. In the case of unmodified lignin samples, lignin esters with decanoic acid (C10) did not improve the  $T_g$ . However, lignin esters with tetradecanoic acid (C14) at 30% gave the maximum  $T_g$  of 72.12 °C and dropped after further incorporation. The glass transition step in DSC curves is distorted in the case of stearic acid (C18), probably due to the heterogeneity of the material (Figure S1). Thus, the result of the present study suggests PLA + lignin C14 ester-30% to be chosen as the best candidate for further application. Photos of PLA + lignin-30% film and PLA + lignin C14 ester-30% film are given in Figure 4.

The thermogravimetry (TG) curves representing the weight loss percentage of PLA/lignin blends are shown in Figure 3b. These curves were obtained at a heating rate of 20 °C/min under a nitrogen atmosphere. The thermal degradation data indicate the rate of weight loss, which can be used to compare the thermal stability characteristics of different lignin materials. As illustrated in Figure 3b, thermal decomposition occurs over two distinct temperature ranges, beginning at approximately 80 and 245 °C. The weight loss at 80 °C is attributed to the evaporation of humidity and chemically bound water.<sup>34</sup> The major decomposition starting at 245 °C marks the initial degradation temperature, with further degradation occurring at higher temperatures. This indicates that the PLA/lignin blends are thermally stable between 210 and 230 °C, making them suitable for 3D printing applications.

**Mechanical Testing.** Based on the tensile test results of PLA/Lignin film (Figures 4 5 and 6a–c and Table S4), the

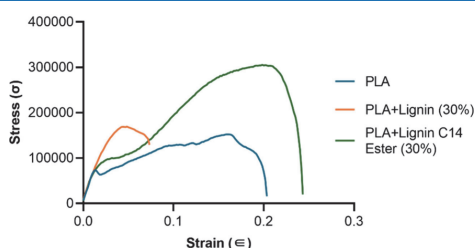


**Figure 5.** Experimental stress–strain curves for PLA, PLA + lignin-30% film, and PLA + lignin C14 ester-30% film.

addition of lignin to PLA affects its mechanical properties. The stress–strain plot (Figure 5) indicates that the mechanical properties of PLA can be significantly altered by blending it with lignin and its ester derivatives. Specifically, pure PLA

shows moderate ductility and stress but does not achieve stress levels as high as those of the PLA-lignin ester blends. PLA + lignin (30%) results in lower strength and strain, suggesting that the material becomes more brittle with lignin addition. PLA + lignin C14 ester (30%) performs the best in terms of both strength and strain, reaching the highest stress and strain values, indicating increased toughness and strength. Overall, the addition of the lignin C14 ester to PLA provides the most beneficial impact on the mechanical properties, making it a promising candidate for applications requiring higher strength and toughness.

The Young's modulus (Figure 6a) of PLA/lignin films (Figure 4a) shows variation based on the lignin used. Incorporation of lignin tends to decrease the stiffness of the PLA matrix, with values generally lower than those of pure PLA. PLA + lignin C14–30% blend had the lowest modulus, indicating a reduction in stiffness. The PLA + lignin C14–30% blend exhibited the highest tensile stress at maximum load (Figure 6b) compared to both neat PLA and PLA + lignin-30% (Figure 4b), indicating that lignin ester can act as a filler that may strengthen the polymer matrix under stress. However, this blend showed a moderate tensile extension at maximum load, slightly lower than that of neat PLA but higher than that of PLA + lignin-30% (Figure 6c), suggesting that modified lignin is a more flexible material. These results suggest that while adding lignin to PLA through a solvent casting method reduces its stiffness; the effect is more pronounced with Lignin C14 ester.

The mechanical properties of the extruded filaments produced at various temperatures and compositions reveal distinct trends (Figure 6d–f and Table S5). Filaments with unmodified lignin and lignin C14 ester at different temperatures exhibited variations in tensile stress, tensile extension, and Young's modulus. The addition of lignin C14 ester significantly improves the tensile stress at maximum load for

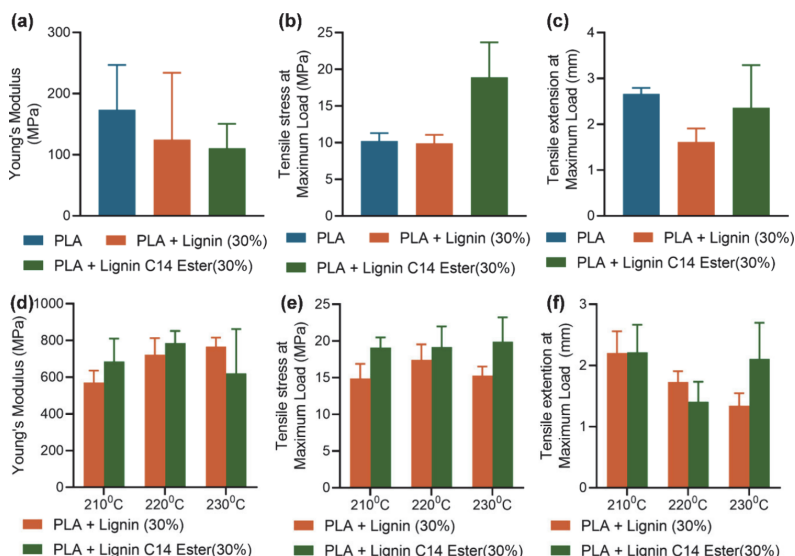


**Figure 6.** (a,d) Young's modulus, (b,e) stress at maximum load, and (c,f) tensile extension at maximum load of PLA/lignin film (a–c) and PLA/lignin extruded filament (d–f).

filament specimens, making them more robust compared to neat material. This improvement is consistent across the different temperatures tested (Figure 6e). The tensile extension decreases with temperature but tends to be higher for filaments with lignin C14 ester at higher temperatures (Figure 6f). The Young's modulus indicates that the blending process and lignin content significantly influence the stiffness. The Young's modulus tends to increase with the processing temperature for both native lignin and lignin C14 ester samples, demonstrating peaks at 230 °C for lignin and 220 °C for lignin C14 ester (Figure 6d).

Similarly, the stress–strain curve (Figure 7) shows that PLA + lignin (30%) at 210 °C exhibits moderate tensile strength

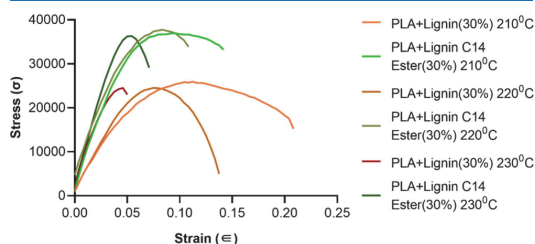


**Figure 7.** Experimental stress–strain curves for PLA and PLA + lignin filaments.

and a reasonable level of strain before fracture. This suggests that these materials have decent flexibility but lower strength compared to others. The PLA+lignin C14 ester (30%) displays the highest tensile strength and strain capability. These materials can endure higher stress and deformation before breaking, indicating that they are the strongest and most flexible in the data set. The filament preparation at 230 °C shows a material with lower tensile strength and a shorter strain range, meaning this material is more brittle, breaking earlier under stress for both lignin and lignin esters. Unmodified lignin with PLA is more brittle (lower strain before failure). However, lignin esters are more ductile, with higher strain values before failure, indicating better flexibility.

In conclusion, the incorporation of lignin into PLA significantly affects the mechanical properties of both films and extruded filaments, demonstrating increased mechanical properties in the composites with significantly higher lignin content compared to the literature.<sup>10,35</sup> Our findings show that the addition of unmodified lignin slightly reduced the tensile stress and extension; however, lignin C14 ester significantly enhanced the tensile stress and extension at the break, suggesting improved compatibility and interaction within the PLA matrix. Lignin generally reduces the Young's modulus of the PLA matrix and can potentially elasticize the polymer composite; it also imparts unique characteristics that might be advantageous for specific applications such as biodegradable packaging and low-load structural components. The findings underscore the importance of optimizing the content and type of lignin for achieving desirable mechanical properties in PLA/lignin composites, particularly for applications in 3D printing and other additive manufacturing technologies where material performance under mechanical stress is crucial.

**Morphological Characterization of 3D-Printed Specimens.** Figure 8 shows individual filaments extruded from a 0.4 mm nozzle at different temperatures for PLA + lignin-30% and

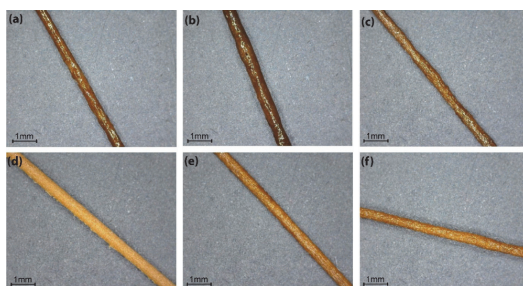


**Figure 8.** Individual filaments extruded from a 0.4 mm nozzle at 210 °C (a, d), 220 °C (b, e), and 230 °C (c, f) for PLA+ lignin-30% (a–c) and PLA + lignin C14 ester-30% (d–f).

PLA + lignin C14 ester-30% composites. The comparison indicates that the addition of lignin C14 ester to PLA results in a filament with improved surface smoothness, especially at higher extrusion temperatures. The smoother surface morphology at 220 °C suggests enhanced compatibility and processing stability for the PLA + lignin C14 ester-30% composite, potentially leading to better mechanical properties and overall material performance.

Figure 9 shows the 3D-printed bone-shaped samples at different temperatures for PLA + lignin-30% and PLA + lignin C14 ester-30% composites. PLA + lignin-30% (Figure 9a–c) samples show significant structural irregularities and poor layer adhesion, indicating suboptimal printing conditions under all three printing conditions. However, PLA + lignin C14 ester-30% (Figure 9d–f) samples demonstrate better structural integrity compared to their PLA + Lignin-30% counterpart at the same temperature but with some visible defects. At 220 °C (Figure 9e) the sample displays the highest quality among all, with a uniform surface texture and strong layer cohesion, indicating optimal printing conditions. The comparison suggests that the incorporation of lignin C14 ester into PLA results in better 3D printability, especially at higher extrusion temperatures. The improved layer adhesion and structural integrity of PLA + lignin C14 ester-30% composites at 220 °C highlight the enhanced compatibility and stability of this material combination, making it more suitable for 3D printing applications compared to PLA + lignin-30%.

## CONCLUSIONS

Organosolv pine lignin was modified through chloromethylation, followed by esterification with decanoic acid (C10), tetradecanoic acid (C14), and stearic acid (C18), and subsequently characterized. Each lignin ester was blended with PLA at four different percentages (10%, 20%, 30%, and 40%) using the solvent casting technique. The blended polymers were subjected to DSC analysis, revealing that the introduction of ester moieties into lignin affected the thermal properties of the polymers. PLA could be filled up to 30% of lignin esters, which results in a slight increase in the  $T_g$  of a composite. PLA/lignin-ester composites were found to be suitable for 3D printing applications. Lignin-esters are compatible with PLA and this increases their thermal stability and mechanical properties, which could be used for the development of high-performance bioplastics with extended working temperature ranges.

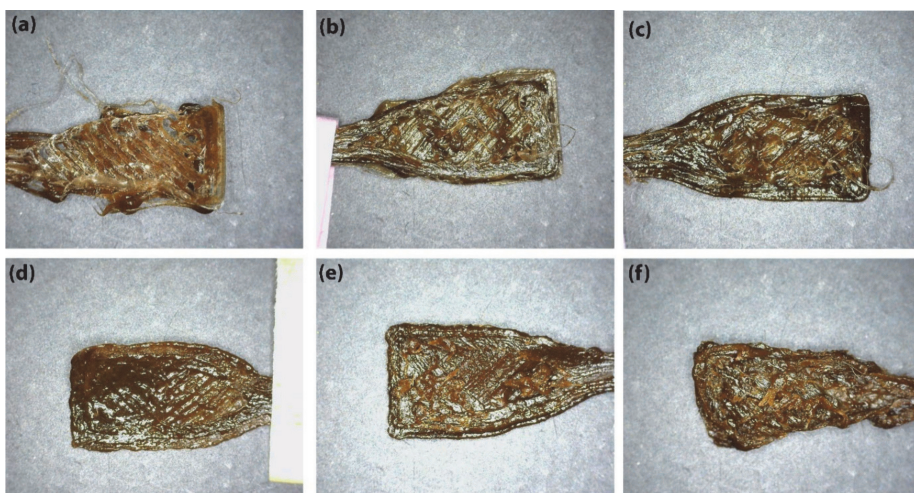


**Figure 9.** 3D-printed bone-shaped samples at 210 °C (a, d), 220 °C (b, e), and 230 °C (c, f) for PLA + lignin-30% (a–c), and PLA + lignin C14 ester-30% (d–f).

Thermogravimetric analyses indicated that the PLA/lignin blends are thermally stable between 210 and 230 °C, with degradation temperatures starting at 245 °C. The addition of lignin and esterified lignin to PLA significantly influenced the mechanical properties of both films and extruded filaments. A comparison of 3D-printed specimens suggests that incorporating lignin C14 ester into PLA results in better 3D printability, especially at higher extrusion temperatures. The improved layer adhesion and structural integrity of PLA + lignin C14 ester-30% composites at 220 °C highlight the enhanced compatibility and stability of this material combination, making it more suitable for 3D printing applications compared to PLA + lignin-30%. The unusual behavior of C14 being both the most flexible and the strongest compared to C10 and C18 carbon chain esters with PLA can be attributed to the optimal balance between chain length and molecular interactions. In the case of C14, the carbon chain is long enough to provide flexibility through increased chain mobility but not so long as to cause excessive chain entanglement or phase separation, which could compromise the strength. In contrast, shorter chains such as C10 may not offer sufficient flexibility, and longer chains such as C18 can lead to more rigid structures due to stronger intermolecular forces or crystallization, reducing overall flexibility. C14 strikes a balance between these effects, leading to an improved flexibility and strength in the composite. This balance between flexibility and strength is less commonly observed but can be explained by the unique interplay of chain length, mobility, and intermolecular interactions specific to this system. Successful incorporation of lignin-based fillers could reduce the price of a bioplastic composite and 3D printing with it. Esterification of lignin is proven to be a greener and more sustainable approach for 3D printing materials development. This strategy to transform biomass into building material gradually reduces greenhouse gas emissions from the building sectors and ensures sustainability, aligning with the United Nations Sustainable Development Goals.

## ■ ASSOCIATED CONTENT

### Supporting Information

The Supporting Information is available free of charge at <https://pubs.acs.org/doi/10.1021/acsomega.4c06680>.

PLA/lignin combinations, elemental composition of lignin esters, DSC values for lignin PLA composites, thermal properties of studied lignin products, mechanical properties of PLA/lignin film, mechanical properties of PLA/lignin extruded filament, and filament fabrication toolpath and process parameters (PDF)

## ■ AUTHOR INFORMATION

### Corresponding Author

Yevgen Karpichev – Department of Chemistry and Biotechnology, Tallinn University of Technology (TalTech), 12618 Tallinn, Estonia; [orcid.org/0000-0003-2322-6750](https://orcid.org/0000-0003-2322-6750); Phone: +372 58 33 75 36; Email: [yevgen.karpichev@taltech.ee](mailto:yevgen.karpichev@taltech.ee); Fax: +372 620 2994

### Authors

Mahendra K. Mohan – Department of Chemistry and Biotechnology, Tallinn University of Technology (TalTech), 12618 Tallinn, Estonia; [orcid.org/0000-0002-6827-592X](https://orcid.org/0000-0002-6827-592X)

Illia Krasnou – Department of Materials and Environmental Technology, Tallinn University of Technology (TalTech), 19086 Tallinn, Estonia; [orcid.org/0000-0002-6459-0199](https://orcid.org/0000-0002-6459-0199)

Tiit Lukk – Department of Chemistry and Biotechnology, Tallinn University of Technology (TalTech), 12618 Tallinn, Estonia; [orcid.org/0000-0001-7765-1707](https://orcid.org/0000-0001-7765-1707)

Complete contact information is available at: <https://pubs.acs.org/doi/10.1021/acsomega.4c06680>

### Author Contributions

The manuscript was written through contributions of all authors. All authors have approved the final version of the manuscript. M.K.M.: conceptualization; methodology; inves-

tigation; validation; data curation; visualization; writing-original draft preparation. I.K.: methodology; investigation; validation; data curation; writing-reviewing and editing. T.L.: conceptualization, methodology; resources; funding acquisition; writing-reviewing and editing; project administration. Y.K.: conceptualization, methodology; resources; funding acquisition; writing -original draft preparation; writing-reviewing and editing; project administration.

### Funding

This study was supported by the Estonian Research Council via project TEM-TA49 (for M.K.M., T.L., and Y.K.)

### Notes

The authors declare no competing financial interest.

## ■ ACKNOWLEDGMENTS

The valuable technical support of Carmen Köster is gratefully acknowledged. The authors acknowledge Prof. Alar Konist for thermogravimetry study.

## ■ ABBREVIATIONS

AcOH, acetic acid; CML, chloromethylated lignin; CHO, formaldehyde; HCl, hydrochloric acid; DMSO, dimethyl sulfoxide; EA, elemental analysis; EtOH, ethanol; FT-IR, Fourier-transform infrared spectroscopy; NMR, nuclear magnetic resonance; PFA, paraformaldehyde; XRF, X-ray fluorescence

## ■ REFERENCES

- (1) Rahim, M.; Douzane, O.; Tran Le, A. D.; Promis, G.; Laidoudi, B.; Crigny, A.; Dupre, B.; Langlet, T. Characterization of Flax Lime and Hemp Lime Concretes: Hygric Properties and Moisture Buffer Capacity. *Energy Build* **2015**, *88*, 91–99.
- (2) Zhang, Y.; Yan, D.; Hu, S.; Guo, S. Modelling of Energy Consumption and Carbon Emission from the Building Construction Sector in China, a Process-Based LCA Approach. *Energy Policy* **2019**, *134*, 110949.
- (3) *Global Plastics Outlook: Economic drivers, environmental impacts and policy options*. OECD. 21 June 2022.
- (4) Chalmin, P. The History of Plastics: From the Capitol to the Tarpeian Rock. *Field Actions Sci. Rep* **2019**, No. Specialissue 19, 6–11.
- (5) Weiss, M.; Haufe, J.; Carus, M.; Brandão, M.; Bringezu, S.; Hermann, B.; Patel, M. K. A Review of the Environmental Impacts of Biobased Materials. *J. Ind. Ecol* **2012**, *16* (s1), S169.
- (6) Ribca, I.; Jawerth, M. E.; Brett, C. J.; Lawoko, M.; Schwartzkopf, M.; Chumakov, A.; Roth, S. V.; Johansson, M. Exploring the Effects of Different Cross-Linkers on Lignin-Based Thermoset Properties and Morphologies. *ACS Sustain Chem. Eng.* **2021**, *9* (4), 1692–1702.
- (7) Adamczyk, J.; Dylewski, R. The Impact of Thermal Insulation Investments on Sustainability in the Construction Sector. *Renewable and Sustainable Energy Reviews* **2017**, *80*, 421–429.
- (8) Elsayy, M. A.; Kim, K.-H.; Park, J.-W.; Deep, A. Hydrolytic Degradation of Polylactic Acid (PLA) and Its Composites. *Renewable and Sustainable Energy Reviews* **2017**, *79*, 1346–1352.
- (9) Haryńska, A.; Janik, H.; Sienkiewicz, M.; Mikolaszek, B.; Kucińska-Lipka, J. PLA-Potato Thermoplastic Starch Filament as a Sustainable Alternative to the Conventional PLA Filament: Processing, Characterization, and FFF 3D Printing. *ACS Sustain Chem. Eng.* **2021**, *9* (20), 6923–6938.
- (10) Bhagia, S.; Bornani, K.; Agrawal, R.; Satlewal, A.; Đurković, J.; Lagaña, R.; Bhagia, M.; Yoo, C. G.; Zhao, X.; Kunc, V.; Pu, Y.; Ozcan, S.; Ragauskas, A. J. Critical Review of FDM 3D Printing of PLA Biocomposites Filled with Biomass Resources, Characterization, Biodegradability, Upcycling and Opportunities for Biorefineries. *Appl. Mater. Today* **2021**, *24*, 101078.
- (11) Balakrishnan, H.; Hassan, A.; Imran, M.; Wahit, M. U. Toughening of Polylactic Acid Nanocomposites: A Short Review. *Polym. Plast Technol. Eng.* **2012**, *51* (2), 175–192.
- (12) Dence, C. W.; Lin, S. Y. Introduction. *Methods in Lignin Chemistry* **1992**, 3–19.
- (13) Awal, A.; Sain, M. Spectroscopic Studies and Evaluation of Thermorheological Properties of Softwood and Hardwood Lignin. *J. Appl. Polym. Sci.* **2011**, *122* (2), 956–963.
- (14) Shi, K.; Liu, G.; Sun, H.; Weng, Y. Polylactic Acid/Lignin Composites: A Review. *Polymers (Basel)* **2023**, *15* (13), 2807.
- (15) Chung, Y.-L.; Olsson, J. V.; Li, R. J.; Frank, C. W.; Waymouth, R. M.; Billington, S. L.; Sattely, E. S. A Renewable Lignin-Lactide Copolymer and Application in Biobased Composites. *ACS Sustain Chem. Eng.* **2013**, *1* (10), 1231–1238.
- (16) Monteil-Rivera, F.; Paquet, L. Solvent-Free Catalyst-Free Microwave-Assisted Acylation of Lignin. *Ind. Crops Prod* **2015**, *65*, 446–453.
- (17) Cachet, N.; Camy, S.; Benjelloun-Mlayah, B.; Condoret, J.-S.; Delmas, M. Esterification of Organosolv Lignin under Supercritical Conditions. *Ind. Crops Prod* **2014**, *58*, 287–297.
- (18) Gordobil, O.; Robles, E.; Egúés, I.; Labidi, J. Lignin-Ester Derivatives as Novel Thermoplastic Materials. *RSC Adv.* **2016**, *6* (90), 86909–86917.
- (19) Thakur, V. K.; Thakur, M. K.; Raghavan, P.; Kessler, M. R. Progress in Green Polymer Composites from Lignin for Multifunctional Applications: A Review. *ACS Sustain Chem. Eng.* **2014**, *2* (5), 1072–1092.
- (20) Mohan, M. K.; Silenko, O.; Krasnou, I.; Volobujeva, O.; Kulp, M.; Ošek, M.; Lukk, T.; Karpichev, Y. Chloromethylation of Lignin as a Route to Functional Material with Catalytic Properties in Cross-Coupling and Click Reactions. *ChemSusChem* **2024**, *17*, No. e202301588.
- (21) Mohan, M. K.; Kaur, H.; Rosenberg, M.; Duvanova, E.; Lukk, T.; Ivask, A.; Karpichev, Y. Synthesis and Antibacterial Properties of Novel Quaternary Ammonium Lignins. *ACS Omega* **2024**, *9* (37), 39134–39145.
- (22) Jöul, P.; Ho, T. T.; Kallavus, U.; Konist, A.; Leiman, K.; Salm, O.-S.; Kulp, M.; Koel, M.; Lukk, T. Characterization of Organosolv Lignins and Their Application in the Preparation of Aerogels. *Materials* **2022**, *15* (8), 2861.
- (23) Hong, S.-H.; Park, J. H.; Kim, O. Y.; Hwang, S.-H. Preparation of Chemically Modified Lignin-Reinforced PLA Biocomposites and Their 3D Printing Performance. *Polymers (Basel)* **2021**, *13* (4), 667.
- (24) Hult, E.-L.; Koivu, K.; Asikkala, J.; Ropponen, J.; Wrigstedt, P.; Sipilä, J.; Poppius-Levlin, K. Esterified Lignin Coating as Water Vapor and Oxygen Barrier for Fiber-Based Packaging. *hfs* **2013**, *67* (8), 899–905.
- (25) Tanase-Opedal, M.; Espinosa, E.; Rodríguez, A.; Chinga-Carrasco, G. Lignin: A Biopolymer from Forestry Biomass for Biocomposites and 3D Printing. *Materials* **2019**, *12* (18), 3006.
- (26) Mousavioun, P.; Halley, P. J.; Doherty, W. O. S. Thermophysical Properties and Rheology of PHB/Lignin Blends. *Ind. Crops Prod* **2013**, *50*, 270–275.
- (27) Sivasankarapillai, G.; Li, H.; McDonald, A. G. Lignin-Based Triple Shape Memory Polymers. *Biomacromolecules* **2015**, *16* (9), 2735–2742.
- (28) Lewis, H. F.; Brauns, F. E.; Buchanan, M. A.; Brookbank, E. B. Lignin Esters of Mono- and Dibasic Aliphatic Acids. *Ind. Eng. Chem.* **1943**, *35* (10), 1113–1117.
- (29) Glasser, W. G.; Jain, R. K. Lignin Derivatives. I. Alkanoates. *hfs* **1993**, *47* (3), 225–233.
- (30) Guo, Z.; Gandini, A.; Pla, F. Polyesters from Lignin. 1. The Reaction of Kraft Lignin with Dicarboxylic Acid Chlorides. *Polym. Int.* **1992**, *27* (1), 17–22.
- (31) Funakoshi, H.; Shiraishi, N.; Norimoto, M.; Aoki, T.; Hayashi, H.; Yokota, T. Studies on the Thermoplasticization of Wood. *Holzforschung* **1979**, *33* (5), 159–166.
- (32) Front Matter. In *Lignin in Polymer Composites*; Elsevier: 2016; p iii. DOI: 10.1016/B978-0-323-35565-0.01001-8.

(33) Li, H.; McDonald, A. G. Fractionation and Characterization of Industrial Lignins. *Ind. Crops Prod* **2014**, *62*, 67–76.

(34) Gkartzou, E.; Koumoulos, E. P.; Charitidis, C. A. Production and 3D Printing Processing of Bio-Based Thermoplastic Filament. *Manuf Rev. (Les Ulis)* **2017**, *4*, 1.

(35) Aguié-Béghin, V.; Di Loreto Campos, N.; Domenek, S.; Maillard, M.-N.; Ducrot, P.-H.; Baumberger, S. The Potential of Lignins as Multifunctional Additives. In *Green Chemistry and Agro-food Industry: Towards a Sustainable Bioeconomy*; Springer Nature Switzerland: 2024; pp 269–290. DOI: [10.1007/978-3-031-54188-9\\_11](https://doi.org/10.1007/978-3-031-54188-9_11)



## Appendix 4






### Publication IV

Mohan, M. K.; Ho, T. T.; Köster, C.; Järvik, O.; Kulp, M.; Karpichev, Y. Tuning Ester Derivatives of Organosolv vs Technical Lignin for Improved Thermoplastic Materials. *Faraday Discuss* **2025**. <https://doi.org/10.1039/D5FD00068H>.

Reprinted with permission from Royal Society of Chemistry



# Tuning ester derivatives of organosolv vs. technical lignin for improved thermoplastic materials†

Mahendra Kothottil Mohan, <sup>‡a</sup> T. Tran Ho, <sup>‡a</sup> Carmen Köster,<sup>a</sup>  
Oliver Järvik, <sup>b</sup> Maria Kulp <sup>a</sup> and Yevgen Karpichev <sup>\*a</sup>

Received 4th May 2025, Accepted 30th June 2025

DOI: 10.1039/d5fd00068h

In this study, lignin from two different sources – organosolv pine and hydrolysis birch – were chemically modified through esterification of hydroxyl groups using octanoyl (C8), lauroyl (C12), and palmitoyl (C16) chlorides, as well as through chloromethylation followed by esterification with tetradecanoic acid (C14) and benzoic acid. Modification of lignin was confirmed by FTIR and NMR spectroscopy. The esterified lignin samples were loaded into polylactic acid (PLA) at loadings of 10%, 20%, and 30% using a solvent casting method. Thermal and mechanical properties of PLA/lignin composites revealed that esterification significantly affected the polymer matrix properties. PLA could sustain as much as 30% lignin ester loading without affecting the film integrity. Among the variations, hydrolysis lignin ester (HLE) and benzoic acid ester (BAEP) enhanced the heat stability of PLA, while esterification with palmitoyl chloride (OHLE\_C16) increased its elasticity through plasticization.

## 1. Introduction

Despite its abundance (up to 35%) and aromatic-rich structure, lignin receives much less attention in biorefineries compared to sugar derivatives in lignocellulosic biomass.<sup>1,2</sup> For instance, the downstream process primarily utilizes black liquor, which contains mostly lignin, for electricity production, a common scenario for every pulp and paper industry worldwide.<sup>3</sup> The difficulties arise in lignin's valorisation due to its heterogeneity of structure and properties that drastically change depending on the botanical origin, as well as the severity of the fractionation process. Lignin's chemistry significantly varies in the compositions of the three main monolignols, *p*-hydroxyphenyl (H), guaiacyl (G), and syringyl (S) (Fig. 1).<sup>4</sup> As

<sup>a</sup>Department of Chemistry and Biotechnology, Tallinn University of Technology (TalTech), Akadeemia tee 15, 12618 Tallinn, Estonia. E-mail: yevgen.karpichev@taltech.ee; Fax: +372 620 2994; Tel: +372 620 4381

<sup>b</sup>Department of Energy Technology, Tallinn University of Technology (TalTech), Ehitaajate tee 5, 19086 Tallinn, Estonia

† Electronic supplementary information (ESI) available. See DOI: <https://doi.org/10.1039/d5fd00068h>

‡ These authors contributed equally to the publication.



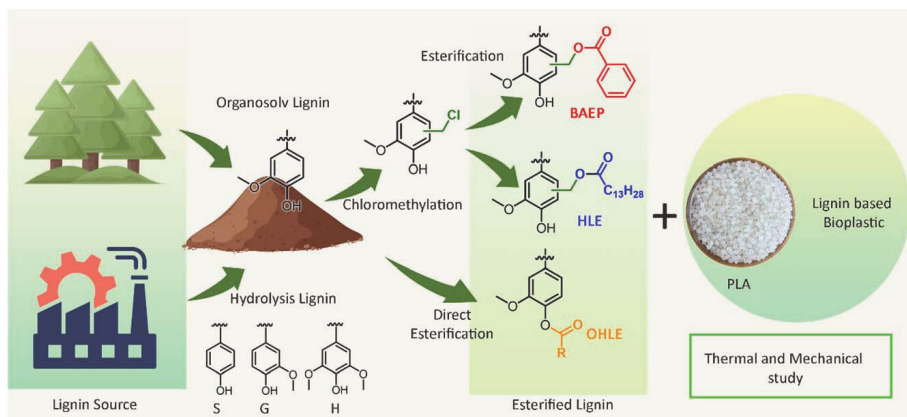


Fig. 1 Esterification of organosolv pine lignin and hydrolysis lignin in three different schemes and their compatibility study with PLA.

a conventional classification, softwood contains mostly guaiacyl units, and minor portions of *p*-hydroxyphenyl and syringyl; while, a hardwood's plant cell wall is predominantly composed of syringyl fragments, and a smaller quantity of guaiacyl; by contrast, all monolignols are present in non-woody biomass.<sup>4,5</sup> On an industrial scale, hydrolysis and organosolv pulping techniques are the two standard practices used to produce technical lignin. The former method focuses on using enzymatic treatment to liberate lignin from the recalcitrant biomass matrix, while the later employs aqueous organic solvents with or without a catalyst for the separation. The native lignin inevitably undergoes structural changes as a consequence of fractionation, which poses a challenge for its high-value-added applications.

Bio-derived polymers face several challenges, including poor interfacial adhesion with synthetic polymers, variations in purity due to differences in raw material sources, and complex extraction processes. These factors can hinder consistent material performance and limit broader applicability.<sup>6</sup> Lignin is a promising candidate for biocomposite production, due to its aromatic structure and high carbon content. The phenolic hydroxyl, carboxyl, and methoxy groups in lignin can be chemically modified to improve its compatibility with a variety of polymers. In recent decades, researchers have been focusing on potential application of lignin in various fields, including automotive components, bioplastics, adhesives, and antimicrobial packaging materials.<sup>7–9</sup> From a sustainability standpoint, lignin and its derivatives present a promising alternative to fossil-based plastics, helping to reduce reliance on petroleum-derived resources while promoting the development of bio-based materials.

Nevertheless, its structural complexity makes direct utilization challenging, which necessitates chemical modification to enhance its functionality and integration. Common modification strategies for lignin include depolymerization, the introduction of new reactive sites, and the functionalization of hydroxyl groups.<sup>7</sup> Techniques such as acetylation, esterification, and phenolation have been widely investigated.<sup>8</sup> Initial attempts to incorporate unmodified lignin into polypropylene often resulted in increased material stiffness but decreased tensile strength and elongation.<sup>9</sup> These drawbacks were primarily due to poor compatibility, specifically the weak adhesion between polar lignin and non-polar



polymers, which is attributed to strong self-interaction driven by inter- and intra-hydrogen bonding, causing lignin particles to agglomerate and act as stress concentrators within the composite.<sup>10</sup> Such limitations underscore the need for suitable chemical modifications to realize lignin's potential in polymer applications completely.<sup>11,12</sup> In contrast, acetylated lignin displays decreased hydrogen bonding because acetyl groups replace the hydroxyl groups during the acetylation. This modification makes acetylated lignin more hydrophobic and enhances its solubility in specific organic solvents.<sup>13</sup>

Esterification is the most frequently chosen pathway among different approaches to improve the thermoplasticity of lignin *via* chemical modification of hydroxy groups.<sup>14</sup> Those functional groups present as one of the significant active sites in lignin that can be functionalized with long-chain hydrocarbons, resulting in materials with improved thermoplasticity, flexibility of the polymer chain, hydrophobicity, and miscibility in nonpolar solvents as a consequence.<sup>15</sup> In a typical fashion, the synthesized material could be obtained by direct esterification with carboxylic acids,<sup>16</sup> acid anhydrides<sup>17</sup> or acid chlorides<sup>18,19</sup> in the presence of suitable catalysts. Recently, we have reported the development of a novel approach to esterify lignin *via* chloromethylation onto the aromatic rings at either the *ortho* or *meta*-position.<sup>20</sup> As an intermediate product, chloromethylated lignin (Fig. 1) offers highly reactive sites towards a variety of functionalization possibilities in which esterification using carboxylic acid is favourable. The obtained material has been successfully studied as a co-polymer blended with polylactic acid (PLA) for 3D printing purposes.<sup>21</sup>

In this work, we present a systematic comparison of two distinct esterification strategies for lignin modification: (i) direct esterification of hydroxyl groups using fatty acid chlorides, and (ii) a two-step process involving chloromethylation followed by reaction with carboxylic acids. The modified lignin samples were blended with polylactic acid (PLA) at varying ratios to assess compatibility and composite performance (Fig. 1). Additionally, the impact of hydrocarbon chain chemistry, such as saturated fatty acids and aromatic acids (*e.g.*, benzoic acid), on the physicochemical properties of the resulting lignin/PLA composites was examined. Two types of lignin were used: hydrolysis lignin from birch (a hardwood) and organosolv lignin from pine (a softwood) to highlight the broad potential of lignin for functionalization and application. The obtained materials were characterized using Fourier transform infrared spectroscopy (FT-IR), phosphorus nuclear magnetic resonance (<sup>31</sup>P NMR), and 2D heteronuclear single quantum coherence (2D-HSQC). Additionally, the resulting biocomposites were characterized using differential scanning calorimetry (DSC), thermogravimetric analysis (TGA), and mechanical testing.

## 2. Materials and methods

### 2.1. Materials

PLA-Ingeo 3D850 from NatureWorks LLC-US, chloroform (99%), lauroyl chloride (98%), triethylamine, octanoyl chloride (99%), and palmitoyl chloride (98%) were purchased from Thermo Fischer Scientific. CDCl<sub>3</sub> and DMSO-*d*<sub>6</sub> from Eurisotop, as well as all reagents used, were of analytical reagent (AR) grade and were procured from Sigma-Aldrich (Taufkirchen, Germany). They were employed without further purification. Four distinct birch-derived hydrolysis lignin (HL)



samples were obtained from Fibenol OÜ (Estonia). The lignin was classified as hydrolysis lignin due to its production process, which involves enzymatic treatment. Longitudinally sawn pine timber sawdust was sourced from Prof. Jaan Kers (Tallinn University of Technology, Tallinn, Estonia).

The preparation of the biomass and organosolv lignin were carried out as described in an earlier study.<sup>22</sup>

## 2.2. Chloromethylation and esterification of lignin

The chloromethylation of organosolv lignin and hydrolysis lignin were carried out following our previously established procedure.<sup>20</sup> Esterification with benzoic acid was carried out by dissolving 2 g (1 eq.) of benzoic acid and 1.48 g (1 eq.) of K<sub>2</sub>CO<sub>3</sub> in 20 mL of THF. The reaction mixture was heated to 70 °C and was maintained at this temperature for 1 hour. Subsequently, 66 mg of KI and 2 g of chloromethylated lignin (previously dissolved in 30 mL of THF) was added. The mixture was then refluxed overnight. After the reaction was completed, the mixture was cooled to room temperature, and the solvent was removed under reduced pressure. The residue was extracted using an ethyl acetate–water system. The organic layer was washed successively with a saturated NaHCO<sub>3</sub> solution, water, and brine, then dried over anhydrous Na<sub>2</sub>SO<sub>4</sub>. Finally, the solvent was removed under reduced pressure, and the product was precipitated in hexane. Esterification of the hydrolysis lignin with tetradecanoic acid was carried out following our previously published procedure.<sup>21</sup>

## 2.3. Chlorine content *via* XRF analysis

X-ray fluorescence (XRF) spectroscopy was used for the determination of chlorine content in chloromethylated lignin. Quantitation was performed using a Bruker S4 PIONEER wavelength-dispersive XRF spectrometer using an Rh anode under vacuum. Lignin samples were pressed into pellets to ensure homogeneity. Chlorine analysis was performed with a PET crystal and with Bruker's pre-calibrated methodology. The theoretical maximum chlorine content of 15.4 wt% was computed from the chloromethylated guaiacyl (G) unit (229.45 g mol<sup>-1</sup>) to facilitate the evaluation of the efficiency of chloromethylation *via* mass-to-mass comparison with the XRF data.

## 2.4. Lignin–OH groups esterification

The direct esterification of organosolv lignin, *via* its hydroxyl groups, was prepared as reported.<sup>23</sup> 1 g of lignin was weighed and dissolved in a 100 mL round-bottom flask containing 10 mL of dry THF. Later, 300 µL of triethylamine (TEA, 1.5 eq. to total OH groups, 2.87 mmol g<sup>-1</sup> of lignin<sup>22</sup>) was added and mixed for 10 minutes. The mixture was then kept in an ice bath for 10 minutes, and fatty acid chlorides (367 µL of octanoyl-C8, 506 µL of lauroyl-C12, or 657 µL of palmitoyl-C16 chlorides) (1.5 equivalents to the total OH groups) were added.<sup>22</sup> The reaction was carried out at room temperature for 4 hours, under vigorous stirring. Upon completion, 50 mL of chloroform was added, and the mixture was transferred to a separatory funnel for liquid–liquid extraction using 30 mL of a 5% sodium hydroxide solution. The organic layer was gathered, and the solvent was evaporated to collect the modified lignin. The final materials were washed three times with 50 mL of 100% ethanol to remove unwanted by-products. The esterified lignin samples were freeze-dried to remove all solvent residue.



## 2.5. PLA/lignin film preparation

PLA was separately dissolved in DCM in a 15 mL glass vial. Lignin was dissolved in THF at room temperature and then mixed to achieve a lignin content of 10% to 30% w/w. Our previous study<sup>21</sup> showed that at 40% lignin esters with PLA, a reduction in  $T_g$  was observed. Based on these results, we have considered only up to 30% as the maximum in this work. The dissolved components were combined in a Petri dish and allowed to dry overnight. After the initial drying phase, the composite material underwent further drying in a vacuum oven at 40 °C for an additional 12 hours.

## 2.6. Fourier transform infrared spectroscopy (FT-IR)

The infrared spectra of the lignins were recorded by IRTracer-100 (Shimadzu, Japan). The measurements were conducted in two modes: diffuse reflection and attenuated total reflection (ATR). All spectra were recorded in the range of 4000–400  $\text{cm}^{-1}$  for 80 scans.

## 2.7. Nuclear magnetic resonance (NMR)

NMR analysis was measured as  $^{31}\text{P}$  for determination of the hydroxyl contents and 2D-heteronuclear single quantum coherence (2D-HSQC) for structural characterization. For the  $^{31}\text{P}$  experiment, approximately 30 mg of lignin was dissolved in 500  $\mu\text{L}$  of pyridine and  $\text{CDCl}_3$  (1.6 : 1 v/v). Upon solubilization, 100  $\mu\text{L}$  of the internal standard (*N*-hydroxy-5-norbornene-2,3-dicarboximide, 20  $\text{mg mL}^{-1}$ ) and 100  $\mu\text{L}$  of relaxation agent (chromium(III) acetyl-acetonate, 5  $\text{mg mL}^{-1}$ ), which were prepared in the same mixture of pyridine and chloroform, were added to the vial containing the solubilized lignin. Finally, 70  $\mu\text{L}$  of 2-chloro-4,4,5,5-tetramethyl-1,3,2-dioxaphospholane, and a phosphorus derivatization reagent, were added.  $^{31}\text{P}$  data were acquired at 25 °C using an inverse gated decoupling pulse sequence (zgig), with 1500 scans, on a Bruker Avance III 400 MHz spectrometer. Data acquisition for 2D-HSQC was carried out on the hydrolyzed lignin and its derivatives. 40 mg of the samples were dissolved in 600  $\mu\text{L}$  of  $\text{DMSO}-d_6$ . Experimental data were achieved using a Bruker Avance III 800 MHz spectrometer with hsqcetgpsisp2.2 pulse sequence, four scans. Data analysis was assisted by the MestReNova software.

## 2.8. Differential scanning calorimetry

Differential scanning calorimetry (DSC) was performed using a PerkinElmer DSC 6000 calorimeter with an IntraCooler II as the cooling system at a constant heating rate of 10 °C  $\text{min}^{-1}$  in a pure nitrogen atmosphere (purity 99.999%, purge at 20  $\text{mL min}^{-1}$ ). A sample mass of 5  $\text{mg} \pm 2 \text{ mg}$  was used for all materials. Samples were pressed into the aluminium crucible using the aluminium lid to improve contact between the material and the crucible.

## 2.9. Thermogravimetry

Thermogravimetric analysis (TGA) was performed using a NETZSCH STA 449 F3 Jupiter® apparatus. The samples were heated in a pure nitrogen atmosphere (purity 99.999%, purge at 40  $\text{mL min}^{-1}$ ) from 25 °C to 400 °C at a constant heating



rate of  $10\text{ }^{\circ}\text{C min}^{-1}$ . The mass of the samples was  $4.8 \pm 0.9\text{ mg}$ . Aluminium crucibles were used.

### 2.10. Mechanical testing

Biocomposites were tested mechanically using an Instron 5866 instrument (ASTM D638 standard) (Instron, US) and a load cell of 2.5 kN (force sensor capable of measuring up to 2.5 kN of force). A grip distance of 30 mm was used for a 10 mm wide film.

## 3. Results and discussion

### 3.1. Characterization of lignin and its modification

We previously demonstrated the esterification followed by chloromethylation of pine lignin, and the same methodology was applied to hydrolysis lignin. NMR proved the chloromethylation procedure to be as efficient for in-house lignin as it was for *in situ* extracted pine lignin. In the  $^1\text{H}$  NMR spectra, the characteristic peak at 4.5–4.75 ppm (Fig. S1 and S2†) confirms the presence of  $\text{CH}_2\text{-Cl}$ . For further confirmation, 2D-HSQC measurement with a higher order in dimension that offers a deeper understanding of lignin structure (*e.g.*, inter-unit linkages, and subunits) was analysed for the hydrolysis of birch lignin.<sup>24,25</sup> As a rule of thumb for the 2D-HSQC interpretation of lignin, focused on two major informative areas: (i) the oxygenated aliphatic side chain (C/H 100–35/6–2.5 ppm), (ii) aromatic or unsaturated carbon (C/H 150–100/8.0–6.0 ppm). All the spectra were calibrated at the solvent signal of DMSO- $\text{d}_6$  (C/H 39.51/2.50 ppm). As a result, the new reactive groups were successfully introduced onto aromatic rings in lignin, as verified by two distinct cross-peaks appearing at C/H 37.97/4.8 and 40.61/4.63 ppm, marked as an asterisk in Fig. 2c, compared to those of the starting material (Fig. 2a). Since the introduction of new functional groups could occur at either the *ortho* or *meta*-position, it explains the emergence of two distinguishable signals in the HSQC spectra. This observation was consistent with the previous  $^1\text{H}$  NMR data. Methoxy is one of the most abundant functional groups in lignin, which supply the intense and stable cross signal at C/H 55.62/3.77 ppm before and after chemical modification, however, the ether linkage ( $\beta\text{-O-4'}$ ) peaks ( $\text{A}_{\beta(\text{S})}$ : C/H 86.06/4.11) undergo substantial decrease in chloromethylation-modified lignin. This can be explained by the fact that the acidic media used in the chloromethylation step depolymerized lignin into smaller fragments by breaking down the labile bond, as also evidenced in our previous study.<sup>20</sup> Moving to the aromatic area of the HSQC spectra, they were strongly indicated by the cross signals of the S and G units as two main monolignols in the hardwood species at C/H 104.30/6.60 and 118.5–110.11/6.90–6.76 ppm, respectively<sup>26</sup> (Fig. 2b). After chloromethylation (Fig. 2d), the intensity of all these peaks drastically declines, confirming that the substitution occurred on the aromatic rings, as per our hypothesis. It is worth noting that, despite the higher degree of methoxylation in S than G units, steric hindrance was not a barrier for introducing new functional groups onto other positions on S-rings.

On the other hand, a  $^{31}\text{P}$  NMR measurement was employed to investigate the impact of the esterification process on the  $\text{-OH}$  groups through the two pathways: using acid chlorides targeting hydroxy groups, and chloromethylation followed by



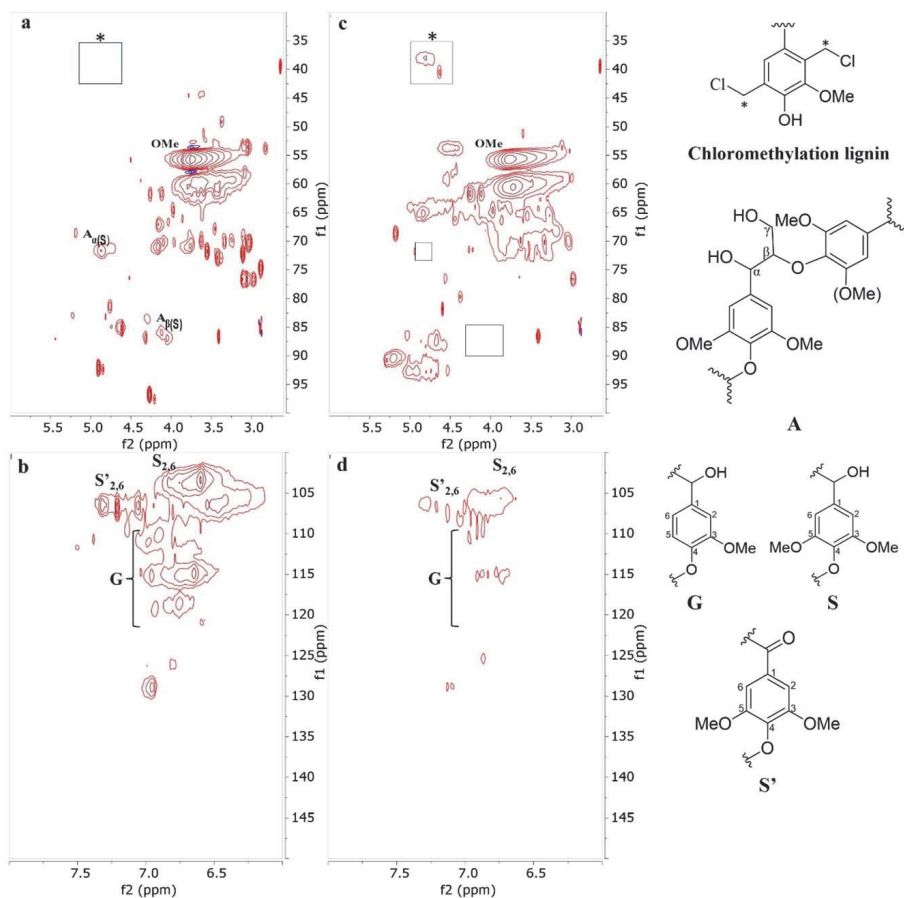


Fig. 2 2D-HSQC of hydrolysis lignin (a and b), chloromethylation lignin (c and d). Two regions of investigation: oxygenated aliphatic side chain (C/H 100–35/6.0–2.5 ppm) (top), aromatic/unsaturated region (C/H 150–100/8.0–6.0 ppm) (bottom). The lignin's subunits are shown on the right side.

esterification. All the spectra were referenced at the internal standard signal of 151.8 ppm before analysis. As a softwood species, phenolic hydroxy groups were predominantly found for G and H units (Fig. S3a<sup>†</sup>).<sup>27</sup> These functional groups were expected to be consumed in the direct esterification approach, as shown in Fig. S3b,† which shows a significant decrease. At the same time, aliphatic hydroxyl groups show a slight change. In the chloromethylated sample (Fig. S3c<sup>†</sup>), there is a profound shift of the origin of OH groups from G units towards the regions of condensed OH (from around 139.0 to 144.0 ppm). Still, it does not disappear, as observed in the first case. The shifting can be explained by two facts: (i) the attachment of chloromethyl to aromatic rings of lignin mimic a similar structure of condensed lignin, (ii) the electronegativity of chloride atoms contributes to the decrease of electron density on the aromatic rings, which causes the shifting towards lower field or higher chemical shift. Later, the grafting of benzoic acid was confirmed by the shift of the signal at approximately 144.0 ppm to a lower chemical shift of 142.4 ppm (Fig. S3d<sup>†</sup>), indicating that the electronegative groups

were replaced successfully, resulting in a balance in electron density due to the attachment of a conjugation system.

XRF analysis further confirms that 13.3% and 13.6% of chlorine is present in the chloromethylated hydrolysis lignin and organosolv pine lignin, respectively. The esterification reaction was confirmed through  $^1\text{H}$  NMR. A comparison study revealed the disappearance of the chloromethylated peak ( $\text{ph-CH}_2\text{-Cl}$ ) and the emergence of a new peak ( $\text{ph-CH}_2\text{-O}$ ), corresponding to the methylene moieties, indicating the formation of the ester (HLE) (Fig. S1†).

The esterification of hydrolysis lignin with tetradecanoic acid (HLE) was confirmed by the enhanced intensity of the two bands around  $2918$  and  $2846\text{ cm}^{-1}$ , which are attributed to  $\text{CH}_2$  stretching vibrations in the methyl and methylene groups of the ester side chains (Fig. 3a). Additionally, a slightly merged absorption band at  $1734\text{ cm}^{-1}$  corresponds to  $\text{C=O}$  stretching vibrations, while the band at  $1575\text{ cm}^{-1}$  and  $1541\text{ cm}^{-1}$  is associated with aromatic skeletal vibrations in lignin, as shown in Fig. 3a. The complex and heterogeneous structure of lignin, with aromatic moieties, makes it challenging to differentiate between peaks arising from native lignin and those introduced through esterification with benzoic acid. The absorption bands arising at  $1740\text{ cm}^{-1}$  and  $1464\text{ cm}^{-1}$  correspond to the ester  $\text{C=O}$  and aromatic stretching vibrations. The  $\text{C-H}$  deformation vibration absorption at  $713\text{ cm}^{-1}$ , typical of monosubstituted benzene compounds, will confirm the benzoic acid ester (BAEP) in Fig. 3b.

For all the direct esterification samples using fatty acid chlorides (C8, C12, C16) (Fig. 3c), the successful modification was confirmed by the appearance of two characteristic signals at  $1740\text{ cm}^{-1}$  and  $1760\text{ cm}^{-1}$  representing aliphatic and

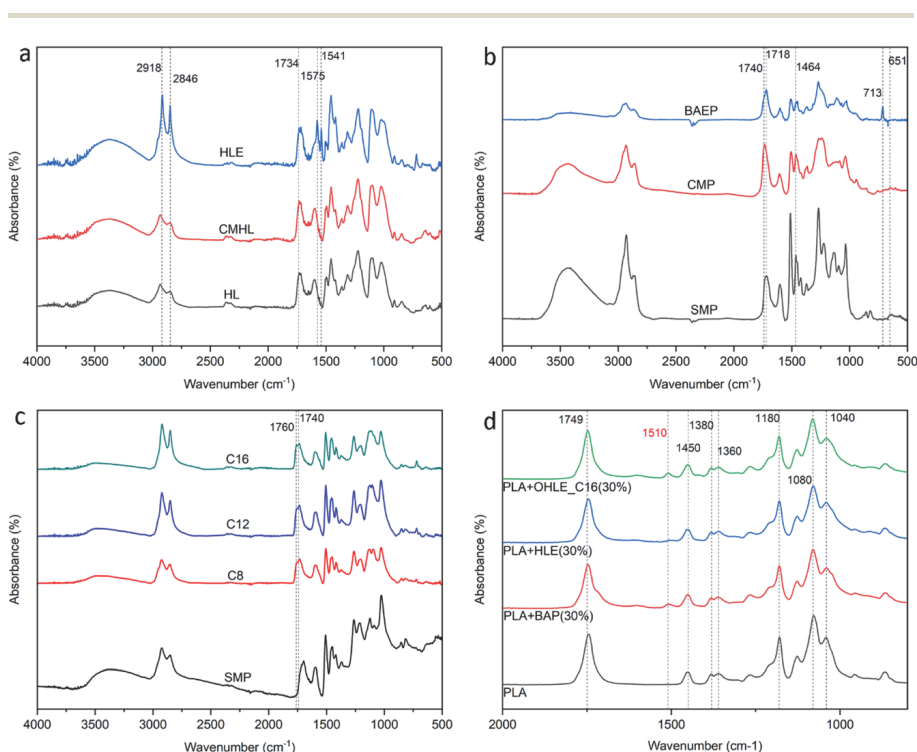


Fig. 3 FT-IR measurements for hydrolysis lignin esters (HLE) (a), lignin benzoic acid ester (BAEP) (b), direct esterified lignin (OHLE) derivatives (c), and PLA/lignin ester films (d).



aromatic esters, respectively.<sup>28</sup> Moreover, the OH stretching vibration band at  $3440\text{ cm}^{-1}$  experienced an incremental decline, which further verifies the consumption of hydroxy groups during the esterification. The variation in attached hydrocarbon chain length (from C8 to C16) was observed as a slight increase within the region of aliphatic C–H stretching  $2918\text{--}2846\text{ cm}^{-1}$ . The work-up procedure was proven to be efficient as the absence of a carbonyl chloride (Cl–C=O) signal at  $1800\text{ cm}^{-1}$ , which originates from unreacted acid chloride,<sup>29</sup> indicated that no side products were detected.

The FT-IR spectra of PLA/lignin composites showed the characteristic band of neat PLA (Fig. 3d). The prominent peak at  $1749\text{ cm}^{-1}$  is attributed to C=O stretching vibrations, and that at  $1450\text{ cm}^{-1}$  is due to antisymmetric bending of  $\text{CH}_3$  groups. Peaks associated with deformation and bending vibrations of CH groups appear at  $1380\text{ cm}^{-1}$  and  $1360\text{ cm}^{-1}$ . C–O–C stretching vibrations are present at  $1180$ ,  $1080$ , and  $1040\text{ cm}^{-1}$ . A weak band at  $1510\text{ cm}^{-1}$  for C=C stretching of an aromatic ring was observed in the biocomposites with lignin.

### 3.2. Thermal behaviour: DSC, TG, and DTG of esterified lignin/PLA composite

The thermal properties of PLA can be systematically altered by incorporating modified lignin at different loadings. Our previous study explored changes in  $T_g$  of PLA loaded with organosolv pine lignin modified with fatty acids. Lignin tetradecanoic acid (C14) at 30% was found to provide the maximum improvement in the glass transition temperature.<sup>21</sup> Similarly, PLA with hydrolysis lignin esters (HLE) resulted in a gradual increase in the glass transition temperature ( $T_g$ ) from  $66\text{ }^\circ\text{C}$  to  $70\text{ }^\circ\text{C}$ , as the concentration increases from 10% to 30%, while reducing  $C_p$  values, indicating enhanced thermal stability of the glassy phase and flexibility of the polymer matrix (Fig. 4a). In contrast, phenolic-OH esterified lignin (OHLE) mixed with PLA exhibited various trends depending on the alkyl chain length. OHLE\_C8 and OHLE\_C12 showed  $T_g$  values close to PLA but moderately increased  $\Delta C_p$ , suggesting balanced flexibility. Remarkably, OHLE\_C16 reduces both  $T_g$  (down to  $55\text{ }^\circ\text{C}$ ) and  $\Delta C_p$ , as shown in Fig. 4b, indicating a strong plasticization effect. Benzoic acid ester lignin (BAEP) with PLA exhibited an increase in  $T_g$ , reaching  $70\text{ }^\circ\text{C}$  at a 30% loading, accompanied by a moderately rising  $\Delta C_p$ , indicating improved thermal properties at higher concentrations. Thus, the results of the present study suggest that HLE-30%, OHLE\_C16-30%, and BAEP-30% should be chosen for further studies.

The thermogravimetric (TG) data (Fig. 4c) reveal the thermal stability of the PLA/lignin esters. All samples show a gradual decrease in mass with increasing temperature. Mass loss occurs in two separate temperature ranges, initiating at around  $80\text{ }^\circ\text{C}$  and again at approximately  $245\text{ }^\circ\text{C}$ . The mass loss observed at  $80\text{ }^\circ\text{C}$  is due to the evaporation of humidity and chemically bound water. Significant thermal decomposition begins at  $245\text{ }^\circ\text{C}$ , marking the onset of substantial degradation, with the degradation rate increasing with the temperature rise. Among them, PLA, BAP-30%, and HLE-30% exhibit a similar trend of degradation, while the OHLE\_C16-30% sample shows the lowest thermal stability. However, BAP-30% shows a slightly higher mass loss at temperatures preceding thermal degradation onset. The differential thermogravimetric (DTG) analysis (Fig. 4d) reveals the differences in thermal degradation behavior. BAP-30% exhibits slightly higher DTG values at the intermediate temperature range of  $80\text{ }^\circ\text{C}$



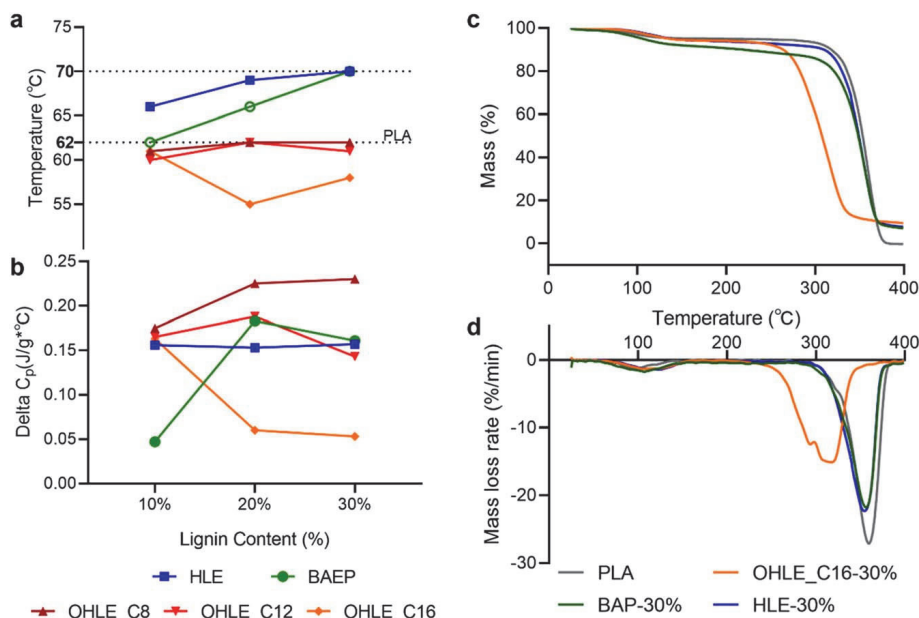


Fig. 4 Glass transition temperature (a),  $\Delta C_p$  (b), thermogravimetric (c), and differential thermogravimetric (d) studies for PLA/lignin film.

to 120  $^{\circ}\text{C}$ . OHLE\_C16-30% exhibits an early degradation trend, whereas HLE-30% and BAP-30% display similar DTG trends to PLA. These results suggest that the OHLE\_C16-30% is the least thermally stable, due to the lack of phenolic hydroxyl groups to form hydrogen bonds. In contrast, esterification through chloromethylation provides the free hydroxyl groups, which are likely to have stronger intermolecular interactions and result in a more thermally stable structure.

Overall, compared to the thermal properties of common fossil-based plastics like polyethylene terephthalate (PET,  $T_g$  70–87  $^{\circ}\text{C}$ ),<sup>30</sup> all esterified lignin/PLA composites show slightly lower glass transition temperatures ( $T_g$  55–70  $^{\circ}\text{C}$ ). The same applies to the selected loading at 30% of modified lignin (OHLE C16, BAP, and HLE) with PLA ( $T_g$  58–70  $^{\circ}\text{C}$ ).

### 3.3. Mechanical properties

Based on the DSC properties, neat PLA and its composites with 30 wt% lignin esters (HLE, OHLE\_C16, and BAEP) were examined for tensile properties, and are listed in Fig. 5 and Table S1.<sup>†</sup> The neat PLA film exhibited the maximum load (15.2  $\pm$  2 N) (Fig. 5a), indicating greater load-carrying capacity compared to other modified composites. Significantly, the PLA + HLE (30%) composite showed reduced maximum load (8.5  $\pm$  2 N) yet the highest tensile stress among all other modified composites (Fig. 5b), which shows improvement in the strength of the material in terms of cross-sectional area after the addition of HLE. In contrast, PLA + OHLE\_C16 (30%) and PLA + BAEP (30%) composites exhibited lower maximum loads and tensile stresses, with PLA + BAEP (30%) recording the lowest tensile stress, indicating a loss of strength.

Tensile extension to the maximum increased upon lignin ester addition (Fig. 5c), showing enhanced ductility of the composite materials. Maximum



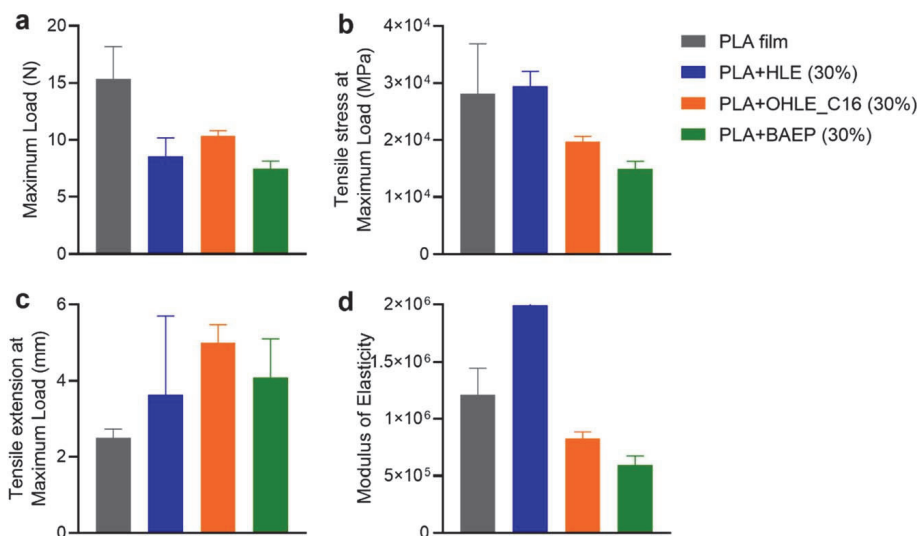


Fig. 5 (a) Maximum load, (b) tensile stress at maximum load, (c) tensile extension at maximum load, (d) Young's modulus of PLA/lignin film.

elongation was observed for PLA + OHLE\_C16 (30%), followed by PLA + HLE and PLA + BAEP, while neat PLA had the minimum extension. This shows that the addition of lignin esters reduces the brittleness of the PLA matrix and enhances its flexibility. The most structurally similar commercial plastic derived from fossil fuel resources, polystyrene (PS), has tensile strength ranging from 35 to 51 MPa,<sup>30</sup> which is lower than PLA itself. This transitive comparison proves that the composite consists of PLA and 30% HLE is a promising material to replace fossil-based plastic.

The modulus of elasticity (Fig. 5d), being a measure of material stiffness, was greatly influenced by the form of lignin ester used. PLA + HLE (30%), followed by neat PLA, possessed the largest modulus, thereby indicating increased stiffness by incorporating HLE. Both the other composites, namely PLA + OHLE\_C16 (30%) and PLA + BAEP (30%), exhibit a lower modulus, indicating a softening effect on the PLA matrix.

In conclusion, the mechanical characteristics of PLA composites depend to a great extent on the nature of the incorporated lignin ester. Among the under-examined samples, PLA + HLE (30%) exhibited higher tensile stress and stiffness, and is therefore most suitable for applications requiring enhanced mechanical strength and rigidity. PLA + OHLE\_C16 (30%) improved ductility at the expense of strength and stiffness, making it ideal for more elastic applications. PLA + BAEP (30%) possessed the worst mechanical properties, suggesting minimal structural reinforcement. This result demonstrates the tunability of the mechanical properties of PLA through lignin ester modification and the potential of HLE as an effective reinforcing agent.

## 4. Conclusions

Lignin isolated by two different processes – organosolv and hydrolysis – were chemically modified through direct esterification at the hydroxyl groups and

esterification *via* chloromethylation. The resulting lignin esters were subsequently characterized and incorporated into PLA at varying concentrations (10%, 20%, and 30%) using the solvent casting technique. Thermal and mechanical analysis of the blended composites revealed that the introduction of ester moieties into lignin affects the thermal and mechanical behaviour of the polymer matrix. Notably, PLA was able to accommodate up to 30% of lignin esters. Among the modifications, HLE and BAEP modifications improve the thermal characteristics of PLA, whereas OHLE\_C16 provides enhanced flexibility through plasticization. These results underscore that the overall characteristics of PLA composites strongly depend on the type of lignin ester introduced. The results demonstrate the potential for tailoring the thermal and mechanical properties of PLA through selective lignin esterification approaches, offering a promising avenue for the production of high-performance, sustainable bioplastics.

## Data availability

The following data associated with this work can be found in the ESI.† <sup>1</sup>H NMR spectra of hydrolysis lignin (HL), chloromethylated hydrolysis lignin (CMHL), and hydrolysis lignin esters (HLE) (Fig. S1†); <sup>1</sup>H NMR spectra of organosolv pine lignin (OPL), chloromethylated pine lignin (CMPL), and benzoic acid ester pine (BAEP) (Fig. S2†); <sup>31</sup>P NMR spectra of organosolv pine lignin (a), C16 ester modified OH of pine lignin (b), chloromethylated pine lignin (c), and benzoic acid ester pine (d) (Fig. S3†); the tensile properties of neat PLA and its composites with 30 wt% lignin esters (HLE, OHLE\_C16, and BAEP) (Table S1†).

## Author contributions

The manuscript was written through the contributions of all authors. All authors have approved the final version of the manuscript. Mahendra K. Mohan: conceptualization; methodology; investigation – organosolv extraction, chemical modification, characterization, thermal and mechanical testing; validation; data curation; visualization; writing – original draft preparation. Tran Ho: methodology; investigation – organosolv lignin extraction, esterification, characterisation, NMR analysis; validation; data curation; writing – original draft preparation. Carmen Köster: investigation – technical lignin characterisation and modification; validation; data curation; writing – original draft preparation. Oliver Järvik: investigation – thermal analysis; validation; data curation; writing – reviewing and editing. Maria Kulp: methodology, writing – reviewing and editing. Yevgen Karpichev: conceptualization, methodology; resources; funding acquisition; writing – reviewing and editing; project administration.

## Conflicts of interest

The authors declare that they have no known competing financial interests or personal relationships that could have appeared to influence the work reported in this paper.



# Acknowledgements

The Estonian Research Council supported this work *via* project TEM-TA49. The valuable technical support of Dr Illia Krasnou, Dr Marina Kudrjašova, and Dr Indrek Reile is gratefully acknowledged. The authors acknowledge Muhammad Afaq Khan for organosolv lignin extraction.

# References

- 1 R. Shorey, A. Salaghi, P. Fatehi and T. H. Mekonnen, *RSC Sustainability*, 2024, **2**, 804–831.
- 2 J. Ralph, C. Lapierre and W. Boerjan, *Curr. Opin. Biotechnol.*, 2019, **56**, 240–249.
- 3 S. Sethupathy, G. Murillo Morales, L. Gao, H. Wang, B. Yang, J. Jiang, J. Sun and D. Zhu, *Bioresour. Technol.*, 2022, **347**, 126696.
- 4 V. K. Ponnusamy, D. D. Nguyen, J. Dharmaraja, S. Shobana, J. R. Banu, R. G. Saratale, S. W. Chang and G. Kumar, *Bioresour. Technol.*, 2019, **271**, 462–472.
- 5 A. V. Faleva, A. Yu. Kozhevnikov, S. A. Pokryshkin, D. I. Falev, S. L. Shestakov and J. A. Popova, *J. Wood Chem. Technol.*, 2020, **40**, 178–189.
- 6 J. Sameni, S. A. Jaffer and M. Sain, *Composites, Part A*, 2018, **115**, 104–111.
- 7 P. Figueiredo, K. Lintinen, J. T. Hirvonen, M. A. Kostiainen and H. A. Santos, *Prog. Mater. Sci.*, 2018, **93**, 233–269.
- 8 F. Taleb, M. Ammar, M. ben Mosbah, R. ben Salem and Y. Moussaoui, *Sci. Rep.*, 2020, **10**, 11048.
- 9 R. Pucciariello, V. Villani, C. Bonini, M. D'Auria and T. Vetere, *Polymer*, 2004, **45**, 4159–4169.
- 10 D. Kun and B. Pukánszky, *Eur. Polym. J.*, 2017, **93**, 618–641.
- 11 C. Wang, S. S. Kelley and R. A. Venditti, *ChemSusChem*, 2016, **9**, 770–783.
- 12 E. A. Agustiany, M. Rasyidur Ridho, M. Rahmi D. N., E. W. Madyaratri, F. Falah, M. A. R. Lubis, N. N. Solihat, F. A. Syamani, P. Karungamye, A. Sohail, D. S. Nawawi, A. H. Prianto, A. H. Iswanto, M. Ghazali, W. K. Restu, I. Juliana, P. Antov, L. Kristak, W. Fatriasari and A. Fudholi, *Polym. Compos.*, 2022, **43**, 4848–4865.
- 13 U. Hwang, B. Lee, B. Oh, H. S. Shin, S. S. Lee, S. G. Kang, D. Kim, J. Park, S. Shin, J. Suhr, S.-H. Kim and J.-D. Nam, *Eur. Polym. J.*, 2022, **165**, 110971.
- 14 S. Laurichesse and L. Avérous, *Prog. Polym. Sci.*, 2014, **39**, 1266–1290.
- 15 A. Lisý, A. Ház, R. Nadányi, M. Jablonský and I. Šurina, *Energies*, 2022, **15**, 6213.
- 16 P. Hafezisefat, L. Qi and R. C. Brown, *ACS Sustain. Chem. Eng.*, 2023, **11**, 17053–17060.
- 17 S. N. Pawar, R. A. Venditti, H. Jameel, H.-M. Chang and A. Ayoub, *Ind. Crops Prod.*, 2016, **89**, 128–134.
- 18 O. Gordobil, E. Robles, I. Egüés and J. Labidi, *RSC Adv.*, 2016, **6**, 86909–86917.
- 19 O. Gordobil, I. Egüés and J. Labidi, *React. Funct. Polym.*, 2016, **104**, 45–52.
- 20 M. K. Mohan, O. Silenko, I. Krasnou, O. Volobujeva, M. Kulp, M. Ošeka, T. Lukk and Y. Karpichev, *ChemSusChem*, 2024, **17**, e202301588.
- 21 M. K. Mohan, I. Krasnou, T. Lukk and Y. Karpichev, *ACS Omega*, 2024, **9**, 44559–44567.
- 22 P. Jõul, T. T. Ho, U. Kallavus, A. Konist, K. Leiman, O.-S. Salm, M. Kulp, M. Koel and T. Lukk, *Materials*, 2022, **15**, 2861.



- 23 E.-L. Hult, J. Ropponen, K. Poppius-Levlin, T. Ohra-Aho and T. Tamminen, *Ind. Crops Prod.*, 2013, **50**, 694–700.
- 24 J.-L. Wen, S.-L. Sun, B.-L. Xue and R.-C. Sun, *Materials*, 2013, **6**, 359–391.
- 25 T.-Q. Yuan, S.-N. Sun, F. Xu and R.-C. Sun, *J. Agric. Food Chem.*, 2011, **59**, 10604–10614.
- 26 Z. Wang and P. J. Deuss, *ChemSusChem*, 2021, **14**, 5186–5198.
- 27 L. Lagerquist, A. Pranovich, I. Sumerskii, S. von Schoultz, L. Vähäsalo, S. Willför and P. Eklund, *Molecules*, 2019, **24**, 335.
- 28 K. A. Y. Koivu, H. Sadeghifar, P. A. Nousiainen, D. S. Argyropoulos and J. Sipilä, *ACS Sustain. Chem. Eng.*, 2016, **4**, 5238–5247.
- 29 R. Shorey and T. H. Mekonnen, *Int. J. Biol. Macromol.*, 2023, **230**, 123143.
- 30 F. Luzi, L. Torre, J. M. Kenny and D. Puglia, *Materials*, 2019, **12**, 471.



## Appendix 5

### Publication V

Mohan, M.K.; Bragina, O.; Mosjakina, S.; Raimundo, J.-M.; Karpichev, Y. Antibacterial Properties of Heteronium Lignin Containing Materials Against ESKAPE Pathogens. *ChemRxiv*. 2025; <https://doi.org/10.26434/chemrxiv-2025-zmlgw-v2>

This content is a preprint and has not been peer-reviewed



# Antibacterial Properties of Heteronium Lignin Containing Materials Against ESKAPE Pathogens

*Mahendra Kothottil Mohan<sup>1 †</sup>, Olga Bragina<sup>1 †</sup>, Sofija Mosjakina<sup>1</sup>, Jean-Manuel Raimundo<sup>2</sup>,  
Yevgen Karpichev<sup>\*1</sup>*

<sup>1</sup>Department of Chemistry and Biotechnology, Tallinn University of Technology (TalTech),  
Akadeemia tee 15, 12618 Tallinn, Estonia

<sup>2</sup> Département Matériaux Polytech Marseille, Aix Marseille University, CINaM UMR CNRS 7325,  
163 Avenue de Luminy, CEDEX 09, 13288 Marseille, France

<sup>†</sup> Contributed equally to the publication

## Corresponding Author:

\*Dr. Yevgen Karpichev, fax: +372 620 2994

E-mail: [yevgen.karpichev@taltech.ee](mailto:yevgen.karpichev@taltech.ee)

## ABSTRACT:

The rise of antibiotic resistance and a declining antimicrobial pipeline pose significant threats to public health. The ESKAPE pathogens—*Enterococcus faecium*, *Staphylococcus aureus*, *Klebsiella pneumoniae*, *Acinetobacter baumannii*, *Pseudomonas aeruginosa*, and *Enterobacter spp.*—are critical multidrug-resistant bacteria urgently needing effective therapies. Lignin has shown promise as a renewable antibacterial material, and its chemical modifications can enhance its antimicrobial activity. In this study, quaternary ammonium (QALs) and quaternary phosphonium (QPLs) lignin materials were derived from softwood (pine) through chloromethylation and further functionalized with tertiary amines and phosphines. Successful synthesis was confirmed via NMR, FT-IR, and elemental analysis. The antibacterial effectiveness of QALs and QPLs against ESKAPE pathogens was evaluated through growth inhibition zone (ZOI) assays and minimum bactericidal concentrations (MBCs). QPLs exhibited greater antibacterial activity than QALs, with QPLs containing a trihexyl carbon chain (C6) demonstrating superior effectiveness compared to those with trioctyl carbon chain (C8). The ZOI test also confirmed that QPLs reached optimal antibacterial activity at C6. The film composed from cellulose acetate (CA) and QPLs containing C6 was obtained by electrospinning in a dimethylacetamide/acetone mixture. The electrospun film of CA-QPL was characterized morphologically using scanning electron microscopy and assessed for its biofilm inhibitory properties against Gram-positive and Gram-negative bacteria. QPL demonstrates dose-dependent cytotoxicity at elevated concentrations; however, it maintains a commendable safety margin relative to its antibacterial efficacy.

**Keywords:** Quaternary ammonium lignin; Quaternary phosphonium lignin, ESKAPE pathogens, Antimicrobial materials, Electrospun films; Sustainable biomaterials, Biofilm inhibition.

## 1. INTRODUCTION

A significant number of resistant infections identified in clinical medicine can be attributed to a specific group of pathogens known as the 'ESKAPE' organisms. This group includes *Enterococcus faecium*, *Staphylococcus aureus*, *Klebsiella pneumoniae*, *Acinetobacter baumannii*, *Pseudomonas aeruginosa*, and other members of the *Enterobacteriaceae* group.<sup>1</sup> These organisms have a common set of characteristics that allow them to thrive in today's healthcare environment. They possess a range of intrinsic or acquired resistance mechanisms, making them a significant cause of resistant infections over time.<sup>2</sup> Several compounds are being developed to target specific virulence factors, aiming to block the pathogenesis or reduce the virulence of ESKAPE organisms.

Quaternary ammonium compounds (QACs) are a well-known class of cationic biocides that exhibit potent antibacterial,<sup>3</sup> fungicidal,<sup>4</sup> antiviral,<sup>5</sup> and antibiofilm<sup>6</sup> activities. QACs consist of a positively charged nitrogen atom bonded to four carbon-containing groups. Numerous hypotheses have been proposed to explain how quaternary ammonium compounds (QACs) work.<sup>7</sup> The prevailing perspective is that QACs are broad-spectrum, nonspecific agents that disrupt cellular membranes.<sup>8</sup> Key factors that influence the effectiveness of QACs include the length and type of their hydrophobic tails, as well as the positive charge of the quaternary nitrogen.<sup>9,10</sup>

Our research group previously proposed a new method for synthesizing a series of quaternary ammonium compounds (QACs) using lignin as the starting material.<sup>11</sup> This approach is cost-effective and straightforward for obtaining quaternary compounds derived from lignin. However, a significant limitation remains: we have only conducted tests against a limited number of clinically isolated bacteria, specifically Methicillin-resistant *S. aureus* and *K. pneumoniae*.

In the mid-20th century, several quaternary phosphonium salts (QPSs), which share structural and biological similarities with quaternary ammonium salts (QASs), were developed and reported as antibacterial agents.<sup>12</sup> Recent reviews have highlighted the potential of these non-nitrogen-based cationic amphiphiles as alternatives to address the issues of resistance and toxicity associated with quaternary ammonium surfactants (QASs).<sup>13</sup> Phosphonium salts were tested in different physical states, either as ionic liquids (liquid state) or as self-assembled nanoparticles derived from ionic liquids, and both forms exhibit potent antimicrobial action.<sup>14,15</sup> These studies highlight that lipophilic, positively charged phosphonium salts exploit microbial membrane vulnerabilities—often more effectively than ammonium analogues.

Lignin, alongside cellulose and hemicellulose, is gaining scientific interest as a source of aromatic compounds, accounting for 30% of all non-fossil organic carbon on Earth. It is produced in large quantities as a byproduct of the pulp and paper industry, where it is primarily burned as a low-efficiency fuel to power paper mills. In addition to its abundance and low cost, lignin is appealing due to its several advantageous properties, including biodegradability, antioxidant activity, high carbon content, high thermal stability, and stiffness, as comprehensively reviewed by Rinaldi et al.<sup>16</sup> These significant characteristics of lignin can be effectively combined with the advanced functionalities of well-defined polymers through covalent bond linkages.<sup>17</sup> Regarding its antibacterial properties, lignin appears to be a promising green alternative to fossil-based agents effective against various harmful microorganisms. Its biocidal activity makes it a more environmentally friendly option compared to silver nanoparticles. Several studies, including our previous work, have demonstrated that lignin exhibits antimicrobial properties.<sup>11</sup> Beyond achieving potent antibacterial effects, it is essential to ensure that lignin-based materials are safe for use in contact with human tissues. For potential biomedical applications such as wound dressings or topical antimicrobial coatings, cytotoxicity must be carefully evaluated. HaCaT cells are spontaneously transformed human keratinocytes that represent the basal epidermal keratinocytes.

In human skin, keratinocytes reside in the epidermal layer alongside Merkel cells, Langerhans cells, and melanocytes. The HaCaT cell line serves as a model system for investigating epidermal homeostasis and skin pathophysiology.<sup>18</sup> They can be used as a model to study the pathogenesis of psoriasis, which is a disease characterized by the hyperproliferation of keratinocytes. They can also be used as an in vitro model to study wound healing, where they represent the highly proliferative epidermis,<sup>19</sup> or as an in vitro model to study the toxic effects of antimicrobial agents on human skin.<sup>20</sup> The spontaneously immortalized HaCaT cell line has been deployed as a keratinocyte model to assess the skin irritation potential of chemicals.<sup>21</sup>

In this study, we developed a new lignin-based phosphonium compound to compare the molecular diversity of quaternary heteronium lignin compounds (QHLs) based on our previous data. The effectiveness of both quaternary ammonium lignins (QALs) and quaternary phosphonium lignins (QPLs) was evaluated through growth inhibition assays and minimum bactericidal concentrations (MBCs) against ESKAPE pathogens. We hypothesize that quaternized phosphonium lignin derivatives exhibit high antibacterial efficacy due to the synergistic effect of positively charged phosphonium groups, which disrupt bacterial membranes, and optimal hydrophobicity, which facilitates membrane penetration. This molecular architecture is proposed to confer both broad-spectrum bactericidal activity and acceptable biocompatibility. The QALs outperformed the previously synthesized compound (C18;  $C_{18}H_{37}N(CH_3)_2$ ), which was used as a positive control in our current studies. We aim to produce electrospun nanofibers from active QLs using cellulose acetate (CA) to evaluate their real-life applications.

## 2. MATERIALS AND METHODS

### 2.1 Materials

All the reagents, CA powder (Mn = 30,000 Da, acetyl content 39.8%), and solvents used were of analytical grade and purchased from Sigma-Aldrich. Pine timber sawdust was provided by Prof. Jaan Kers (Tallinn University of Technology, Tallinn, Estonia). The clinical isolates *Staphylococcus aureus* HUMB 19594 (methicillin-resistant, MRSA), *Enterococcus faecium* HUMB 65620, *Klebsiella pneumoniae* HUMB 01336, and *Pseudomonas aeruginosa* HUMB 4438 D01-10 were obtained from the Estonian Electronic Microbial Database. *Enterobacter cloacae* DSM 109592 and *Acinetobacter baumannii* DSM 25645 were obtained from the German Collection of Microorganisms and Cell Cultures (DSMZ).

### 2.2 Chloromethylation and quaternisation

Organosolv pine extraction and chloromethylation were performed according to the previously described protocol.<sup>11,22</sup> Quaternisation of chloromethylated lignin (CML) (**Scheme 1**) with tertiary amines (triethylamine and trioctylamine) and phosphines (triethylphosphine and trioctylphosphine) is adapted according to our previously reported scheme.<sup>11</sup> 1g of any of the amine or phosphine was added to a solution of CML (1g in 20 ml of acetonitrile), and the mixture was heated at 80°C for 24h. The resulting quaternised lignin (QALs or QPLs) was filtered, washed with hexane, and dried in a vacuum. The resulting quaternary lignin (QLs) were designated as C6, C8, P6, and P8 depending on the number of alkyl chain carbon.

### 2.3 Characterization of QLs

Fourier transform infrared spectroscopy (FT-IR) of QLs was prepared with a concentration of 1:100 KBr pellets. Analysed 80 scans with the resolution of 2 cm<sup>-1</sup> using Shimadzu Lab Solutions software. Proton nuclear magnetic resonance (<sup>1</sup>H NMR, <sup>31</sup>P NMR) spectra of SM, CML, and QLs were acquired using a Bruker Avance III 400 MHz spectrometer (USA). All samples (approximately 60 mg) were dissolved in DMSO-d<sub>6</sub> in a 5 mm NMR tube; MestReNova x64 software was used to plot the <sup>1</sup>H NMR spectra.

Elemental Vario MICRO cube (Langensfeld, Germany) was used for elemental analysis for nitrogen with CHNS mode.

## 2.4 Antibacterial activity assessment

**Growth Inhibition Assay.** A single colony from an overnight culture plate was transferred into 5 mL of LB broth and incubated at 37 °C with shaking at 150 rpm for 16 h. The resulting culture was diluted 1:50 in fresh LB medium and further incubated for 2 h under the same conditions to reach the exponential growth phase. The culture was then adjusted to an optical density at 600 nm ( $OD_{600}$ ) of 0.1, and 100  $\mu$ L of this standardized inoculum was evenly spread on TSA agar plates using sterile glass beads. Plates were allowed to dry for 5 min before applying the test samples. For each plate, 3  $\mu$ L drops of the test compounds (100 mg/mL in DMSO) were dispensed onto the freshly inoculated agar surface. As a control, 3  $\mu$ L of DMSO alone was applied. Plates were incubated at 37 °C for 24 h to allow optimal bacterial growth. Following incubation, the diameter of the clear growth inhibition zone surrounding each drop was measured in millimeters using a caliper. All experiments were performed in three independent biological replicates.

**Minimal Bactericidal Concentration (MBC).** A single colony from an LB agar plate was transferred into LB broth and incubated for 16 h at 37 °C with agitation at 150 rpm. The overnight culture was then diluted 1:50 with fresh medium and further cultivated under the same conditions until reaching the exponential growth phase ( $OD_{600} = 0.6$ ). Cells were harvested by centrifugation at 5000 g for 10 min, and the pellet was resuspended in an equal volume of sterile water. This washing procedure was repeated twice, after which the pellet was finally resuspended in sterile water to achieve a cell density corresponding to  $OD_{600} = 0.2$ . Test compounds were prepared at the required concentrations in 3% DMSO, which was previously confirmed to have no significant effect on bacterial viability after 24 h of exposure. The highest lignin concentration tested in this assay was 6 mg/mL, and the final diluent contained 1.5% DMSO in water. For the MBC assay, 100  $\mu$ L of the bacterial suspension was combined with 100  $\mu$ L of the compound solution and incubated at 37 °C for 24 h. After exposure periods of 1 h and 24 h, 3  $\mu$ L aliquots of the mixture were drop-plated onto LB agar and incubated at 37 °C for 24 h. The minimum bactericidal concentration (MBC) was defined as the lowest compound concentration that resulted in no visible colony formation in the 3  $\mu$ L spot. All MBC determinations were performed in triplicate.

## 2.5 Cell viability assay

The human HACAT cell line, immortalized keratinocytes (ATCC PCS-200-011), was grown in Dulbecco's modified Eagle's medium with 4.5 g/L glucose, L-glutamine, and sodium pyruvate (DMEM, Corning) supplemented with 10% FBS and 1% PEST. Cells were seeded in 96-well plates at a density of  $1 \times 10^5$  cells per well using the Countess Automated Cell Counter (Invitrogen) and incubated overnight at 37 °C, 5%  $CO_2$ , and 95% humidity. After 24 h, 100  $\mu$ L of either fresh medium or fresh medium containing SM and P6 samples at a final concentration of 0.00039 – 0.3 mg/mL (diluted in 3% DMSO) were added to each well, followed by an additional 24 h incubation period. Wells treated with 3% DMSO alone served as the solvent control. Cell viability was assessed using the WST-1 assay (Roche), which enables a colorimetric evaluation based on the reduction of tetrazolium salts to water-soluble formazan by metabolically active cells. The amount of formazan produced is directly proportional to the number of viable cells. Measurements were performed 24 h following treatment. Subsequently, 5  $\mu$ L of WST-1 reagent was added to each well containing 100  $\mu$ L of culture medium, and the plates were incubated at 37 °C for two hours. Absorbance was then measured at 450 nm using a TECAN GENios Pro Microplate Reader (Switzerland).

## 2.6 Electrospinning of CA-Lignin nanofibers

A solution containing 15 wt.% of cellulose acetate (CA) was prepared by mixing acetone and dimethylacetamide in a volume ratio of 2:1 (v/v%) while stirring continuously at room temperature until a homogeneous and transparent solution was achieved. Then, P6 was added to the CA solution to reach a final concentration of 10% (v/v) of P6, and the mixture was stirred again at room temperature to achieve a homogeneous solution.

Cellulose acetate (CA) solutions, both with and without Lignin\_P6 (10%), were electrospun at room temperature using a horizontal electrospinning setup. Each polymer solution was placed in a 5 ml syringe fitted with a needle that had a diameter of 0.6 mm. The electrospinning process was conducted at a voltage of 20–25 kV using a power supply (Gamma High Voltage Research, ES 40R-20W/DM/M1127, Ormond Beach, FL), with the distance between the needle and the collector adjusted to between 8 and 10 cm. The feeding rate was set at 0.8 ml/h, controlled by a syringe pump (NE-1010 Programmable Single Syringe Pump, New Era Pump Systems, Inc.). The electrospun nanofibers were collected on a cylindrical rotary drum, which was covered with non-woven fabric. The CA and CA-Lignin\_P6 membranes were then removed from the non-woven fabric and allowed to dry at room temperature for 24 hours. Scanning electron microscopy (SEM, Zeiss FEG-SEM Ultra-55) was used to assess the morphology and average diameter of the nanofibers.

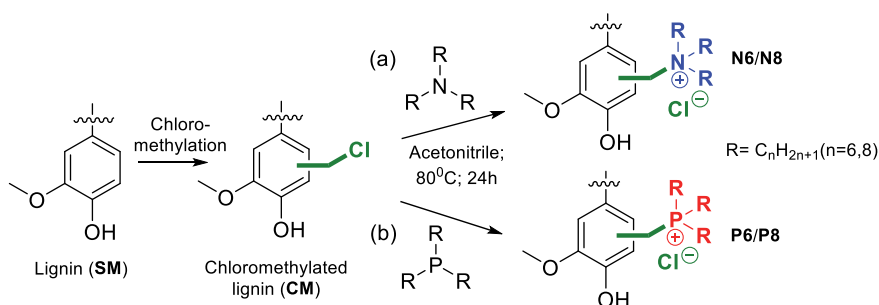
To evaluate the biofilm-inhibitory properties of the tested materials, monospecies biofilms of *Staphylococcus aureus* HUMB 19594 and *Klebsiella pneumoniae* HUMB 01336 were established.<sup>23</sup> Experiments were conducted in sterile 6-well plates (Nunc), using coated samples that were UV-sterilized for 15 minutes before use. Each well was filled with 2 mL of nutrient broth inoculated with approximately  $10^6$  CFU/mL of bacterial suspension prepared in sterile saline. The coated samples were then placed into the wells and incubated at 37 °C for 24 hours to facilitate bacterial adhesion, colonization, and biofilm formation on the material surfaces. Following incubation, the samples were gently rinsed with 1 ml of sterile saline to eliminate planktonic (non-adherent) cells. To recover biofilm-associated cells, the samples were transferred into 1 mL of sterile saline, and biofilms were mechanically disrupted by vigorous vortexing and repeated pipetting. The resulting suspensions containing detached biofilm cells were serially diluted, and 100  $\mu$ L of each dilution was spread onto nutrient agar plates. After 24 hours of incubation at 37 °C, colony-forming units (CFU/mL) were counted to quantify the viable bacteria associated with each sample.

## 2.7 Statistical analysis

Statistical analysis of the data was performed with GraphPad Prism 10.1.1 (GraphPad Software, San Diego, USA). Correlations, multiple linear regression, and analysis of variance (ANOVA), followed by Dunnett's post hoc testing for multiple comparisons at  $p = 0.05$ , were used where appropriate.

## 3. RESULTS AND DISCUSSION

### 3.1 Characterization of lignin and its modification



**Scheme 1.** Schematic synthesis pathway of quaternary ammonium (QALs) and phosphonium (QPLs) lignin, from organosolv lignin (SM), as shown for the G unit of lignin.

A detailed characterization of chloromethylated lignin is described in our previous publication.<sup>11,22,24</sup> Quaternised both ammonium (QALs) and phosphonium lignin (QPLs) were proved by FT-IR measurement (**Figure 1**). Characteristic peaks of CM at 643  $\text{cm}^{-1}$  and 1262  $\text{cm}^{-1}$ , and absorption peaks at 723  $\text{cm}^{-1}$ , 2953  $\text{cm}^{-1}$ , and 1464  $\text{cm}^{-1}$  confirmed both quaternisation of QALs and QPLs.  $^1\text{H}$  NMR spectrum showed high intensity peaks at  $\delta$  0.88 and  $\delta$  1.25 ppm, indicating the presence of  $\text{CH}_3$  and  $\text{CH}_2$  groups that form the hydrophobic tails of the alkyl chains in both QALs and QPLs (**Figure S1**). Furthermore, the  $^{31}\text{P}$  NMR analysis shows a peak at  $\delta$  33.38 for both P6 and P8, confirming the presence of a quaternary phosphonium group in the lignin structure (**Figure S2**). Additionally, CHN analysis proved that all modified QLs have increased C and H% compared to the CM lignin, and the N% was seen only in the QAL samples (**Table S3**).

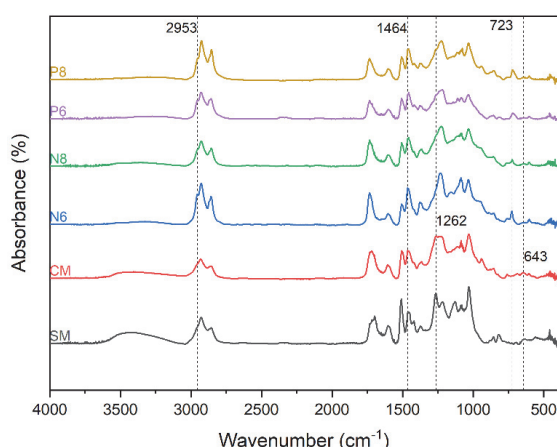


**Figure 1.** FT-IR spectra of organosolv lignin as SM, chloromethylated lignin (CM), quaternary ammonium lignin (N6, N8), and quaternary phosphonium lignin (P6, P8).

### 3.2 Antibacterial activity of lignin

Across all six tested bacterial strains—*Staphylococcus aureus*, *Enterococcus faecium*, *Klebsiella pneumoniae*, *Acinetobacter baumannii*, *Enterobacter cloacae*, and *Pseudomonas aeruginosa*—compound P6 consistently demonstrated the strongest and broadest antibacterial activity. It produced clear and measurable zones of inhibition against every strain tested (**Figure 2**), indicating potent efficacy against both Gram-positive and Gram-negative bacteria, and highlighting its potential as a lead compound for further antimicrobial development. Compound P8 showed moderate activity against five of the six strains, with remarkably consistent inhibition of Gram-negative species, though its overall potency was lower than that of P6. The positive control (PC) exhibited only limited antibacterial effects, with weak inhibition observed against *S. aureus* and *A. baumannii*, and no activity against the other tested bacteria. In contrast, nitrogen-containing quaternary ammonium lignin derivative compounds N6 and N8, as well as SM, showed no detectable antibacterial activity against any of the tested strains, suggesting a lack of intrinsic antimicrobial properties under the conditions used. Overall, P6 stands out as the most promising candidate due to its consistent and high-level activity across a broad spectrum of clinically relevant pathogens.

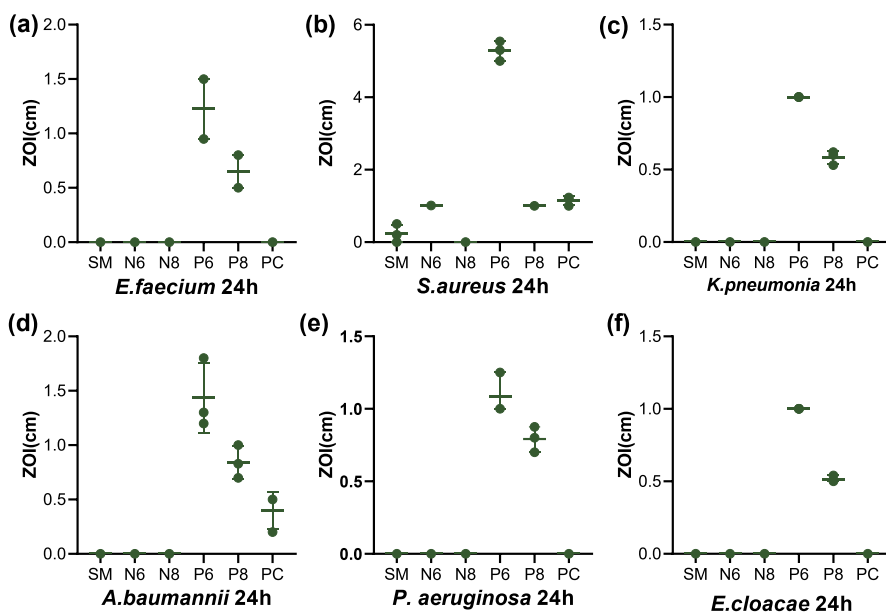


**Figure 2.** The zone of inhibition (ZOI) of lignin samples (QLs) against ESKAPE after 24 h of incubation is plotted. The median and range of three biological replicates are shown.

The comparative analysis of MBCs across six clinically relevant bacterial species (*S. aureus*, *E. faecium*, *K. pneumoniae*, *A. baumannii*, *E. cloacae*, and *P. aeruginosa*) at two different time points—1 hour and 24 hours—demonstrates that the bactericidal efficacy of the tested compounds is both strain-specific and time-dependent. The minimum bactericidal concentration (MBC) against *E. faecium* showed moderate inhibition in both sample groups after 1 hour and 24 hours (**Figure 3a**). Among these, compounds P6 and P8 showed significant effects comparable to the unmodified lignin (SM), while compounds N6 and N8 demonstrated moderate activity. After 24 hours, the most notable improvement was observed for compound P6, indicating a strong time-dependent bactericidal effect. However, the other tested compounds did not alter the MBC even after 24 hours of incubation. In contrast, the lignin sample (SM) showed no inhibition. A similar trend was noted for *S. aureus* (**Figure 3b**). Although initial inhibition at 1 hour was relatively low, most test samples exhibited increased efficacy after 24 hours, particularly for compounds P6 and P8, which performed better than the positive control (PC). Compounds N6 and N8 did not show a significant decrease in MBC, and compound SM remained inactive, consistent with the earlier time point. These results suggest that P6 exhibits strong time-dependent bactericidal activity against gram-positive bacteria and is the most effective compound tested against both *S. aureus* and *E. faecium*. Meanwhile, P8 also shows potential as a moderately active agent.

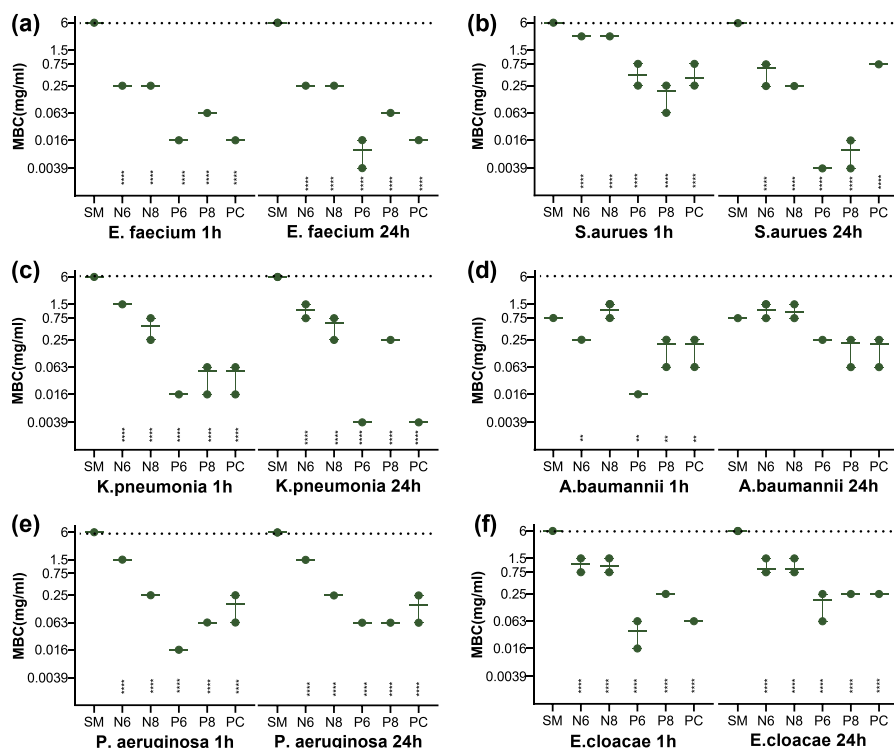


**Figure 3.** Minimal bactericidal concentration (MBC) of lignin samples (QLs) against ESKAPE after one hour and 24 hours of exposure are plotted. The highest concentration (6 mg/ml) was used in the MBC assay. Statistically significant differences from control (SM) are presented above the X-axis for each respective modification, denoted by \*\*\*\* ( $p \leq 0.0001$ ), \*\*\* ( $p \leq 0.001$ ), \*\* ( $p \leq 0.01$ ), and \* ( $p < 0.05$ )

The gram-negative strains exhibited different responses to the tested compounds. For *K. pneumoniae* (Figure 3c), there were significant time-dependent variations in bactericidal efficacy at the 1-hour and 24-hour marks. At the 1-hour point, compounds P6, P8, and PC demonstrated notable activity, while N6 and N8 had moderate effects, and compound SM was inactive. After 24 hours, P6 showed increased potency, with its minimum bactericidal concentration (MBC) decreasing to 0.0039 mg/mL, indicating strong time-dependent activity. Similarly, PC also showed substantial improvement, reaching an MBC of 0.0039 mg/mL, reflecting highly potent bactericidal action. N6 and N8 exhibited a moderate enhancement in efficacy over time.

*A. baumannii* (Figure 3d), *P. aeruginosa* (Figure 3e), and *E. cloacae* (Figure 3f) displayed a complex antibacterial response, highlighting significant differences in compound efficacy over time. At the 1-hour mark, compounds P6, P8, and PC showed the most pronounced bactericidal effects, indicating that all three possess rapid antimicrobial activity against these bacteria. However, after 24 hours, the MBC of P6 increased, suggesting a reduction in potency over extended exposure, possibly due to the activation of bacterial resistance mechanisms such as efflux systems or biofilm formation. In contrast, P8 and PC maintained similar MBC values compared to their 1-hour readings, indicating bacteriostatic activity. These results suggest that P8 has nearly identical activity to PC, whereas P6 retains the highest activity at the 1-hour mark, despite some reduction in efficacy over time. Compounds N6 and N8 exhibited modest or delayed activity, with some improvements noted at the 24-hour mark, indicating

potential for further optimization or use in combination therapy. Conversely, SM remained largely inactive against all tested organisms at both time points, indicating limited bactericidal potential.

The optimal alkyl chain length for antibacterial activity varies between quaternary ammonium lignin and quaternary phosphonium lignin due to the differing chemical properties of their respective cations and their interactions with bacterial membranes. Quaternary ammonium lignin necessitates long hydrophobic single chains (C12–C18) to facilitate adequate membrane penetration and disruption, as the smaller, less polarizable ammonium cation interacts less strongly with lipid bilayers.<sup>11,25</sup> Conversely, quaternary phosphonium lignin demonstrates a stronger inherent affinity for bacterial membranes owing to the larger, more polarizable phosphorus center, which is inherently more lipophilic and capable of effectively penetrating lipid bilayers. Consequently, shorter chains, such as three C6 groups, attain an optimal balance between hydrophobic interaction and water solubility, thereby maximizing antibacterial efficacy. Longer chains in phosphonium derivatives can diminish solubility and restrict surface interactions, whereas shorter, distributed chains sustain robust multivalent contact with bacterial membranes while maintaining adequate dispersibility.

### Cell viability assay

The WST-1 assay revealed distinct biological responses of HaCaT keratinocytes to SM and P6 treatments (Figure 4). Regarding SM, cell viability demonstrated an increase across most tested concentrations, with the peak value recorded at 0.3 mg/mL ( $129.89 \pm \%$ ), followed by 0.15 mg/mL ( $124.11 \pm \%$ ) and 0.025 mg/mL ( $116.53 \pm \%$ ). Even at the lowest concentrations (0.00039–0.0016 mg/mL), viability remained marginally above the control level (105–108%). No tested concentration of SM reduced cell viability below that of the control. Conversely, P6 elicited a pronounced, concentration-dependent decline in viability at higher doses. Specifically, at 0.3 and 0.15 mg/mL, cell viability decreased significantly to 40.62% and 49.38%, respectively, indicating notable cytotoxic effects. At intermediate doses (0.075 mg/mL), viability was 93.19%, whereas lower concentrations ( $\leq 0.025$  mg/mL) did not induce a significant decrease, with values approximating or slightly exceeding 100%.

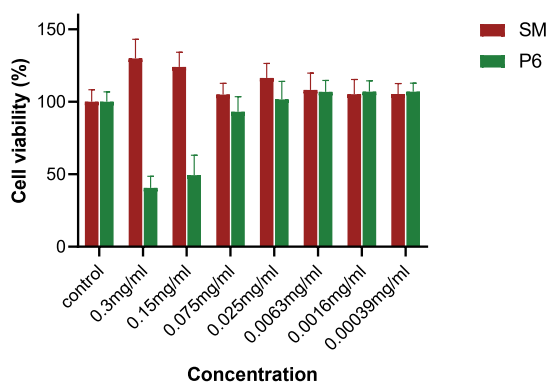


**Figure 4.** Viability of HaCaT after 24 h of exposure at concentrations ranging from 0.00039 to 0.3 mg/mL. Cell viability was expressed as a percentage relative to the control (100%).

Importantly, antibacterial testing demonstrated that the minimum bactericidal concentrations (MBCs) of P6 for the majority of tested bacterial strains were markedly lower than the concentrations at which P6 exhibited cytotoxicity towards HaCaT cells. For instance, MBC values against *S. aureus* and *K. pneumoniae* were as low as 0.0039 mg/mL, whereas cytotoxic effects in keratinocytes were observed only at concentrations of  $\geq 0.15$  mg/mL. Even for less sensitive strains, such as *A. baumannii* (MBC =

0.25 mg/mL) and *E. cloacae* ( $\text{MBC} = 0.19 \pm 0.11 \text{ mg/mL}$ ), bactericidal activity was attained at or below the threshold associated with significant cytotoxicity. This favorable therapeutic window indicates that P6 can achieve effective bactericidal action at doses well below those affecting mammalian cell viability, supporting its potential for safe topical application. Such a margin between antimicrobial potency and cytotoxicity is critical for biomedical materials, as it allows high local concentrations to be applied directly to infected sites while minimizing adverse effects on host tissues. Comparable findings have been reported for other phosphonium- and ammonium-functionalized polymers, where a balance between hydrophobicity, cationic charge, and biocompatibility determined clinical applicability.<sup>26</sup> Given P6's strong antibacterial activity and favorable safety margin, we explored its incorporation into cellulose acetate electrospun fibers to create functional antibacterial surfaces.

### Morphology of CA–Lignin electrospun nanofibres

The SEM images of pure cellulose acetate (CA) electrospun nanofibers and CA-lignin derivatives electrospun nanofibers are presented in **Figure 5**. The pure CA electrospun nanofibers show no bead formation and are thicker and more uniform compared to all other tested samples (see **Figure 5b**). In contrast, the CA-lignin (SM) formations exhibit slight changes in fiber structure, including the presence of beads and thinner fibers (see **Figure 5c**). This effect may be attributed to the complex and irregular structure of lignin, which has a relatively low molecular weight and limited chain entanglement compared to cellulose acetate at this concentration. This disruption in the fiber formation process can encourage bead formation, particularly at high lignin content, such as 10%.

When cellulose acetate is combined with lignin modified with quaternary phosphonium salt (specifically at a concentration of P6-10%), fiber thinning and breakage are observed, as shown in **Figure 5d**. This phenomenon is hypothesized to occur due to the ionic nature of quaternary phosphonium salts. When these salts are added to the solution, they increase the electrical conductivity, which enhances the stretching of the electrospinning jet. However, this can lead to excessive thinning of the fibers, making the jet less stable and often resulting in fiber breakage or spraying instead of continuous fiber formation.

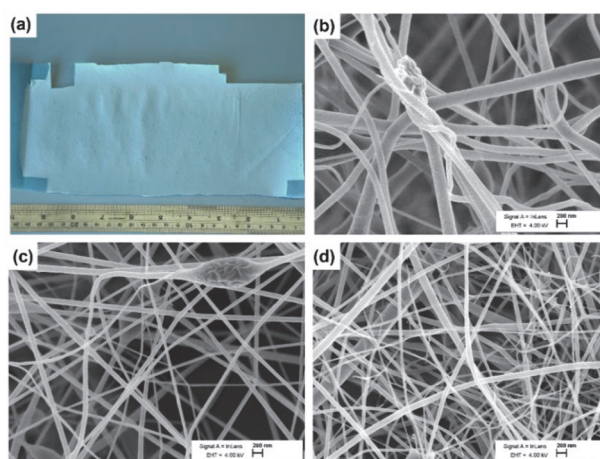


**Figure 5.** Electrospun nanofibers collected on non-woven fabric (a) and SEM images of pure CA nanofibers (b), CA with 10% unmodified lignin(SM) (c), and P6 (d).

### Wettability test

The graph illustrates the change in contact angle as a function of aging time during a wettability test (**Figure 6a**). For all three samples, the contact angle shows a clear decreasing trend with increasing aging time. This trend indicates a progressive enhancement in surface wettability over time, suggesting that the surface becomes more hydrophilic as it ages. The steady decline also implies that the measurements are reliable and reproducible across different trials. Both cellulose acetate (CA, without lignin) and P6 exhibit similar trends in contact angle, starting from approximately 18° and decreasing to around 6.8° at 3.5 seconds. In contrast, SM (cellulose acetate with 10% unmodified lignin) shows a maximum contact angle of approximately 31.5°, which then decreases to about 20.5°. This behavior may be attributed to the hydrophobic nature of organosolv lignin. Conversely, the combination of quaternary phosphonium lignin and CA behaves similarly to cellulose acetate, likely due to the increased polarity from the quaternary groups, resulting in a more hydrophilic surface. Overall, the data support the interpretation of increasing surface hydrophilicity over time, with most contact angles falling within the superhydrophilic range (less than 10°). Beyond morphology, surface properties such as wettability can strongly influence bacterial adhesion and biofilm formation. Therefore, we subsequently evaluated the hydrophilicity of pure CA fibers, CA–SM composites, and CA–P6 composites, followed by an assessment of their anti-biofilm efficacy against representative Gram-positive and Gram-negative bacteria.

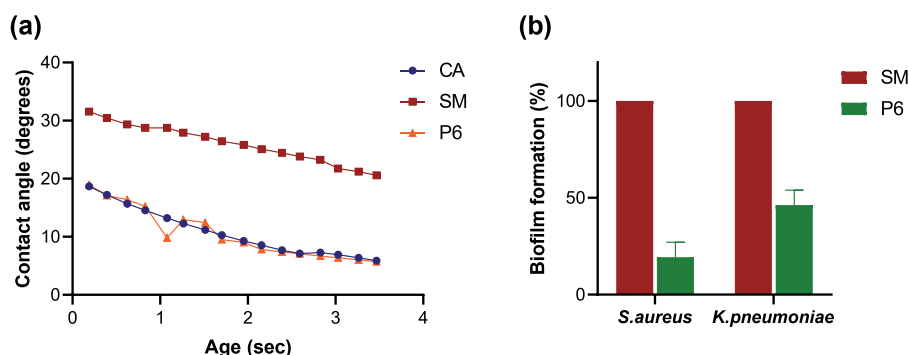


**Figure 6.** (a) Contact angle changes of cellulose acetate (CA-10%), cellulose acetate with 10% unmodified lignin (SM), and cellulose acetate with 10% P6 lignin (P6) over time, and (b) Anti-biofilm properties of the tested materials (SM, P6).

### Anti-Biofilm properties of nanofibers

The anti-biofilm properties of P6 were tested against monospecies biofilms of *Staphylococcus aureus* and *Klebsiella pneumoniae* (**Figure 6b**). The unmodified lignin (SM) served as a control, representing 100% residual biofilm. Previous work has shown that lignin itself can exhibit inherent antibiofilm activity, demonstrating that willow bark-derived fiber bundles, where lignin is a prominent surface component, significantly inhibited *S. aureus* biofilm formation, with bioactivity strongly correlated to the surface lignin content, and noted that activity dropped sharply when coverage fell below ~20%.<sup>27</sup> In our case, the lignin content in P6-based composites was only about 10%, yet phosphonium quaternization enabled substantial antibiofilm effects against both tested species. The results show that P6 significantly reduces biofilm formation by both *Staphylococcus aureus* and *Klebsiella pneumoniae* compared to unmodified lignin. In terms of residual biofilm relative to controls, P6 yielded notably lower levels, especially for *S. aureus*, with biofilm biomass averaging only about 19.4% of the control. This indicates strong anti-adhesive or anti-biofilm effects against Gram-positive bacteria. For *K. pneumoniae*, residual biofilm levels were higher, around 46.2%, but still marked a substantial

decrease relative to untreated surfaces. Interestingly, although the minimum bactericidal concentration (MBC) of P6 was the same for both bacteria (0.0039 mg/mL), their biofilm inhibition effects differed considerably. This demonstrates that bactericidal activity against planktonic cells does not necessarily translate to anti-biofilm effectiveness.<sup>28</sup> Cells within biofilms often show increased resistance due to protective extracellular matrices, altered metabolism, or limited penetration of active agents.<sup>29</sup> Other factors, including biofilm architecture, extracellular polymeric substance (EPS) composition, and cell-surface interaction mechanisms, may also influence biofilm formation and stability on treated surfaces. In the present case, the more potent inhibition observed for *S. aureus* biofilms may be linked to structural differences between Gram-positive and Gram-negative biofilms, including variations in surface charge and extracellular matrix porosity, which can modulate the interaction of cationic lignin derivatives with bacterial communities.

#### 4. CONCLUSIONS

Softwood lignin-based quaternary heteronium compounds (QALs and QPLs) are synthesized and characterized using <sup>1</sup>H NMR, <sup>31</sup>P NMR, FTIR, and elemental analysis. Antibacterial testing against ESKAPE pathogens showed that compound P6 had the strongest and broadest activity profile, with significant time-dependent bactericidal effects against Gram-positive species (*S. aureus*, *E. faecium*) and notable potency against selected Gram-negative strains, especially *K. pneumoniae*. These results align with existing literature indicating that phosphonium cations have greater polarizability and lipophilicity than ammonium analogs, enabling stronger membrane interactions. The C6 chain length appears to strike the best balance between hydrophobic membrane penetration and aqueous dispersibility. Cytotoxicity testing using HaCaT keratinocytes revealed that P6 maintains a favorable safety margin, with bactericidal concentrations well below those causing significant cell viability loss. This profile supports its potential for topical applications, including infected wound management, skin regeneration materials, or antibacterial surface material development. Incorporation of P6 into cellulose acetate electrospun film produced composites with pronounced antibiofilm activity, particularly against *S. aureus*, despite a lignin surface content well below the threshold typically associated with high biofilm inhibition in unmodified lignin systems. This underscores the potential of chemical functionalization to enhance lignin's antimicrobial performance even at reduced loadings. Taken together, these results identify P6 as a promising lead for the development of advanced lignin-based antimicrobial materials. Future studies should aim to elucidate the mechanisms underlying its antibiofilm activity, optimize composite fiber formulations, and validate efficacy and safety in vivo models.

#### ASSOCIATED CONTENT

##### Supporting Information

The following files are available free of charge:

<sup>1</sup>H NMR spectra of starting material (SM), chloromethylated lignin (CML), tertiary amines (triethylamine (N6) and trioctylamine (N8)), and phosphines (triethylphosphine (P6) and trioctylphosphine (P8))(Figure S1); CHN analysis of modified lignin (Table S1); <sup>31</sup>P NMR spectra of phosphines (triethylphosphine (P6) and trioctylphosphine (P8)) (Figure S2).

##### Author contributions

The manuscript was written through the contributions of all authors. All authors have approved the final version of the manuscript.

**Mahendra K. Mohan:** Conceptualization; Methodology; Investigation – synthesis and characterization of studied compounds and materials; Validation; Data curation; Visualization; Writing - Original draft preparation; **Olga Bragina:** Methodology; Investigation – antibacterial and anti-biofilm study; Validation; Data curation; Writing- Original draft preparation; Writing- Reviewing and Editing. **Sofija Mosjakina:** Investigation – antibacterial properties; Validation; Data curation; **Jean-Manuel Raimundo:** Conceptualization; Methodology; Writing - Reviewing and Editing; **Yevgen Karpichev:** Conceptualization, Methodology; Resources; Funding acquisition; Writing - Reviewing and Editing; Project administration.

### Conflict of interest

The authors declare that they have no known competing financial interests or personal relationships that could have appeared to influence the work reported in this paper.

### ACKNOWLEDGEMENTS

This research was funded by Estonian Research Council grants TEM-TA49 (for M.K.M., Y.K.) and PARROT French-Estonian science and technology cooperation programme (for M.K.M., J.-M.R, Y.K.). The valuable technical support of Dr. Illia Krasnou, Dr. Marina Kudrjašova, and Dr. Natalja Savest is gratefully acknowledged.

### REFERENCES

- 1 L. B. Rice, *J Infect Dis*, 2008, **197**, 1079–1081.
- 2 W. R. Miller and C. A. Arias, *Nat Rev Microbiol*, 2024, **22**, 598–616.
- 3 A. Koziróg, B. Brycki and K. Pielech-Przybylska, *Int J Mol Sci*, 2018, **19**, 873.
- 4 A. Zhang, Q. Liu, Y. Lei, S. Hong and Y. Lin, *React Funct Polym*, 2015, **88**, 39–46.
- 5 A. S. Sokolova, O. I. Yarovaya, D. V. Baranova, A. V. Galochkina, A. A. Shtro, M. V. Kireeva, S. S. Borisevich, Y. V. Gatilov, V. V. Zarubaev and N. F. Salakhutdinov, *Arch Virol*, 2021, **166**, 1965–1976.
- 6 S. Takenaka, T. Ohsumi and Y. Noiri, *Japanese Dental Science Review*, 2019, **55**, 33–40.
- 7 A. R. Ahmady, P. Hosseinzadeh, A. Solouk, S. Akbari, A. M. Szulc and B. E. Brycki, *Adv Colloid Interface Sci*, 2022, **299**, 102581.
- 8 R. Dolezal, O. Soukup, D. Malinak, R. M. L. Savedra, J. Marek, M. Dolezalova, M. Pasdiorova, S. Salajkova, J. Korabecny, J. Honegr, T. C. Ramalho and K. Kuca, *Eur J Med Chem*, 2016, **121**, 699–711.
- 9 S. Alkhalifa, M. C. Jennings, D. Granata, M. Klein, W. M. Wuest, K. P. C. Minbiole and V. Carnevale, *ChemBioChem*, 2020, **21**, 1510–1516.
- 10 D. K. A. Kusumahastuti, M. Sihtmäe, I. V. Kapitanov, Y. Karpichev, N. Gathergood and A. Kahru, *Ecotoxicol Environ Saf*, 2019, **172**, 556–565.
- 11 M. K. Mohan, H. Kaur, M. Rosenberg, E. Duvanov, T. Lukk, A. Ivask and Y. Karpichev, *ACS Omega*, DOI:10.1021/acsomega.4c06000.
- 12 S. R. Brayton, Z. E. A. Toles, C. A. Sanchez, M. E. Michaud, L. M. Thierer, T. M. Keller, C. J. Risener, C. L. Quave, W. M. Wuest and K. P. C. Minbiole, *ACS Infect Dis*, 2023, **9**, 943–951.

- 13 R. Odžak, D. Crnčević, A. Sabljic, L. Krce, A. Paladin, I. Primožič and M. Šprung, *Antibiotics*, 2023, **12**, 1231.
- 14 S. Carrara, F. Rouvier, S. Auditto, F. Brunel, C. Jeanneau, M. Camplo, M. Sergent, I. About, J.-M. Bolla and J.-M. Raimundo, *Int J Mol Sci*, 2022, **23**, 2183.
- 15 F. Brunel, C. Lautard, F. Garzino, J.-M. Raimundo, J.-M. Bolla and M. Camplo, *Bioorg Med Chem Lett*, 2020, **30**, 127389.
- 16 R. Rinaldi, R. Jastrzebski, M. T. Clough, J. Ralph, M. Kennema, P. C. A. Bruijninx and B. M. Weckhuysen, *Angewandte Chemie International Edition*, 2016, **55**, 8164–8215.
- 17 H. Liu and H. Chung, *J Polym Sci A Polym Chem*, 2017, **55**, 3515–3528.
- 18 B. Lehmann, *Journal of Investigative Dermatology*, 1997, **108**, 78–82.
- 19 Z. Chen, J. Y. Seo, Y. K. Kim, S. R. Lee, K. H. Kim, K. H. Cho, H. C. Eun and J. H. Chung, *Journal of Investigative Dermatology*, 2005, **124**, 70–78.
- 20 J. López-García, M. Lehotský, P. Humpolíček and P. Sáha, *J Funct Biomater*, 2014, **5**, 43–57.
- 21 A. Hoh and K. Maier, in *Cell and Tissue Culture Models in Dermatological Research*, Springer Berlin Heidelberg, Berlin, Heidelberg, 1993, pp. 341–347.
- 22 M. K. Mohan, O. Silenko, I. Krasnou, O. Volobujeva, M. Kulp, M. Ošeka, T. Lukk and Y. Karpichev, *ChemSusChem*, DOI:10.1002/cssc.202301588.
- 23 I. Liakos, A. Holban, R. Carzino, S. Lauciello and A. Grumezescu, *Nanomaterials*, 2017, **7**, 84.
- 24 M. K. Mohan, T. T. Ho, C. Köster, O. Järvik, M. Kulp and Y. Karpichev, *Faraday Discuss*, DOI:10.1039/D5FD00068H.
- 25 N. Kula, Ł. Lamch, B. Futoma-Kołoch, K. A. Wilk and E. Obłąk, *Sci Rep*, 2022, **12**, 21799.
- 26 Y. Xue, H. Xiao and Y. Zhang, *Int J Mol Sci*, 2015, **16**, 3626–3655.
- 27 J. Dou, P. Ilina, C. D. Cruz, D. Nurmi, P. Z. Vidarte, M. Rissanen, P. Tammela and T. Vuorinen, *J Agric Food Chem*, 2023, **71**, 16554–16567.
- 28 S. Fulaz, S. Vitale, L. Quinn and E. Casey, *Trends Microbiol*, 2019, **27**, 915–926.
- 29 R. Roy, M. Tiwari, G. Donelli and V. Tiwari, *Virulence*, 2018, **9**, 522–554.



# Curriculum vitae

## Personal data

Name: Mahendra Kothottil Mohan  
Date of birth: 20-10-1993  
Place of birth: Olarikkara, Thrissur, Kerala  
Citizenship: India

## Contact data

E-mail: mahendrakmohan@gmail.com

## Education

2021–2025 Tallinn University of Technology, PhD  
2014–2016 Bangalore University, Karnataka, India, MSC (Organic Chemistry)  
2011–2014 Calicut University, Kerala, India, BSC (Chemistry)

## Language competence

English Fluent  
Malayalam Native  
Hindi Limited Working Proficiency  
Estonian Elementary Proficiency, A1

## Professional employment

2016–2021 Research Assistant, Institute for Stem Cell Science and Regenerative Medicine (InStem), NCBS, Bangalore, India

## Short study visit.

2022 Training, University Aix-Marseille, France, 10<sup>th</sup>- 18<sup>th</sup> December  
2023 Training, University of Tartu, Estonia, 8<sup>th</sup> -10<sup>th</sup> March  
2025 MedChem Program: From Organic Chemistry to Pharmaceutical Drugs, Porto University, Portugal, 7<sup>th</sup>-11<sup>th</sup> July

## Honours and awards

2022 Best Flash Presentation Award, Department of Chemistry and Biotechnology Symposium, Tallinn, Estonia  
2022 Two times Dora Plus Short study visit scholarship (T1.1), (The Archimedes Foundation, Estonia)  
2025 Erasmus+ Short-term and blended mobility scholarship

## Teaching experience and supervision

Spring 2022-2025 Laboratory-based training and co-supervision of Green Line Projects for MSc students under the European Master in Bioceb.  
Autumn 2024 Scientific Adviser in High School Scientific Research Project-Aarush Chowdavarapu (Audentes School, Tallinn).  
Autumn 2024 Scientific Adviser in High School Scientific Research Project-Andrei Mihhaidarov (Keskkool, Tallinn 53).  
2023-2025 Supervision of Master's thesis — "Hydrolysis lignin modification via chloromethylation, subsequent esterification, and blend-making with PLA" — Carmen Köster

### Selected Other Publication

Mohan, M. K.; Thorat, K.; Puthiyapurayil, T. P.; Sunnapu O.; Chandrashekharappa, S.; Ravula, V.; Khader, R.; Sankaranarayanan, A.; Muhammad, H.; Vemula, P. K. *Nat Commun*, **2024**, 15, 4844.

### Conference Presentations

#### Oral Presentations:

1. Mohan, M. K. Development of a Green Chloromethylation Process for Lignin and its Diverse Applications// *XI<sup>th</sup> Rencontres de Chimie Organique de Marseille (XI<sup>th</sup>-RCOM)*. 11-12 October **2024**, Marseille, France.
2. Mohan, M. K. Chloromethylation as a versatile chemical route for biomass valorization: an example of lignin, 4<sup>th</sup> TalTech summer seminar on biomass valorization, 26-28 August **2024**, Kata küla, Estonia.
3. Mohan, M. K.; Karpichev, Y. Greener protocol for chloromethylation of lignin and its diverse application// *2024 MRS Spring Meeting & Exhibit*. 22-26 April **2024**, Seattle, WA, USA.
4. Mohan, M. K. Chloromethylation as a versatile chemical route for biomass valorization: an example of lignin// *3<sup>rd</sup> TalTech summer seminar on biomass valorization*. 21-23 August **2023**, Kuressaare, Estonia.
5. Mohan, M. K. Chloromethylation as a versatile chemical route for lignin valorization// *Department of Chemistry and Biotechnology Symposium*, 20 December **2022**, Tallinn, Estonia.
6. Mohan, M. K. Chemically modified lignin as functional materials with catalytic properties in click and cross-coupling reaction// *2<sup>nd</sup> TalTech summer seminar on biomass valorization*. 15-17 August **2022**, Pärnu, Estonia.

#### Poster Presentations:

1. Mohan, M. K.; Köster, C.; Krasnou, I.; Lukk, T.; Karpichev, Y. Novel Softwood Lignin Esters as Advanced Filler to PLA for 3D Printing. In *9<sup>th</sup> Green and Sustainable Chemistry Conference*, 4-6 March, Pune, **2025**.
2. Mohan, M. K.; Kaur, H.; Duvanova, E.; Rosenberg, M.; Dahlem, M.; Ivask, A.; Raimundo, J. M.; Lukk, T.; Karpichev, Y. Synthesis and Antibacterial Properties of Lignin-Based Quaternary Ammonium and Phosphonium Salts. In *International Conference EcoBalt 2023-Chemicals & Environment*, 9-11 October, Tallinn, **2023**.
3. Mohan, M. K.; Lukk, T.; Karpichev, Y. Chloromethylation as a Versatile Route for Lignin Valorization. In *CA17128 LignoCOST Final dissemination event*, 1-3 March, Pisa, **2023**.
4. Mohan, M. K.; Ošeka, M.; Kulp, M.; Lukk, T.; Karpichev, Y. Chemically Modified Lignin as Functional Materials with Catalytic Properties in Click and Cross-Coupling Reaction. In *CA17128 LignoCOST working groups meeting*, 24-25 August, Tallinn, **2022**.
5. Mohan, M. K.; Duvanova, E.; Lukk, T.; Karpichev, Y. Synthesis and Antibacterial Properties of Lignin-Based Amino and Quaternary Ammonium Surfactants. In *Lignin conference on Lignin Valorization organized by CA17128 LignoCOST*, 31<sup>st</sup> May – 3<sup>rd</sup> June, Wageningen, **2022**.
6. Mohan, M. K.; Duvanova, E.; Lukk, T.; Karpichev, Y. Synthesis and Antibacterial Properties of Lignin-Based Amino and Quaternary Ammonium Surfactants. In *5<sup>th</sup> International Symposium on Nanoparticles-Nanomaterials and Applications (5<sup>th</sup> ISN2A-2022)*, 24-27 January, Caparica, **2022**.

## Elulookirjeldus

### Isikuandmed

Nimi	Mahendra Kothottil Mohan
Sünniaeg	20-10-1993
Sünnikoht	Olarikkara, Thrissur, Kerala
Kodakondsus	India

### Kontaktandmed

E-post	mahendrakhmohan@gmail.com
--------	---------------------------

### Hariduskäik

2021–2025	Tallinna Tehnikaülikool, doktorantuur
2014–2016	Bangalore'i Ülikool, Karnataka, India, magistrikraad (orgaaniline keemia)
2011–2014	Calicuti Ülikool, Kerala, India, bakalaureusekraad (keemia)

### Keelteoskus

Inglise keel	Kõrgtase
Malajalami	Emakeel
Hindi	Piiratud tööalane keeleoskus
eesti keel	Algtasemel keeleoskus, A1

### Teenistuskäik

2016–2021	Teadusassistent, Tüvirakkude ja Regeneratiivmeditsiini Instituut (InStem), NCBS, Bangalore, India
-----------	---

### Lühiajalised õppevisiidid

2022	Koolitus, Aix-Marseille'i Ülikool, Prantsusmaa, 10-18 Detsember
2023	Koolitus, Tartu Ülikool, Eesti, 8.–10. Märts
2025	Meditsiinkeemia programm: Orgaanilisest keemiast ravimiteni, Porto Ülikool, Portugal, 7.–11. juuli

### Teaduspreemiad ja tunnustused

2022	Parima lühiettekande auhind, Keemia ja Biotehnoloogia osakonna sümpoosion, Tallinn, Eesti
2022	Kahekordne Dora Plus lühiajalise õpirände stipendium (T1.1), (Sihtasutus Archimedes, Eesti)
2025	Erasmus+ lühiajalise ja kombineeritud liikuvuse stipendium

### Õpetamis- ja juhendamiskogemus

Kevad 2022–2025	Laboratoorne väljaõpe ja kaasujuhendamine magistriõppe projektides (Green Line Projects) Euroopa magistriprogrammi Bioceb raames
Sügis 2024	Teadusnõustaja gümnaasiumi teadusprojektis – Aarush Chowdavarapu (Audentes Kool, Tallinn)
Sügis 2024	Teadusnõustaja gümnaasiumi teadusprojektis – Andrei Mihhaidarov (Tallinna 53. Keskkool)
2023–2025	Magistritöö juhendamine – “Hüdrolüüsiliigniini modifitseerimine klorometüülimise, järgneva esterdamise ja PLA-ga segamise teel” – Carmen Köster



ISSN 2585-6901 (PDF)  
ISBN 978-9916-80-386-8 (PDF)